Development and characterisation of molecularly imprinted suspension polymers

by Rachel Walsh.

Pharmaceutical and Molecular Biotechnology Research Centre
Waterford Institute of Technology
June 2010

A thesis submitted for the degree of
Doctor of Philosophy

Under the supervision of
Dr. Peter McLoughlin
Dr. Patrick Duggan
Dr. Helen Hughes.

Waterford Institute *of* Technology

Declaration

No element of the work described in this thesis, unless otherwise stated, has been previously submitted for a degree at this or any other institution. The work in this thesis has been performed entirely by the author.

Signed: _____

Date: _____

Acknowledgements

First and foremost, I would like to thank my supervisors Dr. Helen Hughes, Dr. Pat Duggan and Dr. Peter McLoughlin for embarking me on this thesis journey. I would like to acknowledge their invaluable assistance as well as their patience, encouragement, guidance and enthusiasm throughout the course of this project. I could not have wished for better supervisors. Your contributions, detailed comments and insight have been of great value to me.

I would also like to thank Dr. June Frisby for her assistance and input into this project. I thank the Tyndall National Institute, Cork for the use of their SEM facilities as part of the National Access Programme.

Thank you to the European Unions INTERREG IIIA programme and the Council of Directors, under the Technology Sector, Strand III, without whose generous funding this research would not have taken place.

I would like to thank the staff in the Department of Chemical and Life Sciences, with a special mention to Pat, Aidan and Karen. Thank you also to the library staff. Let me also say thank you to the staff in the Research Support Unit, especially, Eimear (for helping me at any time) and Rita (for her words of encouragement).

A special word of thanks to my colleagues in the Pharmaceutical and Molecular Biootechnology Research Centre for their advice and support. In particular, my B21 colleague Richie deserves a mention, for his insightful comments and interesting discussions, which kept me in good spirits. I further would like to mention my old B01 buddies Sarah and Maeve for their support and friendship. Thanks, to all the other postgrads (past and present), both biology and chemistry, with whom I shared my time, for their friendship and encouragement.

Last but not least, a big 'thank you' to my family, my parents, Patricia and Robbie, for their unconditional support and encouragement to pursue my interests. I dedicate this thesis to you both.

Abstract

A controlled photo-polymerisation procedure for the synthesis of spherical molecularly imprinted polymer (MIP) beads through the use of a suspension polymerisation methodology is described. As molecular imprinting moves towards commercialisation, the need to produce packing materials with good flow properties is critical.

A comparative study of non-covalent MIPs synthesised by suspension and bulk polymerisation methods using 2-aminopyridine (2-apy) as a template and methacrylic acid (MAA) as functional monomer to produce acrylate polymers is reported. The influence of experimental parameters such as temperature, agitation speed and cross-linker i.e. trimethylolpropane trimethacrylate (TRIM) and ethylene glycol dimethacrylate (EGDMA) was examined in order to assess their impact on binding performance, yield, morphology and particle size distribution in the different polymers. It was concluded that for improved polymer performance, longer polymerisation times and lower temperatures resulted in the best polymer affinity for suspension polymerisation.

A detailed investigation of polymers produced by varying pre-polymerisation composition was performed using binding isotherm analysis. The optimum isotherm for use for MIP analysis was found to be the Langmuir-Freundlich isotherm with additional information subsequently obtained by plotting affinity distribution spectra. A greater number of binding sites with similar binding energies were found in the suspension MIPs in comparison to NIPs. A GC-MS methodology was utilised to characterise the performance of polymers synthesised under varying conditions in the absence of solvent. A direct comparison was found between imprinting performance assessed by a GC-MS methodology and solution phase analysis experiments.

To extend the scope of this study, MIPs were prepared for chlorpheniramine racemate (CP), *d*-chlorpheniramine (*d*-CP), brompheniramine racemate (BP) and *d*-brompheniramine (*d*-BP) as the template molecules respectively employing a novel non-stabilised aqueous suspension polymerisation procedure. A cross-selectivity rebinding study was carried out on the polymers using chiral HPLC analysis. Higher uptake capacities and IF values were found for the BP polymers over the CP polymers. It is speculated the higher binding of BP polymers over CP is related to differences in polarisability between Br and Cl and steric constraints.

The *d*-CP MIP prepared at 9500 rpm was packed as a HPLC stationary phase and the enantioselectivity and chromatographic behaviour of CP and BP was studied using an aqueous mobile phase. The highest enantioselectivity factor (1.19) and resolution (0.88) was obtained for CP over BP. Interestingly, BP was more retained on the *d*-CP MIP column than CP as a result of deprotonation correlating with equilibrium binding observations. The effect of column temperature on the *d*-CP MIP column was also studied for the separation of a mixture of *d*-CP and *d*-BP isomers and concluded that with increase in column temperature improved retention performance was observed with sharper peaks produced and an increase in resolution from 0.61 to 0.86. The *d*-CP imprinted column was also capable of separating pheniramine racemate (PHEN), CP and BP enantiomers using an aqueous mobile phase. The highest retention factor, enantioselectivity and resolution were observed for BP over the PHEN and CP enantiomers. This was explained due to the fact that all compounds possess similar pK_a values and in addition the hydrophobicity is in the order of BP, CP and PHEN. The chromatographic behaviour and separation of CP, *d*-CP, BP and *d*-BP isomers were also studied on a *d*-BP imprinted column using an aqueous mobile phase. The retention, selectivity and resolution of BP and *d*-BP on the *d*-BP imprinted column were greater in comparison to CP and *d*-CP. The results showed that the *d*-CP and *d*-BP imprinted columns each gave the best enantioseparation for its own template.

Physical characterisation of the polymers was carried out using nitrogen sorption porosimetry, particle size distribution, solvent swell studies and SEM. All samples exhibited low specific surface areas, pore volumes and pore diameters indicating non-porous materials. Trends were observed between the polymer properties characterised by the above techniques and the synthesis conditions.

Table of Contents

Chapter 1

Introduction

1.1 Introduction

In nature molecular recognition plays a decisive role in biological activity, for example in receptors, enzymes and antibodies [1]. Utilising this biochemical machinery as a model for a variety of applications, scientists have been working to mimic the molecular recognition of biological molecules [2]. Researchers use a technique called molecular imprinting for the creation of an imprinted material with carefully shaped pores that become artificial receptors. The relationship between the template and the imprinted cavity corresponds to a theory originating in biochemistry, which is called the 'lock-and-key' mechanism proposed by Nobel laureate Emil Fischer explaining enzyme-substrate interaction around 100 years ago [3]. The idea of a matrix designed to recognise a specific substrate remains the foundation of molecular imprinting theory and has been the primary aim of research in this area since the major revival of interest in molecular imprinting in the early 1970s. Chemists are making progress in developing more and more selective recognition systems. The availability of materials that can bind selectively to a target molecule is the answer to releasing a host of new technologies, making the analytical applications of molecular imprinting polymers (MIPs) for real-world analyses more attractive. Preparing a material with designed recognition elements, such as a stable cavity with a defined shape and functional groups, has enabled chemists to synthesis a wide range of structures capable of combining the advantages of synthetic plastics, such as low cost, durability and robustness, with the recognition properties of natural receptors. However, the developments in improving MIP technology with enhanced recognition properties necessitates further research into understanding the governing mechanisms of generating selectivity in molecular imprinted materials.

1.2 The concept of imprinting

Molecular imprinting is a technique whereby selective recognition sites can be created in synthetic polymers. This is achieved by forming a highly cross-linked polymeric matrix between functional monomers and a target compound (template) [4]. There are three approaches to molecular imprinting: covalent, non-covalent and semi-covalent. The crucial part of all these procedures is to ensure that functional groups

of the template molecule fully interact with complementary functional groups of the polymer followed by thermal or photo-initiated radical polymerisation.

A schematic representation for the synthesis of a molecular imprinted polymer (MIP) is shown in Figure 1.1: (a) a pre-polymerisable complex is formed between template molecule (blue) and one or more functional monomers (pink, green and yellow) by either non-covalent, covalent and/or metal-ion coordination imprinting interactions; (b) polymerisation then occurs with an excess of cross-linking agent to produce the MIP (grey); (c) template extraction (blue) is performed by washing and/or extraction, which leaves specific recognition sites that are complementary to the template in terms of size, shape and chemical functionality orientations, thus enabling subsequent recognition of the template during the rebinding process.

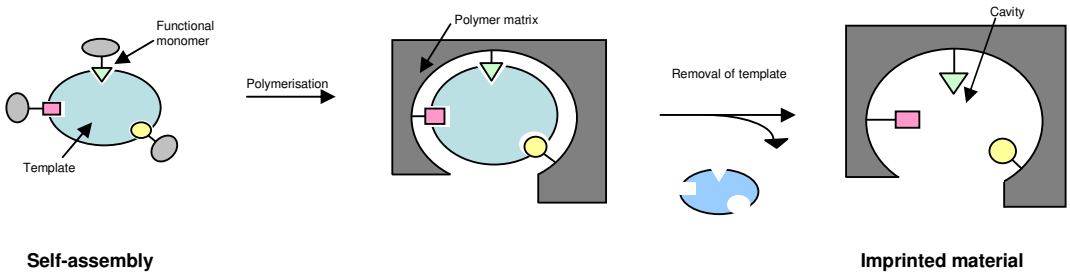

Figure 1.1 **Schematic representation of molecular imprinting (a) formation of a pre-polymerisation complex between template and functional monomers; (b) polymerisation step; and (c) template extraction, adapted from reference [5].**

The first step in constructing a recognition site is choosing an appropriate imprinting strategy. Currently the most common method of forming imprinted polymers is free radical vinyl polymerisation involving non-covalent interactions. The main characteristic of polymers prepared in this way is their high degree of cross-linking (typically between 70 & 95 %).

1.3 History of molecular imprinting

In reviewing the historical origins of molecular imprinting as a technique, it is noted that imprinting was first introduced in the early 1930s by a Soviet chemist M.V.

Polykov [6] who performed a series of investigations on silica for use in chromatography. It was observed that when silica gels were prepared in the presence of a solvent additive the resulting silica demonstrated preferential binding capacity for that solvent. It was the first time that experiments of this kind were accompanied by explanations of this nature. The mechanism proposed by Polykov was largely overlooked by the scientific community.

In 1949 a study was performed by a student of Linus Pauling; Frank Dickey, which involved the development of molecular imprinting in silica matrices in the presence of dyes [7]. Dickey observed that after removal of the 'patterning' dye the silica would rebind the same dye in preference to the others. Dickey's silicas can be considered to be the first imprinted materials.

Dickey's approach to introduce the template in the sodium silicate pre-polymerisation mixture produced a more definite influence on the structure of the silica, whereas Polykov introduced the template after the silica framework had been formed. Dickey's work is similar to present methodologies, thus, this method became the most widely used in subsequent studies.

Silica imprinting continued during the 1950s and 1960s, but the number of publications in the area remained low. Work in the area involved attempting to use imprinted materials for practical separations such as – solid phases in chromatography and in thin layer chromatography. The reasons for the limited interest were related to limitations in the stability and reproducibility of the imprinted silica materials. However, the re-emergence of silica based MIP research has occurred. Pinel *et al*. examined the imprinting of silica gel and showed that regiospecificity for cresols was successfully imprinted by using *o*-cresol as template [8]. Hunnius *et al*. [9] prepared porous silicas through a sol-gel process, which were developed for the generation of selective adsorption sites by molecular imprinting. Depending on the preparation conditions, microporous silica show surprising adsorption selectivities. These selectivities are not related to imprinting effects but must be attributed to unpredictable changes in surface polarity of the final porous materials. More recently the potential use of titanium alkooxide as precursors to imprinted media have been illustrated by Kunitake and co-workers [10]. A study published in 2005 by T-R. Ling

involved the recognition of catecholamine using a molecular imprinted silica-alumina gel [11]. Shiomi *et al*. [12] tested a new molecular imprinting technique to synthesise protein-imprinted silica using covalently immobilised template haemoglobin for biological application.

The introduction of molecular imprinting applied to organic polymers was first reported by a group led by Günter Wulff in the early 1970's. Since then, molecular imprinting has advanced significantly, and a number of companies now sell tailor-made imprints. For example, MIP technologies AB, Lund, Sweden; POLYIntell, Rouen, France and Semorex Inc., North Brunswick, NJ, USA.

1.4 Principal methodologies of assembling recognition site functionality

This section describes some of the principal methodologies employed in assembling recognition site functionality: covalent, non-covalent and semi-covalent.

1.4.1 The covalent approach

Covalent imprinting is one in which the polymerisable derivatives are co-polymerised with a cross-linking monomer pioneered by Günter Wulff and co-workers [1]. These derivatives are obtained by forming covalent bonds between the template and suitable polymerisable monomers to produce an 'exact fit' recognition site, in which the same chemical bonds in the initial template monomer complex reform during any subsequent binding of the imprinted polymer cast. In order to remove the template from the polymer and free up the binding sites, these covalent bonds have to be chemically cleaved. The functionality remaining in the binding site is capable of binding the target molecule by re-establishment of the covalent bond. Only a restricted range of functional groups (alcohols (diols), aldehydes, ketones, primary amines and carboxylic acids) can be imprinted by this approach. The bulk of covalent imprinting strategies involve condensation reactions requiring addition or loss of a water molecule during the cleavage or rebinding processes respectively. Examples of templates that can be imprinted in this way, include 1,2- and 1,3-diols (boronate ester

and ketal/acetal), aldehyde (acetal and Schiff's base), ketone (ketal) and amine (Schiff's base).

Shea *et al*. [13;14] and Damen and Neckers [15-17] have imprinted carboxylic acids using carboxylic ester linkages. Following template cleavage, rebinding occurred by reaction of carbonyl chloride with an alcohol, or through the displacement of bromide by a carboxylate anion. However, because of the slow rebinding kinetics and the requirement for activated intermediates, carboxylic acids have limited use in the covalent approach.

The benefit of the covalent imprinting method is that the reversible bond between the functional groups is only associated with the template site, and that functional groups responsible for binding are only located in the binding cavities, therefore restricting non-specific binding effects. The most prevalent covalent approach for the imprinting of templates contains pairs of hydroxyl-groups (1,2-diol and 1,3-diol functionality) utilising boronate esters; the reason being that boronic esters undergo a fast and reversible reaction with diols. Wulff and co-workers imprinted molecules by the covalent approach including derivatives of mannose, 4-nitrophenyl-α-D-mannopyranose [18;19]. A schematic representation of such a reaction is shown in Figure 1.2.

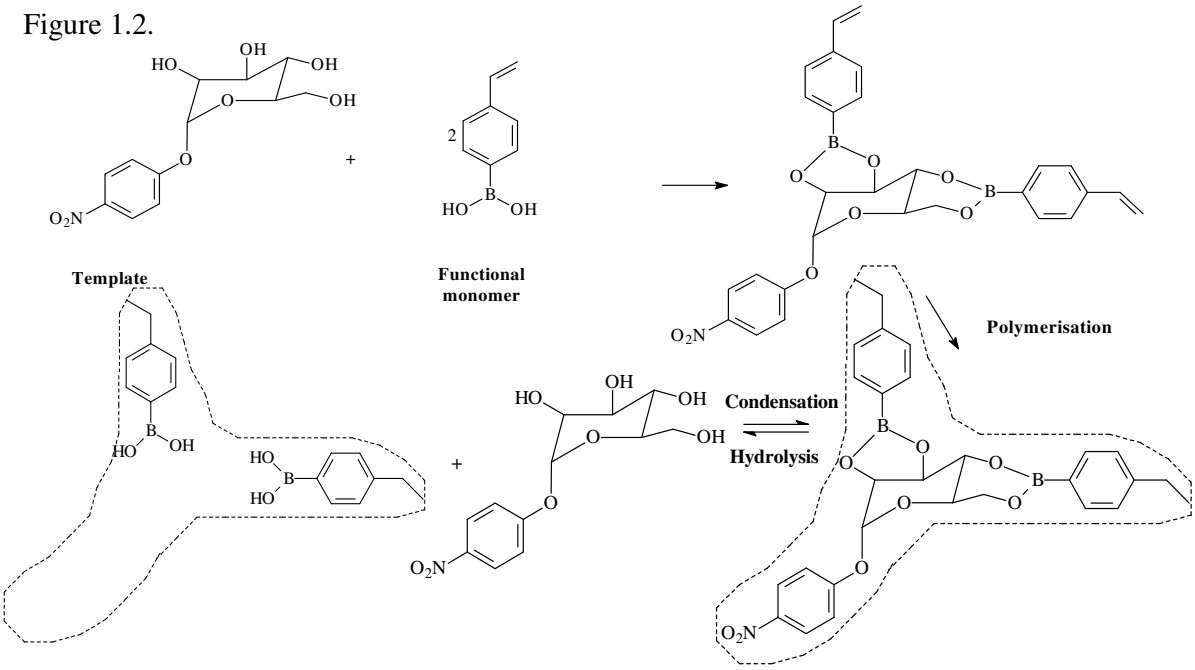

Figure 1.2 **Schematic illustration of the covalent imprinting of 4-nitrophenyl-α-D-mannopyranose using 4-vinylphenylboronic acid as functional monomer [18].**

For this study two molecules of 4-vinylphenylboronic acid were bonded covalently to the hydroxyl groups of the sugar molecule by an ester linkage which formed two cyclic boronate ester groups. Subsequently this template-monomeric complex was incorporated into a polymer matrix by the polymerisation of the vinyl function of the monomer with a high proportion of cross-linking monomer. Later hydrolysis of the ester linkages resulted in the formation of a cavity within the polymer structure, which is able to covalently rebind the templated molecule.

It must be noted that rebinding involves the reformation of those previously cleaved bonds. The kinetics of template-monomer formation and cleavage are sufficiently fast to allow chromatographic applications in the case of boronic esters [20;21].

1.4.2 Non-covalent approach

Non-covalent imprinting was developed by Klaus Mosbach and Arshady [22], who exclusively used non-covalent forces such as ionic interactions, hydrogen bonding, and dipole-dipole interactions. The approach relies on the formation of a pre-polymerisation complex between monomers carrying suitable functional groups and the template.

The interaction between functional monomer and template during polymerisation are complementary to those between polymer and template in the rebinding step. Due to the complementarity of the binding sites between polymer and the template a host-guest relationship is produced. As a result, the non-covalent approach is the one most frequently used for imprinting, as it is open to a wide range of templates. In addition to the simple processes used to extract the template a greater number of higher affinity sites are generated. The need to chemically cleave and reform covalent bonds in the covalent process is not required in the non-covalent approach.

Non-covalent interactions have been assigned to a broader range of template molecules. A series of functional monomers is commercially available, and have been tested in non-covalent imprinting. The most common acidic functional monomer, methacrylic acid (MAA) was first reported by Mosbach *et al*. [23].

Amongst the basic monomers, 4-vinyl pyridine (4-vpy) is the most extensively employed [24;25]. A neutral monomer, 2-hydroxyethyl methacrylate (HEMA) [26] has also been used, and the incorporation of HEMA in methacrylate-based MIPs makes the polymers less hydrophobic which aids in the diffusion of hydrophilic templates [27].

The appeal of non-covalent imprinting is the simplicity and versatility of the procedure. This can address elements of the template structure that are not influenced by covalent imprinting, by using a range of chemical interactions (ionic, dipolar and H-bonding) as shown in Figure 1.3. The major disadvantage of non-covalent imprinting is the variety of binding sites obtained as a result of the assembly of complexes that form between monomers and templates during the initial stages of polymerisations. Additionally, the need to increase non-covalent interactions responsible for complex formation during polymerisation limits the choice of solvents and reaction conditions.

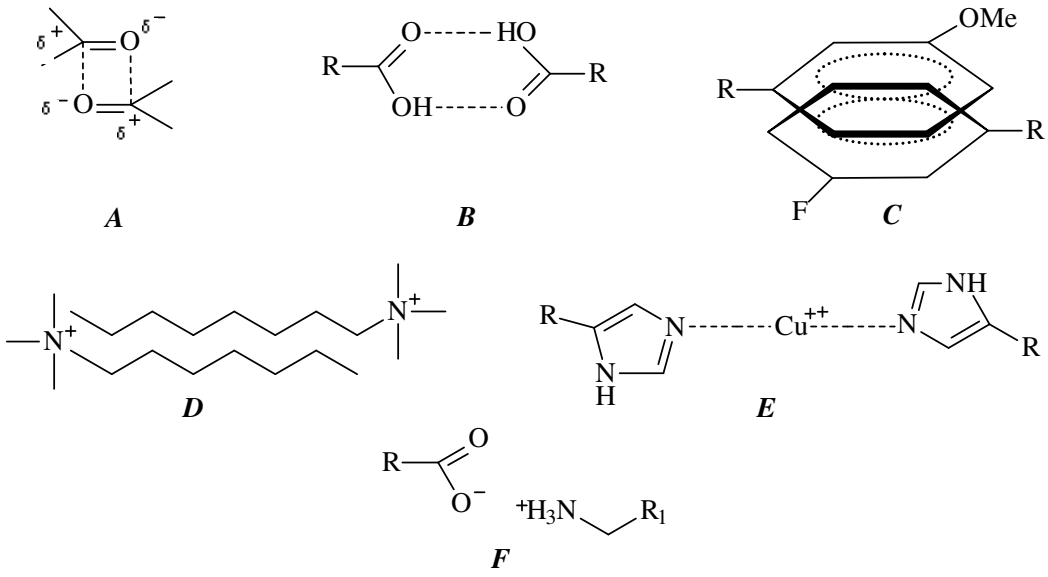

Figure 1.3 **Examples of interactions found in non-covalent imprinting. *A;* electrostatic: dipole-dipole, *B;* hydrogen bonding, *C;* π-π stacking, *D;* van der Waals, *E;* coordination bond, *F;* electrostatic ion-ion [28].**

The binding constants in non-covalent imprinting are essentially weak due to the nature of the interactions involved in comparison to the strength of bonds used in

covalent imprinting. In order to compensate for the effect of the weak interactions, an excess proportion of functional monomer is added.

A major contributor to the molecular recognition afforded by MIPs is the binding affinity. Binding affinity refers to the strength of the binding interaction, often given as a binding constant (K, mol^{-1}) or as free energy (ΔG, kcal/mol). Table 1.1 gives the ranges of binding energies for several major types of non-covalent interactions.

Table 1.1 Range of binding energies for non-covalent interactions [28].

	Type of binding interaction	**Range of binding energies (kcal/mol)**
1.	Electrostatic	
	a. ion-ion	20 – 80
	b. ion-dipole	12 – 50
	c. dipole-dipole	1 – 10
2.	Coordination bond	20 – 50
3.	Hydrogen bond	1 – 30
4.	π-π stacking	0 – 12
5.	van der Waals	0 – 1.5

Umpleby *et al*. [29] have employed affinity distribution diagrams to help explain the heterogeneity in MIPs prepared by non-covalent imprinting. For example, a very wide range of binding constants (K) have been reported for MIPs from 10^{-2} to 10^{-8} M^{-1} illustrating broad heterogeneous distributions.

Yu *et al*. [30] performed an investigation to analyse the mechanism of the non-covalent chiral recognition in MIPs of N-*tert*-butoxycarbonyl-tryptophan, schematically illustrated in Figure 1.4.

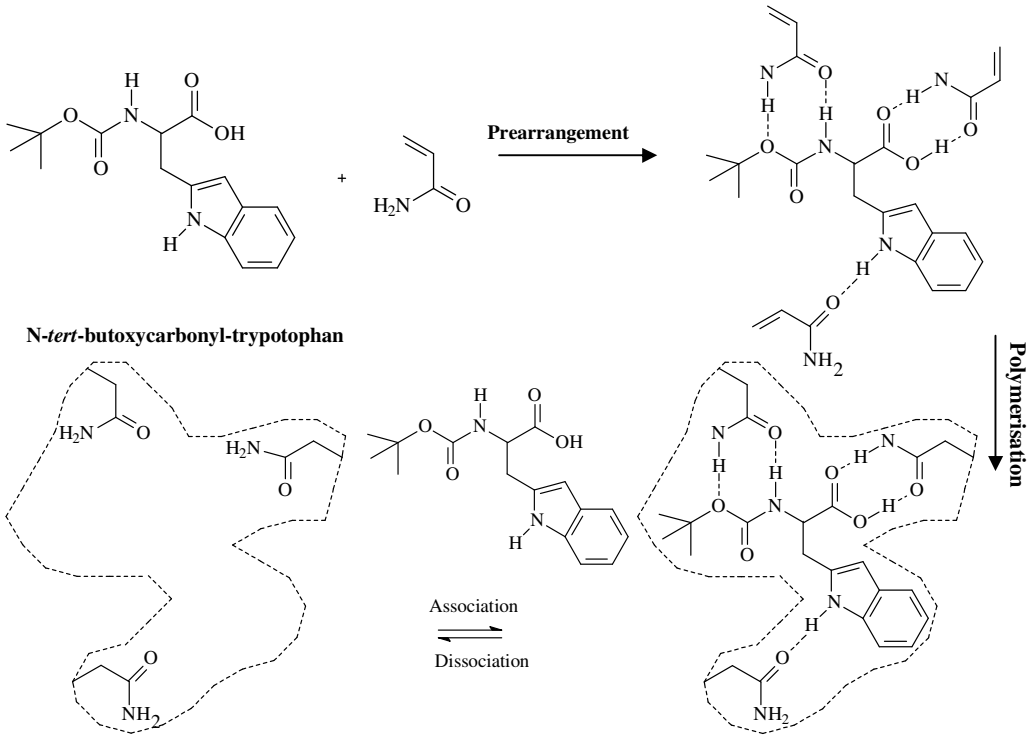

Figure 1.4 **Schematic illustration of the non-covalent imprinting of N-*tert*-butoxycarbonyl-tryptophan [30].**

The non-covalent template-monomer complex formations are controlled by equilibria and excess functional monomer ensures an equilibrium shift towards complex formation during pre-polymerisation. The binding sites are of variable conformities, which gives heterogeneity to the imprinted polymer. The effect can be minimised in certain cases by optimisation of the polymerisation conditions and by using stoichiometric ratios of template to monomer.

1.4.2.1 Stoichiometric non-covalent approach

Stoichiometric non-covalent interactions represent a very valuable method for binding the template during the molecular imprinting procedure. In stoichiometric non-covalent interactions template and functional monomer react in a 1:1 molar ratio during polymerisation. It is possible to introduce binding site functional groups nearly exclusively inside the imprinted cavities. Ninety eight percent re-uptake of template to the imprinted polymer is achievable. It is, therefore, not necessary to use

any excess of binding site monomers in order to saturate the template completely. This can only be achieved when the association constant for the template-monomer interaction is considerably high ($K_a > 10^3$ M^{-1}) [31]. Stoichiometric non-covalent interaction shows in most cases both the advantages of covalent and non-covalent interactions without showing their corresponding disadvantages.

Since all cavities can be reloaded these polymers show high capacity (e.g., for preparative applications) and are especially suited for the synthesis of catalytically active imprinted polymers. Wulff's group designed and synthesised polymerisable amidines (including guanidines) which form strong 1:1 complexes with carboxylic acids [32]. The use of the amidine group as binding site monomer is of interest and their equilibria has been investigated. The interaction of amidines with carboxylates is rather strong since it uses a combination of electrostatic as well as bidentate hydrogen bonds.

Wulff and Schönfeld [32] carried out NMR titrations of amidinium complexes to study the underlying binding reaction. Systematic investigations showed that unsubstituted amidines often form insoluble complexes with carboxylic acids. This problem can be overcome by using *N,N*-dialkylated benzamidines. Out of a large series of compounds *N,N*-diethyl-4-vinylbenzamidine proved to be the most favourable binding site monomer in this respect; complexes being soluble even in non-polar solvents like chloroform and benzene.

Lübke *et al.* [33] imprinted ampicillin by designing and employing two different electroneutral functional monomers which are capable of forming strong interactions with the carboxylic acid functionality and amine functionality of the template. The functional monomer, shown in Figure 1.5 ***B*** (5-(4‘ ‘‘-vinyl)benzyloxy-1,3-bis[2‘-(3‘ ‘,3‘ ‘,4‘ ‘,4‘ ‘-tetramethyl-2‘ ‘,5‘ ‘-dioxaborolanyl)phenylcarbomoyl]benzene) was selected to interact with the carboxyl groups and had an association constant of K_a = 2.8 x 10^2 M^{-1} with the ampicillin salt (DMSO-d_6). The structure of 1.5 ***C*** (2-(4-vinylphenyloxy)-3,5,6-trichlorobenzoquinone) was used for n - π interactions with the amino group of ampicillin. For polymer formation both of the functional monomers employed were used in a 1:1 stoichiometric ratio with the template (tetrabutylammonium salt of ampicillin). Ampicillin bound the MIP more strongly

than the NIP. In addition, the imprinted polymer also preferentially bound the ampicillin over structurally related analogues.

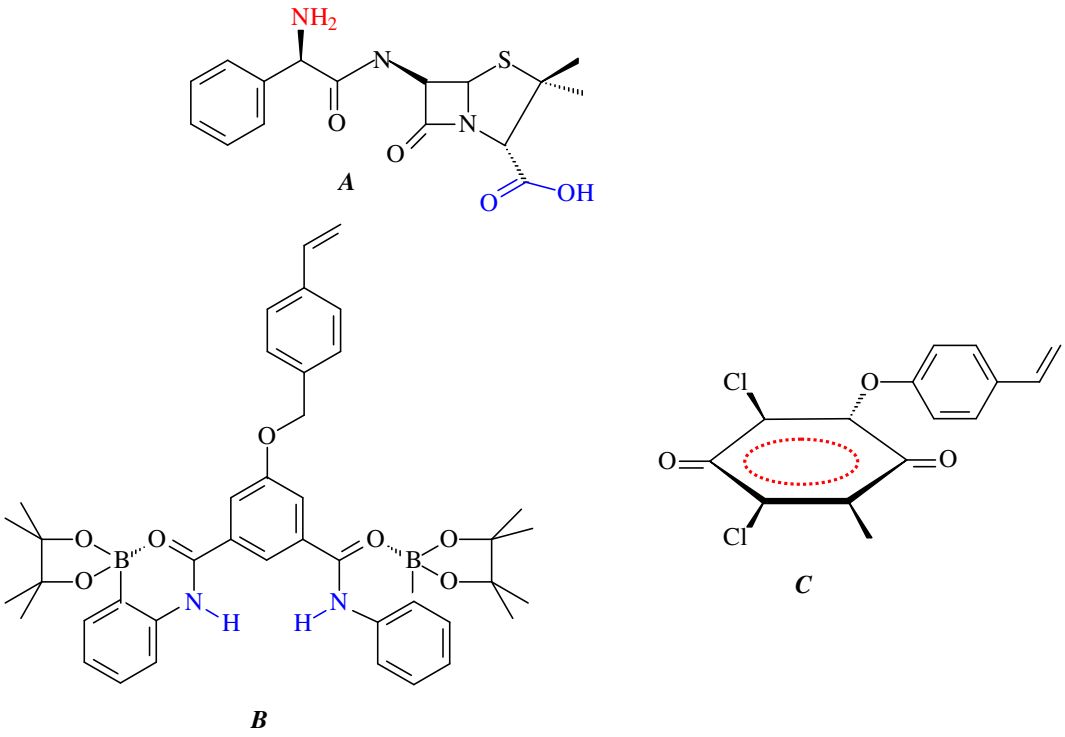

Figure 1.5 **Example of precursors used in stoichiometric imprinting. *A*; ampicillin, *B*; and *C*; the functional monomers employed (adapted from reference [33]). Corresponding interacting functionalities are highlighted using the same colour.**

Strikovsky *et al.* [34] reported that optimising conditions in stoichiometric non-covalent interaction yields improved catalytic performance results. For imprinting procedures involving non-covalent bonds with sufficiently high association constants, complexes possessing a 1:1 ratio of template to binding site are given. The advantages of the novel stoichiometric non-covalent interaction, based on *N*,*N*-diethyl(4-vinylphenyl)amidine (DEVPA) as functional monomer and diphenyl phosphate (DPP) as template molecule was studied.

1.4.3 Semi-covalent approach

The semi-covalent approach also aims to unite the advantages of the covalent and non-covalent approach. The template is covalently bound to a polymerisable group,

the functionality is recovered after cleavage of the templates found in the binding site, and rebinding takes place via non-covalent interactions. Wulff *et al*. introduced the idea of the semi-covalent approach, when it was used together with the (reversible) covalent approach. The template, glyceric acid, was attached to boronic acid and 4-vinylaniline by an amide bond. The template reformed a covalent boronate ester bond in the rebinding process but interacted with the amine group by way of ion pair formation [35;36]. Sellergren and Andersson [37] imprinted the template, *p*-aminophenylalanine ethyl ester. A structural analogue was employed which had two polymerisable groups attached through ester linkages. Following hydrolysis the carboxylic acid groups remaining in the polymer binding site rebinds the amino acid through a mixture of hydrogen bonding and electrostatic interactions.

Presently two semi-covalent methodologies have been developed and can be distinguished; (i) the template and the monomer are connected directly [38] or (ii) the template and the monomer are connected using a spacer group. The sacrificial spacer method was introduced by Whitcombe *et al*. [39], in order to avoid crowding in the binding site cavity and to allow unhindered non-covalent rebinding to occur. The semi-covalent imprinting of the template cholesterol was the first example of the use of the sacrificial spacer approach (Figure 1.6). As cholesterol has limited functionality it was a difficult molecule to imprint through conventional routes. Cholesterol was attached via a carbonyl spacer to 4-vinylphenol giving cholesteryl 4-vinylphenyl carbonate as the template monomer. Following polymerisation, the cholesterol was cleaved from the polymer by base hydrolysis. A phenolic hydroxyl group is left in the binding site which is able to interact with cholesterol through hydrogen bond formation. Adequate space between functional groups remained in order to establish hydrogen bonding and creation of an imprinted site displaying a recognition site matching that of the cholesterol molecule as shown in Figure 1.6. MIPs for cholesterol prepared in this way showed higher chromatographic efficiency relative to non-covalent imprinted polymers when used as stationary phases in HPLC [40]. In addition, the MIP prepared by semi-covalent imprinting was found to bind more cholesterol.

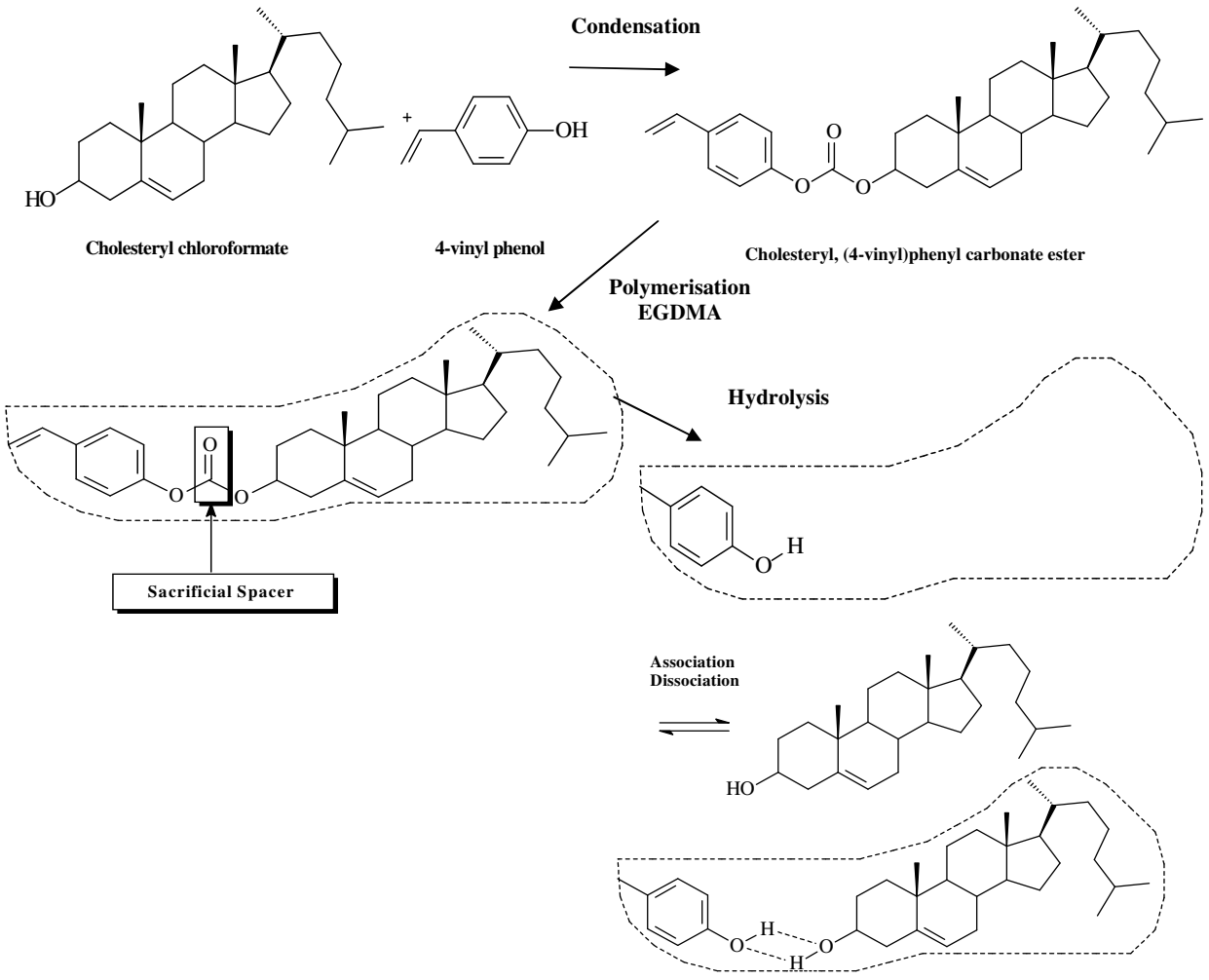

Figure 1.6 **Schematic illustration of the sacrificial spacer approach to the molecular imprinting of Cholesterol [39].**

1.5 Factors affecting the imprinting process

The methodology of molecular imprinting is quite straightforward. However the rational design of MIPs is very complicated because of a number of experimental variables, for example the template, functional monomer(s), ratio of functional monomer(s) to template, cross-linker(s), ratio of functional monomer(s) to cross-linker(s), pre-polymerisation interactions, solvent(s), initiator, thermodynamic considerations, temperature, pressure, methodology and polymerisation parameters. Binding site orientation, stability and accessibility are governed by the structural characteristics of the polymeric matrix and are essential to recognition of the

polymers formed. For this reason, investigating and optimising various parameters is essential in order to make progress in maximising recognition effects.

1.5.1 Template

The shape, size and chemical functionality of the template species has significant bearing on the imprinting approach utilised. At present, imprints of several hundred template species have been accomplished, including a vast range of molecular sizes, shapes and functionality. Generally, with regard to choice of template, factors should be considered such as: solubility in organic solvents, possession of electrostatic functionalities, being chemically inert under polymerisation conditions in order to be compatible with free radical polymerisation. For larger molecules imprinting can be difficult to achieve.

While the features of the template species are the most important aspect of the imprinting process, it is inclined to be the most restrictive in terms of potential variations. Removal of the template provides a cavity, which matches the physical and chemical characteristics of the template species. Any variation from the structure of the desired species to a structurally similar entity may result in loss of selectivity. It is not always possible to imprint using the desired template due to high cost of purchase or the difficulty in obtaining the template which may result in the imposed use of a 'surrogate' or 'dummy' template [41]. Their use may also be required if the species demonstrates sensitivity to the conditions of polymerisation.

Cummins *et al*. [42] performed a systematic cross-selectivity study of a series of substituted nitrogen heterocycles. The factors responsible for template receptor binding in molecularly imprinted polymers were evaluated. All species were non-covalently imprinted in thermoinduced methacrylic acid-ethylene glycol dimethacrylate co-polymers. The electrostatic effects, principally hydrogen-bonding, were investigated through rebinding in chloroform and acetonitrile. All imprinted polymers exhibited varying degrees of selectivity except for 2-dimethylaminopyridine, with which no selective effects were seen. Evaluations of

template properties showed that a relationship exists between non-specific binding and template basicity for a series of structural isomers.

Template effects in covalent imprinting of sugars using boronic acid derivatives was investigated and appears to be dependent on the spatial distribution of functional groups rather than absolute structure, implied by cross-selectivity of a D-galactose-imprinted polymer with L-fructose and vice-versa [43].

Template removal is an issue in non-covalent MIPs. Template bleed can occur which can interfere with analyte detection. The use of 'dummy' templates may help avoid these problems [44]. The effect of very high monomer to template ratios has been studied and significant imprinting effects were observed with very low template concentrations [45]. The effect of template size on the selectivity of MIPs has been examined. The amount of template and porogen used was varied in order to selectively extract a wide range of phenylurea herbicides of close structural selectivity. The results showed that the size and structure of the template in terms of the strength of interaction was of utmost importance to the success of the imprinted polymer. [46]. It was found that the isoproturan-imprinted polymer was able to recognise all the herbicides studied whereas fenuron-imprinted polymers were highly selective in rebinding only fenuron from a mixture of phenylureas. This fact proves that the size of the cavities obtained for the fenuron-imprinted polymer is appropriate only to fenuron. The effect of intermolecular H-bonding in the template on its imprint [47] was also evaluated. By comparing the structures of the three templates, it was found that molecular recognition ability will decrease when the template itself is able to form intramolecular hydrogen bonds in the molecular imprinting process.

Yu and Mosbach compared the performance of acrylamide-based MIPs prepared with a range of N-protected amino acids [48]. MIPs prepared using acrylamide as the hydrogen bonding functional monomer exhibited good enantiomeric recognition properties in aqueous solutions.

1.5.2 Functional monomer

The chemical characteristics of the functional monomer are of primary importance to the imprinting process. The functional monomer is selected to assist the formation of strong non-covalent interactions between it and the template.

A detailed review of the different approaches employed in optimising MIP design has been put forward by Karim *et al*. [49]. Interactions occurring in the pre- and post-polymerisation media and the different techniques used to assess them were reviewed.

Figure 1.7 illustrates some frequently used non-covalent functional monomers, which are divided into groups corresponding to their acidic, basic or neutral character.

Acidic

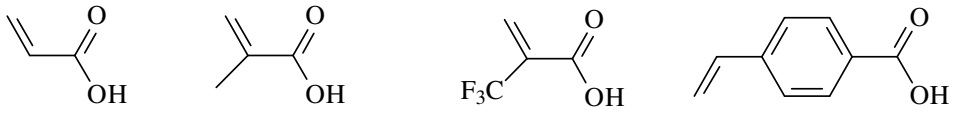

Acrylic acid (AA) | Methacrylic acid (MAA) | Trifluoromethacrylic acid (TFMAA) | 4-Vinylbenzoic acid (4-VBA)

Basic

4-Vinylpyridine (4-VPY) | 1-Vinylimidazole (1-VIm) | 4-Vinylimidazole (4-VIm) | Allylamine (AA)

Neutral

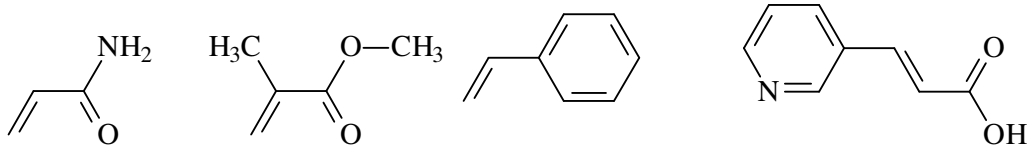

Acrylamide (ACM) | Methyl methacrylate (MMA) | Styrene (S) | Trans-3-(3-pyridyl)-acrylic acid (TPAA)

Figure 1.7 A range of functional monomers used in non-covalent molecular imprinting.

The most frequently used functional monomer in molecular imprinting is methacrylic acid (MAA). It has the capability to get involved in many interactions (ion-ion, ion-dipole and dipole-dipole) due to its amphoteric nature (i.e. it can simultaneously act as a Lewis acid and base), and hydrogen donating and accepting properties. The most successful non-covalent imprinting systems are based on MAA which is cross-linked with ethylene glycol dimethacrylate (EGDMA) [50]. Spivak *et al.* [51] reported that MAA has the capability of forming stable cyclic hydrogen bonds with appropriate templates. MAA is a suitable functional monomer for theophylline, since carboxylic acid groups can form hydrogen bonds with the functional groups on theophylline. A study was conducted by Pavel and Lagowski [52] to gain an understanding of intermolecular interactions in the molecular imprinting of theophylline.

The choice of functional monomers is very important to preserve stable monomer-template complexes during the imprinting process. The functional group is chosen as to complement the chemical functionality of the template molecule. In general, for templates with acid groups, monomers with basic functionality are preferred. For instance, MAA is commonly used for basic templates [53]. For templates carrying carboxylic acid moieties, vinylpyridine is the monomer of preference.

Molecular dynamics (MD) simulations were performed in different molecular systems in order to predict interaction energies and closest approach distances for molecular imprinting of theophylline and its derivatives. It was found that simulated functional groups of monomers interacting with ligands tend to be carboxylic acid and double bonds. Figure 1.8 presents an example of an optimised configuration of the H-bonding interactions between four molecules of methacrylic acid and one molecule of theophylline [52].

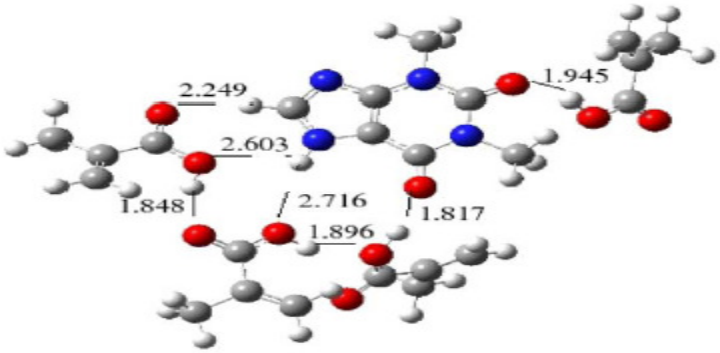

Figure 1.8 **Example of an optimised configuration for four molecules of methacrylic acid and one molecule of theophylline [52].**

Matsui *et al*. [54] used the more acidic functional monomer 2-(trifluoromethyl)acrylic acid (TFMAA) for molecular imprinting of a strongly basic template nicotine. Chromatographic studies using the nicotine imprinted polymer as stationary phase indicated that TFMAA used for imprinting resulted in a high affinity nicotine-selective polymer. The molecule (TFMAA) is more acidic in comparison to the conventional functional monomer MAA, owing to the electron-withdrawing effect of the trifluoromethyl group. Haginaka and Sambe [55] reported the use of a common basic functional monomer 4-vinylpyridine (4-vpy) for imprinting of an acidic template (*S*)-naproxen.

The stoichiometric ratio of template to functional monomer is very significant to the ultimate performance of the imprinted polymer, in particular where interactions are non-covalent. Together, the type and the stoichiometric ratio of the functional monomer to template will govern the pre-arrangement complex structure and strength. In covalent imprinting the nature of the template-monomer bond is uniform and non-equilibrium based. The conditions of the polymerisation will not have an influence on this bond. However in a non-covalent system, the template-monomer complex formation is equilibrium based. Binding constants are comparatively low and a stoichiometric excess of functional monomer is often needed to guarantee a high degree of template-monomer complexation. As a result a proportionally large quantity of functional monomer is distributed indiscriminately throughout the polymer matrix which does not play a part in the creation of specific binding sites. The effect of this is to expose a high proportion of non-specific binding sites to the imprinted polymer. Baggiani *et al* [56] examined the effect of adjusting the molar ratio between template and functional monomer for 2,4,5-trichlorophenoxyacetic acid acrylic imprinted polymer. It was determined that in HPLC applications, column capacity, selectivity and imprinting effect were inversely proportional to the template-monomer mole ratio.

The difficulty in molecular imprinting is the choice of the correct functional monomer, as there is a vast range of functional monomers available. In theory it is possible for an imprinted phase of any stable molecular species to be constructed. This is not the case in practice, due to possible monomers being both time-consuming and expensive in their construction.

1.5.3 Cross-linking monomers

Creating a recognition site and deciding on an appropriate imprinting strategy is just the first step in making an imprint. The next step is to prepare the polymer. Free radical vinyl polymerisation is the most common method of forming imprinted polymers. The main feature of polymers prepared in this way is their high degree of cross-linking due to a substantial proportion (typically between 70 and 95 per cent). This high level of cross-linking serves an important function: it provides an element of rigidity in the recognition sites by forming the supporting matrix.

A range of organic based cross-linking monomers used in the non-covalent approach to molecular imprinting are shown in Figure 1.9.

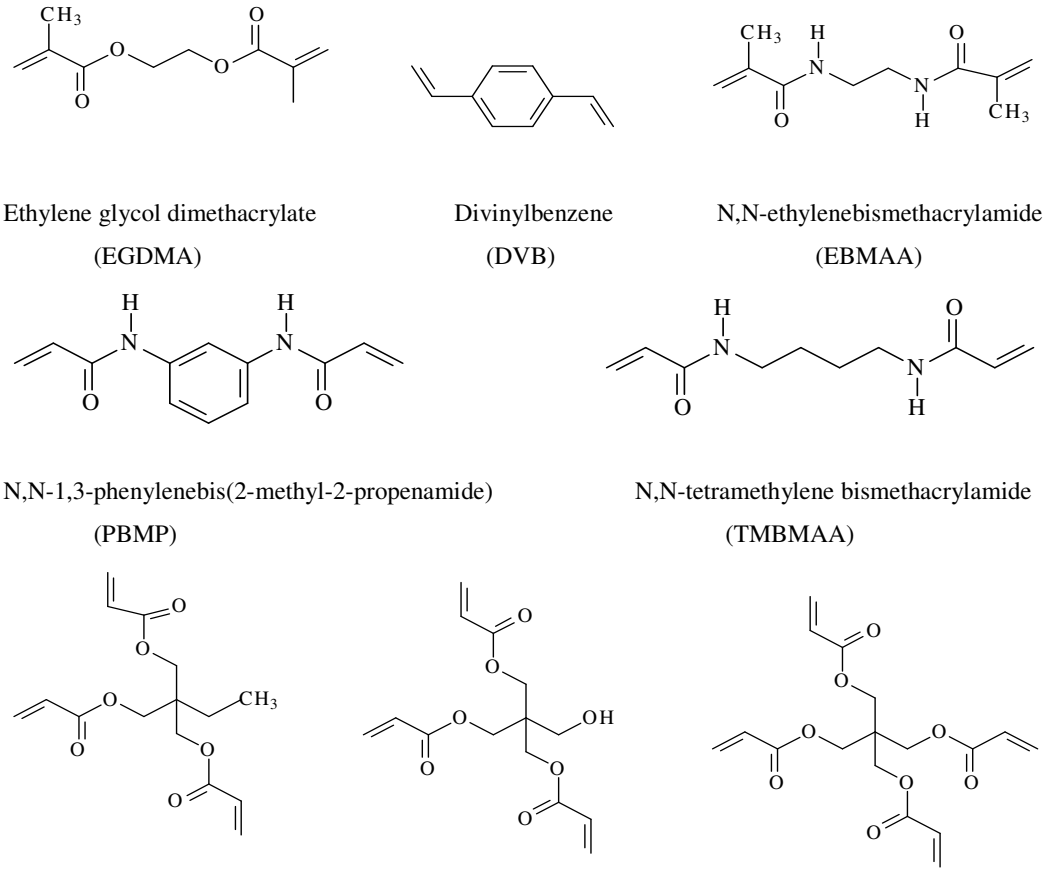

Figure 1.9 **A range of organic based cross-linking monomers used in the non-covalent approach to molecular imprinting.**

Wulff and co-workers compared a series of commercial and synthetically produced styrenic and methacrylate cross-linkers in some early studies [57], including pure isomers of divinylbenzene (DVB) (a commercial material which is a mixture of isomers) in the covalent study of α–D-mannopyranoside. The selectivity during racemic resolution was determined. Ethylene glycol dimethacrylate (EDGMA) was found to be the best cross-linking agent used. This was accredited to the combination of a short flexible linker and the rigidity and pro-chiral character of the methacrylate groups of EGDMA.

Cross-linkers used in organic based molecular imprinting in the past have been limited to monomers with two (meth)acrylate groups. Generally, these polymers were prepared with EGDMA. Trimethylolpropane trimethacrylate (TRIM) with three (meth)acrylate groups such as have been shown to be superior to EGDMA in some applications as reported by Kempe and Mosbach [58]. The system described in that study involved the copolymerisation of TRIM as cross-linker with MAA as functional monomer in the presence of a dipeptide acting as template. Greater load capacities and improved resolutions were achieved using TRIM as cross-linker.

A suitable degree of cross-linking is important in preserving binding specificity of an imprinted polymer. When functional groups are not satisfactorily attached by cross-linking, i.e. levels of cross-linking are too low, the binding specificity by the imprinted polymer decreases. On the other side, when the levels are too high, the loading capacity of the polymers is reduced, and the diffusion of substrates into the imprinted cavities during rebinding may also be obstructed. Generally the poly (MAA-*co*-TRIM) has a higher load capacity to the poly (MAA-*co*-EGDMA), since TRIM has one more vinyl group than EGDMA and therefore less is required to ensure the same backbone rigidity that contributes to binding specificity [58].

Holland *et al.* prepared a series of 2-aminopyridine (2-apy) imprinted methacrylic acid-ethylene glycol dimethacrylate (MAA-EGDMA) copolymers under identical conditions but with varying amounts of cross-linker [59]. Polymer composition, morphology and performance was examined by a thermal desorption GC-MS methodology, nitrogen sorption, solvent swell effects and solution-phase binding. The thermal desorption GC-MS technique demonstrated the ability to facilitate

template removal, the extent of which was dependant on varying the amounts of cross-linker employed in polymer synthesis. A higher amount of cross-linker resulted in a higher amount of template retention. These results correlated with porosity data; a larger number of pores were formed for polymers prepared with a decrease in EGDMA, which would facilitate the release of template from the polymers. Results in this study suggested that a reduction in cross-linker indicated a higher degree of flexibility of the polymers. A higher quantity of displaced template would imply that there are more unoccupied binding sites within the polymer network. Rebinding studies were also assessed in solution phase for the polymers in order to validate the thermal desorption technique. Direct correlations between both characterisation techniques were found.

Villamena and De La Cruz [60] report a study on the caffeine selectivity of divinyl benzene (DVB) cross-linked polymers in aqueous media. A high binding affinity and selectivity of DVB cross-linked polymers for caffeine in aqueous media was shown in comparison to EGDMA and TRIM based polymers. Analytes with hydrophilic and electron-withdrawing groups lowered their binding affinity with the polymer. The nature of the caffeine-DVB imprinted polymer interaction appeared to be predominantly a hydrophobic π-π interaction but partly due the presence of the caffeine specific sites.

Spivak and Sibrian-Vasquez [61] developed new classes of cross-linked polymers to optimise the performance of molecularly imprinted polymers. A simple molecular imprinting method was designed using a single cross-linking monomer *N*,*O*-*bis*methacryloyl ethanolamine (NOBE) in addition to template, initiator, and solvent. The structure of NOBE is represented in Figure 1.10. The term "OMNiMIPs" (*O*ne *M*o*N*omer *M*olecularly *I*mprinted *P*olymers) was conceived to describe this approach, which eradicates variables such as choice of functional monomer and cross-linker, the ratio of functional monomer/cross-linker, and the ratio of functional monomer/template in order to simplify MIP design. Binding and selectivity using NOBE in the OMNiMIP approach was investigated. Polymers were imprinted with a range of templates and compared with polymers imprinted with the traditionally used MIP formulation EGDMA/MAA. Higher binding capacities (i.e. the number of binding sites) were observed for the MIPs using NOBE against the traditional

EGDMA/MAA formulation, approximately 20 – 25 % template loading with respect to the monomer [62].

However, in a follow up study increased loadings of multiple templates to greater than 25 mol% resulted in gradual loss of binding capacity and a significant lowering of the imprinting effect [63]. Therefore, the binding capacity was maximised at 25 mol% template loading, where the ratio of monomer to template was 3:1, suggesting that the binding affinity sites require approximately three monomers surrounding the template molecule.

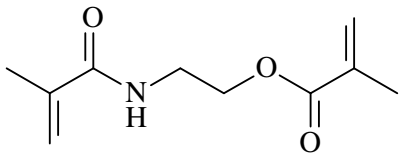

Figure 1.10 **Structure of single cross-linking monomer *N*,*O*-*bis*methacryloyl ethanolamine (NOBE).**

1.5.4 Solvent/Porogen

Both the imprinting process and the physical state (morphology, pore size distribution, pore structure, swellability and toughness) is shaped by the choice and amount of the porogenic solvent used in the polymerisation recipe for the MIP as reported by Sellergren and Shea [64]. The influence of the polymerisation solvent has multiple roles:

(i) It solubilises all the monomers in the pre-polymerisation mixture before polymerisation
(ii) It stabilises template-monomer pre-polymerisation complexes
(iii) It acts as a 'porogen' helping to control the porosity of the resulting polymer.

The most considerable influence of the porogen in non-covalent imprinting is its ability to stabilise template-monomer complexes. The properties of the solvent (porogen) used in the imprinting step in terms of hydrogen bond capacity and polarity is likely to influence the strength of interactions. In a study by Sellergren and Shea

[64], it was observed there was no apparent link between selectivity and polymer morphology, but there was a connection between the hydrogen bonding capacity of the porogen and polymer selectivity. A loss of selectivity was observed with increasing polarity of the solvent used for the imprinted polymers, which was linked to the template used.

Yoshizako *et al*. [65] prepared polymers and demonstrated that optimum rebinding of *ortho*- or *para*-xylene was observed using the solvent employed in the polymerisation. A major restriction in organic acrylic based molecular imprinting is that all species are soluble in the organic solvent. Therefore imprinting of template molecules that are only soluble in aqueous media are usually not an option. A promising alternative to overcome this constraint is sol-gel imprinting. Cummins *et al*. [66] analysed the binding properties in both acrylic based polymers and sol-gel polymers. It was reported that hydrogen bonding plays an important function in the molecular recognition of acrylic based polymers and to a less significant degree in sol-gel polymers. Another interesting finding showed that with acetonitrile as the porogen acrylic polymers demonstrated only negligible performance of MIP over NIP. Sol-gel polymers produced a considerable difference between MIP and NIP. The sol-gel functional monomer system was chosen to include two functional monomers phenyltrimethoxysilane (PTMOS) containing an aromatic ring facilitating the formation of possible π-π interactions with the aromaticity of the pyridine ring, and 3-aminopropyltriethoxysilane (APTES), capable of hydrogen bonding with both the amine and the pyridyl nitrogen of the template (2-apy). This demonstrates the ability of sol-gels to maintain better recognition in a more polar environment.

Andersson reported that incubation of MIPs in solvents and aqueous buffers could be performed equally well by displaying successful recognition [67]. In this situation a change in recognition mechanism from H-bonding to hydrophobic recognition was illustrated by a loss of recognition in intermediate aqueous-organic mixtures [68;69]. The effect of binding to MIPs in HPLC by the use of organic modifiers, for example acetic acid, has been analysed [70]. Non-specific interactions with both MIP and control were found to be reduced. The employment of surfactants as modifiers in aqueous-based recognition studies and in SPE and chromatography has also been investigated and reviewed [71-73].

1.5.5 Initiator

The most common method of initiation in the synthesis of MIPs is by the formation of free radicals. Free radical formation has generally been performed thermally or photolytically. Figure 1.11 outlines the structures of the most common initiators used in organic based molecular imprinting.

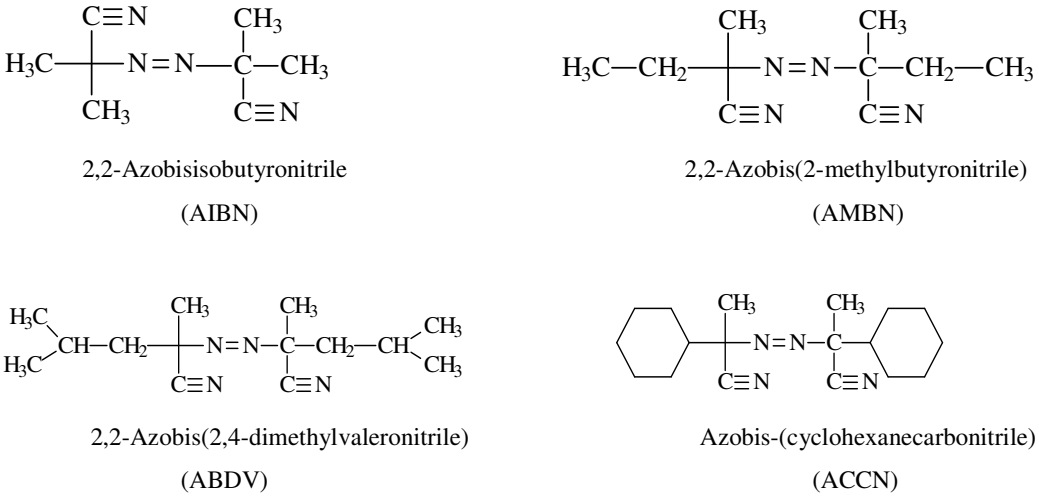

Figure 1.11 Structures of initiators used in organic based molecular imprinting.

The azobisnitriles are decomposed by heat (ABDV:40 °C; AIBN:60 °C) or ultraviolet light [74;75]. This decomposition results in the departure of nitrogen to leave metastable radicals.

The polymerisation mechanism involves three distinct phases: initiation, propagation and termination as demonstrated in Figure 1.12. ***Initiation*****,** where a free radical resulting from the decomposition of the initiator (AIBN) attacks the double bond of the vinyl monomer molecule, forming a heterodimer, possessing a free radical functionality; ***Polymerisation***, where the reaction continues, a chain transfer is formed from the reaction of a free radical and a new monomer unit and propagation occurs rapidly by addition of new monomers under the formation of a growing radical chain; ***Termination***, can occur in many ways, the most important, is by transfer of an active centre to another molecule where the radicals of two growing polymer chains are

coupled, resulting in the removal of radicals from the polymerisation process. This can occur by two different mechanisms (i) combination or (ii) disproportionation.

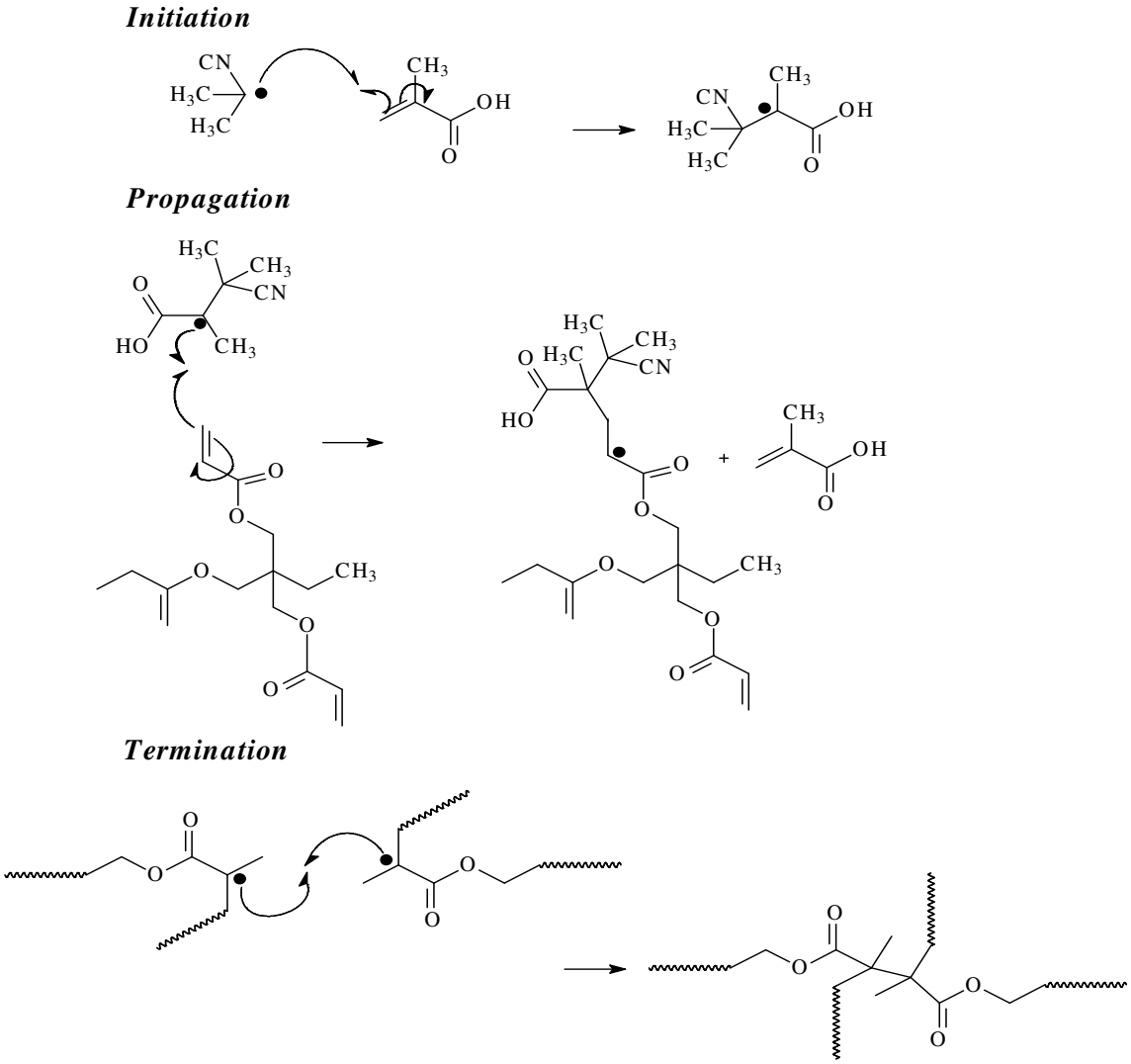

Figure 1.12 **The three stages of free radical polymerisation: *Initiation*, free radical initiation of AIBN with MAA; *Polymerisation;* and *Termination* occurring by the combination of two radicals.**

Free radical polymerisations must be performed in an inert environment, usually by purging the monomer mixture with nitrogen gas, as the presence of oxygen, which can easily accept an electron from the radicals may result in early chain-termination prior to polymerisation.

Various studies of initiation methods have been performed. Azonitriles are commonly used initiators. The initiator 2,2'-azo-bis-(cyclohexyl carbonitrile) (ABCHC) is a better quality initiator at low temperatures due to its greater solubility in comparison to AIBN. Skudar *et al*. reported this may be an advantage in photochemical initiation [76]. O'Shannessy *et al*. [77] prepared polymers with azobisnitriles using photochemical and thermal initiation methods at a range of temperatures from 0 to 60 ^{o}C. Enantioselectivity was evaluated by HPLC. Results show that polymers prepared at low temperature using photolytic homolysis of azobisnitriles significantly increased enantioselectivity. Sreenivasan [78] compared the use of γ-irradiation to thermal and photochemical methods. A major advantage of employing γ-irradiation negates the use of an additional initiator since the radiation provides a continuous source of radicals.

Reaction times for polymerisations are between 16 to 48 hrs depending on batch size and format. Piletsky *et al*. [79] imprinted a set of polymers with (-)-ephedrine using thermal and UV initiation. Significant differences in the enantioselective properties were observed in polymers prepared by either thermal or photo initiation methods. Polymerisation time also had a dramatic effect on polymer morphology. Increasing polymerisation time increases the rigidity of the polymer structure and facilitates the formation of imprinting cavities with a better defined shape. An increase in MIP selectivity upon increase in polymerisation time seems to be related to an increase in polymer rigidity. In order to demonstrate and prove this, the swelling of the polymers synthesised using thermo-initiation and a "weak" UV lamp (0.016 W/cm^2) was measured in chloroform. The experiments showed a proportional decrease in polymer swelling when the polymerisation time was increased represented in Figure 1.13.

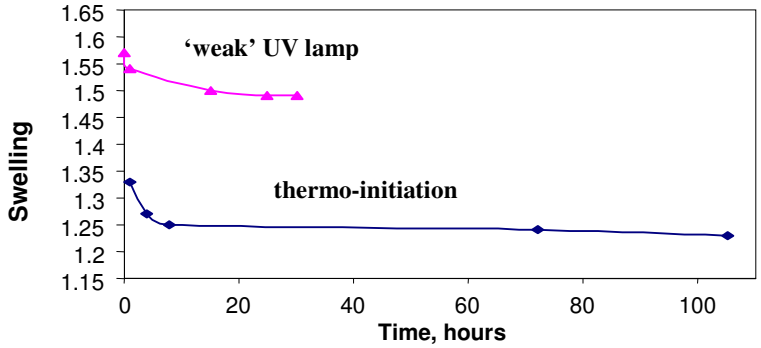

Figure 1.13 **Dependence of the polymer swelling in chloroform on the polymerisation time, adapted from reference [79].**

A second study was performed by Piletsky *et al* [74], to examine the influence of the initiator and the effects of different polymerisation conditions such as time, temperature and percentage initiator using a set of polymers imprinted with (-)-ephedrine.

The best recognition properties for MIPs were observed with lower quantities of initiator which generated lower temperatures during polymerisation. In conclusion MIPs should be synthesised for a long period of time with low concentration of initiator and low temperature. Employing a thermal initiator can jeopardise the efficiency of the imprinting process. As a result, initiators with low activation energy should be used, or initiation should be photolytically activated, particularly if the template is thermolabile.

1.5.6 Temperature

The formations of monomer-template complexes are equilibrium based and are thus sensitive to their thermal environment. The effect of polymerisation temperature on MIP performance has been the subject of several studies [74;77;79]. MIPs polymerised at lower temperatures form polymers with greater selectivity in contrast to polymers prepared at higher temperatures. To polymerise at colder temperatures it is necessary to use photochemical polymerisation.

Mosbach *et al*. [77] presented a study on enantioselectivity of L-phenylalanine anilide imprinted polymers. Initiation was conducted at 60, 40 and 0 ^{o}C. The results of this study showed that better selectivity was obtained at the lower temperatures as opposed to the identical polymers thermally polymerised. The reason for this has been postulated on the basis of Le Chatelier's principle, analysis of the thermodynamic parameters predicts that reduced temperatures will steer the pre-polymer complex toward complex formation, therefore increasing the number and perhaps, the quality of binding sites formed [80].

Piletsky *et al* [81] analysed the impact of polymerisation temperature on MIPs affinity and specificity in polymer performance by chromatographic experiments. A

computational approach to designing MIPs was used. Employing a virtual library of the most commonly used functional monomers, computer modelling was used to design a MIP specific for cyano-bacterial toxin microcystin-LR, a toxin from aquatic micro-organisms. Using the same monomer composition (MAA/EGDMA) a group of polymers was prepared by imprinting with (-)-ephedrine at six different temperatures, -30, -20, -10, 0, 20, and 80 ^{o}C. Experimental results [81] suggest that the polymer was able to 'memorise' the temperature used in the polymerisation process in a style similar to previously documented 'memory' effects for MIP systems for the template and polymerisation solvent. While lower initiation temperatures may assist MIP preparation in some cases, the opinion from the observations made, was that the internal temperature contained within the monolith was greater than the surroundings. This was due to the exothermal nature of the polymerisation process. The affinity of ephedrine enantiomers was examined at -10, 0, 10, 20, 30, 40, 50 and 55 ^{o}C. By decreasing the polymerisation temperature the polymer's affinity and specificity were significantly improved. Analysis of the thermodynamic parameters of the polymer-template interactions shows that the template binding by the synthesised MIP at low temperature in contrast to binding at higher temperature is most likely entropy driven. This results from a release of solvent molecules from the cavities and from the conformational changes in the polymer induced by the template. The computer modelled MIP was based on the formation of the pre-polymer complex and outperformed the control MAA/EGDMA MIP. Therefore, thermodynamic control is an important parameter in determining MIP performance when comparing the template binding by the synthesised MIP at low temperature in contrast to binding at higher temperature.

Lu *et al.* [75] performed a study investigating the influence of polymerisation temperature on the molecular recognition of imprinted polymers using 3-L-PheNHPh as the template molecule. It was suggested that a lower polymerisation temperature is advantageous to the stability of the template-functional monomer assemblies in the pre-polymerisation mixture. However, a higher polymerisation temperature was favourable for completeness of polymerisation reaction, which consequently improves the quality and quantity of MIPs recognition sites [75].

Osmani *et al*. [82] employed FTIR spectroscopy to observe the effect of temperature on the pre-polymerisation solution containing 2-apy (template) and MAA (functional monomer) at 22 ^{o}C and 0 ^{o}C. IR spectra showed that lower temperature led to more stabilised interactions of the hydrogen-bonded complexes.

1.5.7 Rational design of MIPs

1.5.7.1 Combinatorial approach

A method in which potentially suitable monomers can be detected without the problem of trial and error analyses is by use of a combinatorial approach. One of the first reports of the combinatorial approach to optimising the performance of MIPs was carried out by Takeuchi and co-workers [83]. A semi-automated approach was utilised to prepare a selection of MIPs by changing the proportions of functional monomers. Polymer synthesis and analysis employed programmable liquid-handling equipment to prepare small-scale MIPs (≈ 30 mg) on the bottom surface of glass vials. The polymers were analysed *in situ* by binding assays.

Similarly, Lanza and Sellergren independently developed and employed a semi-automated, scaled-down production of MIPs allowing *in situ* processing and evaluation of the synthesised materials to optimise the choice of functional monomer [84]. Six imprinted polymer formulations were prepared with different functional monomers. After photochemical irradiation of the vials, the resultant 'mini-MIPs' (≈ 55 mg) were subjected to two screening steps to determine MIP capacity.

Sellergren *et al*. synthesised triazine-targeted MIPs while Takeuchi targeted sulphonylurea herbicides. Both experiments have successfully employed the combinatorial screening for rapid evaluation and selection for the optimum composition of the MIP components.

The selection of the most favourable composition can be eased by the employment of the experimental design and multivariate analysis. Cedefur *et al*. [85] produced a library of molecularly imprinted polymers (MIPs) which were synthesised by radical bulk polymerisation using the β-lactam antibiotic penicillin G as the template.

Diversity of the library was obtained by combining various functionalised monomers and cross-linkers and by varying the stoichiometry of the concentration of the components in the pre-polymerisation mixtures. The 52 polymers produced were subsequently processed and evaluated. The MIP candidate, showing the highest selectivity for penicillin G, was prepared from MAA and TRIM as the functionalised monomer and cross-linker, respectively.

1.5.7.2 Computational approach

Batra and Shea [86] published a review reporting the combinatorial and computational approaches employed to optimise MIP formulation. The components of an imprinting system, i.e. monomers, solvents, initiators and templates were systematically changed on a small scale in an automated system. A large number of polymers can be quickly and effectively prepared in this manner. The 'Mini-MIPs' produced were investigated for their performance, and the optimum composition established.

Theoretical molecular modelling is a similar approach; the technique relies on the ability of computational calculations to predict potential monomers for an intended application. The process removes all practical aspects of MIP synthesis until the required formula is detected. The advantage of the strategy was demonstrated by Subrahmanyam *et al.* [87] who presented an improvement in recognition of creatinine over that of polymers prepared without modelling. MIPs created by the traditional methods using MAA were unable to differentiate between creatine and creatinine. A rational method for the selection of functional monomers was developed in order to improve the polymer's affinity for creatinine. Fluorescent measurements were employed and the computational designed MIP was capable of recognising creatine and creatinine by generating a fluorescent signal proportional to the analyte concentration. Nevertheless, the technique is based on calculations of the thermodynamic properties of the pre-polymer solution. The changing thermodynamic conditions which occur during polymerisation are not accounted for.

1.5.7.3 Study of pre-polymerisation interactions

The extent of self-assembly of functional monomer-template complexes pre-polymerisation mixtures has been characterised by UV spectroscopic analysis [88]. This analysis presents a method for determining the degree of template complexation in methacrylic acid-ethyleneglycol dimethacrylate cross-linked network copolymers and estimates the number of selective recognition sites in a polymer prepared with a known monomer/template composition. Another study was performed to identify the nature of template functional monomer interactions present in the molecular imprinting of bupivacaine in methacrylic acid–ethylene glycol dimethacrylate co-polymers using ^{1}H-NMR studies. It was shown that these electrostatic interactions survive the polymerisation process, up until the stage of gelation [89].

Osmani *et al*. performed a detailed investigation into the functional groups responsible for the formation of a non-covalent complex between 2-aminopyridine (template) and methacrylic acid (functional monomer) using FTIR spectroscopy and confirmed by ^{1}H NMR spectroscopic data [82]. From the FTIR results, a two-point cooperative interaction between 2-apy and MAA can be deduced as shown in Figure 1.14. FTIR and ^{1}H NMR data complement each other in identifying the stoichiometry of interaction by titrations giving a better understanding of the pre-polymerisation and prediction of MIP performance was gained by using FTIR.

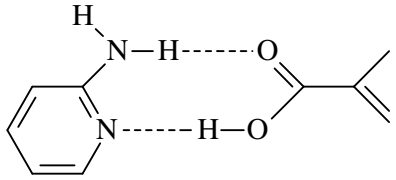

Figure 1.14 **Proposed interaction mechanism between 2-aminopyridine and methacrylic acid.**

1.6 Methods of polymerisation

The variety of requirements for different analytical applications has imposed restrictions on the choice of polymer system and the method of preparation employed, such as beads, films and nanoparticles.

Different polymerisation methods include:

- Monolith synthesis
- Suspension polymerisation in liquid perfluorocarbon producing spherical beads (beads vary between 5 – 50 μm) [90].
- Suspension polymerisation in mineral oil producing micron-sized spherical beads [91].
- Suspension polymerisation in a spiral micro-channel [92].
- Aqueous two-step swelling methods producing monodisperse micron-sized beads [93].
- Multi-step swelling producing micron-size particles [94].
- Precipitation polymerisation generating monodisperse sub-micron particles [95].
- Surface imprinting to produce submicrometer core-shell emulsion particles [96].
- MIP films grafted onto surfaces and particles [97;98].

However, while the production of polymeric beads is fairly straightforward it does not necessarily imply the techniques are readily transferable to industrial applications, due to high losses and inefficiencies in preparation. Also most of the above polymerisation techniques employ certain conditions which are not readily applicable to all molecular imprinting recipes [99]. For instance, a limitation in the fluorocarbon suspension method is that acetonitrile does not work favourably if used as a solvent. Conversely for the mineral oil suspension method only insoluble porogenic solvents such as acetonitrile are compatible. Aqueous phase methods, such as core-shell nanoparticles and two-step swelling work unsuccessfully with more polar templates. A further drawback to the production of bead formations is that the majority of imprinting techniques are based on non-covalent interactions. For example, template-monomer interactions based mainly on hydrogen-bonding may not be suitable as aqueous based bead formats. As a result methods of preparing beaded polymers which are amenable with the chemistry of the imprinting procedure have been investigated. Methods of creating novel MIP formats are an active research area.

In 2004, work by Pérez-Moral and Mayes [100] comprehensively compared different methods such as bulk, suspension, precipitation, two-step swelling and emulsion core-shell polymerisation for the preparation of MIPs. The morphology of the polymers produced by the different methods was characterised and assessed by scanning electron micrographs (SEM) and transmission electron micrographs (TEM) as shown in Figure 1.15. Suspension and two-step swelling polymers prepared were spherical in shape and 6 – 40 µm in diameter. The core-shell polymers produced were spherical and monodisperse with a diameter of 72 nm. For precipitation polymers, particles were 700 nm and slightly irregular in shape.

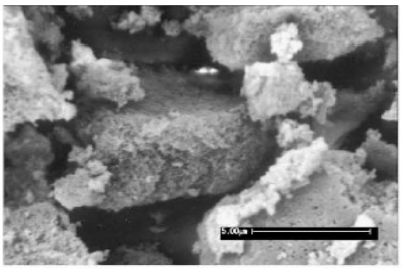

(a) Bulk Polymerisation (Scale 5 µm)

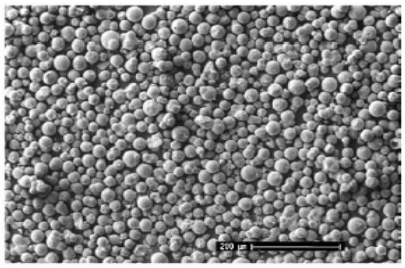

(b) Suspension Polymerisation (Scale 200 µm)

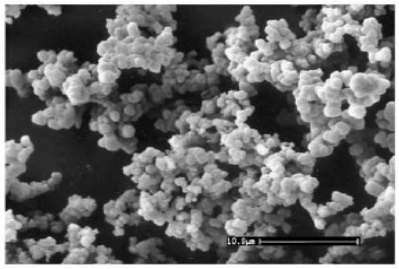

(c) Precipitation Polymerisation (Scale 10 µm)

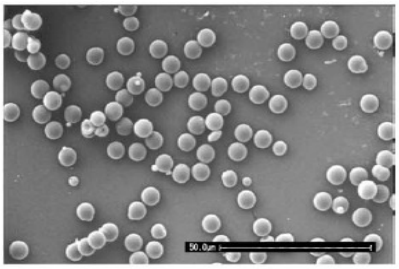

(d) 2-Step Swelling Polymerisation (Scale 50 µm)

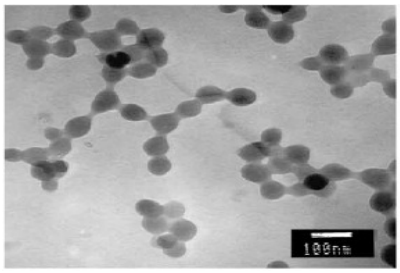

(e) Emulsion Core-Shell Polymerisation (Scale 100 nm)

Figure 1.15 **SEM and TEM micrographs of the polymers obtained by different polymerisation procedures [100].**

The following section describes the different types of polymerisation methods used for imprinting polymers.

1.6.1 Monolith synthesis

MIPs are prepared as monoliths using the bulk polymerisation technique, due to its ease and adaptability. As a result the material requires grinding and sieving to obtain particles generally in the 25 – 50 μm size range. Before the particles can be used the final step consists of sedimentation to remove fine particles. Even though bulk polymerisation is the most common method employed to prepare MIPs it is not, however, the most effective. Bulk polymerisation is a time consuming process, labour intensive and wasteful. During the grinding and sieving process a considerable amount of material is lost, with a moderate amount of usable material remaining (30 – 40 %) depending on the particle size required [101]. The particles produced by bulk polymerisation are irregular in shape and of variable geometry with heterogeneous binding sites, which are caused partly by the grinding and sieving process.

Irregular shaped particles can cause flow problems when packed into HPLC columns. In chromatographic applications the overall efficiency and separation is reduced as a result of the irregularity of the particle size produced as high back pressures are generated. This, therefore, makes this technology unattractive to industry being both wasteful and problematic for scale-up; hence beaded polymers are preferable in the majority of cases.

An interesting point to note is that improvements in chromatographic parameters may enhance the packing conditions of chromatographic columns resulting in improvement of the performance of irregularly shaped particles. In investigations reported by Tóth and colleagues [102] the performance of different particle types in HPLC were compared. It was proposed that particle geometry did not demonstrate a great influence on the binding performance. The inconsistency in comparison was attached to the chromatographic theory used for peak determination.

1.6.2 Imprinted bead formation

For many applications especially HPLC, capillary electrophoresis chromatography (CEC) and solid phase extraction (SPE), ground and sieved, irregularly shaped particles have limited scope for direct use. This has lead to the introduction of methods of preparing polymer formats and systems that are compatible to analytical applications.

Alternative strategies for generating imprinted bead particles have been developed to improve on the characteristics of the bulk monolith formations. MIPs with adjustable morphologies such as those prepared by suspension and precipitation polymerisation have been prepared and developed.

The potential advantages of imprinted beads include:

- Fast and efficient route to the production of imprinted polymer beads yielding usable particles for intended application.
- Uniform particle size distribution is obtained
- Spherical beads possess superior flow characteristics in chromatographic applications to those packed with crushed materials.
- Spherical particles of uniform geometry pack more efficiently in columns and have better flow properties which results in efficient separations

1.6.2.1 Suspension polymerisation in water

The alternative techniques used to address the problems associated with bulk polymerisation in order to generate MIP's in beaded form have been reviewed extensively in the literature [103-105].

Aqueous based suspension methods for production of spherical beads is a well-established and highly developed technology. Attempts have been made to use suspension techniques for producing beads from acrylic monomers which can contain imprinted molecules. In addition, because of the high solubility of acidic monomers in water, random co-polymerisation of monomers and cross-linkers is not achieved.

Suspension polymerisation using water as the continuous phase has been applied as a molecular imprinting technique to prepare a MIP for L-histidine (L-His) [106]. The histidine imprinted beads were prepared by the suspension polymerisation of *N*-methacryloyl-L-His-copper(II)-L-His [MAH-Cu(II)] and ethylene glycol dimethacrylate. After polymerisation, the template, L-His was removed from the resultant polymer, producing the MIP specific for L-His. Histidine imprinted beads were used for recognition of cytochrome *c* and ribonuclease A (surface histidine exposed proteins) and enantiomeric separation of D- and L-histidine by HPLC.

A MIP for benzo[a]pyrene (BAP) was synthesised by bulk polymerisation and aqueous micro-suspension polymerisation [107]. Three monomers and two cross-linkers were investigated. Non-covalent imprinting showed similar affinity for bulk and suspension polymerisation when DVB and 4-vpy were used as cross-linker and functional monomer. No obvious difference in the affinity was observed between polymers prepared by either bulk or suspension polymerisation. In this system, strong hydrophobic interactions could compensate for the weakening of electrostatic interactions.

MIPs were prepared using 4-aminopyridine (4-apy) as an imprinting molecule by aqueous suspension polymerisation [108]. The template, functional monomer (MAA), cross-linker (EDGMA), porogen (chloroform) and the initiator (AIBN) were mixed and sonicated to aid dissolution. Polyvinyl alcohol 400 was dissolved in water and used as the dispersing agent. The resultant polymeric microspheres had diameters between 8 – 25 μm (Figure 1.19) which were packed into stainless steel column (250mm × 4.6mm i.d.) for selective separation and quantitative determination of 4-apy and 2-aminopyridine (2-apy). The mobile phase was adjusted with different pH buffers and the influences on capacity factors were investigated. In mobile phase (pH > 5.5), 4-apy gave a larger retention factor than 2-apy. It is suggested that ionic and hydrophobic interactions could be used for the recognition of 4-apy on the MIP.

1.6.2.2 Suspension polymerisation in liquid perfluorocarbon

An approach to overcome the problem posed by the presence of water is the use of a non-aqueous media to disperse the droplets of imprinting mixture. The method introduced by Mayes and Mosbach in 1996 [90] utilised liquid perfluorocarbon as the dispersing phase producing spherical polymer beads. The liquid perfluorocarbons are a suitable inert phase for suspension polymerisation due to being largely immiscible with most organic compounds. However, the main problem encountered was the stabilisation of the suspension of the imprinting mixture in the fluorocarbon liquid. This required the design, synthesis and testing of a range of polymeric surfactants. In this approach an acrylate polymer was used to stabilise the suspension of initiator/crosslinker/imprint molecule/porogenic solvents and fluorinated surfactants.

By altering the amount of added stabilising polymer the size of the obtained beads could be varied between 5 and 50 μm. Mayes and Mosbach found that the optimum emulsion stability of an imprinting mixture in liquid perfluorocarbon was achieved using a copolymer of acryloyl PFA1 and acryloyl PEG2000MME (mole ratio 20:1, termed PPFS) [90].

A comprehensive chromatographic study of the polymer beads established that values and resolution factors were comparable to those achieved with traditional ground and sieved imprinted polymers. However, a major advantage of the small (5 μm) beaded packings was that it gave low back pressure and rapid diffusion which yielded good separation at high flow rates. The use of a liquid perfluorocarbon dispersant produced spherical particles which are polydisperse (mean diameter = 19.7 ± 0.6 μm). A custom-synthesised fluorinated polymer surfactant was required to stabilise the formation of droplets in the dispersant, liquid perfluorocarbon. The dispersant was convenient to handle as it is not toxic or flammable. The disadvantage of the process is the cost of the synthesis. However, most of the dispersant can be recycled at the end of the polymerisation and reused.

In 2006, Pérez-Moral and Mayes [109] proposed a new method for rapid synthesis of MIPs in a beaded form. The method utilised a liquid perfluorocarbon as the

dispersing phase for the synthesis of spherical particles. In this study, polymer beads were polymerised under UV light in solid phase extraction (SPE) cartridges. Four different functional monomers, (MAA, AA, HEMA and 2-VPY) were used for the imprinting of morphine and propranolol. This resulted in a direct and rapid synthesis method for the production of MIPs. Using this method, the time and speed of rotation of the micro-homogeniser controls the final diameter of the particles.

From Figure 1.16 it was shown that both procedures produced beads. Image (b) has broader size distribution in comparison to image (a). A possible reason could be due to droplet coalescence. However, an obvious advantage of the rapid synthesis method in SPE cartridges over the fluorocarbon suspension polymerisation in the conventional reactor is that the time required for the synthesis is considerably reduced. The polymers produced are directly obtained in particle bead formats, with no waste of polymer.

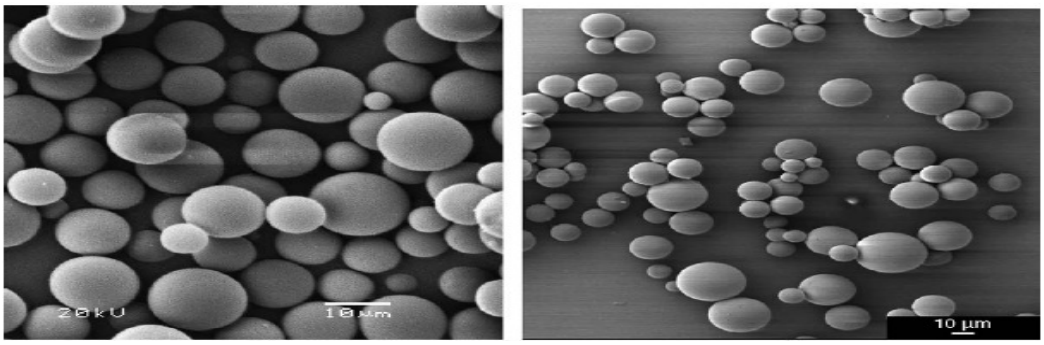

(a) **(b)**

Figure 1.16 **Scanning electron micrographs of particles made by (a) conventional suspension polymerisation in fluorocarbon using a stirred reactor and (b) rapid synthesis in an SPE cartridge [109].**

Fairhurst *et al*. [110] prepared similar particles using fluorocarbon suspension polymerisation. In this study a direct comparison of the performance of beads, ground monolithic imprinted polymers and silica-grafted MIPs was performed using HPLC and Turbulent Flow Chromatography (TFC) techniques.

Enantiomeric separations of β-blockers for the three different polymers were evaluated. In conclusion, the beaded material synthesised was the quickest, simplest

and most efficient to prepare. A degree of enantioseparation for the β-blockers was obtained also, with an overall improvement in peak shape in comparison to the ground monolithic polymers.

Suspension polymerisation in liquid perfluorocarbon suffers from some disadvantages: (i) it is expensive and (ii) it needs a fluorinated stabiliser to stabilise the droplets.

1.6.2.3 Suspension polymerisation in mineral oil

Another suspension polymerisation method in a non-aqueous medium was reported using mineral oil. The method was developed for the synthesis of spherical beads by Kempe and Kempe in 2004 [91;111]. The method described in the first communication [91] was used to synthesise propranolol imprinted polymer libraries with MAA as functional monomer and TRIM as cross-linker. MIP microspheres of 1 – 100 μm in diameter were obtained. In a typical procedure a dispersing phase was developed which consisted of the formation of droplets of pre-polymerisation solution directly in mineral oil by vigorous mixing followed by transformation of the droplets into solid spherical beads by photo-induced free-radical polymerisation. An advantage of this method to prepare MIP beads is that no detergents or stabilisers were required for the droplet formation.

Important to the success of the method is that the pre-polymerisation mixture consisting of template, functional monomer, cross-linker, free-radical initiator and porogen should all be insoluble in the mineral oil. This places a restriction on the choice of solvent to dissolve the components of the pre-polymerisation mixture. As acetonitrile is insoluble in mineral oil it is commonly employed as the solvent (porogen) of choice.

A second study [111] undertook a detailed investigation of the polymerisation procedure, identifying factors affecting the quality of the beads formed. Spherical MIP beads were compared and evaluated with irregularly shaped particles prepared by grinding and sieving of polymer monoliths. Both beads and irregularly shaped

particles showed similar characteristics in terms of elemental composition, surface area, pore diameter and pore volume. However, the binding capacity was higher for the beads than the irregularly shaped particles in most of the solvents and solvent mixtures investigated. This might be the result of a better accessibility of the recognition sites in the polymer network of the beads (i.e. the higher number of recognition sites). The key advantages of the described procedure lie in the attractive format of the MIPs produced and the simple production method. Throughout the synthesis, the suspension step was quick. However, suspension polymerisation in mineral oil produced a wide range of bead sizes which required extensive sieving to get a narrow size distribution.

1.6.2.4 Suspension polymerisation in a spiral micro-channel flow reactor

Both suspension polymerisation methods using liquid perfluorocarbon and mineral oil can generate MIPs in beaded form. However, neither method can reliably produce monodisperse MIP particles with controllable size for a wide range of different templates in a variety of porogenic solvents. A study to prepare uniform spherical MIP beads by controlled suspension polymerisation in a spiral micro-channel using mineral oil and perfluorocarbon liquid as continuous phases was reported by Zourab *et al*. [92]. Monodisperse droplets containing the monomers, template, initiator, and porogenic solvent were introduced into the micro-channel (Figure 1.17), and particles of uniform size were produced by subsequent UV polymerisation. This was a rapid process, without any loss of polymer materials. The droplet/particle size could be varied by changing the flow conditions in the micro-fluidic device. Beads from the micro-reactor were nearly monodisperse (Figure 1.18) with an average diameter of 24 µm compared to the beads from the conventional fluorocarbon suspension method and those from the mineral oil suspension method had larger bead size of > 30 µm. Figure 1.17 shows a schematic of the spiral micro-flow reactor showing the overall layout and the sample and oil inlet points.

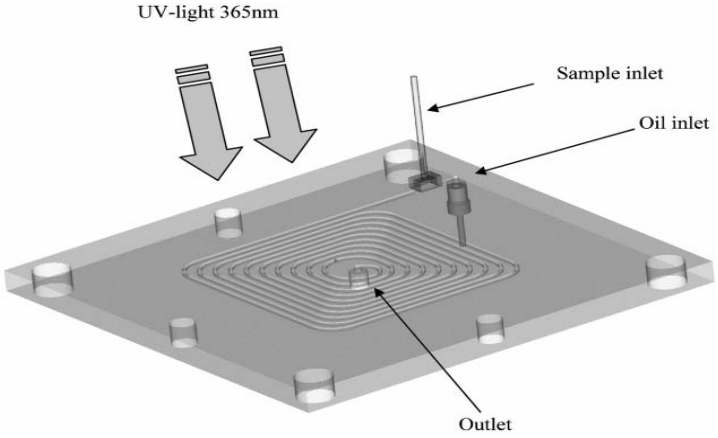

Figure 1.17 **Schematic of the spiral micro-flow reactor showing the overall layout and the sample and oil inlet points [92].**

The SEM images (Figure 1.18) show that the micro-reactor beads are near-monodisperse compared to the standard suspension methods.

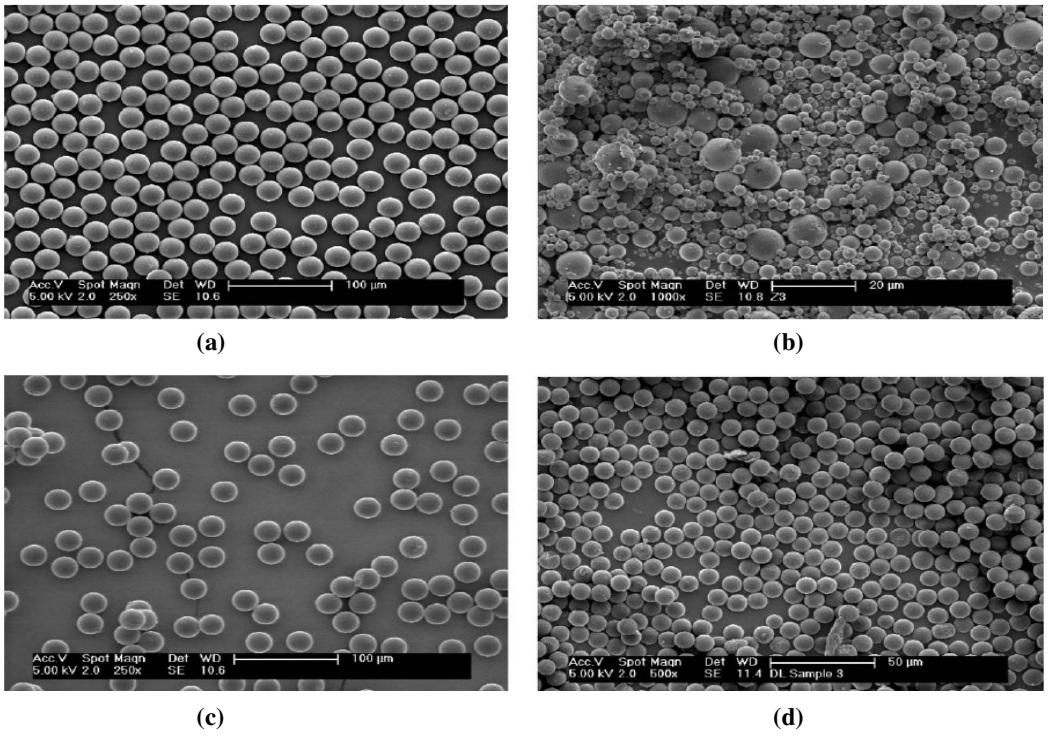

(a) **(b)**

(c) **(d)**

Figure 1.18 **Scanning electron micrographs (SEM) of typical beads produced in oil using (a) the micro-reactor and (b) dispersing device (standard suspension polymerisation in oil) and beads produced in liquid fluorocarbon using (c) the micro-reactor and (d) conventional suspension polymerisation (stirred reactor) [92].**

Binding values for the beads produced by conventional suspension methods and in the micro-reactor were found to have similar binding properties. The most important finding from the study is that the size distributions in suspension polymerisation can be reduced by careful reactor design and process optimisation.

1.6.2.5 Suspenion-Epitope polymerisation

To improve the problems associated with the molecular imprinting of large protein molecules, the 'epitope approach' has been reported in the literature [112]. Employing this technique, only a small sequence of amino acids contained in the larger protein, is used as a template molecule. When a protein, containing this specific amino acid sequence is brought together with the MIP prepared via the epitope approach, the entire protein can be recognised and bound. The 'epitope approach' is a promising method for the separation of recombinant proteins.

Kotrotsiou *et al*. [113] synthesised MIP microparticles produced by suspension and inverse suspension (i.e. oil in water and water in oil) methods using the 'epitope approach'. The hydrophobic (i.e., Boc-Trp-Trp) or hydrophilic (i.e., His-Phe) oligo-peptides were employed as templates. The suspension polymerisation method was employed to produce MIPs with specificity towards the hydrophobic tripeptide of tryptophan. MIPs specific to the hydrophilic His-Phe dipeptide were prepared by the inverse suspension method. Both types of suspension polymerisation methods led to the formation of microparticles. Evaluation of the microparticles towards the template molecules by rebinding experiments demonstrated good specificity and selectivity in both cases [113].

1.6.2.6 Precipitation polymerisation

Micro-spherical particles with more uniform size can be obtained by the method of precipitation polymerisation. The technique was first reported by Ye *et al*. [95;114]. Precipitation polymerisation is carried out in experimental conditions that are similar to those of bulk polymerisation mixture (template, monomer and cross-linker) but

using 2 to 10 times the amount of porogen. The particles formed were placed in a Soxhlet extraction system for template removal, without the need for grinding and sieving. In a cross-linking co-polymerisation, increasing the amount of solvent and cross-linker causes the growing polymer chain from occupying the entire reactor volume, and therefore a dispersion of micro-spherical particles in the solvent is formed. Further dilution leads to a reduction in the size of the micro-spheres. The imprinted polymers can be created by varying composition during precipitation polymerisation controls morphologies, i.e. micro- and nanospheres [115]. The precipitation method can deliver micro-spheres bearing imprinted binding sites similar to the traditional grinding and sieving method, rapidly and in good yield but with improved binding kinetics. The method is generally applicable to a large variety of target molecules. While the reaction solvent influences micro-spheres, the presence of a print molecule, the functional monomer and cross-linker also affects the particle size of the obtained micro-spheres. The composition of the imprinting solvent is very important in order to control the phase separation to yield uniform MIP micro-spheres. Therefore the choice of reaction solvent is very significant [115].

Wang *et al*. [116] prepared mono-dispersed theophylline-imprinted and non-imprinted spherical, polymer particles of about 5 µm in diameter using MAA as functional monomer. Mono-dispersed microspheres resulted from the copolymerisation of DVB in a mixture of acetonitrile and toluene. The MIPs prepared were used for HPLC separation of theophylline.

Turiel *et al*. [117] prepared polymer microspheres with average particle diameter of 3.5 µm. The imprinted microspheres were packed directly into columns for HPLC-fluorescence (HPLC-F) determination of the fungicide thiabendazole (TBZ) in fruit extracts. Castell *et al*. [118] prepared monodisperse propranolol imprinted polymer microspheres [*p*(divinylbenzene-*co*-methacrylic acid)] by precipitation polymerisations. The mean particle diameter measured was found to be 3.6 µm.

Results from a study by Wei *et al*. [119] for comparison of the specific binding properties of imprinted polymers for 17β-estradiol prepared by different synthetic routes yielded particulates produced from bulk polymers, microspheres, and sub-microspheres. Microspheres prepared by precipitation polymerisation showed

excellent rebinding properties at equilibrium binding conditions, and mean particle diameter of 3 µm. Sambe *et al*. [120] prepared uniformly-sized MIPs for (*S*)-nicotine using MAA or TFMAA as a functional monomer and DVB as a cross-linker in a mixture of toluene and acetonitrile. The mono-dispersed micro-spheres were about 4 µm in diameter. Enantioseparation of nicotine was achieved using the (*S*)-nicotine-imprinted MAA-co-DVB polymers.

Yoshimatsu *et al*. [121] have studied the effect of a cross-linking monomer on the final size of MIPs by varying the ratio of DVB and TRIM. Particle size of the MIP beads obtained ranged from 130 nm to 2.4 µm by varying the ratio of two cross-linking monomers, while maintaining excellent recognition properties.

Mono-dispersed MIPs were prepared by precipitation polymerisation using other cross-linkers and polymerisation media. Tamayo *et al*. [122] prepared MIPs for fenuron with EGDMA as a cross-linker and toluene as the polymerisation medium, with the mean particle diameter of ca. 1 µm. Spherical imprinted polymers were prepared in the presence of sulfasalzine as a template with EGDMA as cross-linker and a mixture of toluene and acetonitrile as solvent [123]. The diameters of the beads were 4 µm for sulfasalzine. The release rate of the bioactive agent at different pHs was studied; the beads are able to re-bind the bioactive agent and to release it when there is a substantial change of pH (from 1.0 to 6.8).

The advantages of the precipitation polymerisation method include quick delivery of high quality imprinted polymers with minimal optimisation in a one-step process and it is surfactant-free.

1.6.2.7 Dispersion polymerisation

The production of imprinted particles by dispersion is the least common method for generating MIP bead formats. The monomer and not the polymer is soluble in the dispersion medium with the formation of well-defined spherical beads. Dispersion polymerisation is also defined as a ‘modified precipitation polymerisation’ [124].

Büyüktiryaki *et al*. [125] produced methylmercury-imprinted beads by the dispersion polymerisation technique with use of a methylmercury-MAC complex monomer and EDGMA. This technique proved successful for the generation of methylmercury imprinted polymeric micro-beads that can effectively be used for the removal of the methyl mercury ions from aqueous solutions by solid-phase extraction.

In the mid 1990's Sellergren demonstrated the dispersion polymerisation technique by preparing a MIP for pentamidine using MAA as functional monomer, EGDMA as cross-linker and 2-propanol-water as porogen. This resulted in the in situ formation of micro-porous beads imprinted with pentamidine in the absence of a stabiliser in the chromatographic column [124;126]. It was found that pentamidine was more strongly bound on the MIP for pentamidine than that for benzamide, the reference polymer. By changing the mobile phase pH, the selective enrichment of pentamidine in urine samples was accomplished with the absorption and desorption of pentamidine [124]. Due to the polar nature of the dispersion phase only templates capable of strongly interacting with functional monomers were open to imprinting.

More recently, applications of the dispersion technique have been based on the imprinting and recognition of ions. The ability of Cu (II) imprinted beads to selectively recognise and bind Cu (II) ions from a metal solution was demonstrated by Say *et al*. [127]. In an accompanying study the dispersion method was also applied to the imprinting of the cyanide ion [128]. The selective binding of the cyanide ion could be determined even in the presence of a number of similar ions in aqueous solution.

The main difference between bulk and dispersion/precipitation polymerisation methods is the volume of polymerisation medium used. Larger volumes of polymerisation medium are required in dispersion/precipitation techniques.

1.6.2.8 Multi-step swelling polymerisation

Multi-step swelling polymerisation used in molecular imprinting was first described by Hosoya *et al*. [129]. A series of uniformly sized diaminonaphthalene imprinted

particle beads were prepared in an aqueous two step swelling and polymerisation method for HPLC. The process was based on the non-aqueous technique employed by Matsui *et al*. [130] for the formation of imprinted rod materials. The ability of applying the method in aqueous media was shown by the selective recognition of templates in both procedures.

Monodisperse particles were produced by the step-wise swelling of a polystyrene seed particle with a mixture of fresh monomer and an activating solvent (dibutylphthalate). In the second stage, non cross-linked seed particles prepared by suspension polymerisation can be swollen with porogen, template, functional monomer and cross-linker for the preparation of uniform-sized MIP particles by photo or thermal polymerisation. A typical multi-step swelling and polymerisation method is shown in Figure 1.19.

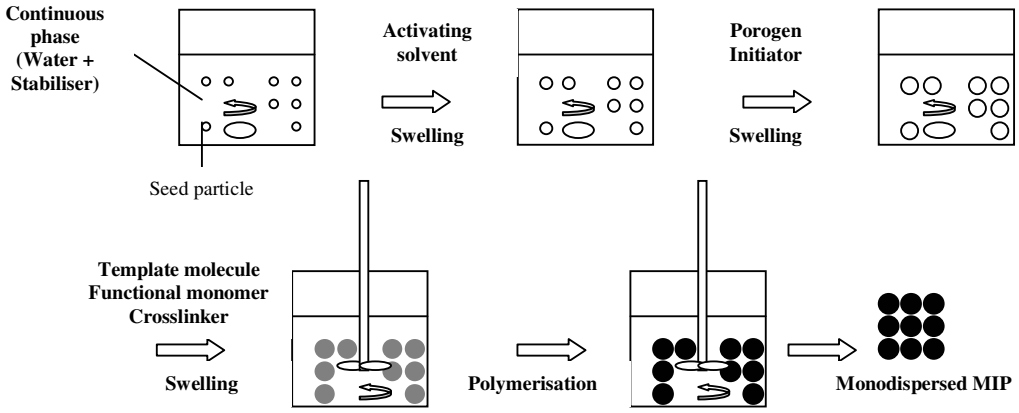

Figure 1.19 **Preparation method of mono-dispersed MIP by multi-swelling and polymerisation, adapted from reference [131].**

Mono-dispersed MIPs are easy to prepare. However, a disadvantage of the method is that template molecule and functional monomer interactions could be disrupted as water is used as a continuous phase.

The groups of Hosoya and Haginaka [55;129] have utilised the multi-step swelling technique for the imprinting and application of polymeric beads with different templates and functional monomers. MIPs for β-estradiol and bisphenol A (BPA)

[132], catechin gallate [94] were prepared using 4-vpy and 2-vpy as functional monomers respectively. A hydro-organic mobile phase (for example a mixture of phosphate buffer and organic modifier such as acetonitrile, ethanol or 2-propanol as an eluent) was employed for the specific recognition of each template molecule. Hydrogen bonding interactions between a template molecule and pyridinyl groups on the polymer mainly worked for its template recognition and its shape recognition. Furthermore, MIPs for other template molecules were prepared and evaluated using a hydro-organic mobile phase. Cinchona alkaloids [133] and atropine [134] were prepared using MAA or acrylamide as a functional monomer. Ionic and hydrophobic interactions worked for template recognition in both studies.

Additionally, MIPs for chiral templates such as (*S*)-naproxen [55;135], (*S*)-ibuprofen [136], (*S*)-propranolol [137], *d*-chlorpheniramine (*d*-CP) [138], *d*-brompheniramine (*d*-BP) [139;140], *N*-protected L-amino acids [141] and (-)-ephedrine [142] were prepared by multi-step swelling and polymerisation. A hydro-organic mobile phase or organic mobile phase was used to get baseline or near baseline resolution of enantiomers. A high degree of chiral discrimination was exhibited by ibuprofen and partial resolution of structural analogues was attained [136]. Chromatographic conditions were optimised by elevating the column temperature and reducing the flow rates applied to naproxen imprinted beads [55].

Multi-step swelling and polymerisation was also applied to the imprinting of the β-blocker propranolol [143]. The imprinted beads demonstrated ability to enantioselectively discriminate between enantiomers of structurally related compounds. This strategy employed for (*S*)-propranolol was then applied for imprinting of the chiral template *d*-CP [138] which was optimised in a cross-selectivity study [139]. The retentive and enantioselective properties of *d*-CP, *d*-BP and their structurally related compounds using the MIPs were studied using hydro-organic mobile phases. Ion exchange and hydrophobic interactions work mostly for the retention and enantioseparation of *d*-CP and *d*-BP on both MAA-*co*-EGDMA and TFMAA-*co*-EDMA polymers in hydro-organic mobile phases. MIPs gave the highest enantioselectivity for the template molecule. In addition, MIPs for *d*-CP and *d*-BP gave very similar enantioselectivity and resolution for chlorpheniramine (CP) and

brompheniramine (BP). Therefore, CP or BP could be used as a structural analogue to each other to prevent the leakage of a template molecule.

1.6.2.9 Core-shell emulsion polymerisation

Core-shell particles are formed in a two-stage process from a seed latex. This is in contrast to the multi-stage swelling polymerisation described above. The seed particle which may be cross-linked is surrounded by a shell of new polymer in a second emulsion polymerisation, which allows the imprinted sites to be positioned near or at the surface of the beads. Pérez *et al*. [96] prepared sub-micrometer surface-imprinted particles for cholesterol by a two-stage aqueous emulsion polymerisation with a poly(divinylbenzene) shell over a cross-linked poly(styrene) core. Particles were produced with hydrophobic recognition cavities in the surface of a hydrophilic bead by using a specially designed template-surfactant. Both a template surfactant (TS) pyridinium 12-(cholesteryloxycarbonyloxy)dodecanesulfate and a polymerisable surfactant (PS) (pyridinium 12-(4-vinylbenzyloxycarbonyl)dodecanesulfate were synthesised in the second polymerisation step and used in the preparation of surface-imprinted core-shell particles. A distinguishing aspect of this type of surface imprinting is that the template is positioned at a predefined distance from the polymer surface at the same time stabilising the particles during the second polymerisation step.

1.7 Polymer evaluation and characterisation

The molecular recognition abilities of imprinted polymers form the basis for the applicability of MIPs in chromatography, sensors and catalysis [144]. The following sections review the use of different characterisation techniques for the verification of the imprinting process.

1.7.1 Binding sites and their distribution

The analysis of the binding properties of MIPs is based on methods developed for characterising antibodies and other biological receptors. The most important

characteristic of MIPs is their binding properties. Monomer-template complex formation in non-covalent imprinting is equilibrium dependent. Consequently, imprinting yields a broad distribution of binding sites with a range of binding affinities. A heterogeneous system contains binding sites of varying affinity and selectivity as illustrated in Figure 1.20 and is more common in non-covalent systems [29].

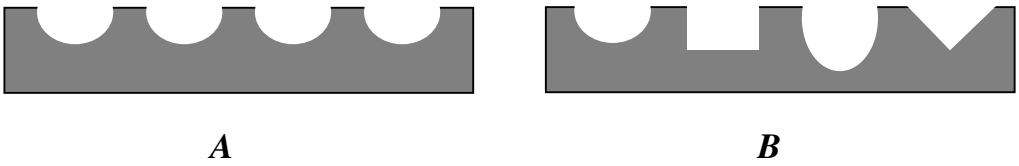

Figure 1.20 ***A;*** **homogeneous binding sites and** ***B*****; heterogeneous binding sites, adapted from reference [29].**

As a result of this there is a limitation in practical and economical terms on imprinted material. Batch rebinding studies are a characterisation method providing the first insight into the binding properties of a specific MIP. Fitting of binding isotherms to a Langmuir model [39] has generally been preformed by a graphical method such as Scatchard plots or using curve-fitting software to analyse the isotherms. Typical characterisation studies are based on a homogeneous distribution of binding sites possessing uniform affinity and distribution. Thus, two binding affinity constants (*N* and *K*) are obtained from the fitting parameters. The variables *N* and *K* correspond to the number of binding sites and the association constant of the binding sites, respectively. These types of binding behaviour are seen in structurally homogeneous systems such as enzymes and antibodies [144].

However, the binding sites in MIPs vary greatly in size, shape and rigidity. MIPs are commonly characterised by low average binding affinities and a high degree of binding site heterogeneity [145]. The high degree of binding site heterogeneity is particularly important for MIP applications in separation techniques, as it is the main cause of chromatographic peak asymmetry and peak tailing [146]. In addition, binding site heterogeneity is among the main restrictions responsible for cross-reactivity in sensing applications [147]. However, the Langmuir isotherm (LI) does not provide an accurate description of the binding behaviour of non-covalent

imprinted MIPs which has led to the investigation of other binding models such as the Freundlich (FI) [29] and Langmuir-Freundlich (L-FI) [148] isotherms. These isotherms accurately reflect the unimodal distribution of heterogeneous binding sites in MIPs, and can measure site heterogeneity. Umpleby *et al.* also proposed the affinity spectrum as a general description of the distribution of binding site affinity in MIPs [149]. Fitting of experimental isotherms to the Freundlich model provided excellent agreement for MIPs against L-phenylalanine anilide [150], aminoantipyrine [151] and haemoglobin [152]. Furthermore, it was shown that this model is applicable to isotherms measured at low concentration or sub-saturation levels [153]. Each of these models (LI, FI and L-FI) has their advantages and disadvantages, which were examined in detail in review papers in 2007 by García-Calzón and Díaz García [154] and in 2004 by Umpleby [29].

Figure 1.21 illustrates the proposed broad affinity distribution of imprinted systems and the area which each of the mentioned binding models represents. *N* is the number of binding sites and *K* is the binding energy.

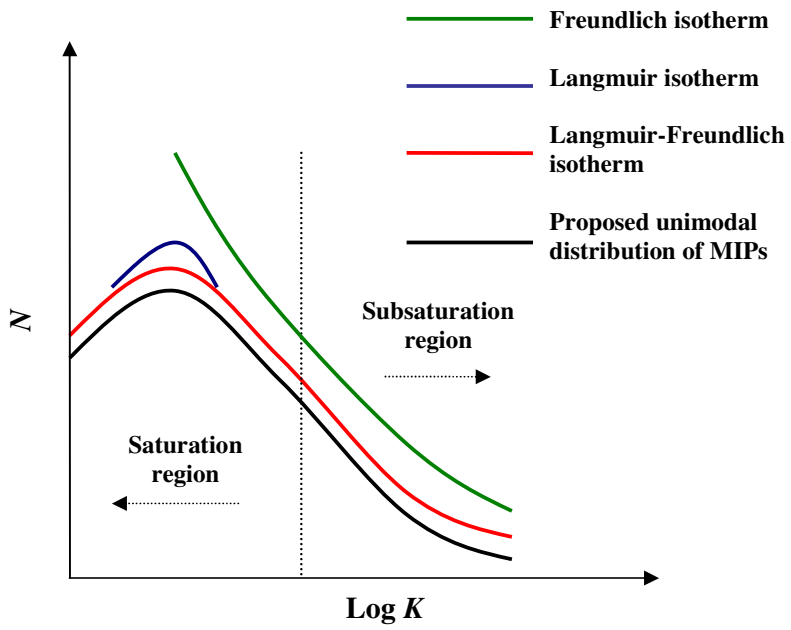

Figure 1.21 **The proposed broad affinity distribution of imprinted systems and the area which each of the binding models represents (Note: This figure is extracted from data presented in reference [29]).**

1.7.1.1 Discrete distribution models: Langmuir isotherm

The simplest and most frequently used model in adsorption studies is the Langmuir isotherm (LI) as shown in Equation 1.1. Haupt *et al*. [45] used the LI to determine the affinity of a series of theophylline imprinted polymers. It is then assumed that once a template molecule occupies a site, no further adsorption can take place at that site. Therefore, in theory, a saturation value is reached beyond which no further sorption can take place. This value allows the calculation of the surface binding capacity.

The Langmuir model can be expressed as:

$$B = \frac{N_t\, aF}{1 + aF} \qquad \textbf{Equation 1.1}$$

Where; B and F are the concentration of template bound and free in solution after equilibration,

N_t is the total number of binding sites,

a is related to the average binding affinity K_o via $K_o = a^{1/m}$,

m is the heterogeneity index. The value of which varies from zero to one (with one being homogeneous and values approaching zero being increasingly heterogeneous).

By plotting ($1/B$) versus ($1/F$) the LI can express the experimental data in linear form, where a is the y-intercept/slope (and is related to the binding affinity) and N_t is 1/y-intercept [154].

1.7.1.2 Continuous distribution models: Freundlich isotherm

The Freundlich isotherm (FI) is the most easily applied of the three models as it consists of two-fitting parameters, a and m, shown in Equation 1.2. The empirical form of the FI [155] has been widely used for modelling heterogeneous surfaces. The FI describes the relationship of the concentration of bound (B) and free (F) guest molecules as:

$$B = aF^{\,m} \qquad \textbf{Equation 1.2}$$

The two fitting parameters a and m, shown in Equation 1.2, yield a measure of physical binding parameters, where a is related to the median association constant $K_o = a^{1/m}$, and the second fitting parameter m is the heterogeneity index. The value can vary from zero to one, with one being homogeneous and values approaching zero being increasingly heterogeneous.

To determine the suitability of the FI in assessing the binding behaviour of MIPs the experimental binding isotherm is plotted in log B versus log F format.

However, the FI is only accurate over a specific concentration range [153]. The FI cannot yield the global binding parameters such as the total number of binding sites (N_t) or the overall average affinity constant (K_o) [149]. Accurate measurements of these values in heterogeneous systems as well as the heterogeneity index requires hybrid models that can accomodate both saturation and sub-saturation regions of a binding isotherm such as the Langmuir-Freundlich (L-FI) isotherm.

1.7.1.3 Langmuir-Freundlich isotherm

The L-FI isotherm has been successful in modelling the adsorption behaviour of many heterogeneous systems [148]. The model was introduced for MIPs by the groups of Umpleby *et al*. [149]. As the name implies, the L-FI isotherm is a composite of the Langmuir and Freundlich isotherms and has previously been shown to model the binding behaviour of MIPs more accurately than the LI or the FI individually.

Unlike the LI and the FI, the L-FI is capable of modelling the binding characteristics of imprinted polymers at both high and low concentrations for heterogeneous and homogeneous systems [154]. L-FI describes a specific relationship between the equilibrium concentration of bound (B) and free (F) guest in heterogeneous systems (Equation 1.3) with three fitting coefficients: N_t, a and m.

$$B = \frac{N_t a F^{m}}{1 + aF^{m}} \qquad \textbf{Equation 1.3}$$

Although a linear analysis is not possible for a three parameter isotherm, the experimental data is fitted to the L-FI (log B vs log F) following the method of Umpleby *et al.* [148]. The *Solver* function of Microsoft Excel optimises the fitting parameters N_t, a and m so as to maximise the correlation coefficient [148], R^2 (i.e. the difference between the experimental model and the model-predicted bound concentrations).

The L-FI has been successful in modelling the adsorption behaviour of many heterogeneous systems. The L-FI can reduce to either L or F isotherms at its limits. For example, when $m = 1$, the L-FI (Equation 1.3) reduces to the LI (Equation 1.1) in which a corresponds directly to the binding affinity (K). Alternatively, as either F or a approaches 0, the L-FI reduces to the FI (Equation 1.2). The L-FI reduces for all systems to the Freundlich at the low concentrations.

Once the binding parameters have been determined from L-FI an affinity distribution can be calculated giving the number of binding sites with respect to association constant for those sites [156].

1.7.1.4 Affinity distribution analysis

Several models have been proposed to describe the heterogeneity of binding sites in MIPs. Shimizu and co-workers investigated the affinity distribution (AD) analysis which makes use of analytical approximations made by the LI, FI and LF-I models [148]. From the literature, five MIPs, both covalent and non-covalent were assessed by applying the three different models to each system. Three of the systems had been assessed in the saturation and sub-saturation concentration regions. Applying all three models to each individual experimental isotherm, it was found that the LF-I was found to have a better fit compared to the LI or FI due to the fact that it is a three parameter model in contrast to a two parameter LI or FI model. A more important reason is that the LF-I is physically more appropriate, due to the proposed heterogeneity in MIPs.

Affinity distribution (AD) spectra can be generated by fitting the L-FI experimental binding data into Equation 1.4, using the Microsoft Excel Solver function [148]. The number of binding sites (N_t) are plotted with a particular association constant (K_i), by substituting the L-FI fitting parameters N_t, a and m into Equation 1.4.

$$N_t = \frac{\left[N_t am \left(\frac{1}{K_i} \right)^m \left(1 + 2a \left(\frac{1}{K_i} \right)^m + a^2 \left(\frac{1}{K_i} \right)^{2m} + 4a \left(\frac{1}{K_i} \right)^m m^2 - a^2 \left(\frac{1}{K_i} \right)^{2m} m^2 - m^2 \right) \right]}{1 + a \left(\left(\frac{1}{K_i} \right)^m \right)^4}$$

Equation 1.4

Where; K_i = log (1/(F/1000)) and F is the concentration of free analyte in solution post-equilibrium.

A more informative depiction of the binding parameters is provided by the (AD) approach, as it plots a distribution of the binding sites and their related association constants in units of log K, in comparison to other methods commonly used to characterise MIPs (e.g. Scatchard plots).

Chemical post-modification of polymers has emerged as a technique to get round the problem of heterogeneity. Shimizu *et al.* [157] successfully applied this technique to improve the binding characteristics of an ethyl adenine-9-acetate (EA9A) selective polymer. This was achieved by preferentially eliminating the low-affinity binding sites by esterification with diazomethane or phenyldiazomethane. Selectivity in the esterification reaction was achieved using a guest molecule as an *in situ* protecting group that preferentially shields the high-affinity sites and leaves the low affinity sites exposed toward the reaction. Affinity distribution analysis suggested a higher percentage of high affinity binding sites when the polymers had been subjected to an esterification reaction.

1.7.1.5 Trends in binding data in MIP materials

In a typical imprinted polymer, there is usually a variety of binding sites with different affinities for the analyte ranging from high dissociation constants in the mM range to low dissociation constants in the μM – mM range. However, the binding properties in MIPs are generally measured only in a narrow concentration range, which corresponds to only a subset of the sites in MIPs. For instance, polymers that have strong interactions between monomer and template or have been covalently imprinted yield a more homogeneous distribution and are characterised by the LI. Whitcombe *et al*. synthesised a covalently imprinted polymer which was modelled by the LI [39]. In the literature the FI has been shown to be useful in modelling the binding properties of non-covalently imprinted polymers, with an acceptable fit (R^2 = 0.97 – 0.99) [148;153;157]. Wei and Mizaikoff used the FI fitting parameters to assess the binding behaviour of imprinted polymers for 17 β-estradiol prepared by different synthetic routes (bulk polymers, microspheres and sub-micropheres) [119]. The goodness of fit, R^2 value for the bulk was 0.969 and 0.973 for the imprinted microspheres. The binding affinity constants for all three formats were compared. The sub-microspheres provided the lower median binding affinity constant ($2.5 \times 10^{-3} \pm 4.5 \times 10^{-4}$ mM^{-1}) in comparison to the bulk polymers ($9.0 \times 10^{-3} \pm 5.3 \times 10^{-4}$ mM^{-1}), and the microspheres ($1.3 \times 10^{-2} \pm 4.8 \times 10^{-4}$ mM^{-1}). From the calculation of binding site distribution the number of low binding sites (K = 0.028 mM) is 20 times higher than the number of high binding sites (K = 2.13 mM) for bulk MIPs. It was concluded there was a dominating amount of low affinity binding sites. As equal amounts of polymer and solvent were employed for the binding studies, it can be included that the binding site distributions for all three MIP formats are comparable [119]. The FI is able to accurately measure the heterogeneity of a MIP, although it is usually restricted to the tailing region of the affinity distribution (AD) spectra. Therefore, the FI does not provide enough information to find a reliable solution for AD. This is because a suitable measurement of the total number of binding sites would be required. Extra physical measurements are needed to improve the AD found.

Holland *et al*. [158] prepared a series of 2-apy non-covalent MIPs by bulk polymerisation with varying amounts of cross-linker (EGDMA) and characterised the MIPs by utilising LI, FI, L-FI and affinity distribution (AD) spectra. The L-FI

isotherm was judged to be the most appropriate isotherm for analysis in the concentration range used. This was as a result of improved linear regression values obtained when it was fit to the experimental data. The obtained R^2 values for each MIP composition prepared with varying amounts of EDGMA (40 – 10 (mmol)), ranged from 0.892 – 0.921. Furthermore, the L-FI isotherm was sensitive to changes in the binding site energies with changes in composition. The total number of binding sites increased with decreasing EGDMA, N_t: 88.6 – 281.9. This trend was expected due to increasing flexibility which allowed intrinsic sites of the polymer to become occupied; this resulted in an overall higher capacity of the polymers. Correspondingly the average binding energy of the sites decreased with decreasing EGDMA amounts. The MIP prepared with 40 (mmol) of EGDMA is characterised by a higher binding affinity constant (K_o = 0.94 mM^{-1}) in comparison to the MIP prepared with 10 (mmol) of EGDMA, (K_o = 0.46 mM^{-1}). The reduction in binding energy may be attributed to the presence of less defined binding sites in the MIP prepared with lower amounts of cross-linker. This emphasises the importance of the cross-linker in maintaining the conformity of the binding sites during polymerisation. AD spectra were found to be an excellent method of displaying the relationship between the number of binding sites and their associated energy [158].

1.7.2 Nitrogen sorption analysis

Although the binding and selectivity of imprinted polymers in chromatographic or rebinding studies are not reliant on macroporosity, the applications of MIPs in drug delivery could possibly depend on mass-transfer kinetics related to porosity. Therefore, direct physical characterisation methods for MIPs such as surface area and porosity measurements are required. The morphology of the imprinted polymer can be investigated employing nitrogen sorption porosimetry. The technique involves a fixed mass of dry polymer being exposed to nitrogen gas at a series of fixed pressures. As the pressure increases the gas condenses and fills the pores. The amount of gas is measured as a function of pressure. Isotherms can be constructed (Figure 1.22) from which information on the specific pore surface area (m^2 g^{-1}), specific pore volume (cm^3 g^{-1}), average pore diameter and pore size distribution can be obtained [159].

1.7.2.1 Gas isotherm analysis

Nitrogen sorption porosimetry is a particularly useful method for analysing in detail medium-sized (meso-) and small (micro-) pores [159]. IUPAC [160] classifies the size of pores as macropores for pore diameters greater than 50 nm (typical values for surface area of imprinted polymers are in the range 100 – 400 $m^2 g^{-1}$), mesopores for the pore range 2 to 50 nm and micropores for pore diameters less than 2 nm.
There are 6 types of adsorption isotherms shown in Figure 1.22, which can be used to gain information on porosity [160]:

- Type I - the most common isotherm encountered, which is characteristic of materials having extremely small pores.
- Type II - are indicative of non-porous or macroporous materials. The inflection point or knee of the isotherm is called Point B, this point indicates the stage at which monolayer coverage is complete and multilayer adsorption begins.
- Type III - describe adsorption on non-porous or macroporous adsorbent with weak adsorbate-adsorbent interactions, it is the least encountered isotherm.
- Type IV - are typical for mesoporous materials. The most characteristic feature of the type IV isotherm is the occurrence of hysteresis loops. Hysteresis loops arise from different adsorption/desorption mechanisms. The initial part of the Type IV can be attributed to monolayer-multilayer adsorption as in the case of Type II [160].
- Type V - represent pore condensation and hysteresis (pores present in the mesopore range).
- Type VI - is a special case, which represents stepwise multilayer adsorption on a uniform, non-porous surface, it is rarely encountered.

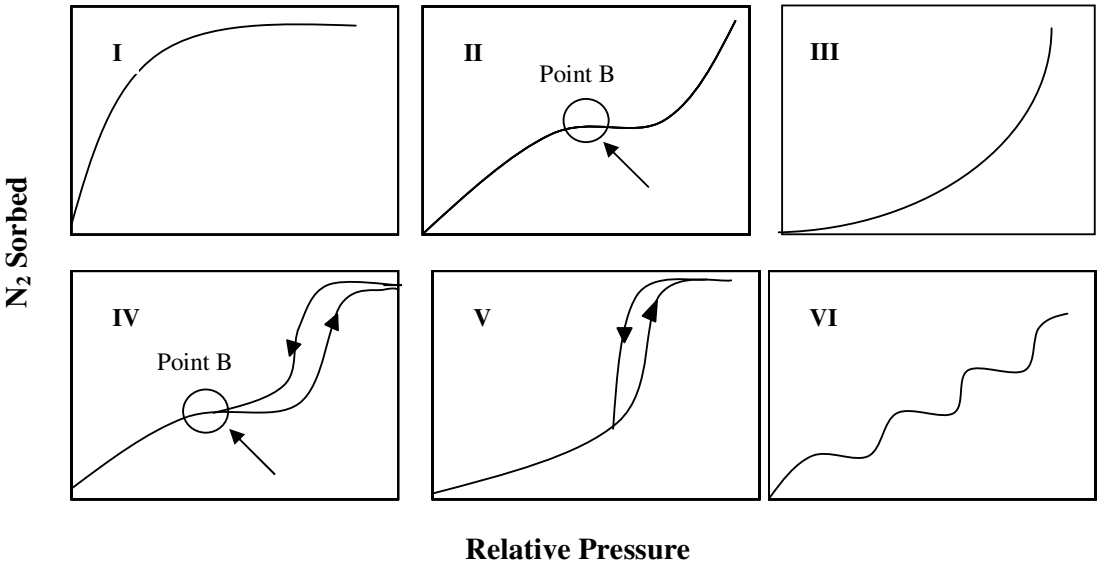

Figure 1.22 **The IUPAC classification for adsorption isotherms (Types I-VI) with the x-axis representing the relative pressure and the y-axis denoting the amount of gas adsorbed, adapted from reference [160].**

The surface area of the polymers can be derived from the adsorption isotherm, in the P/P_o range < 0.3 for a six point plot, using Brunauer, Emmett and Teller (BET) analysis [161;162]. An expression for the BET equation is derived and written in the linear form [160].

Specific pore volume ($cm^3 g^{-1}$), average pore diameter and pore size distribution of the polymers were calculated according to the Barrett, Joyner and Halden (BJH) method [161]. Pore radii at each P/P_o point were determined using the Kelvin equation [160]. The application of the Kelvin equation is corrected for multilayer thickness on the pore walls using the Halsey equation [160]. Differential pore volumes were generated by plotting dV/dD versus D (V is the pore volume and D is the pore diameter) [161]. Where t is the thickness of the adsorbed liquid (monolayer coverage is an assumption), and 3.54 and 5.00 are empirical values [162].

In general, molecularly imprinted polymers typically reveal Type IV isotherms, which indicate mesoporous structures, with surface areas ranging between 100 – 400 m^2g^{-1} [64]. Spivak reported that parameters that control surface area and pore distribution include the percentage of cross-linking monomer, type and amount of porogen and the

reaction temperature [163]. The solvent or 'porogen' used in polymerisation plays an important role in the formation of the porous structure of the MIPs. Porosity takes place from phase separation of the porogen and the growing polymer during polymerisation. Porogens with low solubility phase separate early and provide polymers that form larger pores with lower surface areas [163]. Sellergren and Shea [64] employed nitrogen sorption to characterise MIPs made with MAA/EGDMA monomers using L-phenylalanine anilide as template. Different porogens were employed to compare the effect on surface areas, pore volume and the average pore size of the MIPs. The polymers showed a wide distribution of surface areas and pore volumes. They found that the polymers made with chloroform as porogen were non-porous and had very low surface area (3.5 m^2g^{-1}) [64]. In general polymers made with hydrophobic solvents such as chloroform and toluene tend to have lower surface area to polymers made in solvents such as acetonitrile [164].

Urraca *et al*. determined the effect of different templates and functional monomers on the textural properties of photochemically polymerised bulk MIP and NIP polymers prepared at 4 °C (cold room). The nitrogen adsorption plots yielded Type IV isotherms. Regardless of the template used the MIPs prepared had higher surface areas and more developed porous texture than the corresponding NIPs which might be attributed to the cavities left after removal of template. Employing 1-allyl piperazine as functional monomer the surface area of the MIP was 146 m^2g^{-1} and NIP was 13 m^2g^{-1}. The MIP and NIP values using 2-(diethylamino)ethyl methacrylate as functional monomer were (MIP: 146 m^2g^{-1}; NIP: 13 m^2g^{-1}) respectively.

The porosity of imprinted polymers can be adapted by the type and amount of solvent, the concentration of cross-linking monomers, the reaction temperature and the method of polymerisation [158;159]. Holland *et al*. [158] investigated the effect of morphology and the performance of MIPs prepared with varying amounts of cross-linker (EGDMA). Through the use of physical characterisation techniques, porosity, surface area and swell studies were linked to performance related parameters i.e. the affinity of the polymer for the template, the total number of binding sites and the binding energy. As discussed in the previous section, the LF-I and AD spectra was applied to study the effect of varying amount of cross-linker on the binding characteristics of MIPs. The total number of binding sites increased with decreasing

EGDMA. This trend was expected due to increasing flexibility which allowed intrinsic sites of the polymer to become occupied; this resulted in an overall higher capacity of the polymers. The average pore diameter decreased with increasing amount of EGDMA content in the polymer, which lead to an overall lower capacity (lower number of binding sites). The flexibility and various porous structures of the polymers (as a consequence of being prepared with varying amounts cross-linker), combined with the swelling of the polymer in chloroform may have resulted in greater access within the polymer which resulted in a higher degree of binding (both specific and non-specific) [158].

Wei and Mizaikoff [119] compared the relationships between the particle porosity and rebinding properties for 17 β-estradiol imprinted polymers generated by three different synthetic routes yielding bulk polymers, microspheres and sub-microspheres respectively. The surface areas of these polymers determined by BET analysis were ranked by increasing surface area as sub-microspheres (10.30 m^2g^{-1}), bulk material (552.89 m^2g^{-1}) and microspheres (706.98 m^2g^{-1}). They confirmed that porosity of imprinted polymers plays an important role in their rebinding characteristics. Bulk polymer monoliths with larger surface area gave superior binding. Additionally, the cross-linking density was investigated and optimised for maintaining a balance between the structural rigidity of the binding sites and the porosity of the resultant MIPs. The findings from the investigation presented aided in establishing a rational basis for fine tuning of imprinted materials for analytical applications such as HPLC.

1.7.3 Particle size distribution analysis

Particle size distribution measurements of polymer samples are carried out based on a laser diffraction technique employed by the Malvern Mastersizer 2000 analyser. The non-imaging technique is based upon the physical principle of the interaction between the light beam and the particle. The scattered light pattern formed at the detector is a summation of the scattering pattern produced by each particle that is being sampled. The type of laser diffraction instrument used for analysis of samples is based on the Mie optical model, which enables analysis to about 0.1 μm [165]. The 'Mie theory' predicts how light is scattered by a particle of known size as light is absorbed. The

Mastersizer 2000 uses the Mie theory in reverse i.e. it knows the light scattering pattern generated for a given sample (measured) and if the refractive index of the material is known is calculates the particle size. A predictive model is generated and a comparison for fit is made between the predicted model and the measured data. For the application of the Mie theory, three properties need to be known:

- The refractive index (RI) of the dispersant (Real) – describes the amount of scattering that takes place as a result of light interacting with the particle. This value is found in the Malvern RI appendix.
- The refractive index of the sample material.
- The imaginary refractive index of the sample material (Imaginary) – describes the amount of absorption that takes place as the light enters the particle.

1.7.3.1 Particle size studies to investigate the effect of solvents on MIPs

The effect of solvents on the morphology of MIPs is also an important consideration. The type and nature of the solvent used in the rebinding step will influence the relative swelling of the polymer. Therefore, particle size distribution of MIPs is an important aspect related to polymer swelling. Farrington *et al*. [166] studied the particle size distribution of ibuprofen MIPs using a Malvern Mastersizer 2000 equipped with light scattering technology. Particle size studies were investigated on exposure of the MIP to different solvents (i.e. water, methanol and acetonitrile). It was shown that solvent greatly affected the particle size distribution. Exposure to water caused the least reduction in average particle size compared to methanol and acetonitrile. Results showed that a higher degree of swelling corresponded to poorer rebinding studies in the same solvent. Investigations on particle size distribution have received little attention to date in the literature on MIPs. This is linked to the fact that traditional bulk polymerisation method requires grinding and sieving of the polymer yielding particle sizes within the range 25 and 75 μm [121].

1.7.4 Scanning electron microscopy (SEM) studies

The scanning electron microscopy (SEM) technique is frequently used to examine the structure and surface morphology of imprinted polymers. Its excellent resolution makes it a one of the best tools for this purpose. González *et al*. [167] synthesised non-covalent MIPs by bulk polymerisation using digoxin as template. These MIPs were synthesised using different functional monomers and porogens. A comparative study of the MIPs was determined by examining differences in the surface morphology by SEM. It was found that the morphological studies were connected to the structural characteristics of MIPs synthesised under different conditions with the results of binding assays.

1.7.5 Nuclear Magnetic Resonance (NMR) studies

NMR spectroscopy is becoming a widely used technique within the field of molecular imprinting to predict the most appropriate ratios of template to functional monomer. Farrington [166] used ^{1}H NMR experiments and molecular modelling to investigate the pre-polymerisation mixture. Additionally, NMR has been employed by O'Mahony *et al*. [168] to investigate the hydrophobicity and ion pair interactions as forces influencing the selectivity by imprinted polymers.

1.7.6 Fourier Transform Infra-Red (FTIR) analysis

FTIR spectra of MIPs can be obtained using KBr pellets containing the prepared materials. Analysis of the distinct monomer bands to those of the polymer can give an indication of the extent of monomer incorporation into the polymer network. For instance, MAA has distinct bands at 1638 cm^{-1} and 950 cm^{-1} which may be revealing regarding the degree of unreacted double bonds within the polymer [169]. FTIR characterisation also enables the extent of non-covalent interactions, particularly hydrogen bonds formed between polymer and template to be investigated. Kyzas *et al*. [164] prepared two water-compatible MIPs for the selective adsorption of a Reactive Red (RR) and Basic Red dye (BR). FTIR spectra were used for characterisation of the obtained dye-MIPs. Structural differences between MIP and

NIP were affirmed by the absence of dye molecules in the NIP spectrum. In addition, the strong ionic interactions between the negatively charged carboxylic groups of the functional monomer (MAA) and the positively charged dye molecules are revealed by the shift of the peak from 1661 cm^{-1} in B-NIPs to 1653 cm^{-1} in BR-MIPs. The electrostatic interations between sulfonate groups of the dye and protonated amide groups of the acrylamide (functional monomer) were presented through the shift of the peak from 1691 cm^{-1} in the R-NIP to 1682 cm^{-1} in the RR-MIP.

1.7.7 Solid-State Nuclear Magnetic Resonance spectroscopy

Solid-state NMR technique facilitates the acquisitioned NMR spectra of insoluble polymers. Different types of carbon atoms present in the polymer network can be analysed by ^{13}C NMR. This technique is utilised in estimating the number of un-reacted carbon-carbon double bonds present after polymerisation [169]. The use of NMR for rebinding 1,3-diacetylbenzene to its imprinted polymers has been demonstrated by Shea and Sasaki [170]. The technique was used to monitor the fidelity with which the functionalised sites are maintained within the imprinted polymer.

1.8 MIP applications

The process of molecular imprinting is a simple concept that creates macromolecular matrices that exhibit selective molecular recognition behaviour. Owing to the ease of preparation and relatively low cost, stability against high temperatures and pressures, chemical resistance to harsh environments, and the ability to act as synthetic biological receptors, imprinted polymers have lead to useful applications in several areas. Novel physical configurations of MIPs have been obtained in the past few years using different preparation methods. As a result advances in this direction have brought better use of MIPs in (1) affinity separations (2) solid-phase extraction (3) sensors (4) drug delivery.

1.8.1 Affinity separation

At present the biggest application for imprinted polymers is affinity separation [4]. Their use as stationary phases in high performance liquid chromatography (HPLC) continues to be an important research path, although existing limitations such as low capacity and heterogeneous binding sites are well acknowledged and reported. One of the most convenient methods for evaluating the efficiency of a new imprinting protocol is by HPLC using an imprinted stationary phase. Other important fields of research in the affinity separation area include membranes and capillary electrophoresis (CE).

1.8.1.1 MIPs as chiral stationary phases in HPLC

Requirements to administer potent drugs in enantiomerically pure form have led to the rise of technologies aimed at producing the chiral entities on a preparative scale [171]. Non-imprinted column stationary phases have been applied for many years in HPLC for the separation of molecules. The advantage of employing an imprinted polymer over conventional stationary phases is the ability of the imprinted phase to selectively recognise a specific molecule. MIPs have been used as chiral stationary phases (CSPs) since the pioneering work of Wulff in the 1970s [18].

A fundamental application of MIPs is that they possess the ability to differentiate between the enantiomers of a drug solute containing one or more stereogenic centres. CSPs are prepared by packing a HPLC column with an imprinted polymer synthesised with one enantiomer of a drug compound, in bead format or as ground particles. The enantiomer used in the preparation of the MIP is always the one that is more strongly retained therefore the elution order is predictable [172]. MIPs employed as CSPs for use in any separation technique possess predetermined three dimensional spatial cavities which have the ability to recognise one enantiomer over the other. A significant amount of racemates have been resolved on CSPs employing MIPs. The most extensive studies on MIPs as CSPs have been performed using amino acids [64] and their derivatives [90;93;173;174] as templates.

MIPs perform best in the solvent employed during synthesis (usually an aprotic organic solvent such as chloroform or acetonitrile) as hydrogen bond and electrostatic interactions between analyte and MIP are expected to be maximised [64]. Additionally, the swelling of the polymer remains similar and binding sites are not distorted employing the same porogen as used during polymer formation. Yu and Mosbach conducted an investigation into the elements which affect the enantiomeric recognition properties of MIPs in HPLC. Their results showed that the recognition properties of MIPs are greatly influenced by the mobile phase used. For polymers prepared in chloroform, chloroform-based mobile phases gave much better separation than acetonitrile-based mobile phases [175].

When MIPs are employed as chiral stationary phases for chromatographic separations, the differences in binding strengths of various imprinted sites are exhibited. These differences result in extreme tailing of the more retained peak [64]. Peak broadening and tailing effects can be attenuated by careful optimisation of the synthetic and chromatographic conditions, injecting smaller amounts of analyte and using a reduced flow rate. Resolution can be improved by increasing column length but would require a longer run time [172]. The mechanism of analyte retention on MIPs was proposed to be due to an ion-exchange model as described in a literature review discussing the separation of drug enantiomers using MIPs via HPLC with aqueous mobile phases by Ansell [172]. It can be illustrated that in such a system retention is proportional to the product α^*_B x α^*_A where α^*_B is the degree of ionisation of the solute and α^*_A the degree of ionisation of the polymer at a given pH. The ion-exchange model of analyte retention was developed by Sellergren and Shea [64].

An important limitation to employing MIPs as a chiral stationary phase is that only a restricted number of racemates can be resolved employing a specific template. As a result, one column per pair of enantiomers to be separated could be required. Although in a lot of cases several different racemates may have been injected onto the imprinted column aside from the imprinted compound and its enantiomers. Furthermore, poor column efficiency leading to problems in peak quantitation can be improved if the MIPs are monodisperse spherical particles [90].

Pharmaceuticals have been used in chromatographic studies such as chlorpheniramine (CP) and brompheniramine (BP) [138;139]. Haginaka *et al*. successfully separated the enantiomers of CP and BP using chiral MIPs as stationary phases employing an aqueous mobile phase, with elution of the *d*-isomer occurring second. Other classes of compounds that have been used in chromatographic studies include rigid aromatic compounds [90], sugars and sugar derivatives [43;176], pesticides [177], naproxen [178], β-blockers [110;119;132], peptides [173], sterols [40]. High selectivity is often observed employing MIPs as chiral stationary phases, however the technique is not without its difficulties. Binding site heterogeneity and slow mass transfer leads to peak broadening [64]. Columns packed with irregular polymer particles that have polydisperse distributions result in poor column efficiency and high back pressures. Further improvements in efficiency and kinetics are desirable by preparation of MIPs in bead format in order to overcome these difficulties.

1.8.1.2 Enantioseparation by capillary electrophoresis

Capillary electrophoresis (CE) presents a number of advantages to HPLC, the amount of sample and separation buffer required is much less. Additionally, higher efficiencies and shorter analysis times are obtained in comparison to HPLC. However, the disadvantages of CE to HPLC are the lower reproducibility and poorer sensitivity. CE is the migration of charged solutes in solvent under the influence of an electrical field. CE techniques are categorised by two approaches, direct or indirect CE. The direct CE method utilises chiral selectors as additives to the electrolyte.

Nilsson *et al*. [179] first reported the use of MIPs in electrical driven separations through polymeristion of MAA and EGDMA *in situ* with template (L-phenylanaline analide (L-Phe-An), benzamidine (BAM) or pentamidine (PAM)) and porogen directly in the capillaries that were used in the electrophoresis system. However, the enantiomers of D,L-Phe-An on an L-Phe-An imprinted polymer were not separated, which was attributed to the low ratio of cross-linkers to monomers utilised.

The first example of enantioseparation of a racemic mixture of D,L-Phe-An using the CE technique was reported by Lin *et al*. [180]. Optimum resolution was obtained employing a 5:1 molar ratio of cross-linker:monomer.

Nilsson *et al.* [181] comprehensively reviewed the techniques used in the development of imprinted polymers for use in CE and capillary electrochromatography (CEC). A wide range of molecules have been separated using CE, these include, amino acids [180], ephedrine [182], propranolol [72] and fungicide (thiabenzadole in citrus samples) [183].

1.8.2 Solid-phase extraction

For the detection of contaminants in foodstuffs, such as pesticides, herbicides, hormones and antibiotics fast analytical tools for sample preparation are required. Before analysing biological and environmental compounds, many samples require pre-concentration (enrichment) or clean up. In addition to liquid chromatography, imprinted polymers as selective SPE media have risen in popularity in recent years, as it is an easily automated technique and a wide range of phases are available [184]. It is by far the most advanced technical application of MIPs. A vast amount of papers have been published with the use of MIPs as sorbents in SPE, namely molecularly imprinted solid phase extraction (MISPE). The use of MIPs as selective sorbent materials enables performing a customised sample treatment step prior to the final determination. This is necessary when the sample is a complex matrix and the presence of interferences could prevent final quantification by typical chromatographic techniques coupled to detectors [185]. Table 1.2 lists some of the molecules in which MISPE has been applied.

Table 1.2 Examples of molecules in which MISPE has been employed.

Analyte	Sample/Matrix	Reference
Cholesterol	Cheese products	[186]
Triazines	Grape juice and soil extract	[187]
Caffeine	High caffeine soft drink	[188]
Benzo[a]pyrene	Water and coffee samples	[107]
Malachite green	Fish water and fish samples	[189]
Mepivacaine, Ropivacaine and Bupivacaine	Human plasma	[73]
Carbamazepine and Oxcarbazepine	Human urine	[190]
Naproxen	Urine samples	[191]
Dioxynivalenol	Wheat and pasta	[192]

One of the main disadvantages with the MIP for SPE applications is the difficulty in removing the template molecule. This leads to leaching of the template in actual samples being processed and subsequent inaccurate results. This problem has been circumvented by using a structural analogue of the template or imprinting using a 'dummy template'. Despite this possible drawback, MIPs have great potential for commercial applications owing to their low cost, speed of preparation and excellent well-constructed affinities.

MISPE is based on the conventional SPE procedures, therefore conditioning, loading, clean-up and elution steps are performed as a matter of course [193].

MISPE can be performed in off-line or on-line modes when coupled to a chromatographic technique such as HPLC. The vast majority of MISPE studies published were developed in off-line mode [107;128;187;191;193;194]. Relatively simple instrumentation is required and in addition stronger elution conditions can be used without compromising the analytical instrumentation due to solvent, pH or organic modifier.

On-line MISPE protocols have mainly been developed by coupling a pre-column packed with (≈ 50 mg) imprinted polymer into the loop of the injection valve of a liquid chromatography (LC) system [193]. The first application of the on-line MISPE procedure coupled to a HPLC was reported by Masqué *et al*. [195] for the selective extraction of 4-nitrophenol from environmental water. Publications of on-line MISPE studies have increased in the last five years [196-199]. In these studies the analyte of interest has been extracted from an array of matrices, such as biological, environmental and food substances.

1.8.3 Sensors

Sensors are analytical devices comprising a sensing element that recognises a specific target molecule in a complex matrix which creates an output signal. The use of MIPs in sensor applications is advantageous as MIPs possess high mechanical and thermal stability.

There are two principal types of sensors which have been developed; (1) affinity sensors and (2) receptor sensors [200]. The detection in affinity sensor devices is based on the concentration of template bound to the MIP, which is immobilised on the detector surface. Receptor sensors investigate a MIPs ability to change conformation upon binding with the template, leading to a change in a measurable property such as conductivity, permeability or surface potential [201]. Alternatively, sensors can be created which take advantage of the ability of the functional monomer to change its property upon interaction with the template species. Some examples of MIP based sensors used to detect template species include: atrazine [202], caffeine [203], cholesterol [204], carboxylic acids [205], 2,4-dichlorophenoxyacetic acid [206], sorbitol [207], polyaromatic hydrocarbons (PAHs) [208], cocaine, deoxyephedrine and methadone [209].

The advantages of MIPs in sensor applications include their high binding, specificity and affinity for a molecule, which makes them promising alternatives to antibodies and natural receptors. However, there are limitations to the development of MIP sensors including: (i) absence of a general procedure for MIP preparation (ii) difficulties in integrating the polymer with the transducer, (iii) difficulty in transforming the binding event into an electrical signal and (iv) poor performance of MIPs in aqueous solution [200].

1.8.4 Drug-delivery

Allender *et al.* [210] prepared an imprinted polymer for propranolol and investigated its use as a rate attenuating selective excipient in a transdermal patch. Drug diffusion studies indicated that the MIPs released the drug at a considerably lower rate in comparison to the NIP. The lower diffusion from the MIP provided evidence of how the specific binding of such a material could be used to control the drug release.
In terms of 'in vivo' evaluation, Hiratani *et al.* [211] employed imprinted hydrogels which have been used for the opthalmic delivery of timolol from therapeutic soft contact lenses. The imprinted contact lenses were also found to be far superior in controlling the drug release relative to the non-imprinted contact lenses.

The value of molecular technology to drug-delivery i.e. administering drugs by different routes (e.g. oral, ocular or transdermal) also requires the consideration of safety and toxicological concerns [212].

1.9 Aims of research

The main aims of this research were:

- To compare and evaluate the performance of spherical beads produced by suspension polymerisation in parallel with corresponding irregular shaped particles prepared from polymer monoliths in terms of binding properties, yield of system and morphology. In addition, evaluate both methodologies using different cross-linkers to identify correlations in relation to binding performance with physical characteristics of the polymers.
- To examine and optimise suspension polymers produced at different agitation speeds and temperature in order to assess the impact on the overall performance of the spherical beads in terms of affinity, yield, morphology, particle size distribution and solvent swell.
- To assess the applicability of binding isotherm modelling for evaluating the binding behaviour of MIP spherical beads and irregular shaped particles. To gain a better understanding of the rebinding properties of the imprinted polymer formats under different conditions.
- To utilise direct probe thermal desorption GC-MS to evaluate polymer affinity and specificity for spherical and irregular shaped polymers in the absence of solvent.
- To prepare MIPs for CP, *d*-CP, BP and *d*-BP by aqueous suspension polymerisation procedure employing MAA as the functional monomer and trimethylolpropane trimethacrylate (TRIM) as the cross-linker and chloroform as the porogen.
- To optimise a HPLC method for chiral separation and determination of CP and BP enantiomers in terms of resolution and capacity values using the chiral MIPs. To assess the polymer performance by equilibrium binding studies using HPLC.

- To prepare HPLC columns using imprinted polymers and assess their ability to separate CP and its structural analogues using an aqueous mobile phase in terms of enantioselectivity and retention properties. To examine the effect of column temperature on the retention factors, enantioseparation factors and resolution of CP and structurally related compounds using the *d*-$CP_{MIP(9500rpm)}$ column.
- To compare and evaluate the physical characteristics of MIPs prepared for CP, *d*-CP, BP and *d*-BP by suspension polymerisation method in an aqueous medium using different agitation speeds, (9500 rpm, 13500 rpm and 24000 rpm respectively) to identify the most suitable polymer for use as stationary phase.

Reference List

1. Wulff, G.; Sarhan, A. *Angewandte Chemie-International Edition In English* **1972,** *11*, 341.

2. Pauling, L. *Journal of the American Chemical Society* **1940,** *62*, 2643-57.

3. Fischer, E. *Berichte der Deutschen Chemischen Gesellschaft* **1894,** *27*, 2895.

4. Haupt, K.; Mosbach, K. *Trends in Biotechnology* **1998,** *16*, 468-75.

5. Takeuchi, T.; Haginaka, J. *Journal Of Chromatography B-Analytical Technologies In The Biomedical And Life Sciences* **1999,** *728*, 1-20.

6. Polyakov, M. V. *Zhur, Fiz.Khim* **1931,** *2*, 799-805.

7. Dickey, F. H. *Proceedings Of The National Academy Of Sciences Of The United States Of America* **1949,** *35*, 227-29.

8. Pinel, C.; Loisil, P.; Gallezot, P. *Advanced Materials* **1997,** *9*, 582-85.

9. Hunnius, M.; Rufinska, A.; Maier, W. F. *Microporous And Mesoporous Materials* **1999,** *29*, 389-403.

10. Kunitake, T.; Lee, S. W. *Analytica Chimica Acta* **2004,** *504*, 1-6.

11. Ling, T. R.; Syu, Y. Z.; Tasi, Y. C.; Chou, T. C.; Liu, C. C. *Biosensors and Bioelectronics* **2005,** *21*, 901-07.

12. Shiomi, T.; Matsui, M.; Mizukami, F.; Sakaguchi, K. *Biomaterials* **2005,** *26*, 5564-71.

13. Shea, K. J.; Thompson, E. A. *Journal Of Organic Chemistry* **1978,** *43*, 4253-55.

14. Shea, K. J.; Thompson, E. A.; Pandey, S. D.; Beauchamp, P. S. *Journal Of The American Chemical Society* **1980,** *102*, 3149-55.

15. Damen, J.; Neckers, D. C. *Journal Of The American Chemical Society* **1980,** *102*, 3265-67.

16. Damen, J.; Neckers, D. C. *Tetrahedron Letters* **1980,** *21*, 1913-16.

17. Damen, J.; Neckers, D. C. *Journal Of Organic Chemistry* **1980,** *45*, 1382-87.

18. Wulff, G.; Vesper, R.; Grobe-Einsier, R.; Sarhan, A. *Makromolekulare Chemie-Macromolecular Chemistry and Physics* **1977,** *178*, 2799-816.

19. Wulff, G.; Poll, H. *Makromolekulare Chemie-Macromolecular Chemistry and Physics* **1987,** *188*, 741-48.

20. Wulff, G.; Vesper, W. *Journal of Chromatography* **1978,** *167*, 171-86.

21. Wulff, G.; Stellbrink, H. *Recueil des Travaux Chimiques des Pays-Bas - Journal of the Royal Netherlands Chemical Society* **1990,** *109*, 216-21.

22. Arshady, R.; Mosbach, K. *Macromolecular Chemistry and Physics-Makromolekulare Chemie* **1981,** *182*, 687-92.

23. Vlatakis, G.; Andersson L.I.; Müller R.; Mosbach, K. *Nature* **1993,** *361*, 645-47.

24. Kempe, M.; Fischer, L.; Mosbach, K. *Journal Of Molecular Recognition* **1993,** *6*, 25-29.

25. Haginaka, J.; Sanbe, H. *Chemistry Letters* **1999,** *28*, 757-58.

26. Sreenivasan, K. *Talanta* **1997,** *44*, 1137-40.

27. Kugimiya, A.; Takeuchi, T. *Analytical Sciences* **1999,** *15*, 29-33.

28. Spivak, D. A. "Selectivity in molecularly imprinted matrices", *Molecularly Imprinted Materials: Science and Technology*., Yan, M.; Ramstrom, O., Eds.; (Marcel Dekker, New York, **2005**) Chapter 15, 395-417.

29. Umpleby, R. J.; Baxter, S. C.; Rampey, A. M.; Rushton, G. T.; Chen, Y.; Shimizu, K. D. *Journal of Chromatography B* **2004,** *804*, 141-49.

30. Sun, R. F.; Yu, H. M.; Luo, H.; Shen, Z. Y. *Journal of Chromatography A* **2004,** *1055*, 1-9.

31. Wulff, G.; Knorr, K. *Bioseparation* **2002,** *10*, 257-76.

32. Wulff, G.; Schönfeld, R. *Advanced Materials* **1998,** *10*, 957-59.

33. Lübke, C.; Lübke, M.; Whitcombe, M. J.; Vulfson, E. N. *Macromolecules* **2000,** *33*, 5098-105.

34. Strikovsky, A. G.; Kasper, D.; Grun, M.; Green, B. S.; Hradil, J.; Wulff, G. *Journal of the American Chemical Society* **2000,** *122*, 6295-96.

35. Wulff, G.; Sarhan, A. *Angewandte Chemie-International Edition* **1972,** *11*, 341.

36. Wulff, G.; Sarhan, A.; Zabrocki, K. *Tetrahedron Letters* **1973,** *14*, 4329-32.

37. Sellergren, B.; Andersson, L. *Journal Organic Chemistry* **1990,** *55*, 3381-83.

38. Bystrom, S. E.; Borje, A.; Akermark, B. *Journal of the American Chemical Society* **1993,** *115*, 2081-83.

39. Whitcombe, M. J.; Rodriguez, M. E.; Villar, P.; Vulfson, E. N. *Journal of the American Chemical Society* **1995,** *117*, 7105-11.

40. Hwang, C. C.; Lee, W. C. *Journal of Chromatography A* **2002,** *962*, 69-78.

41. Mullett, W. M.; Dirie, M. F.; Lai, E. P. C.; Guo, H.; He, X. *Analytica Chimica Acta* **2000,** *414*, 123-31.

42. Cummins, W.; Duggan, P.; McLoughlin, P. *Biosensors and Bioelectronics* **2006,** *22*, 372-80.

43. Wulff, G.; Schauhoff, S. *Journal Organic Chemistry* **1991,** *56*, 395-400.

44. Matsui, J.; Fujiwara, K.; Takeuchi, T. *Analytical Chemistry* **2000,** *72*, 1810-13.

45. Yilmaz, E.; Mosbach, K.; Haupt, K. *Analytical Communications* **1999,** *36*, 167-70.

46. Martin-Esteban, A.; Turiel, E.; Stevenson, D. *Chromatographia* **2001,** *53*, S434-S437.

47. Zhang, T. L.; Liu, F.; Chen, W.; Wang, J.; Li, K. *Analytica Chimica Acta* **2001,** *450*, 53-61.

48. Yu, C.; Mosbach, K. *Journal Organic Chemistry* **1997,** *62*, 4057-64.

49. Karim, K.; Breton, F.; Rouillon, R.; Piletska, E. V.; Guerreiro, A.; Chianella, I.; Piletsky, S. A. *Advanced Drug Delivery Reviews* **2005,** *57*, 1795-808.

50. Sellergren, B. *Journal of Chromatography A* **2001,** *906*, 227-52.

51. Spivak, D.; Gilmore, M. A.; Shea, K. J. *Journal Of The American Chemical Society* **1997,** *119*, 4388-93.

52. Pavel, D.; Lagowski, J. *Polymer* **2005,** *46*, 7528-42.

53. Andersson, L. I.; Mosbach, K. *Journal of Chromatography* **1990,** *516*, 313-22.

54. Matsui, J.; Doblhoff-Dier, O.; Takeuchi, T. *Analytica Chimica Acta* **1997,** *343*, 1-4.

55. Haginaka, J.; Sanbe, H. *Journal of Chromatography A* **2001,** *913*, 141-46.

56. Baggiani, C.; Anfossi, L.; Giovannoli, C.; Tozzi, C. *Talanta* **2004,** *62*, 1029-34.

57. Wulff, G.; Vietmeier, J.; Poll, H. G. *Makromolecular Chemistry* **1987,** *188*, 731-40.

58. Kempe, M.; Mosbach, K. *Tetrahedron Letters* **1995,** *36*, 3563-66.

59. Holland, N.; Duggan, P.; Owens, E.; Cummins, W.; Frisby, J.; Hughes, H.; McLoughlin, P. *Analytical and Bioanalytical Chemistry* **2008,** *391*, 1245-53.

60. Villamena, F. A.; De La Cruz, A. A. *Journal of Applied Polymer Science* **2001,** *82*, 195-205.

61. Sibrian-Vasquez, M.; Spivak, D. A. *Journal Of The American Chemical Society* **2004,** *126*, 7827-33.

62. LeJeune, J.; Spivak, D. A. *Analytical and Bioanalytical Chemistry* **2007,** *389*, 433-40.

63. LeJeune, J.; Spivak, D. A. *Biosensors and Bioelectronics* **2009,** *25*, 604-08.

64. Sellergren, B.; Shea, K. J. *Journal of Chromatography A* **1993,** *635*, 31-49.

65. Yoshizako, K.; Hosoya, K.; Iwakoshi, Y.; Kimata, K.; Tanaka, N. *Analytical Chemistry* **1998,** *70*, 386-89.

66. Cummins, W.; Duggan, P.; McLoughlin, P. *Analytica Chimica Acta* **2005,** *542*, 52-60.

67. Andersson, L. I. *Analytical Chemistry* **1996,** *68*, 111-17.

68. Baggiani, C.; Giraudi, G.; Giovannoli, C.; Trotta, F.; Vanni, A. *Journal of Chromatography A* **2000,** *883*, 119-26.

69. Chen, W.; Liu, F.; Xu, Y.; Li, K. A.; Tong, S. *Analytica Chimica Acta* **2001,** *432*, 277-82.

70. Sellergren, B.; Mosbach, K.; Lepisto, M. *Journal of the American Chemical Society* **1988,** *110*, 5853.

71. Siemann, M.; Andersson, L. I.; Mosbach, K. *Journal of Agricultural and Food Chemistry* **1996,** *44*, 141-45.

72. Schweitz, L.; Andersson, L. I.; Nilsson, S. *Analyst* **2002,** *127*, 22-28.

73. Andersson, L. I.; Abdel-Rehim, M.; Nicklasson, L.; Schweitz, L.; Nilsson, S. *Chromatographia* **2002,** *55*, S65-S69.

74. Mijangos, I.; Navarro-Villoslada, F.; Guerreiro, A.; Piletska, E.; Chianella, I.; Karim, K.; Turner, A.; Piletsky, S. *Biosensors and Bioelectronics* **2006,** *22*, 381-87.

75. Lu, Y.; Li, C.; Wang, X.; Sun, P.; Xing, X. *Journal of Chromatography B* **2004,** *804*, 53-59.

76. Skudar, K.; Bruggemann, O.; Wittelsberger, A.; Ramstrom, O. *Analytical Communications* **1999,** *36*, 327-31.

77. O'Shannessy, D. J.; Ekberg, B.; Mosbach, K. *Analytical Biochemistry* **1989,** *177*, 144-49.

78. Sreenivasan, K. *Polymer Gels And Networks* **1997,** *5*, 17-22.

79. Piletsky, S. A.; Mijangos, I.; Guerriro, A.; Piletska, E. V.; Chianella, I.; Karim, K.; Turner, A. P. F. *Macromolecules* **2005,** *38*, 1410-14.

80. Spivak, D. A. *Advanced Drug Delivery Reviews* **2005,** *57*, 1779-94.

81. Piletsky, S. A.; Piletska, E. V.; Karim, K.; Freebairn, K. W.; Legge, C. H.; Turner, A. P. F. *Macromolecules* **2002,** 35, 7499-504.

82. Osmani, Q.; Hughes, H.; Flavin, K.; Hedin-Dahlstrom, J.; Allender, C.; Frisby, J.; McLoughlin, P. *Analytical and Bioanalytical Chemistry* **2008,** *391*, 1229-36.

83. Takeuchi, T.; Fukuma, D.; Matsui, J. *Analytical Chemistry* **1999,** *71*, 285-90.

84. Lanza, F.; Sellergren, B. *Analytical Chemistry* **1999,** *71*, 2092-96.

85. Cedefur, J.; Pei, Y. X.; Meng, Z. H.; Kempe, M. *Journal Of Combinatorial Chemistry* **2003,** *5*, 67-72.

86. Batra, D.; Shea, K. J. *Current Opinion in Chemical Biology* **2003,** *7*, 434-42.

87. Subrahmanyam, S.; Piletsky, S. A.; Piletska, E. V.; Chen, B.; Karim, K.; Turner, A. P. F. *Biosensors and Bioelectronics* **2001,** *16*, 631-37.

88. Andersson, H. S.; Nicholls, I.A. *Bioorganic Chemistry* **1997,** *25*, 203-11.

89. Karlsson, J. G.; Karlsson, B.; Andersson, L. I.; Nicholls, I. A. *Analyst* **2004,** *129*, 456-62.

90. Mayes, A. G.; Mosbach, K. *Analytica Chimica Acta* **1996,** *68*, 3769-74.

91. Kempe, H.; Kempe, M. *Macromolecular Rapid Communications* **2004,** *25*, 315-20.

92. Zourob, M.; Mohr, S.; Mayes, A. G.; Macaskill, A.; Pérez-Moral, N.; Fielden, P. R.; Goddard, N. J. *Lab on a Chip* **2006,** *6*, 296-301.

93. Hosoya, K.; Yoshizako, K.; Shirasu, Y.; Kimata, K.; Araki, T.; Tanaka, N.; Haginaka, J. *Journal of Chromatography A* **1996,** *728*, 139-47.

94. Haginaka, J.; Tabo, H.; Ichitani, M.; Takihara, T.; Sugimoto, A.; Sambe, H. *Journal of Chromatography A* **2007,** *1156*, 45-50.

95. Ye, L.; Cormack, P. A. G.; Mosbach, K. *Analytical Communications* **1999,** *36*, 35-38.

96. Perez, N.; Whitcombe, M. J.; Vulfson, E. N. *Macromolecules* **2001,** *34*, 830-36.

97. Sellergren, B.; Ruckert, B.; Hall, A. J. *Advanced Materials* **2002,** *14*, 1204-08.

98. Piletsky, S. A.; Matuschewski, H.; Schedler, U.; Wilpert, A.; Piletska, E. V.; Thiele, T. A.; Ulbricht, M. *Macromolecules* **2000,** *33*, 3092-98.

99. Mayes, A. G.; Whitcombe, M. J. *Advanced Drug Delivery Reviews* **2005,** *57*, 1742-78.

100. Perez-Moral, N.; Mayes, A. G. *Analytica Chimica Acta* **2004,** *504*, 15-21.

101. Brüggemann, O.; Haupt, K.; Ye, L.; Yilmaz, E.; Mosbach, K. *Journal of Chromatography A* **2000,** *889*, 15-24.

102. Toth, B.; Laszlo, K.; Horvai, G. *Journal of Chromatography A* **2005,** *1100*, 60-67.

103. Perez-Moral, N.; Mayes, A. G. *Bioseparation* **2002,** *10*, 287-99.

104. Cacho, C.; Turiel, E.; Martin-Esteban, A.; Perez-Conde, C.; Camara, C. *Journal of Chromatography B* **2004,** *804*, 83.

105. Nantasenamat, C.; Isarankura-Na-Ayudhya, C.; Naenna, T.; Prachayasittikul, V. *Biosensors and Bioelectronics* **2007,** *22*, 3309-17.

106. Ozcan, A. A.; Say, R.; Denzili, A.; Ersoz, A. *Analytical Chemistry* **2006,** *78*, 7253-58.

107. Lai; J.P; Niessner, R.; Knopp, D. *Analytica Chimica Acta* **2004,** *522*, 137-44.

108. Lai, J. P.; Lu, X. Y.; Lu, C. Y.; Ju, H. F.; He, X. W. *Analytica Chimica Acta* **2001,** *442*, 105-11.

109. Perez-Moral, N.; Mayes, A. G. *Biosensors and Bioelectronics* **2006,** *21*, 1798-803.

110. Fairhurst, R. E.; Chassaing, C.; Venn, R. F.; Mayes, A. G. *Biosensors and Bioelectronics* **2004,** *20*, 1098-105.

111. Kempe, H.; Kempe, M. *Analytical Chemistry* **2006,** *78*, 3659-66.

112. Rachkov, A.; Minoura, N. *Journal of Chromatography A* **2000,** *889*, 111-18.

113. Kotrotsiou, O.; Chaitidou, S.; Kiparissides, C. *Materials Science and Engineering: B* **2009,** *165*, 256-60.

114. Ye, L.; Cormack, P. A. G.; Mosbach, K. *Analytica Chimica Acta* **2001,** *435*, 187-96.

115. Ye, L.; Mosbach, K. *Reactive and Functional Polymers* **2001,** *48*, 149-57.

116. Wang; J.F; Cormack, P. A. G.; Sherrington, D. C.; Khoshdel, E. *Angewandte Chemie-International Edition* **2003,** *42*, 5336-38.

117. Turiel, E.; Tadeo, J. L.; Cormack, P. A. G.; Martin-Esteban, A. *Analyst* **2005,** *130*, 1601-07.

118. Castell, O. K.; Allender, C. J.; Barrow, D. A. *Biosensors and Bioelectronics* **2006,** *22*, 526-33.

119. Wei, S.; Mizaikoff, B. *Biosensors and Bioelectronics* **2007,** *23*, 201-09.

120. Sambe, H.; Hoshina, K.; Moaddel, R.; Wainer, I. W.; Haginaka, J. *Journal of Chromatography A* **2006,** *1134*, 88-94.

121. Yoshimatsu, K.; Reimhult, K.; Krozer, A.; Mosbach, K.; Sode, K.; Ye, L. *Analytica Chimica Acta* **2007,** *584*, 112-21.

122. Tamayo, F. G.; Casillas, J. L.; Martin-Esteban, A. *Analytica Chimica Acta* **2003,** *482*, 165-73.

123. Puoci, F.; Iemma, E.; Muzzalupo, R.; Spizzirri, U. G.; Trombino, S.; Cassano, R.; Picci, N. *Macromolecular Bioscience* **2004,** *4*, 22-26.

124. Sellergren, B. *Journal of Chromatography A* **1994,** *673*, 133-41.

125. Büyuktiryaki, S.; Say, R.; Denizli, A.; Ersöz, A. *Talanta* **2007,** *71*, 699-705.

126. Sellergren, B. *Analytical Chemistry* **1994,** *66*, 1578-72.

127. Say, R.; Birlik, E.; Ersöz, A.; Yilmaz, F.; Gedikbey, T.; Denizli, A. *Analytica Chimica Acta* **2003,** *480*, 251-58.

128. Say, R.; Ersöz, A.; Turk, H.; Denzili, A. *Separation and Purification Technology* **2004,** *40*, 9-14.

129. Hosoya, K.; Yoshikazo, K.; Tanaka, N.; Kimata, K.; Araki, T.; Haginaka, J. *Chemistry Letters* **1994,** 1437-38.

130. Matsui, J.; Kato, T.; Takeuchi, T.; Suzuki, M.; Yokoyama, K.; Tamiya, E.; Karube, I. *Analytical Chemistry* **1993,** *65*, 2223-24.

131. Haginaka, J. *Journal of Chromatography B* **2008,** *866*, 3-13.

132. Sanbe, H.; Haginaka, J. *Journal Of Pharmaceutical And Biomedical Analysis* **2003,** *30*, 1835-44.

133. Haginaka, J.; Kagawa, C. *Analytical Sciences* **2003,** *19*, 39-42.

134. Nakamura, M.; Ono, M.; Nakajima, T.; Ito, Y.; Aketo, T.; Haginaka, J. *Journal Of Pharmaceutical And Biomedical Analysis* **2005,** *37*, 231-37.

135. Haginaka, J.; Takehira, H.; Hosoya, K.; Tanaka, N. *Journal of Chromatography* **1998,** *816*, 113-21.

136. Haginaka, J.; Sanbe, H.; Takehira, H. *Journal of Chromatography A* **1999,** *857*, 117-25.

137. Haginaka, J.; Sakai, Y.; Naimatsu, S. *Analytical Sciences* **1998,** *14*, 823-26.

138. Haginaka, J.; Kagawa, C. *Journal of Chromatography A* **2002,** *948*, 77-84.

139. Haginaka, J.; Kagawa, C. *Journal Of Chromatography B-Analytical Technologies In The Biomedical And Life Sciences* **2004,** *804*, 19-24.

140. Haginaka, J.; Tabo, H.; Kagawa, C. *Journal Of Pharmaceutical And Biomedical Analysis* **2008,** *46*, 877-81.

141. Haginaka, J.; Kagawa, C. *Analytical and Bioanalytical Chemistry* **2004,** *378*, 1907-12.

142. Li, Y. C.; Fu, Q. Q.; Zhang, Q. Q.; He, L. C. *Analytical Sciences* **2006,** *22*, 1355-60.

143. Haginaka, J.; Sakai, Y. *Journal Of Pharmaceutical And Biomedical Analysis* **2000,** *22*, 899-907.

144. Shimizu, K. D., "Binding Isotherms", *Molecularly Imprinted Materials: Science & technology*, Ramstrom, Y. A., Ed.; (Marcel Dekker, New York, **2005**) 419-434.

145. Andersson, H. S.; Koch-Schmidt, A. C.; Ohlson, S.; Mosbach, K. *Journal Of Molecular Recognition* **1996,** *9*, 675-82.

146. Sellergren, B.; Shea, K. J. *Journal of Chromatography A* **1995,** *690*, 29-39.

147. Allender, C.; Brain, K. R.; Heard, C. M. *Chirality* **1997,** *9*, 233-37.

148. Umpleby, R. J.; Baxter, S. C.; Chen, Y. Z.; Shah, R. N.; Shimizu, K. D. *Analytical Chemistry* **2001,** *73*, 4584-91.

149. Umpleby, R. J.; Bode, M.; Shimizu, K. D. *Analyst* **2000,** *125*, 1261-65.

150. Szabelski, P.; Kaczmarski, K.; Cavazzini, A.; Chen, Y. B.; Sellergren, B.; Guiochan, G. *Journal of Chromatography A* **2002,** *964*, 99-111.

151. Yang, G.; Wang, D.; Li, Z.; Zhou, S.; Chen, Y. *Chromatographia* **2003,** *58*, 53-58.

152. Guo, T. Y.; Xia, Y. Q.; Hao, G. J.; Song, M. D.; Zhang, B. H. *Biomaterials* **2004,** *25*, 5905-12.

153. Rushton, G. T.; Karns, C. L.; Shimizu, K. D. *Analytica Chimica Acta* **2005,** *528*, 107-13.

154. Garcia-Calzon, J. A.; Diaz-Garcia, M. E. *Sensors and Actuators B: Chemical* **2007,** *123*, 1180-94.

155. Freundlich, H. *Colloid and Capillary Chemistry Metheun, London* **1926,** *1926*.

156. Umpleby, R. J.; Baxter, S. C.; Bode, M.; Berch, J. K.; Shah, R. N.; Shimizu, K. D. *Analytica Chimica Acta* **2001,** *435*, 35-42.

157. Umpleby, R. J.; Rushton, G. T.; Shah, R. N.; Rampey, A. M.; Bradshaw, J. C.; Berch, J. K.; Shimizu, K. D. *Macromolecules* **2010,** *34*, 8446-52.

158. Holland, N.; Frisby, J.; Owens, E.; Hughes, H.; Duggan, P.; McLoughlin, P. *Polymer* **2010,** *51*, 1578-84.

159. Cormack, P. A. G.; Elorza, A. Z. *Journal of Chromatography B* **2004,** *804*, 173-82.

160. Sing, K. S. W. *Pure and Applied Chemistry* **1982,** *54*, 2201-18.

161. Lowell, S.; Shields, J.; Thomas, M.; Thommes, M. *Characterisation of Porous Solids and Powders: Surface Area, Pore Size and Density,* (Kluwer Academic Publishers., Dordrecht, The Netherlands., **2004**).

162. Webb, P. A.; Orr, C. *Analytical Methods in Fine Particle Technology,* 1st Edition.; (Micromeritics Instrument Corp., **1997**).

163. Spivak, D. A. *Advanced Drug Delivery Reviews* **2005,** *57*, 1779-94.

164. Kyzas, G. Z.; Bikiaris, D. N.; Lazaridis, N. K. *Chemical Engineering Journal* **2009,** *149*, 263-72.

165. Malvern Instruments, http://www.malvern.co.uk./, (**2008**).

166. Farrington, K.; Regan, F. *Biosensors and Bioelectronics* **2007,** *22*, 1138-46.

167. Gonzalez, G. P.; Hernando, P. F.; Alegria, J. S. D. *Analytica Chimica Acta* **2006,** *557*, 179-83.

168. O'Mahony, J.; Molinelli, A.; Nolan, K.; Smyth, M. R.; Mizaikoff, B. *Biosensors and Bioelectronics* **2005,** *20*, 1884-93.

169. Sellergren, B.; Hall, A. J. "Fundamental aspects of the synthesis and characterisation of imprinted polymer networks", *Molecularly imprinted polymers. Man-made mimics of antibodies and their applications in analytical chemistry.*, Sellergren, B., Ed.; (Elsevier, Amsterdam, **2001**) 21-55.

170. Shea, K. J.; Sasaki, D. Y. *Journal of the American Chemical Society* **1991,** *113*, 4109-20.

171. Sellergren, B. *Journal of Chromatography A* **2001,** *906*, 227-52.

172. Ansell, R. J. *Advanced Drug Delivery Reviews* **2005,** *57*, 1809-35.

173. Nicholls, I. A.; Ramstrom, O.; Mosbach, K. *Journal of Chromatography A* **1995,** *691*, 349-53.

174. Dauwe, C.; Sellergren, B. J. *Journal of Chromatography A* **1996,** *753*, 191-200.

175. Yu, C.; Mosbach, K. *Journal of Chromatography A* **2000,** *888*, 63-72.

176. Wulff, G. *Angewandte Chemie-International Edition* **1995,** *34*, 1812-32.

177. Tamayo, F. G.; Martin-Esteban, A. *Journal of Chromatography A* **2005,** *1098*, 116-22.

178. Kempe, M.; Mosbach, K. *Journal of Chromatography A* **1994,** *664*, 276-79.

179. Nilsson, K.; Lindell, J.; Norrlöw.O.; Sellergren, B. *Journal of Chromatography A* **1994,** *680*, 57-61.

180. Lin, J. M.; Nakagama, T.; Uchiyama, J.; Hobo, T. *Chromatographia* **1996,** *43*, 585-91.

181. Nilsson, J.; Spégel, P.; Nilsson, S. *Journal of Chromatography A* **2004,** *804*, 3-12.

182. de Boer, T.; Mol, R.; de Zeeuw, R. A.; de Jong, G. J.; Sherrington, D. C.; Cormack, P. A. G.; Ensing, K. *Electrophoresis* **2002,** *23*, 1296-300.

183. Cacho, C.; Schweitz, L.; Turiel, E.; Perez-Conde, C. *Journal of Chromatography A* **2008,** *1179*, 216-23.

184. MIP Technologies, http://www.miptechnologies.com/, (**2009**).

185. Tamayo, F. G.; Turiel, E.; Martin-Esteban, A. *Journal of Chromatography A* **2007,** *1152*, 32-40.

186. Puoci, F.; Curcio, M.; Cirillo, G.; Iemma, F.; Spizzirri, U. G.; Picci, N. *Food Chemistry* **2008,** *106*, 836-42.

187. Chapuis, F.; Pichon, V.; Lanza, F.; Sellergren, B.; Hennion, M.-C. *Journal of Chromatography B* **2004,** *804*, 93-101.

188. Farrington, K.; Magner, E.; Regan, F. *Analytica Chimica Acta* **2006,** *566*, 60-68.

189. Li, Y. H.; Yang, T.; Qi, X. L.; Qiao, Y. W.; Deng, A. P. *Analytica Chimica Acta* **2008,** *624*, 317-25.

190. Beltran, A.; Marcé, R. M.; Cormack, P. A. G.; Borrull, F. *Journal of Chromatography A* **2009,** *1216*, 2248-53.

191. Caro, E.; Marce, R. M.; Cormack, P. A. G.; Sherrington, D. C.; Borull, F. *Journal of Chromatography B* **2004,** *813*, 137-43.

192. Pascale, M.; De Girolamo, A.; Visconti, A.; Magan, N.; Chianella, I.; Piletska, E. V.; Piletsky, S. A. *Analytica Chimica Acta* **2008,** *609*, 131-38.

193. Caro, E.; Marce, R. M.; Borrull, F.; Cormack, P. A. G.; Sherrington, D. C. *TrAC Trends in Analytical Chemistry* **2006,** *25*, 143-54.

194. Luo, W.; Zhu, L.; Yu, C.; Tang, H.; Heqing, T.; Yu, H.; Li, X.; Zhang, X. *Analytica Chimica Acta* **2008,** *618*, 147-56.

195. Masque, N.; Marce, R. M.; Borrull, F.; Cormack, P. A. G.; Sherrington, D. C. *Analytical Chemistry* **2000,** *72*, 4122-26.

196. Ou, J.; Hu, L.; Hu, L.; Li, X.; Zou, H. *Talanta* **2006,** *69*, 1001-06.

197. Caro, E.; Marce, R. M.; Cormack, P. A. G.; Sherrington, D. C.; Borrull, F. *Journal of Chromatography A* **2003,** *995*, 233-38.

198. Mullett, W. M.; Walles, M.; Levsen, K.; Borlak, J.; Pawliszyn, J. *Journal Of Chromatography B-Analytical Technologies In The Biomedical And Life Sciences* **2004,** *801*, 297-306.

199. Zhang, Z.; Zhang, H.; Hu, Y.; Yao, S. *Analytica Chimica Acta* **2010,** *661*, 173-80.

200. Piletsky, S.; Turner, A. "A new generation of chemical sensors based on MIPs", *Molecular Imprinting Polymers.*, Piletsky, S.; Turner, A., Eds.; (Landes Bioscience, **2004**) Chapter 9.

201. Piletsky, S. A.; Piletska, E. V.; Panasyuk, T.; Elskaya, A. V.; Levi, R.; Karube, I.; Wulff, G. *Macromolecules* **1998,** *31*, 2137-40.

202. Prasad, K.; Prathish, K. P.; Gladis, J. M.; Naidu, G. R. K.; Rao, T. P. *Sensors and Actuators B: Chemical* **2007,** *123*, 65-70.

203. Alizadeh, T.; Ganjali, M. R.; Zare, M.; Norouzi, P. *Electrochimica Acta* **2010,** *55*, 1568-1574.

204. Piletsky, S.; Piletskaya, E. V.; Sergeyeva, T.; El'Skaya, A.; Panasyuk, T. *Sensors and Actuators B: Chemical* **1999,** *60*, 216-20.

205. Chen, P.-Y.; Vittal, R.; Nien, P.-C.; Liou, G.-S.; Ho, K.-C. *Talanta* **2010,** *80*, 1145-51.

206. Gobi, K. V.; Tanaka, H.; Shoyama, Y.; Miura, N. *Sensors and Actuators B: Chemical* **2005,** *111-112*, 562-71.

207. Feng, L.; Liu, Y.; Tan, Y.; Hu, J. *Biosensors and Bioelectronics* **2004,** *19*, 1513-19.

208. Dickert, F. L.; Hayden, O. *Trac-Trends in Analytical Chemistry* **1999,** *18*, 192-99.

209. Piletska, E. V.; Guerreiro, A. R.; Romero-Guerra, M.; Chianella, I.; Turner, A. P. F.; Piletsky, S. A. *Analytica Chimica Acta* **2008,** *607*, 54-60.

210. Allender, C. J.; Richardson, C.; Woodhouse, B.; Heard, C. M.; Brain, K. R. *International Journal of Pharmaceutics* **2000,** *195*, 39-43.

211. Hiratani, H.; Fujiwara, A.; Tamiya, Y.; Mizutani, Y.; Alvarez-Lorenzo, C. *Biomaterials* **2005,** *26*, 1293-98.

212. Alvarez-Lorenzo, C.; Concheiro, A. *Journal Of Chromatography B-Analytical Technologies In The Biomedical And Life Sciences* **2004,** *804*, 231-45.

Chapter 2

Synthesis and evaluation of suspension and bulk imprinted polymers using 2-aminopyridine as template

2.1 Introduction

In this study molecularly imprinted polymers (MIPs) were prepared using 2-aminopyridine (2-apy) as the template molecule employing two different polymerisation strategies: suspension and bulk methods. The size and shape of the MIP particles are important to their performance. The development of novel MIP materials including spheres, involves taking into account the required molecular recognition properties along with the material format.

Improvements in the morphology of MIP particles have been achieved using suspension or precipitation polymerisation procedures that allow one to obtain microspheres with regular size and shape [1]. Kempe *et al*. [2] developed a straight-forward route to prepare spherical MIP beads using a method that involved the formation of droplets in mineral oil by vigorous mixing followed by transformation of these droplets into beads by photo-induced free radical polymerisation.

Knowledge of particle sizes and the size distribution of a polymer is an essential requirement for the controlled production of spherical polymer beads. Particle size and size distribution have a significant effect on the mechanical strength, density, chemical and thermal properties of the finished polymer. The use of particle size and size distribution data as relative measurements is very significant when monitoring size distribution as a process control indicator [3;4].

The particle size distribution of the MIP is related to polymer swelling. Particle size studies were performed by Turner *et al*. [5], investigating the influence of swelling. A polar aprotic solvent dimethylformamide (DMF) was used in the production of a MIP capable of recognising ochratoxin A under aqueous conditions. It was found that polymer swelling caused changes in the binding site cavities. It was also found that a MIP with a higher average particle size performed poorly relative to a MIP with a smaller average particle size.

Alternative MIP formats including microspheres synthesised by suspension polymerisation [2;6] and precipitation [7] methods have been reported. However, the differences in actual rebinding characteristics of different MIP formats, based on

molecular interactions under a variety of rebinding conditions received little attention, until a comprehensive study was carried out recently by Wei *et al*. [1]. The study was aimed at correlating the obtained porosities for different polymer formats (particles, microspheres and sub-microspheres) with differences observed during rebinding studies. These results provided useful guidelines for controlling the particle properties for desired applications such as HPLC separations.

The template species utilised in this study, 2-apy, is a heterocyclic compound. Aminopyridines are widely used in pharmacological and medical applications [8;9]. Some of them show anaesthetic properties and have been used in the preparation of drugs for certain brain diseases [9]. The molecular structure of the 2-apy molecule is shown in Figure 2.1.

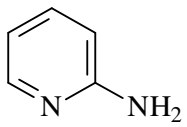

Figure 2.1 Molecular structure of 2-aminopyridine (2-apy).

The role of non-covalent interactions in the association of aminopyridines is a particularly attractive area for study for a number of reasons. Firstly,, 2-apy has high solubility in a variety of solvents over a range of polarities. Secondly, 2-apy presents limited functionality as it only possesses a pyridyl nitrogen capable of acting as a hydrogen acceptor (i.e. base) and an amino function capable of acting as both a hydrogen donor and acceptor in hydrogen bonding interactions [10]. Indeed, molecules which have 'structural parameters such as an embedded 2-apy sub-structure allow for good molecular recognition properties' [11]. Thirdly, 2-apy has demonstrated non-covalent molecular imprinting using methacrylic acid (MAA) by Jie *et al*. [12]. Furthermore, Cummins *et al*. [10] have molecularly imprinted 2-apy by non-covalent imprinting in a bulk monolith polymerisation using an acrylic polymer system. Both the template, 2-apy, and the functional monomer, MAA have the potential to interact via two point hydrogen bonding with each other. It is very important that the template and functional monomer form stable host guest complexes in the pre-polymerisation mixture, as the principle of molecular imprinting lies in the

preservation of the pre-polymerised host guest structure into a polymer matrix. Jie and He [12] employed ^{1}H NMR spectroscopy to investigate the pre-polymerisation mixture before polymerisation takes place. Chloroform was the solvent chosen in their study as it is of low polarity and does not interfere with hydrogen bonding. It was proposed that the interactions characterised between 2-apy and MAA were mainly co-operative hydrogen bonding interactions as demonstrated in Figure 2.2. The hydrogen and/or nitrogen of the amino group of 2-apy were involved in hydrogen bonding formation and the pyridyl nitrogen could also be involved in hydrogen bonding as a hydrogen acceptor.

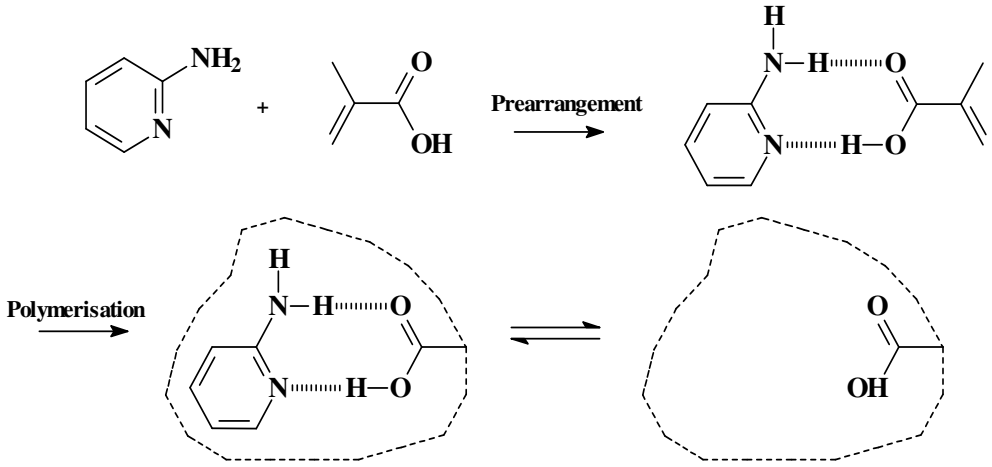

Figure 2.2 **Proposed interaction mechanism of 2-apy template with MAA as functional monomer [12].**

Cummins et al. [13] reported a systematic cross-selectivity study which extended the work carried out by Jie and He [12] in order to develop a further understanding of the imprinting and recognition process. The template 2-apy and 10 structural analogues were imprinted in order to assess binding characteristics in a cross-selectivity study. The species chosen were selected in order to facilitate the assessment of various characteristics of template structure crucial to selective recognition. All polymers demonstrated varying degrees of selectivity with the exception of one species 2-dimethylaminopyridine (2-dmapy) [13]. Conclusions drawn from the study suggest that while the ability of the 10 species to form a co-operative hydrogen-bonding interaction may be advantageous it is not a requirement.

In this chapter the MIPs and corresponding NIPs (non-imprinted polymers) prepared by suspension and bulk polymerisation methods were characterised and evaluated with respect to their binding ability and morphology. Additionally, solvent swell studies were also conducted on these polymers.

The surface morphology of the microspheres and irregular shaped particles was studied by scanning electron microscopy (SEM) analysis. Size analysis by SEM enabled direct observation of the polymer sample under study and consequent determination of size based on a defined measurement of the diameter. The primary benefit of SEM is that it provides information not only on particle size but on particle shape and surface texture. However, limitations in the SEM method arise from sample preparation and image irregularities. Dry powder specimens exhibit agglomerative effects, which do not accurately reflect the true distribution. Thus, a key way of ensuring accurate particle size distribution is by the use of non-imaging methods of size determination such as a laser diffraction particle size analyser which presents more meaningful data. In this study the influence of speed, temperature and cross-linker on particle size distribution of beads and ground particles was investigated by a particle size analyser in order to consolidate the morphology results by SEM.

Objectives of the research

The main objectives of the work in this chapter were:

- To compare and evaluate binding properties, yield of system and morphology of 2-apy imprinted polymers prepared by suspension and bulk polymerisation methods (employing mineral oil as the continuous phase) and bulk polymerisation methods,
- To examine and optimise the suspension polymerisation method under different synthetic conditions, i.e. different agitation speeds and different temperatures in order to assess the impact on the overall performance of the spherical beads in terms of affinity, yield, morphology and particle size distribution,

- To investigate the degree of swelling on exposure to different organic solvents to ascertain physical characteristics of the suspension polymers which would aid in understanding the nature of recognition in MIPs and
- To assess suspension and bulk polymerisation methodologies using different cross-linkers and characterise these by equilibrium binding studies, SEM and particle size distribution in order to investigate the influence of a different cross-linker on the overall performance of the MIP.

2.2 Experimental

2.2.1 Materials

Table 2.1 List of reagents employed

Reagent	Supplier	Assay
Methacrylic acid	Aldrich	99 %
Trimethylolpropane trimethacrylate	Aldrich	
Ethylene glycol dimethacrylate	Aldrich	98 %
*Mineral oil, white, heavy	Aldrich	
2,2′-Azo bis(2-methylpropionitrile)	Aldrich	98 %
1,1-Azobis(cyclohexanecarbonitrile)	Aldrich	98 %
2-Aminopyridine	Aldrich	99 + %
Acetonitrile	Romil	> 99.9 %
Acetone	Riedel-de Haën	> 99 %
Methanol	Romil	> 99.9 %
Chloroform	Riedel-de Haën	> 99.8 %
Acetic Acid	Fluka	> 99.8 %
Water	Fluka	99.8 %
Molecular sieves	Aldrich	3Å 3.2 mm

* Mineral oil: Viscosity Dynamic > 110 - 130 mPas

Viscosity kinematic approx. 34.5 mm^2/s

All the above reagents were purchased from Sigma-Aldrich (Dublin, Ireland). HPLC grade solvents were obtained from Lennox (Dublin, Ireland) and were used without

further purification. To maintain the absence of moisture, chloroform, acetonitrile and methanol were stored over molecular sieves.

2.2.2 Equipment

- 20 mL VGA-220-241K glass vials.
- VGA-221-506R 20 mm rubber stoppers.
- VGA-221-510-D 20 mm crimp seals.
- Endicott test sieves: 25 – 75 µm - Lennox Laboratory Supplies.
- Sterile syringes: Omnifix – Lennox Laboratory Supplies.
- Syringe nylon filters: 0.45 µm, 13 mm diameter – Antech Technologies Ltd.
- Eppendorf tubes
- Stuart Scientific Orbital Incubator S150.
- Vortex, Disruptor Gene, Scientific Industries.
- Desktop Centrifuge, Sigma Aldrich.

2.2.3 Instrumentation

2.2.3.1 Dispersing device equipped with dispersing tool.

The generation of droplets for the production of suspension mixtures was carried out with a DI 25 basic dispersing device equipped with a S25-N18G dispersing tool (IKA®-Werke, Gmbh & Co., Germany). The dispersion tool consists of a shaft and a dispersion head. The bearing of the S25 N shaft is made of PTFE suitable for use with solvents. The dispersion head 18G is used to produce suspensions with particle sizes in the micrometer scale range. The 5 speed settings range from 8000 – 24000 rpm.

2.2.3.2 Photochemical mini-reactor model.

A Rayonet photochemical mini-reactor model RMR-600 (Branford, CT, USA), was used to polymerise suspension polymers. The homogenised mixture was placed in the photochemical mini-reactor equipped with eight 'black-light blue' lamps (USHIO

F4T5/BLB, 8 W each) and polymerised at 350 nm at room temperature for approximately 2 h.

2.2.3.3 UV/Visible spectrophotometer

UV analysis was used to follow the removal of both template and acetic acid from the filtrate stream (Section 2.2.7). The sized and washed polymer particles and beads were used in UV equilibrium binding studies (Section 2.2.8) which were performed on a Varian CARY 50 Ultraviolet-Visible spectrophotometer (JVA Ireland Ltd) to determine binding to the polymer and to assess target affinity.

2.2.3.4 Scanning electron microscope

The morphology of the polymers was characterised by SEM, using a Hitachi S4000 SEM System and Sputter Coater – Unit PS3 Agar Aids for Electron Microscopy.
Polymer samples were attached to 10 mm diameter metal mounts using carbon tape and sputter coated with gold under vacuum in an argon atmosphere. The coated samples were then analysed using SEM with a voltage of 20 keV. The surface of the polymer samples was then scanned at the desired magnification to study the morphology of the beads and particles. Triplicate analysis was performed for suspension polymers. Data was based on the average diameter of 9 beads taken from three images.

2.2.3.5 Viscometer

The viscosity of mineral oil was measured using a Brookfield DV-II+ Programmable Viscometer (Brookfield Engineering Labs., Inc., Middleboro, MA, USA) with a temperature probe.

2.2.3.6 Particle size analyser

Particle size measurements were conducted on the Malvern Mastersizer 2000 (Malvern Instruments Ltd., Worcestershire, UK) equipped with light scattering

technology. The Mastersizer was used in conjunction with a sample dispersion unit, ''Hydro 2000S'' that allows wet samples to be measured.

Water was unsuitable for this study as the polymer particles floated on the surface. Methanol was chosen as the suspension medium (dispersant) when measuring a wet sample. The operating parameters in this study (Table 2.2) were chosen based on using the estimated RI (based on typical values for similar acrylate materials) as a starting point and examining the fit to confirm the suitability of the value chosen.

Table 2.2 Operating parameters for particle size analysis using Mastersizer 2000 particle size analyser.

Properties	Values
Obscuration Limits	5 - 12 %
Stirrer speed	2100 rpm
Optical property of sample	1.52
Dispersant R.I	1.33
Absorption	0.1
Model	'General purpose – Spherical/Irregular'

2.2.4 Synthesis of spherical beads by suspension polymerisation in mineral oil

The methodology used for synthesis of spherical beads in this study, was an adapted method employed for MIP preparation by suspension polymerisation in mineral oil [14]. For the preparation of the 2-apy imprinted polymer (MIP), a pre-polymerisation solution was prepared by dissolving 0.1882 g (2 mmol) of the template 2-apy and 0.258 g (3 mmol) of the functional monomer (MAA). Into the mixture, 3.38 g (10 mmol) of the cross-linker (TRIM) and 0.115 g (0.7 mmol) of the initiator (AIBN), with (8 mL) of the porogen (acetonitrile) were added. The pre-polymerisation solution was purged with a stream of nitrogen gas for 3 min, and 3 mL of the solution were suspended in 57 mL of mineral oil in a 100 mL graduated cylinder. Reference non-imprinted polymer (NIP) beads were synthesised following the same procedure as the MIP but without the addition of the 2-apy template. The pre-polymerisation mixtures were dispersed at five different speeds, ranging from 8000 – 24000 rpm for 30 s with homogeniser DI 25 basic dispersing device, equipped with an S25-N18G dispersing tool. The homogenised mixture was placed in a Rayonet photochemical

mini-reactor and polymerised at 350 nm at room temperature for approximately 2 h. The oil-bead mixtures were filtered and washed with approximately 200 mL of chloroform and acetone to remove the mineral oil.

2.2.5 Synthesis of ground particles by bulk monolith polymerisation

For comparison bulk monolith polymers were prepared according to the method described by Cummins *et al*. [13]. Bulk monoliths were polymerised employing the same pre-polymerisation composition as the suspension polymerisation method in a 20 mL glass vial fitted with 20 mm rubber stopper and sealed. Reaction vessels were sealed using 20 mm crimp seals. As the polymerisation initiator is activated by exposure to a heat source the initiator ACCN was used instead of AIBN, employed in the production of suspension polymers. The reference non-imprinted polymer (NIP) was prepared in an identical manner but in the absence of the template species. The glass vials were placed in a 60 ^{o}C oven overnight during which polymerisation occurred. The resulting polymer monoliths were ground using a mortar and pestle and wet-sieved in acetone using Endicott test sieves. Size fractions of between 25 – 75 μm diameters were collected.

2.2.6 Viscosity measurements of mineral oil at varying temperatures

The viscosity of the mineral oil at a range of temperatures (4.5 – 30 ^{o}C) was measured in triplicate, in the Low Form Griffin 200 mL beaker accompanying the Brookfield Viscometer. Spindle no.1 at a shear rate of 10 rpm, for mineral oil was used, which resulted in measurements of 10 to 100 on the instrument % Torque scale. The same spindle/speed combination was used for all analysis. Before taking measurements it was ensured that the mineral oil was free from entrapped air. A constant temperature bath was used to maintain the temperature of the mineral oil. After the temperature of the inside wall of the container reached the lowest temperature of approximately 4.5 ^{o}C, the motor speed was turned on. Spindle no.1 was rotated in the mineral oil in the beaker for approximately 10 min prior to reading to ensure temperature equilibration. The viscosity measurement was continual at a constant shear rate of 10 rpm, keeping rotation speed of the spindle constant. The temperature was systematically varied by

increasing the temperature of the sample container to cover the desired range (4.5 – 30 ^{o}C).

2.2.7 Template removal

The same method was used for the removal of the template from both particle and bead polymers. Particles and beads were agitated in a hot solution of acidified methanol (with acetic acid) (10 % v/v), for 15 min and then gravity filtered with approximately 50 mL of hot methanol. Continual washing with hot methanol was performed until both template and acetic acid had been removed from the polymers. Acetic acid was employed as it disrupts non-covalent interactions and methanol being polar in nature also aids in the removal of the template, as it competes with the functional monomer for hydrogen bonding interactions. UV analysis was used to follow the removal of both template and acetic acid from the filtrate stream. Washing continued until the template could no longer be detected in the filtrate (λ_{max} = 290 nm). Particles and beads were re-suspended in 50 mL of hot methanol and Buchner filtered followed by washing with a further 50 mL of hot methanol to remove residual acetic acid and oven dried at 80 ^{o}C to a constant mass.

2.2.8 Equilibrium binding analysis

Batch rebinding studies were performed to determine binding to the polymer and to assess target affinity. The sized and washed polymer particles and beads were used in UV equilibrium binding studies. Triplicate 50.0 mg quantities of both MIP and NIP polymers were accurately weighed and placed in 10 mL volumetric flasks. Each polymer was loaded with 5 mL of 0.2 mM 2-apy in the chosen solvent (acetonitrile or chloroform). Flasks were stoppered and oscillated at 25 ^{o}C for 16 h. After equilibration, polymer solutions were filtered to remove polymer particles using 10 mL syringes fitted with a nylon filter tip. The quantity of reloaded template 2-apy bound to the polymer, *Q*, was analysed by UV analysis at the pre-determined wavelength (2-apy: λ_{max} = 290 nm). The amount of 2-apy bound to the polymers, *Q*, was calculated by subtracting the absorbance of free substrate remaining in the post

equilibrium solution, from the initial concentration (0.2 mM 2-apy solution). Average values of triplicate independent results were obtained.

2.2.9 Procedure for making particle size measurements

A representative sample of polymer particles (≈ 100 mg) were suspended in the dispersant solvent methanol using a bench top sonicator for 20 min until no particle aggregate was observed. The parameters in Table 2.2 were chosen for particle size analysis. The suspended sample was gradually added, until laser obscuration was within the limits (Table 2.2).

The scattering pattern from the prepared sample was measured. The detector array within the optical bench is made up of many individual detectors. Each detector collects the light scattering from a particular range of angles. The detector array takes a 'snapshot' of the scattering pattern, 1000 measurement snaps were taken over a measurement time of 6 s. The average of three measurements was reported by the software for each analysis and each polymer was analysed in triplicate.

The particle size values were calculated on a volume basis assuming a normal distribution, as this best reflects the sensitivity of the system. The results are expressed as Dv10, Dv50 and Dv90 and are the default percentiles shown in the analysis report. The median of a particle size distribution (Dv50) is the most critical and is defined as the size (in μm) above and below which 50% of the particles lie. The Dv10 is the size of particle below which 10 % of the sample lies and Dv90 is the size of particle below which 90 % of the sample lies.

It is important that a good sample background is obtained to ensure accurate results. Dirty cell windows can lead to a poor background due to light scattering from the contaminant. The system was repeatedly washed with water and then methanol prior to each sample analysis to guarantee confidence in the results obtained. Additionally, the instrument was calibrated with a 9 μm diameter NIST traceable latex standard prior to analysis and the results were within specification.

2.2.10 Swelling studies

Analysis of polymer swelling was carried out based on a method described by Piletsky *et al*. [15]. Swelling ratios (S_r) of the suspension polymers were measured using three different solvents: acetonitrile, methanol and chloroform. 50 mg of the polymers were weighed in an Eppendorf tube and 1 mL of the appropriate solvent was added and the tube was sealed. The tubes were mixed using a vortex and put on a shaker at 250 rpm for 24 h at room temperature during which equilibrium was achieved. The tubes were centrifuged at a high speed (13500 rpm) for 5 min, the excess solvent was drained off and the tube was then weighed. Because the density of chloroform (1.484 g mL^{-1}) hindered centrifuging, the swelling effect on the polymers was determined by adding 100 μL increments of chloroform to the polymers until saturation was achieved. The chloroform was left to equilibrate with the polymers for 1 h between each addition. The swelling ratio (S_r) was calculated using the Equation 2.1:

$$S_r = \frac{\text{Mass of swollen polymer - Mass of dry polymer}}{\text{Mass of dry polymer}} \qquad \textbf{Equation 2.1}$$

2.3 Results and discussion

2.3.1 Comparative study of suspension versus bulk polymers

Spherical beads formed at 8000 rpm were compared to irregularly shaped particles prepared by the standard bulk monolith method. For this study, 2-apy as template, MAA as functional monomer, TRIM and EGDMA as cross-linkers were utilised in the preparation of polymers. In addition, mineral oil was employed as the continuous phase in the suspension method. Comparison of binding results obtained with an imprinted polymer and one prepared in the absence of the template can provide insight into the contribution of specific and non-specific binding. Specific binding formed during the imprinting procedure results in recognition sites selective for the template. Non-specific binding is due to random interactions within the polymer material and is measured by estimating the binding to the non-imprinted polymer where the template has been omitted from the polymer synthesis.

Imprinting factor (IF) is a quantitative measurement of specificity. The IF values were calculated from the equilibrium binding studies results. Rebinding experiments were conducted in both acetonitrile and chloroform to investigate the effect of solvent polarity on the retention of the substrate materials. The IF expresses the ratio of specific to non-specific binding for each polymer system.
IF can be expressed in Equation 2.2 as:

$$IF = \frac{Qbound_{MIP}}{Qbound_{NIP}} \qquad \textbf{Equation 2.2}$$

Where *Qbound* = quantity of analyte bound to the polymer.

Table 2.3 lists the IF values obtained for reloading 2-apy in acetonitrile and chloroform.

Table 2.3 **IF values obtained for suspension and bulk imprinted polymers reloaded in the chosen solvent (acetonitrile and chloroform). Results are based on triplicate analysis with errors based on ± 1 standard deviation.**

Solvent	Suspension polymer	Bulk imprinted polymer
Acetonitrile	2.1 ± 0.0008	2.1 ± 0.0004
Chloroform	1.5 ± 0.0004	1.3 ± 0.0010

An increase in IF values for suspension and bulk monolith imprinted polymers reloaded in acetonitrile was observed relative to the polymers reloaded in chloroform. A graphical illustration of the results in Table 2.3 is presented in Figure 2.3.

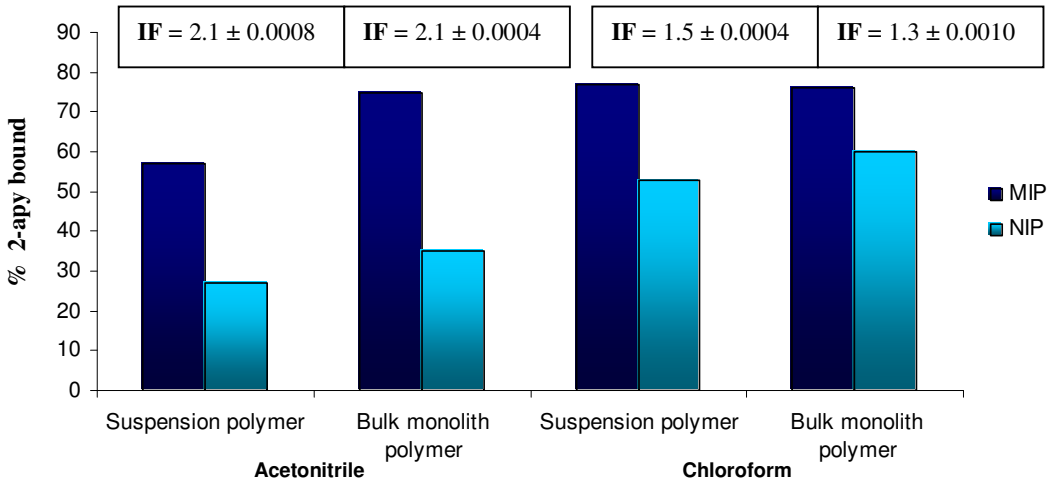

Figure 2.3 **Comparison of equilibrium binding results for suspension (8000 rpm) and bulk monolith imprinted polymers reloaded in acetonitrile and chloroform, respectively. Results are based on triplicate analysis with error bars based on ± 1 standard deviation.**

In all cases, the results demonstrate that the affinity or degree of binding of the template species for the imprinted polymer is greater than for the non-imprinted polymer. This is consistent with more specific binding sites as the MIP was prepared in the presence of the template and should have cavities specific to the template, whereas the NIP does not. Cummins *et al.* [13] demonstrated similar binding results in a previous study, i.e. the MIP was capable of reloading the template with much

higher affinity than the NIP. The binding of a 2-apy imprinted polymer in chloroform gave a specificity of 1.59 and the binding of a 2-apy imprinted polymer in acetonitrile gave a specificity of 2.29 [13].

Analysis of the binding characteristics in acetonitrile in this study for both sets of polymers demonstrated identical IF values, i.e. IF = 2.1 for both suspension and bulk polymers. However, there was a slightly greater capacity in the bulk polymer monolith compared to the suspension polymer.

Analysis of the binding characteristics in chloroform for both sets of polymers showed similar results in terms of affinity. IF values were quite similar, IF = 1.5 for the suspension polymer and IF = 1.3 for the bulk polymer monolith. The NIP profiles for the binding of 2-apy were higher in chloroform in comparison to acetonitrile, indicating substantial non-specific binding which could be due to the polarity of the solvent as mentioned. Another possible reason for higher binding in chloroform is its solvating power for 2-apy, i.e. relative binding to polymer versus solvent. The overall capacity for bulk polymers in chloroform was greater than in acetonitrile.

As mentioned in the introduction, Jie and He [12] investigated the pre-polymerisation mixture between 2-apy and MAA in chloroform. As the solvent has low polarity it is thought it does not interfere with hydrogen bonding, hence enhancing pre-polymerisation complex formation between template molecule and the functional monomer, and as a result optimising binding states. Spivak *et al*. reported that the best conditions for rebinding the template are generally achieved in the same solvent as the one used during polymer preparation so as to mimic the interactions existing prior to and during the polymerisation [16]. This was evident by the optimum rebinding of *ortho*- or *para*-xylene using the solvent employed in the polymerisation demonstrated by Yoshizako *et al*. [17]. In this study, acetonitrile was the porogen employed in polymer synthesis. As it is a more polar than chloroform a possible disruptive effect with the co-operative hydrogen bonding interaction would be expected to occur thus reducing the degree of both specific and non-specific binding. Cummins *et al*. [13] investigated this hypothesis in a previous study by reloading bulk polymers in chloroform and acetonitrile. The MIP produced a reduction in capacity for 2-apy in acetonitrile relative to chloroform.

2.3.1.1 Percentage yield recoveries of suspension versus bulk polymers

An important requirement for any analytical system is the ability of the system to act in a reproducible way. Percentage yield recoveries for the MIP and NIP polymers prepared for suspension and bulk polymerisations are presented in Table 2.4. The percentage yields quoted are the average of three syntheses.

Table 2.4 **Percentage yield recoveries for suspension (8000 rpm) and bulk imprinted polymers. Results based on average values for triplicate synthesis with errors based on ± 1 standard deviation.**

% Suspension MIP	% Suspension NIP	% Bulk MIP	% Bulk NIP
48 ± 0.16	45 ± 0.20	45 ± 0.09	43 ± 0.08

The recoveries in terms of polymer yield were similar for both suspension and bulk polymerisation methodologies. A slightly higher percentage yield recovery for suspension MIPs was noticed. This may be linked to the integrity of the light in the UV photochemical reactor. Suspension polymerisation temperature was initiated at 36 ^{o}C. Bulk monolith polymers were placed in a 60 ^{o}C oven to start the polymerisation process. Predominantly polymerisations were performed at room temperature.

Furthermore, the polymer monoliths were ground and sieved to obtain size fractions of between 25 – 75 µm diameters. This resulted in loss of useable polymers which impacted on the percentage yield recoveries shown in Table 2.4.

2.3.2 Characterisation of spherical beads and ground particles by SEM analysis

The surface morphologies of the bulk monolith and suspension polymers were assessed by scanning electron microscopy (SEM). Figure 2.4 illustrates the SEM images for the ground MIP particles prepared by bulk polymerisation (a) and MIP beads prepared by suspension polymerisation at 8000 rpm (b) respectively.

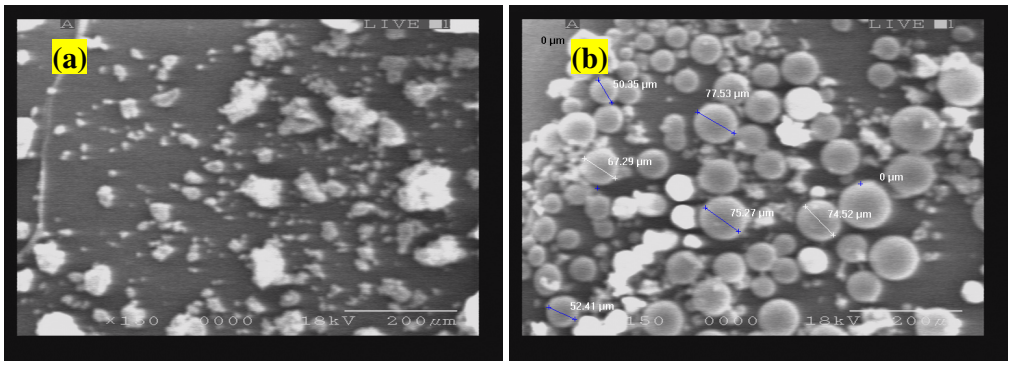

Figure 2.4 **SEM images of (a) MIP particles prepared by bulk polymerisation and (b) MIP beads prepared at a speed of 8000 rpm. Accelerating voltage: 18 kV; Working magnification of 150 X in both panels.**

Different morphologies were revealed between the polymers as exemplified by the SEM images. In Figure 2.4 (a) the crushed bulk materials provide irregularly shaped particles with dimensions of 25 – 75 µm. As clearly seen in Figure 2.4 (b), the polymeric beads have a spherical form and the majority of the beads had a smooth surface, but some had a rough exterior due to adsorbed smaller particles onto the surface. The average bead size of the suspension polymer was 78 µm ± 4.1 µm in diameter. The greater number of smaller particles in the bulk polymer monoliths could also indicate a link to the increased overall capacity observed in rebinding studies as seen in Section 2.3.1.

The SEM results obtained for this comparative study of beads and particles agree with those in the literature. In previous work by Kempe *et al.* [14], similar trends were observed. The majority of the beads were spherical with a smooth surface although some appear to be fused, and the average bead size was 19 µm. The bulk particles possessed an irregular shape with size fractions of 25 – 50 µm. Due to the uniform size and shape of spherical beads, they are preferred over bulk particles for most applications of MIPs, especially stationary phases in chromatography [14].

2.3.3 Optimisation of suspension polymerisation procedure

The key aim of this research element was to optimise the suspension polymerisation method for the production of controlled particle size molecularly imprinted polymers. A number of parameters were investigated to optimise the suspension polymers which

included agitation speeds, temperature, and cross-linker on the suspension and bulk polymerisation methods in order to optimise affinity and particle size.

2.3.3.1 Influence of agitation speed on suspension polymers

Suspension polymerisations were carried out at 5 different speeds: 8000, 9500, 13500, 20500 and 24000 rpm. Percentage yield recoveries for the MIP and NIP polymers are presented in Table 2.5.

Table 2.5 **Percentage yield recoveries for suspension imprinted polymers carried out a 5 speeds. Results based on average values for triplicate synthesis with errors based on ± 1 standard deviation.**

Polymer	% 8000 rpm	% 9500 rpm	% 13500 rpm	% 20500 rpm	% 24000 rpm
MIP	48 ± 0.16	55 ± 0.20	56 ± 0.10	57 ± 0.21	55 ± 0.15
NIP	45 ± 0.20	52 ± 0.24	55 ± 0.26	51 ± 0.20	55 ± 0.15

Spherical beads were produced at all 5 speeds with comparable % yields for all polymers.

U.V equilibrium binding analysis was performed for the suspension polymers in 0.2 mM 2-apy in acetonitrile as detailed in Section 2.2.8. The results are displayed in Figure 2.5 and Table 2.6.

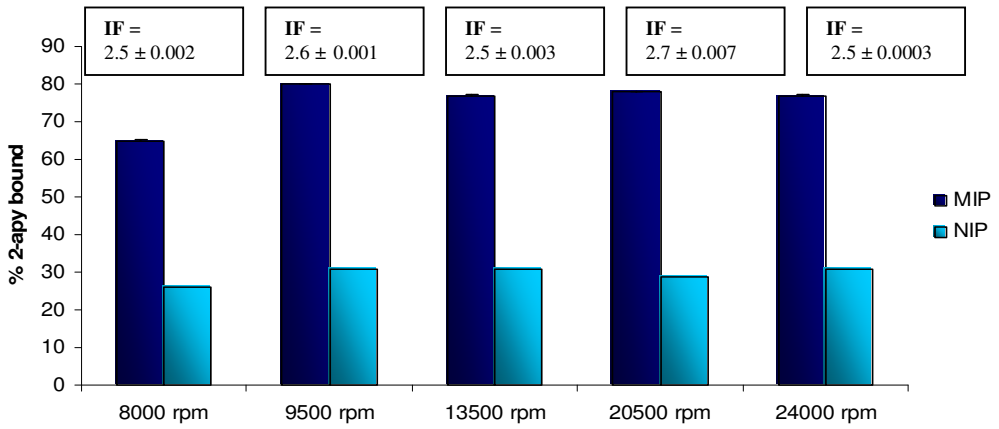

Figure 2.5 **Comparison of equilibrium binding analysis of 2-apy suspension imprinted polymers prepared at different agitation speeds. Results are based on triplicate analysis with error bars based on ± 1 standard deviation.**

Table 2.6 **IF values obtained for suspension polymers performed at 5 different speeds reloaded in acetonitrile. Results are based on triplicate analysis with errors based on ± 1 standard deviation.**

Polymer (rpm)	% MIP BOUND	% NIP BOUND	IF
8000	65 ± 0.01	26 ± 0.02	2.5 ± 0.002
9500	80 ± 0.01	31 ± 0.01	2.6 ± 0.001
13500	77 ± 0.02	31 ± 0.01	2.5 ± 0.003
20500	78 (± 0.001)	29 ± 0.06	2.7 ± 0.007
24000	77 ± 0.01	31 ± 0.01	2.5 (± 0.0003)

Very little difference was seen across the 5 speeds of polymers in terms of IF values. The highest capacity was observed for 9500 rpm, with negligible deviation seen in affinity values (i.e. % bound results) for speeds above 9500 rpm. A similar degree of specificity was maintained across the 5 speeds, (IF: 2.5 and 2.7). A slight increase in specificity was seen for 9500 and 20500 rpm polymers (IF = 2.6 and 2.7) respectively. Equilibrium binding results demonstrated robustness in the design of the suspension polymerisation procedure.

2.3.3.2 Characterisation of MIP beads prepared at low and high speeds by SEM analysis

SEM images were taken of the beads prepared at 9500 rpm and 24000 rpm respectively, as shown in Figure 2.6 (a) and (b).

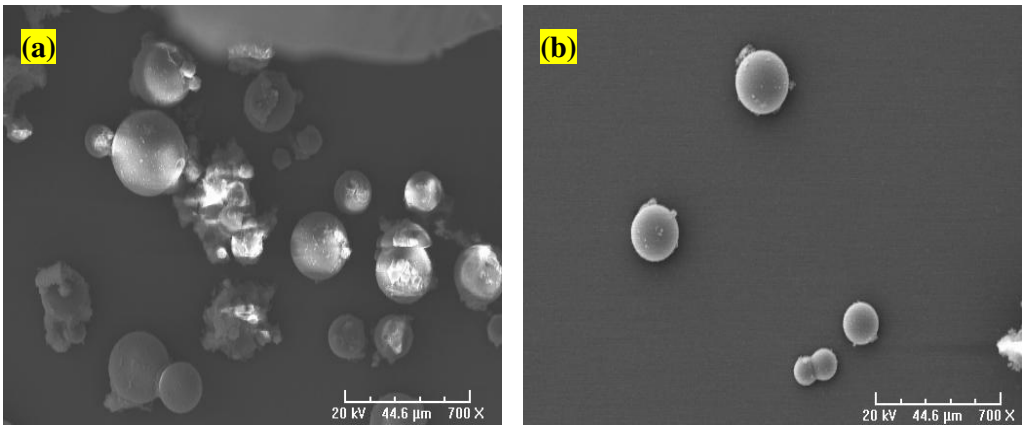

Figure 2.6 **SEM images of beads prepared at (a) 9500 rpm (b) 24000 rpm. Accelerating voltage: 20 kV; Working magnification 700X in both panels.**

The beads show more agglomeration at 9500 rpm (Figure 2.6 (a)) in comparison to the surface morphology of the beads prepared at 24000 rpm (Figure 2.6 (b)). The majority of beads at 9500 rpm were spherical although some appear to be fused. A noticeable difference between images (a) and (b) was the size distribution of the beads. At the higher speed, 24000 rpm the size distribution was shifted toward decreased bead diameters, with average bead sizes of 22 µm ± 1.5 µm found. Mixing at 9500 rpm, the average bead size of the suspension polymer was 39 µm ± 2.2 µm in diameter.

2.3.3.3 Influence of different speeds on the size distribution of spherical polymers

The particle size distribution results are presented in Table 2.7 for the suspension polymers prepared at five different speeds.

Table 2.7 **Results obtained from particle size studies for suspension MIP and NIP polymers prepared at 5 different agitation speeds with TRIM as cross-linker. Results based on triplicate analysis with errors based on ± 1 standard deviation.**

Polymer (rpm)	Dv10(µm)	Dv50(µm)	Dv90(µm)
8000 MIP	4.13 ± 0.004	24.38 ± 0.005	79.19 ± 0.054
8000 NIP	2.99 ± 0.055	25.74 ± 0.043	97.41 ± 0.467
9500 MIP	4.67 ± 0.034	23.78 ± 0.017	187.25 ± 0.158
9500 NIP	3.99 ± 0.082	22.57 ± 0.023	258.95 ± 0.360
13500 MIP	2.59 ± 0.063	22.26 ± 0.072	101.44 ± 0.689
13500 NIP	3.86 ± 0.099	21.66 ± 0.137	229.50 ± 0.722
20500 MIP	2.51 ± 0.023	17.30 ± 0.029	54.29 ± 0.066
20500 NIP	2.17 ± 0.087	17.47 ± 0.049	84.07 ± 0.112
24000 MIP	2.35 ± 0.014	15.06 ± 0.041	85.91 ± 0.182
24000 NIP	3.71 ± 0.004	16.80 ± 0.002	306.85 ± 0.017

In agreement with SEM images shown in Figure 2.6, an evident trend for Dv50 values was observed for spherical polymers prepared at different speed rates. As the speed increased, the Dv50 value correlated with a decrease in particle size, this was graphically illustrated in Figure 2.7. The smallest particle size measurement was obtained at the highest speed, 24000 rpm MIP = 15.06 ± 0.041 µm (Table 2.7).

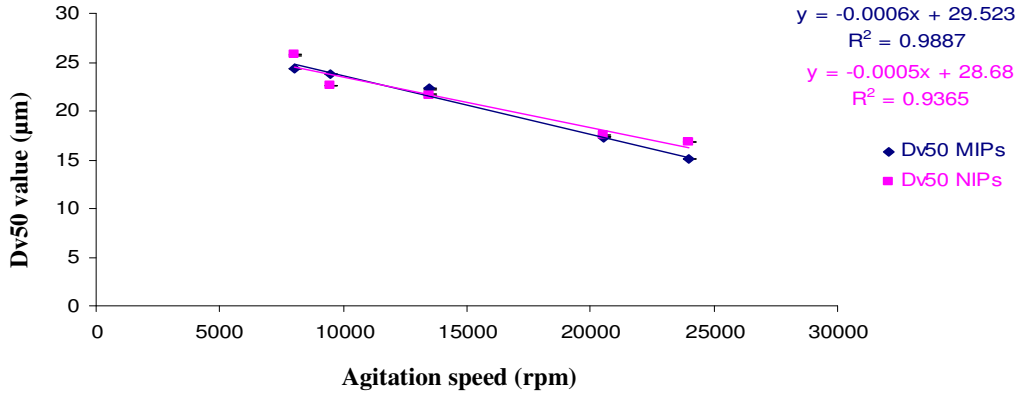

Figure 2.7 **The Dv50 values plotted against agitation speed.**

Another interesting observation of MIP versus NIP at each speed is that the Dv50 value for the NIP was larger in the majority of cases, except for 9500 rpm. Kempe *et al*. [14] also characterised the MIPs in their study by particle size distribution and found that agitation speed affected the size of the beads. The size distribution was shifted toward decreased bead diameter with increasing rate, mixing at 8000, 13500 and 20500 rpm for 30 s resulted in average bead sizes of 22, 18 and 16 µm, respectively.

A trend was observed for Dv10 values across the speeds, the values decreased going from 8000 rpm to 24000 rpm (with the exception of 9500 rpm) for MIP polymers, the NIP polymers exhibited random distribution of sizes. The Dv90 values of the NIP for all speeds also showed a random distribution of sizes. A trend was observed between the MIPs and NIPs at each speed, where the NIPs exhibited greater Dv90 values in comparison to the MIPs. Figure 2.8 represents the overlay of the five speeds for suspension (a) MIP and (b) NIP polymers prepared with TRIM as cross-linker.

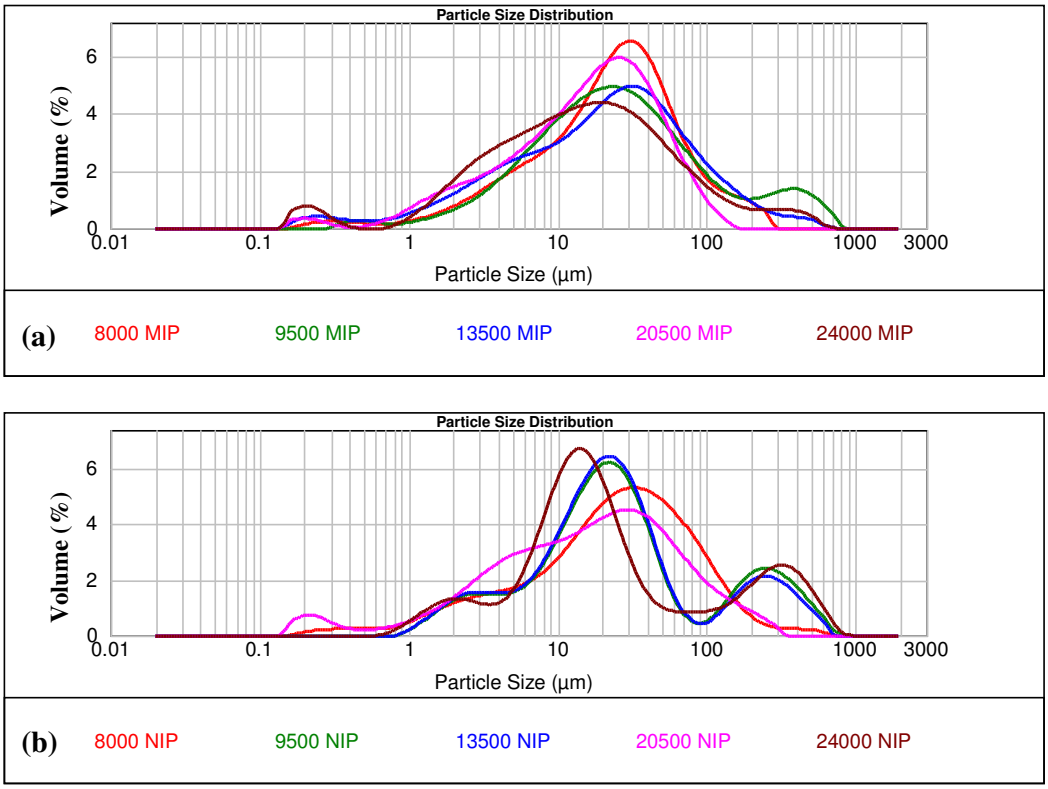

Figure 2.8 **Overlay of suspension (a) MIP and (b) NIP polymers prepared at 5 speeds using TRIM as cross-linker.**

From the overlays of the size distributions for suspension MIP and NIP polymers, it was observed that the particle size distribution was broad across all speed sizes, as the speed increased the distribution shifted and the particle size for the higher speeds had a smaller diameter size. The approximate spread in particle size distribution for suspension MIP and NIP polymers in Figures 2.8 (a) and (b) was determined by calculating the peak widths at half the peak height. Bimodal distributions, i.e. two peak maxima were observed for some NIP polymers in Figure 2.8 (b). The results are shown in Table 2.8.

Table 2.8 **The approximate spread in particle size distribution determined by calculating the peak widths at half the peak height for suspension MIP and NIP polymers prepared at 5 speeds.**

Polymer (rpm)	Particle size spread (µm)
8000 MIP	103
8000 NIP	1st Peak = 98 & 2nd Peak = 314
9500 MIP	62
9500 NIP	1st Peak = 25 & 2nd Peak = 301
13500 MIP	78
13500 NIP	1st Peak = 39 & 2nd Peak = 287
20500 MIP	57
20500 NIP	76
24000 MIP	67
24000 NIP	1st Peak = 121 & 2nd Peak = 360

In Table 2.8, the particle size spread for MIP and NIP polymers prepared at lower speeds exhibited broad distributions which gradually decreased as the speed increased. For instance, suspension MIPs prepared at 8000 rpm had an average particle size spread 103 µm in contrast to MIPs prepared at 24000 rpm with average spread of 67 µm. Bimodal distributions, i.e. two peak maxima were observed for some NIP polymers in Figure 2.8 (b). The ratio of these NIP polymers varied a lot (Table 2.8). For the NIPs, particle size spreads were measured for 8000 rpm: 1st peak = 98 µm and 2nd peak = 314 µm and 24000 rpm: 1st peak = 121 µm and 2nd peak = 360 µm, respectively. In the majority of cases the NIPs exhibited a broader spread in comparison to the MIPs which was possibly due to more aggregates being present in the NIPs over the MIPs.

The particle size distribution results for suspension polymers prepared at different speeds (Table 2.7) indicated that mixing rate had an impact on the size distribution of polymers. By increasing the rate, polymers moved towards decreased bead diameters. Suspension polymerisation methods are very sensitive to parameters such as stirrer speed [18]. To achieve the formation of droplets of pre-polymerisation solution in mineral oil, vigorous agitation of the two phases was required. Using a homogeniser, agitation and the formation of the droplets could be carried out effectively in a cylinder-shaped vessel. Kempe *et al*. [14] reported that the volume of the pre-polymerisation solution in the mineral oil suspension mixture affected the yield, size, and shape of the polymers formed. It was found that using 30 % volume or more of the pre-polymerisation solution in mineral oil, rapid phase separation of the droplets in the oil occurred which resulted in the formation of large-sized particles. Employing 5 % volume of the pre-polymerisation solution, the suspension of droplets in the oil was more stable during polymerisation [14]. Consequently a ratio of 1:19 volume portions of pre-polymerisation solution to mineral oil was used in the formation of polymers beads in this study.

2.3.3.4 Swelling study analysis

In order to better elucidate the difference between the dry state and the solvent swollen state of the MIP polymers, swelling tests were performed in acetonitrile, methanol and chloroform. The method was adapted from Piletsky *et al*. [15], who calculated and presented their results in terms of weight ratio. The data for MIP and NIP suspension polymers prepared at 5 different speeds are represented in Table 2.9.

Table 2.9 **Results obtained from solvent swell studies in acetonitrile, methanol and chloroform for suspension MIP and NIP polymers prepared at 5 different speeds using TRIM as cross-linker. Results based on triplicate analysis with errors based on ± 1 standard deviation.**

	Swell Ratio (S_r)		
Polymer (rpm)	**Acetonitrile**	**Methanol**	**Chloroform**
8000 MIP	3.61 ± 0.43	3.41 ± 0.17	9.89 ± 0.07
8000 NIP	3.64 ± 0.20	3.58 ± 0.06	10.88 ± 0.22
9500 MIP	3.64 ± 0.01	4.11 ± 0.06	11.05 ± 0.17
9500 NIP	3.96 ± 0.04	4.21 ± 0.71	11.26 ± 0.10
13500 MIP	3.78 ± 0.14	4.36 ± 0.36	11.10 ± 0.13
13500 NIP	3.90 ± 0.03	4.54 ± 1.05	10.99 ± 0.24
20500 MIP	4.57 ± 0.20	4.47 ± 0.74	11.07 ± 0.01
20500 NIP	4.53 ± 0.05	4.77 ± 0.08	11.09 ± 0.03
24000 MIP	4.89 ± 0.35	4.65 ± 0.46	11.12 ± 0.10
24000 NIP	4.96 ± 0.09	4.69 ± 0.53	11.18 ± 0.03

In Table 2.9, nearly all the polymers had the lowest swelling factors in acetonitrile. Secondly, acetonitrile and methanol exhibited similar swelling to each other. Swelling in chloroform was significantly greater in comparison to acetonitrile and methanol. Koohpaei *et al*. [19] reported that swelling is most pronounced in chlorinated solvents, such as chloroform, as compared with solvents like acetonitrile. An obvious trend was observed across the three solvents employed in Table 2.9, as the rate of agitation increased, the swelling ratio increased in all three solvents in the MIPs. The reason for the increased swell ratio at higher agitation speeds could be due to the polymers being more flexible. For swell analysis 50 mg of each polymer was weighed. The total surface area of these polymers would increase as the sphere diameter decreases, i.e. more particles for a given mass, thus implying that a greater number of pores exist, leading to a greater volume of solvent sorbed and therefore a higher solvent swell ratio.

As methanol was employed as dispersant in particle size analysis, the solvent swell study in methanol for suspension MIPs prepared at five different speeds is graphically illustrated in Figure 2.9.

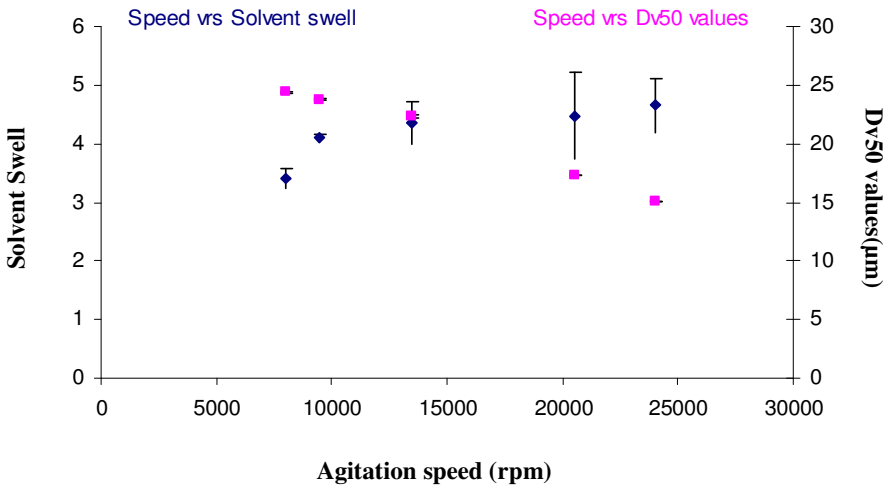

Figure 2.9 **Plot of solvent swell in methanol for suspension MIPs against five different speeds and their corresponding Dv50 values. Errors based on ± 1 standard deviation from triplicate analysis.**

In Figure 2.9, an increase in the solvent swell ratio in methanol for suspension MIPs correlated with increasing agitation speed, and a corresponding decreasing particle size. Therefore, the particle size study compared well with the swelling analysis in the same solvent.

2.3.3.5 Influence of temperature on viscosity of mineral oil

The viscosity of the mineral oil at a range of temperatures (4.5 – 30 ^{o}C) was measured in triplicate using the Brookfield Viscometer. The averages of the three readings of viscosity versus temperature for the mineral oil are plotted in Figure 2.10.

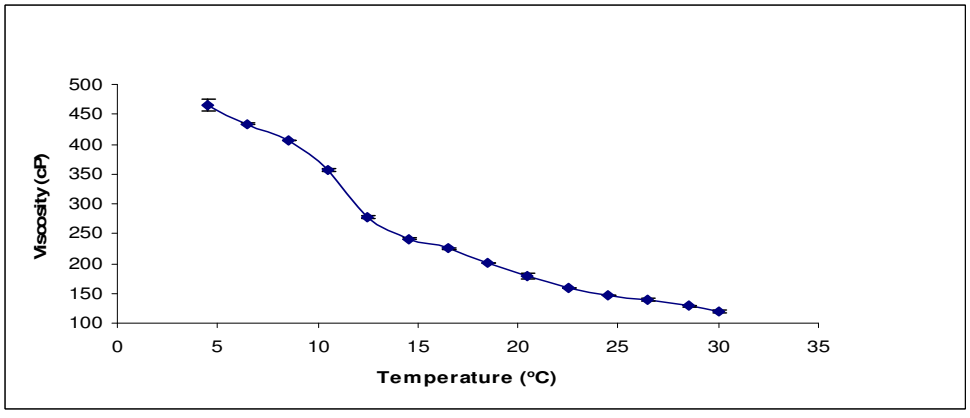

Figure 2.10 **Viscosity versus Temperature profile for mineral oil obtained from Brookfield Viscometer. Errors based on ± 1 standard deviation from triplicate analysis.**

During the polymerisation process, variation of physical properties such as viscosity can largely influence the droplet size distribution [20]. The objective of this study was to evaluate the effect of temperature on the viscosity of mineral oil at a range of temperatures (4 – 30 ^{o}C). A relatively small variation in temperature resulted in a significant change in viscosity as seen in Figure 2.10. Of significant importance is the sudden change in viscosity at 10 ^{o}C. It was reported that by increasing the viscosity of a suspension mixture the cohesive force will be enhanced thus promoting the droplets stability against break-up [21]. Increasing the viscosity of the continuous phase (mineral oil) can result in an increase in droplet stability by decreasing the droplet collision frequency [22]. In the following section suspension polymerisation of 2-apy imprinted polymers at two temperatures (4 and 25 °C) was carried out to study the effect of temperature variation on particle size.

2.3.3.6 Influence of different temperature on suspension polymers

U.V equilibrium binding analyses as detailed in Section 2.2.8 were performed for suspension polymers prepared at 4 °C in a cold room at a speed of 8000 rpm. Included for comparison purposes is the equilibrium binding results for suspension polymer prepared at 25 °C at a speed of 8000 rpm. The results including binding data for the 2 temperatures are displayed in Figure 2.11 and Table 2.10.

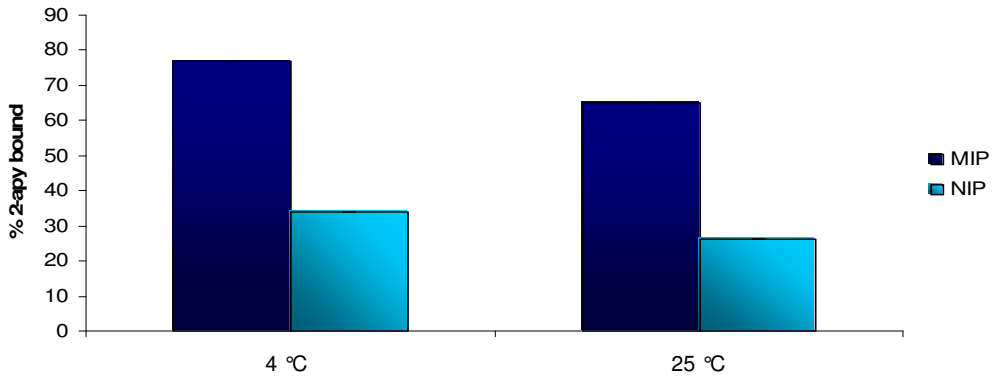

Figure 2.11 **Comparison of equilibrium binding analysis for 2-apy suspension imprinted polymers (8000 rpm) prepared at 2 different temperatures using a 0.2 mM 2-apy standard in acetonitrile. Results are based on triplicate analysis with error bars based on ± 1 standard deviation.**

Table 2.10 **IF values for suspension polymers (8000 rpm) performed at 2 different temperatures. Results are based on triplicate analysis with errors based on ± 1 standard deviation.**

Temperature °C	% MIP BOUND	% NIP BOUND	IF
4	77 ± 0.007	34 ± 0.003	2.3 ± 0.001
25	65 ± 0.005	26 ± 0.015	2.5 ± 0.002

Comparing the binding results there is a slight difference for the polymers prepared at 4 and 25 °C in terms of affinity values. A higher overall binding capacity was observed for both MIP and NIP polymers prepared in a 4 °C cold room in comparison to polymers prepared at 25°C. Agreeing with literature results, the lower temperature showed strongest binding [23]. The specificity was found to be slightly higher at 25 °C, (IF = 2.5) in comparison to 4 °C, (IF = 2.3). In a recent study by Koohpaei *et al*. [19] multivariate analysis was applied to the screening of MIPs. A higher temperature produced a negative influence on polymer performance. Thus, the lowest possible temperature must be selected, to avoid binding site degradation. Similar results were concluded in a study carried out by Piletsky *et al*. [24] who found that increased temperature exhibited a negative influence on complex formation between template and functional monomer.

Percentage yield recoveries for the MIP and NIP polymers prepared at two different temperatures, 4 and 25 °C are presented in Table 2.11.

Table 2.11 **Percentage yield recoveries for suspension polymers (8000 rpm) prepared at two different temperatures. Results based on average values for triplicate analysis with errors based on ± 1 standard deviation.**

4 °C		**25 °C**	
% MIP	**% NIP**	**% MIP**	**% NIP**
50 ± 0.20	45 ± 0.15	45 ± 0.31	45 ± 0.19

The recoveries in terms of polymer yield were better for suspension polymers prepared at 4 °C in comparison to 25 °C. The present results indicated that the polymerisation temperature played a role in the performance of the synthesised material. It is worthy of note, that the percentage yield recoveries of the NIPs remained the same. However, an improvement in percentage yield is seen in the MIP prepared at 4 °C, which is possibly linked to the stronger pre-equilibrium complex at

lower temperature. In this study, it was found that when synthesising polymers in the 4 °C cold room the photo-polymerisation time needed to be increased from 2 h to 6 h. Navarro *et al*. [23] have previously reported that polymers which were obtained by photo-initiation at the lowest temperature (4 °C) showed the strongest binding. They proposed that this effect is due to more stable interactions between monomer and the imprint molecule in the pre-polymerisation mixture at low temperature, leading to better defined imprinted sites in the polymer [23].

In this study, polymers prepared at 25 °C (room temperature) were initiated at 36 °C inside a UV reactor and the actual temperature inside the reaction vessel during polymerisation may be a lot higher than the initial temperature. As a result the temperatures of photo-polymerisations performed in a 4 °C cold room and at 25 °C in this study were monitored using a thermocouple which was placed in the middle of the reaction cylinder. As expected a higher temperature was reached during UV polymerisation, in a 4 °C cold room the reaction temperature was 22 °C and for polymerisations performed at 25 °C the reaction temperature was 48 °C.

2.3.3.7 Characterisation of MIP beads prepared at two temperatures by SEM analysis

The effects of reaction temperature (4 °C and 25 °C) on the physical properties were assessed by SEM analysis as shown in Figures 2.12 (a) and (b).

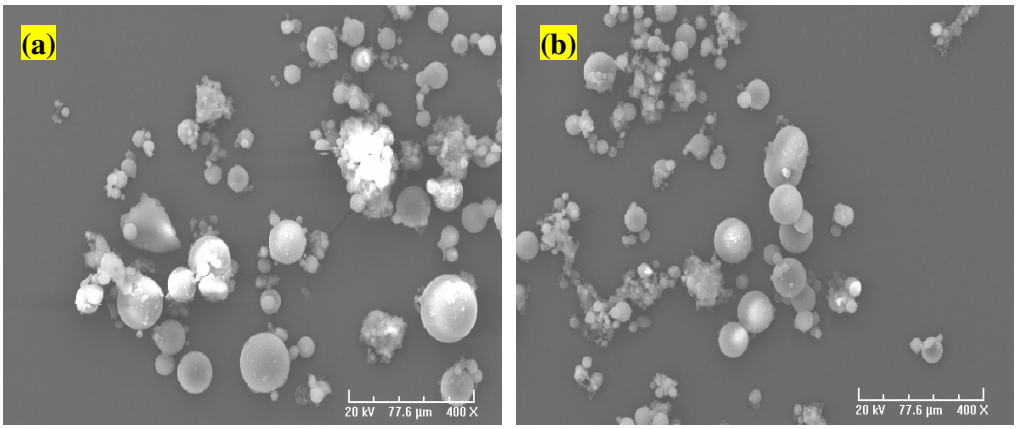

Figure 2.12 **SEM images of MIP beads 8000 rpm prepared (a) at 25 °C (b) in 4 °C cold room. Accelerating voltage: 20 kV; Working magnification 400X in both panels.**

Some obvious morphological differences were observed between the polymers. A decrease in temperature reduced the bead diameters as seen in Figure 2.12 (b). Less aggregation was also observed in the beads prepared at lower temperature. The average size of the beads was 56 µm ± 3.4 µm at 25 °C and 49 µm ± 4.3 µm at 4 °C.

The effect of temperature on UV initiated polymerisation on bead formation was investigated by SEM analysis and compared to polymers prepared in a thermostat-controlled water-bath by Gonzalez *et al*. [25]. Polymers were synthesised under UV light (365 nm) at 10 °C for 24 h and in a 60 °C water-bath for 20 h. SEM analysis demonstrated different textures of the resulting polymers. Polymers obtained with UV initiation, showed a more microporous structure compared to the particles obtained in the heated initiated polymerisation in the water-bath, which were larger. The slow polymerisation process by UV light in a colder environment gave more time for homogeneous, spherical particles to form.

2.3.3.8 Influence of different temperature on the size distribution of polymers

Extending the study in Section 2.3.3.6, polymers were prepared at two different speeds, 9500 and 24000 rpm in a 4 °C cold room. The results of the particle size distribution results are presented in Table 2.12.

Table 2.12 **Results obtained from particle size studies obtained for 9500 and 24000 rpm suspension MIP and NIP polymers at 4 °C and 25 °C with TRIM as cross-linker. Results based on triplicate analysis with errors based on ± 1 standard deviation.**

Polymer (rpm)	Dv10(µm)	Dv50(µm)	Dv90(µm)
9500 MIP 4 °C	2.51 ± 0.013	17.30 ± 0.021	54.29 ± 0.011
9500 NIP 4 °C	2.98 ± 0.003	18.41 ± 0.023	62.83 ± 0.240
9500 MIP 25 °C	4.67 ± 0.017	23.78 ± 0.058	187.25 ± 0.347
9500 NIP 25 °C	3.99 ± 0.006	22.57 ± 0.021	258.95 ± 0.141
24000 MIP 4 °C	2.37 ± 0.007	10.69 ± 0.022	30.97 ± 0.035
24000 NIP 4 °C	2.54 ± 0.008	14.49 ± 0.013	46.64 ± 0.017
24000 MIP 25 °C	2.35 ± 0.005	15.06 ± 0.022	85.91 ± 0.035
24000 NIP 25 °C	3.71 ± 0.010	16.80 ± 0.009	306.85 ± 0.342

Table 2.12 includes results for 9500 and 24000 rpm polymers prepared at the same speeds but at 25 °C (Table 2.7). Comparing the Dv50 values of the 9500 and 24000 rpm polymers at 4 °C and 25 °C, the size distribution for the polymers changed. The 9500 rpm MIP value decreased at the lower temperature from 23.78 to 17.30 µm, and the NIP value was smaller going from 22.57 to 16.55 µm. A similar trend was also observed for the 24000 rpm MIPs and NIPs at lower temperature (Table 2.12). By polymerising at a colder temperature a significant drop in the particle size distribution was exhibited in comparison to polymerisation at 25 °C. This was possibly due to the particles being more stabilised at the lower temperature which could account for the smaller bead sizes. Dv10 and Dv90 values exhibited a similar trend at the lower temperature for both speeds were lower for the MIPs and NIPs (Table 2.12).

Figure 2.13 represents the overlays of the MIP and NIP suspension polymers for (a) 9500 rpm and (b) 24000 rpm prepared at 4 °C and 25 °C respectively.

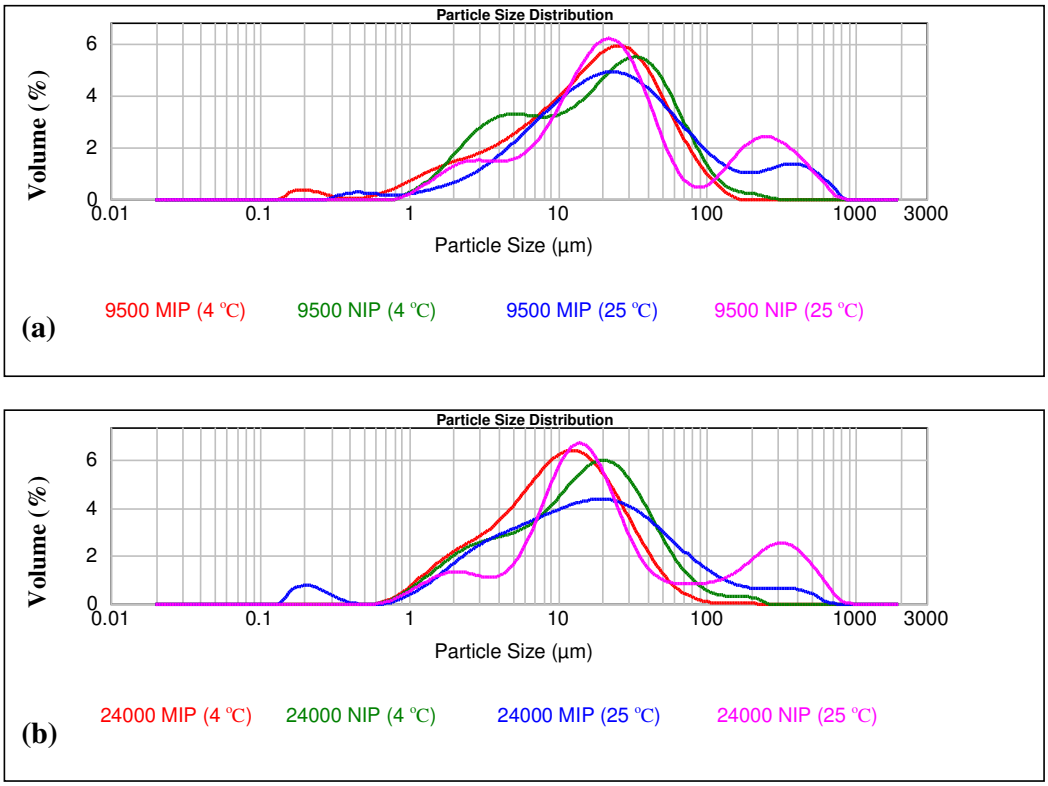

Figure 2.13 **Overlays of MIP and NIP suspension polymers for (a) 9500 rpm and (b) 24000 rpm prepared at 4 °C and 25 °C respectively with TRIM as cross-linker.**

From the graphical illustrations in Figures 2.13 (a) and (b), it is evident that the drop in polymerisation temperature caused a shift to lower particle size distributions for both the 9500 rpm and 24000 rpm suspension MIP and NIP polymers. The approximate spread in particle size distribution was determined by calculating peak widths at half the peak height, the spread is illustrated in Table 2.13.

Table 2.13 **The approximate spread in particle size distribution determined by calculating the peak widths at half the peak height for 9500 and 24000 rpm suspension MIP and NIP polymers prepared at 4 °C and 25 °C.**

Polymer (rpm)	Particle size spread (µm)
9500 MIP 4 °C	57
9500 NIP 4 °C	73
9500 MIP 25 °C	62
9500 NIP 25 °C	1st Peak = 25 & 2nd Peak = 301
24000 MIP 4 °C	32
24000 NIP 4 °C	46
24000 MIP 25 °C	67
24000 NIP 25 °C	1st Peak = 121 & 2nd Peak = 360

From Table 2.13 it was evident that there was a change in the spread in particle size distribution for both the 9500 and 24000 rpm suspension MIP and NIP polymers prepared at 4 °C and 25 °C. The particle size spread for 9500 rpm MIP and NIP polymers prepared at 4 °C decreased in comparison to the same polymers prepared at 25 °C, i.e. 9500 rpm MIP prepared at 4 °C = 57 µm but the MIP prepared at 25 °C = 62 µm. The same trend in decreasing particle size spread was observed for the 24000 rpm polymers prepared at the lower temperature.

2.3.4 Influence of different cross-linker on suspension and bulk polymerisation

Results presented to date in this chapter were prepared using TRIM as cross-linker. In order to assess the effect of cross-linker on the resulting MIP, a similar series of polymers were prepared using EGDMA as cross-linker. The binding characteristics of MIP and NIPs prepared using suspension and bulk polymerisation methods with EGDMA were assessed and compared to polymers prepared with TRIM as cross-

linker. The flexibility of the polymer chain could have an effect on the rigidity of the resultant polymers thus affecting binding affinity in the polymers. The same composition ratios as in Section 2.2.4 were applied in the preparation of polymers.

MIPs, synthesised by the non-covalent approach, most commonly use MAA as the functional monomer and EGDMA as the cross-linker. In the last 10 years or so, TRIM, containing three polymerisable units has been utilised in non-covalent molecular imprinting.

Percentage yield recoveries for suspension and bulk imprinted polymers prepared using EGDMA and TRIM as cross-linkers respectively are presented in Table 2.14.

Table 2.14 **Percentage yield recoveries for suspension (9500 rpm) and bulk imprinted polymers prepared using EGDMA and TRIM as cross-linkers respectively. Results based on average values for triplicate synthesis with errors based on ± 1 standard deviation.**

Cross-linker	% Suspension MIP	% Suspension NIP	% Bulk MIP	% Bulk NIP
EGDMA	54 ± 0.17	58 ± 0.27	42 ± 0.04	51 ± 0.01
TRIM	55 ± 0.20	52 ± 0.24	43 ± 0.09	45 ± 0.08

The yield data show that employing a different cross-linker had negligible impact on percentage yields for both sets of polymers as exhibited in Table 2.14.

U.V. equilibrium binding analysis as detailed in Section 2.2.8 was performed on suspension polymers prepared at 9500 rpm and bulk imprinted polymers prepared with both cross-linkers, EGDMA and TRIM. The results are illustrated in Figure 2.14.

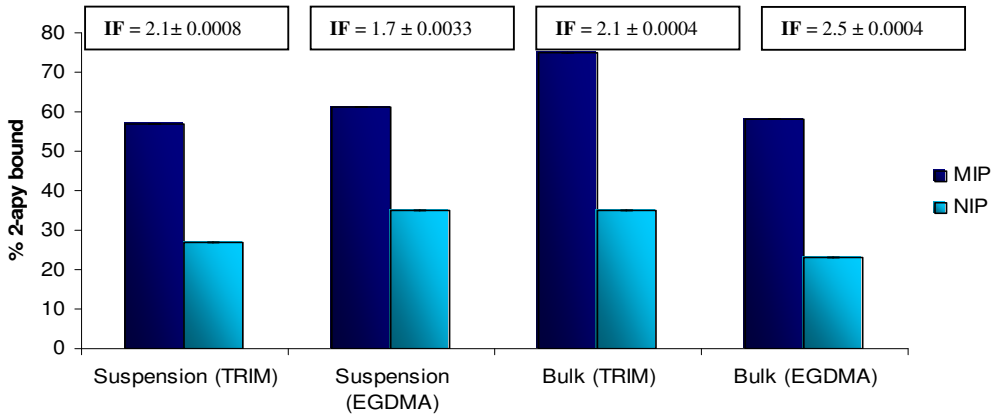

Figure 2.14 **Comparison of equilibrium binding analysis of 2-apy suspension and bulk imprinted polymers prepared with TRIM and EGDMA as cross-linkers. Results are based on triplicate analysis with error bars based on ± 1 standard deviation.**

The IF values for both suspension and bulk polymers prepared with EGDMA as cross-linker, indicated a high IF for the poly(MAA-*co*-EGDMA) system in the bulk method, IF = 2.5 The specificity was lower in the suspension imprinted polymer employing EGDMA as cross-linker (IF = 1.7). There was very little difference in the overall capacity between MIPs for the suspension and bulk polymers employing EGDMA, but there was less non-specific binding in the bulk (EGDMA) system. In the poly(MAA-*co*-TRIM) system the opposite trend was seen, with less non-specific binding in suspension imprinted polymer using TRIM. The bulk polymers in the poly(MAA-*co*-TRIM) system exhibited greater overall capacity in comparison to the poly(MAA-*co*-EGDMA) bulk polymer monolith.

In the literature similar opposing results were seen in some previous studies. Yu *et al.* [26] compared the performance of MAA-*co*-EGDMA to MAA-*co*-TRIM MIPs. The results indicated that the structural differences between these two kinds of imprinted polymers did not influence their recognition properties significantly as previously believed. Navarro *et al.* [23] also investigated EGDMA and TRIM as cross-linkers in the synthesis of bisphenol A using thermal and UV initiation polymerisation. The binding profiles showed a similar trend for the photo-initiated imprinted and non-imprinted polymers prepared at low temperatures.

Kempe and Mosbach prepared a TRIM based MIP [27] and results demonstrated that when a chiral stationary phase was used in liquid chromatography, the MIP exhibited improved load capacity, selectivity, and resolving capacity compared to EGDMA-based MIPs. However, in another study performed by Andersson *et al*. [28] the enantioselectivity of the EGDMA-derived MIPs was superior to the TRIM based MIPs.

2.3.4.1 SEM analysis of polymers using EGDMA as cross-linker

SEM images of suspension MIP and NIP polymers prepared using EGDMA are shown in Figures 2.15 (a) and (b). MIP and NIP bulk polymer monoliths prepared using EGDMA are shown in Figures 2.14 (c) and (d). Different morphological shapes are revealed between both suspension and bulk polymers as exemplified by the SEM images. The SEM image of the suspension MIP polymer prepared at 9500 rpm with TRIM as cross-linker was shown in Figure 2.6 (a) Section 2.3.3.2.

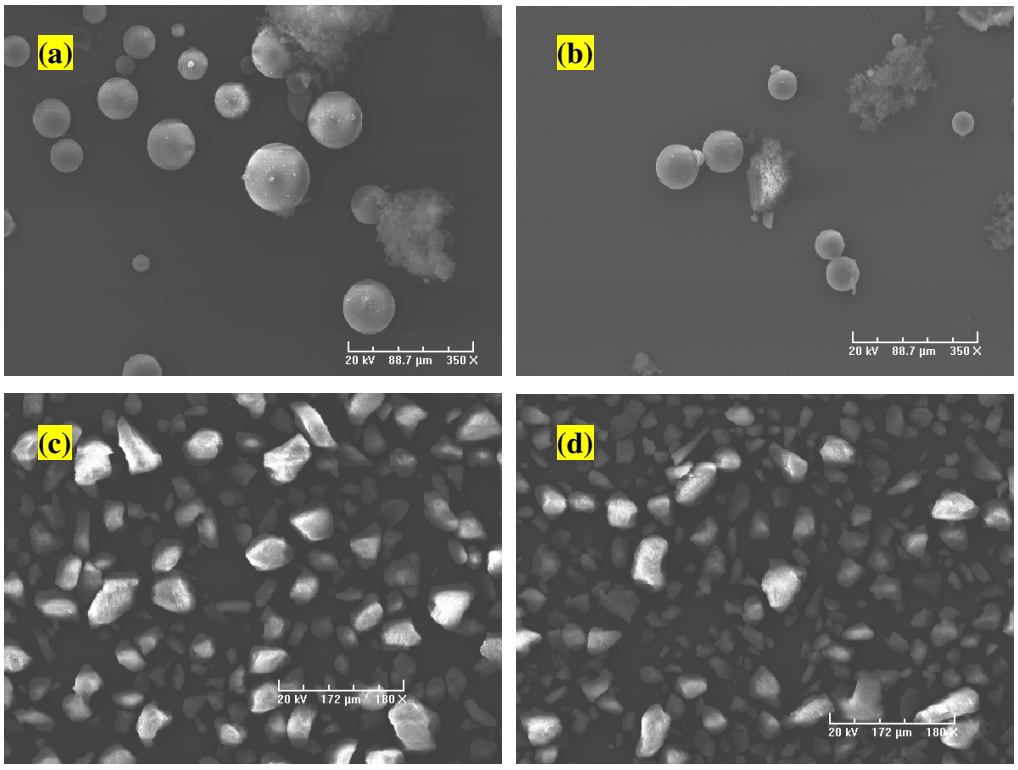

Figure 2.15 **SEM images of suspension polymers prepared at 9500 rpm using EGDMA as cross-linker (a) MIP (b) NIP beads. Accelerating voltage: 20 kV; Working magnification of 350 X in panel (a) and 300 X in panel (b). Bulk particles prepared using EGDMA as cross-linker (c) MIP particles (c) NIP. Accelerating voltage: 20 kV; Working magnification of 180X in panels (c) and (d).**

Figure 2.15 (a) and (b) showed that the images obtained for MIP and NIP suspension polymers employing EGDMA as cross-linker comprised of spherical beads. The average size of the beads was 43 µm ± 11.5 µm for suspension MIP and 36 µm ± 5.2 µm for suspension NIP. The template in the poly(MAA-*co*-EGDMA) suspension system may physically stabilise the suspension resulting in a larger bead size. An opposite trend was seen for the suspension MIP polymer shown in Figure 2.6 (a) (Section 2.3.3.2) using TRIM as cross-linker. The average size of the beads was 32.7 µm ± 8.81 µm for the suspension MIP prepared using TRIM as cross-linker. These results indicate the differences in morphologies of polymers prepared employing different cross-linkers.

Irregular shaped particles for MIP and NIP (EGDMA bulk polymer monoliths) are shown in Figure 2.15 (c) and (d). The particle diameters in the NIP appeared smaller than the MIP. This observation has a possible link to binding results obtained. Smaller particle sizes may imply more access to binding sites due to greater surface area per unit mass of polymer material resulting in an increase in non-specific binding. Evidently, changing cross-linker in polymer synthesis has a definite affect on the binding affinity and final polymer morphology obtained. A poly(MAA acid-*co*-TRIM) system has previously been shown to produce MIPs of high selectivity and load capacity [29]. From the results in this study the most favourable cross-linker for polymerising spherical beads is a system employing TRIM.

2.3.4.2 Influence of different cross-linkers on the size distribution of polymers

Table 2.15 presents the size distribution results analysis for bulk and suspension MIP and NIP polymers prepared with EGDMA and TRIM as cross-linkers. The suspension polymers were prepared at 9500 rpm.

Table 2.15 **Results obtained from particle size studies for bulk and suspension MIP and NIP polymers with EGDMA and TRIM as cross-linkers respectively. Results based on triplicate analysis with errors based on ± 1 standard deviation.**

Polymer	Dv10(µm)	Dv50(µm)	Dv90(µm)
Bulk (EGDMA) MIP	15.10 ± 0.009	36.41 ± 0.003	66.67 ± 0.003
Bulk (EGDMA) NIP	13.35 ± 0.001	36.49 ± 0.002	67.03 ± 0.007
Bulk (TRIM) MIP	9.89 ± 0.001	33.81 ± 0.004	64.71 ± 0.002
Bulk (TRIM) NIP	14.84 ± 0.003	37.12 ± 0.001	68.44 ± 0.004
Suspension (EGDMA) MIP	4.08 ± 0.011	24.37 ± 0.002	78.99 ± 0.026
Suspension (EGDMA) NIP	2.97 ± 0.051	25.91 ± 0.064	97.45 ± 0.022
Suspension (TRIM) MIP	3.41 ± 0.043	23.46 ± 0.015	101.22 ± 0.016
Suspension (TRIM) NIP	3.42 ± 0.034	23.70 ± 0.021	104.06 ± 0.033

The average Dv50 values for particle sizes of MIP and NIP bulk polymers prepared using EGDMA and TRIM as cross-linkers, are in the range of ≈ 33 – 34 µm for MIPs and ≈ 36 – 37 µm for NIPs. The particle size of bulk polymers is mainly affected by grinding and sieving (sieve: 25 – 75µm). Therefore, there was no difference in the size distribution for bulk polymers using two different cross-linkers.

The suspension MIP and NIP polymers used in this study were prepared at 9500 rpm. There was a significant difference between the MIP and NIP particle size distribution Dv50 values for the polymers prepared with TRIM and EGDMA. Smaller particle sizes for MIPs (≈ 24 µm) were found in the suspension polymers prepared with EGDMA in contrast to suspension polymer prepared at the same speed with TRIM which was 40 µm for MIP and 33 µm for NIP respectively.

For Dv10 values for the bulk MIP and NIP polymers prepared with EGDMA and TRIM, the MIP values were significantly smaller (Table 2.15). The same trend was seen for the Dv90 values but the MIP values were only slightly smaller than the NIPs. A similar trend in Dv10 and Dv90 values was also observed for the suspension MIP and NIP polymers prepared with EGDMA and TRIM, with one exception for the

suspension polymer prepared using EGDMA as cross-linker, Dv10 value MIP = 4.08 ± 0.011µm and NIP = 2.97 ± 0.051 µm.

Figure 2.16 represents the overlay of bulk and suspension polymers (a) MIPs and (b) NIPs prepared with different cross-linkers.

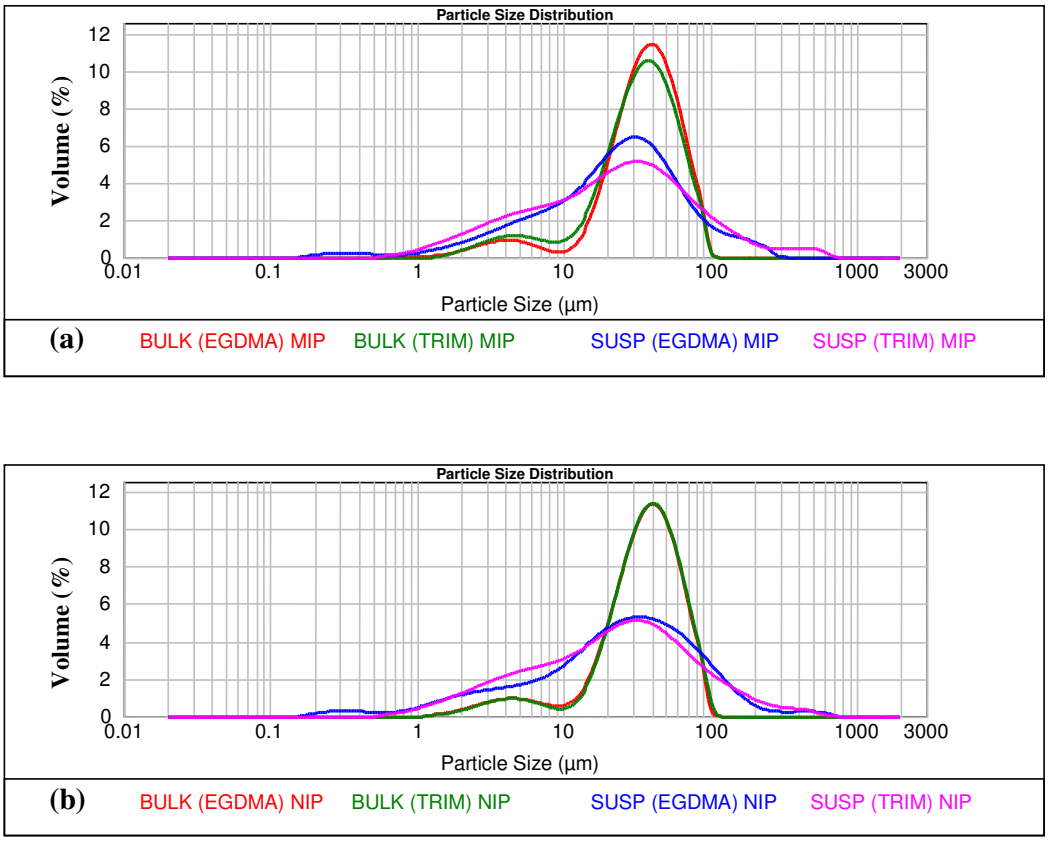

Figure 2.16 **Overlay of bulk and suspension (9500 rpm) polymers (a) MIPs and (b) NIPs prepared with different cross-linkers (EGDMA and TRIM).**

From the overlay of bulk and suspension MIP and NIP polymers with TRIM and EGDMA as cross-linkers in Figure 2.16 (a) and (b), both bulk MIP and NIP polymers were very similar. The suspension MIP and NIP polymers prepared from both cross-linkers also exhibited similar trends to each other. However, the suspension polymers gave broader size distributions to the bulk polymers. This trend is evident in Table 2.16, which illustrates the spread of particle size distributions for bulk and suspension MIP and NIP polymers prepared with EGDMA and TRIM respectively.

Table 2.16 **The approximate spread in particle size distribution determined by calculating the peak widths at half the peak height for bulk and suspension MIP and NIP polymers with EGDMA and TRIM as cross-linkers respectively.**

Polymer	Particle size spread (µm)
Bulk (EGDMA) MIP	50
Bulk (EGDMA) NIP	52
Bulk (TRIM) MIP	48
Bulk (TRIM) NIP	52
Suspension (EGDMA) MIP	55
Suspension (EGDMA) NIP	95
Suspension (TRIM) MIP	77
Suspension (TRIM) NIP	93

The imprinted polymers in this study were synthesised by heat-initiated (bulk) and light-initiated (suspension) polymerisation techniques. The bulk procedure involves grinding and sieving of the polymer within the particle size range of 25 – 75 µm. The spread of particle size distribution for bulk polymers in Table 2.16 was reflecting the sieve mesh sizes and therefore does not reveal a lot of information.

In this study, varying the cross-linker had a significant effect on suspension polymerisation in comparison to bulk technique where virtually no change was observed. For the suspension polymers prepared with TRIM as cross-linker the Dv50 values were slightly smaller than the suspension polymers prepared with EGDMA (Table 2.16). However, the spread in particle size distribution was much broader for the MIP polymers prepared with TRIM in comparison to MIP polymer prepared with EGDMA. The particle size spread was very similar for NIPs prepared with different cross-linkers.

Yoshimatsu *et al*. [4] reported that the size of the NIP beads were bigger than the imprinted particles for a study imprinting propranolol using TRIM and divinylbenzene (DVB). This was explained by the fact that the functional monomer MAA can exist in different forms in the imprinted and non-imprinted system. MAA can form hydrogen-bonded dimers in the non-imprinted system. But in the imprinted system, there is an additional molecular interaction between MAA and the template,

which somehow affected the cross-linker polymer nuclei resulting in smaller polymer beads.

The particle size distribution histograms for the suspension polymers prepared under a number of parameters: agitation speed, temperature and cross-linker in this study produced broad distributions. The suspension polymerisation method is very sensitive to the parameters examined and the outcomes were variable as seen in the results in Tables 2.7, 2.13 and 2.16. However, spherical beads are reported to have superior hydrodynamic and diffusion properties compared to irregularly shaped particles [30].

2.4 Conclusions

The successful preparation of spherical MIP beads was achieved employing a suspension polymerisation method in mineral oil. The novel aspect of this study is an attempt to explain and connect the morphology and structure of the polymers synthesised under different conditions (speed, temperature and cross-linker) with the results of equilibrium binding analysis, SEM, particle size distribution and solvent swell analysis. The important outcome of the study was to optimise the conditions of synthesis in suspension polymerisation in mineral oil. The key findings were:

The binding properties and morphologies of 2-apy imprinted polymers prepared by suspension and bulk polymerisation was investigated.

- Employing acetonitrile as porogen revealed very little difference in terms of affinity and specificity, with identical I.F values of 2.1 for both suspension and bulk polymers. There was a slightly greater capacity in the bulk polymer compared to the suspension polymer.
- The influence of a different solvent (chloroform) on the binding characteristics for both sets of polymers was investigated. I.F values were similar also, I.F = 1.5 for suspension polymer and I.F = 1.3 for bulk polymer monolith. An increase in non-specific binding in suspension and bulk polymers was seen, which could be due to the polarity of the solvent.

Parameters affecting the suspension polymerisation method were examined i.e. different speeds, temperature and cross-linker.

- The performance of the beads evaluated by equilibrium binding analysis varied little with agitation speed. In terms of equilibrium binding no difference in non-specific binding was observed across the 5 speeds with changes in polymer sizes. However, there was an impact on capacity at 9500 rpm.
- Morphologies observed in the SEM micrographs, revealed interesting observations in the resultant polymers, i.e. decreased bead diameters with increasing speed. This was also supported by particle size analysis which was a more accurate method for calculating particle size distribution. The mixing

rate obviously affects the size of the beads, as a direct link between increasing speed and a decrease in particle size distribution was found to exist.

- Solvent swell analysis was performed on all suspension polymers prepared at five different speeds in three different solvents and swelling was greatest in chloroform. Additionally, the swelling ratio increased in all three solvents in the MIPs as the rate of agitation increased.

- Suspension polymerisations of 2-apy at two temperatures (4 and 25 °C) were performed. Varying temperature in the preparation of spherical beads showed noticeable changes in binding affinity for the template. Linking binding data with the results of SEM images and particle size distribution it was concluded that for improved polymer performance, longer polymerisation time and low temperature results in improved polymer affinity with less agglomeration and smaller particle size. The lower temperature is possibly stabilising the template and monomer interactions in the pre-polymerisation mixture with the generation of well defined sites, which could also account for smaller bead sizes.

- EGDMA and TRIM were compared as cross-linkers, the relationships between rebinding properties, SEM images and particle size distributions were detailed. Noticeable changes in binding affinity, surface morphologies and particle size for the template were observed employing different cross-linkers. The most favourable cross-linker was a system employing TRIM, as the best binding affinity and smallest particle size was seen. This is possibly due to the fact the TRIM produced more rigid polymers with stable recognition sites.

In summary, upon optimising the conditions for synthesis in suspension polymerisation in mineral oil and assessing percentage yields, binding conditions, morphology results and particle size analysis it was found that the best MIP bead was produced employing acetonitrile as the solvent (porogen) for polymerisation and rebinding analyses, a high agitation speed (24000 rpm), low temperature (4 °C) and TRIM as cross-linker. This polymerisation method is a promising candidate for the preparation of MIPs as HPLC stationary phases.

Reference List

1. Wei, S.; Mizaikoff, B. *Biosensors and Bioelectronics* **2007,** *23*, 201-09.

2. Kempe, H.; Kempe, M. *Macromolecular Rapid Communications* **2004,** *25*, 315-20.

3. Tunc, Y.; Hasirci, N.; Yesilada, A.; Ulubayram, K. *Polymer* **2006,** *47*, 6931-40.

4. Yoshimatsu, K.; Reimhult, K.; Krozer, A.; Mosbach, K.; Sode, K.; Ye, L. *Analytica Chimica Acta* **2007,** *584*, 112-21.

5. Turner, N. W.; Piletska, E. V.; Karim, K.; Whitcombe, M.; Malecha, M.; Magan, N.; Baggiani, C.; Piletsky, S. A. *Biosensors & Bioelectronics* **2004,** *20*, 1060-67.

6. Mayes, A. G.; Mosbach, K. *Analytica Chimica Acta* **1996,** *68*, 3769-74.

7. Ye, L.; Weiss, R.; Mosbach, K. *Macromolecules* **2000,** *33*, 8239-45.

8. Boyd, A. S. F.; Frost, M. J.; Howarth, N. M. *Journal Of Molecular Structure* **2004,** *688*, 149-58.

9. Lin, J. L.; Wu, R. H.; Tzeng, W. B. *Chemical Physics Letters* **2002,** *353*, 55-62.

10. Cummins, W.; Duggan, P.; McLoughlin, P. *Analytica Chimica Acta* **2005,** *542*, 52-60.

11. Spivak, D.; Shea, K. J. *Journal Of Organic Chemistry* **1999,** *64*, 4627-34.

12. Jie, Z.; Xiwen, H. *Analytica Chimica Acta* **1999,** *381*, 85-91.

13. Cummins, W.; Duggan, P.; McLoughlin, P. *Biosensors and Bioelectronics* **2006,** *22*, 372-80.

14. Kempe, H.; Kempe, M. *Analytical Chemistry* **2006,** *78*, 3659-66.

15. Piletsky, S. A.; Piletska, E. V.; Karim, K.; Freebairn, K. W.; Legge, C. H.; Turner, A. P. F. *Macromolecules* **2002,** 35, 7499-504.

16. Spivak, D.; Gilmore, M. A.; Shea, K. J. *Journal Of The American Chemical Society* **1997,** *119*, 4388-93.

17. Yoshizako, K.; Hosoya, K.; Iwakoshi, Y.; Kimata, K.; Tanaka, N. *Analytical Chemistry* **1998,** *70*, 386-89.

18. Zourob, M.; Mohr, S.; Mayes, A. G.; Macaskill, A.; Pérez-Moral, N.; Fielden, P. R.; Goddard, N. J. *Lab on a Chip* **2006,** *6*, 296-301.

19. Koohpaei, A. R.; Shahtaheri, S. J.; Ganjali, M. R.; Forushani, A. R.; Golbabaei, F. *Talanta* **2008,** *75*, 978-86.

20. Alexopoulos, A. H.; Kiparissides, C. *Chemical Engineering Science* **2007,** *62*, 3970-83.

21. Jahanzad, F.; Sajjadi, S.; Yianneskis, M.; Brooks, B. W. *Chemical Engineering Science* **2008,** *63*, 4412-17.

22. Dowding, P. J.; Vincent, B. *Colloids and Surfaces A: Physicochemical and Engineering Aspects* **2000,** *161*, 259-69.

23. Navarro-Villoslada, F.; Vicente, B. S.; Moreno-Bondi, M. C. *Analytica Chimica Acta* **2004,** *504*, 149-62.

24. Mijangos, I.; Navarro-Villoslada, F.; Guerreiro, A.; Piletska, E.; Chianella, I.; Karim, K.; Turner, A.; Piletsky, S. *Biosensors and Bioelectronics* **2006,** *22*, 381-87.

25. Gonzalez, G. P.; Hernando, P. F.; Alegria, J. S. D. *Analytica Chimica Acta* **2006,** *557*, 179-83.

26. Yu, C.; Mosbach, K. *Journal of Chromatography A* **2000,** *888*, 63-72.

27. Kempe, M.; Mosbach, K. *Tetrahedron Letters* **1995,** *36*, 3563-66.

28. Andersson, L. I.; Muller, R.; Vlatakis, G.; Mosbach, K. *Proceedings Of The National Academy Of Sciences Of The United States Of America* **1995,** *92*, 4788-92.

29. Maria Kempe *Analytical Chemistry* **1996,** *68*, 1948-53.

30. Fairhurst, R. E.; Chassaing, C.; Venn, R. F.; Mayes, A. G. *Biosensors and Bioelectronics* **2004,** *20*, 1098-105.

Chapter 3

A detailed examination of 2-aminopyridine suspension and bulk binding characteristics using binding isotherms and affinity distribution spectra

3.1 Introduction

In Chapter 2, equilibrium binding experiments on the polymers were reported, in an attempt to investigate the affinity of the imprinted polymer for 2-apy. Interest has grown in recent years to develop a more in depth understanding of the heterogeneous nature of binding sites of MIPs [1].

Most applications of MIP materials are often restricted by their binding properties. The formation of a distribution of binding sites possessing a range of binding affinities is an intrinsic characteristic of molecular imprinting. The imprinting concept may suggest a homogeneous binding site distribution, however experimental work has demonstrated that a heterogeneous distribution is the common situation [1]. One reason suggested by Diaz Garcia *et al*. [1] for the heterogeneous binding sites in imprinted polymers could be due to dissociation of the template-functional monomer complex in solution. It is assumed that each template-functional monomer complex in the pre-polymerisation mixture produces an imprinted binding site within the imprinted polymer matrix. If excess amounts of functional monomer are used to shift the equilibrium toward full formation of the aggregates (Le Chatelier's principle) most of the functional monomer may be free and randomly oriented in the mixture. Therefore a spectrum of binding sites with different association constants is produced. In a typical non-covalent imprinted polymer, there is usually a variety of binding sites with different affinities for the analyte ranging from high dissociation constants in the mM range to low dissociation constants in the μM – mM range. However, the binding properties in MIPs are generally measured only in a narrow concentration range, which corresponds to only a subset of the sites in MIPs. Generally, MIPs are characterised by comparatively low binding affinities and a high degree of binding site heterogeneity [2]. This limited analytical range and binding site heterogeneity of MIPs leads to inaccuracies and inconsistencies in the estimation of their binding properties in contrast to natural receptors, which rather limits their analytical applications in e.g. chromatography, binding assays, solid phase extractions and sensing [3]. In the literature, Sellergren and Shea demonstrated how the origins of peak asymmetry for the enantiomeric separation of D- and L-phenylanaline anilide (D, L-PA) on a L-PA imprinted column was caused by the heterogeneous nature of the binding sites [4]. Allender *et al*. [5] used Scatchard plots to demonstrate that the cross

reactivity observed for a series of Boc-D,L-amino acid imprinted polymers was also due to the heterogeneous nature of the imprinted polymers. Consequently, improving and thoroughly characterising the binding properties of MIPs should be a driving force toward next generation MIP technology.

3.2 Adsorption isotherms

An adsorption isotherm is described as a measure of the relationship between the equilibrium concentrations of bound and free guest over a certain concentration range and is readily generated from equilibrium batch rebinding studies [6]. Binding properties can be calculated from the binding isotherm by fitting the adsorption isotherm to specific binding models. In this study binding isotherms were used to characterise binding sites in MIPs prepared by bulk and suspension polymerisation. The quantity of binding sites and binding energy of the MIPs was examined by using Langmuir, Freundlich and Langmuir-Freundlich analysis and the most suitable model identified. The aim was to reveal information involved in the selective process of molecular recognition. Also Langmuir-Freundlich affinity distribution analysis facilitates the calculation of an affinity distribution (AD) for MIPs in the concentration range, yielding an estimate of number, affinity, and heterogeneity for this subset of binding sites. For a detailed explanation of the binding models mentioned refer to Section 1.7.1.

Objectives of the research

The main objectives of the work in this chapter were:

- To assess the best model for non-covalent imprinted polymer systems,
- To determine the binding energy and total number of binding sites (N_t) for MIPs produced by different synthetic mechanisms,
- To compare trends between binding data and synthetic method used and
- To utilise affinity distribution (AD) diagrams to study the binding affinity in non-covalent MIP systems.

3.3 Experimental

3.3.1 Experimental binding isotherm analysis

The reagents and equipment as described in Section 2.2, Chapter 2. Binding isotherms were generated for 5 sets of MIP and NIP suspension polymer combinations prepared at different speeds and bulk polymers synthesised using the same monomer composition. The method of preparation for the polymers was described in Section 2.2.4 – 2.2.5, Chapter 2. Ten different solutions of 2-apy in acetonitrile covering the concentration range from 0.02 – 8.0 mM were prepared. Triplicate 50.0 mg quantities of polymer were suspended in 5 mL of 2-apy solution and binding analysis was performed as in Chapter 2. Appropriate dilutions were carried out prior to analysis for the higher concentration analyte solution, post-equilibrium. The absorbance value for a control solution was prepared by making up a 1mM 2-apy solution in acetonitrile. The absorbance value, A_F, is the absorbance of free 2-apy in solution. The free concentration, F, was calculated by rearranging the Beer-Lambert law as $F = A_F/\varepsilon l$, where ε is the molar absorptivity of 2-apy in acetonitrile (2687 mol^{-1} cm^{-1} at 290 nm). The bound amount (B) was calculated by subtracting the concentration of free amount (F) from the initial 2-apy concentration.

Experimental binding isotherms for MIP and NIPs were analysed individually using the LI, FI and L-FIs which were implemented in three steps to establish the presence of template-selective binding sites and to determine the dependence of template uptake on polymer concentration: (1) The experimental data was plotted in log B versus log F format. (2) The data was analysed using LI, FI and L-FI via linear regression which yielded the LI, FI and L-FI fitting parameters in Table 3.1. Linear regression is often used to determine the best fit isotherm for two-parameter isotherms. Linearised forms of FI, LI and L-FI equations are shown in Table 3.1.

Table 3.1 Different linearised forms of isotherm models

Isotherm model	Linearised form	Plot	Parameters
Langmuir	$1/B = (1/NK) + (1/F)$	$(1/B)$ vs. $(1/F)$	K = intercept/slope N_t =1/intercept
Freundlich	$\log B = m \log F + \log a$	$\log B$ vs. $\log F$	$a = 10^{-\text{intercept}}$ m = slope
Langmuir-Freundlich	Solver function[a]	$\log B$ vs. $\log F$	N_t, a, m, K_o

[a] L-F adsorption isotherms were fitted to the log-log plot of the experimental adsorption isotherms using the Solver function in Microsoft Excel by varying the fitting parameters to reach a value of 1 for R^2as described by Shimizu and co-workers [6].

The parameters to be determined from the various isotherms are:

- N_t is the total number of binding sites,
- a is related to the average binding affinity K_o via $K_o = a^{1/m}$,
- m is the heterogeneity index and the value of which varies from zero to one (with one being homogeneous and values approaching zero being increasingly heterogeneous).

Using the experimentally derived L-FI fitting parameters, a and m, the affinity distribution (AD) was calculated. The limits over which the calculated AD is valid are set by the limits (K_{min} and K_{max}) determined by the concentration range of the experimental binding isotherm shown in Equation 3.1:

$$K_{max} = \frac{1}{F_{\min}} \quad \text{and} \quad K_{min} = \frac{1}{F_{\max}} \qquad \textbf{Equation 3.1}$$

3.4 Results and discussion

Polymers used in this study were prepared using 2-apy as template, MAA as functinoal monomer and TRIM as cross-linker which were polymerised by bulk and suspension methods. All data was determined from average *B* and *F* values from triplicate analysis used to generate experimental isotherms, which was then fitted to LI, FI and LF-I using Microsoft Excel Solver function as described by Shimizu and co-workers [6].

Binding energy and N_t values were determined for MIP and NIP polymers produced at 8000 – 24000 rpm and bulk polymer monoliths utilising the Langmuir and Freundlich Isotherms.

Fitting the LI parameters to suspension and bulk polymers, the binding energies (*K*) for MIPs was significantly higher than for NIPs. The *K* values for the bulk polymers were lower than for the suspension polymers, i.e. bulk polymers (MIP: 2.480 mM^{-1} and NIP: 1.855 mM^{-1}) in comparison to the 24000 rpm polymers (MIP: 3.004 mM^{-1} and NIP: 2.275 mM^{-1}). An opposing trend was seen for the N_t values, where the total number of binding sites was greater in the NIPs compared to the MIPs for both suspension and bulk polymers, i.e. 24000 rpm (MIP: 0.525 $\mu molg^{-1}$ and NIP: 0.715 $\mu molg^{-1}$) and bulk polymers (MIP: 0.440 $\mu molg^{-1}$ and NIP: 0.567 $\mu molg^{-1}$), respectively.

Fitting the FI parameters to suspension and bulk polymers, the binding affinity values were greater for NIPs than for the MIPs in suspension and bulk polymers, i.e. 24000 rpm (MIP: 0.012 mM^{-1} and NIP: 0.040 mM^{-1}) and bulk polymers (MIP: 0.005 mM^{-1} and NIP: 0.017 mM^{-1}), respectively. The total number of binding sites (N_t values) was greater in the MIPs than in the NIPs for all suspension polymers. But the N_t value was less for the bulk MIP in comparison to the NIP (MIP: 2200 $\mu molg^{-1}$ and NIP: 4513 $\mu molg^{-1}$). The trends observed for the heterogeneous parameter (*m* values) of the FI was that the MIPs had a slightly lower heterogeneity index for both suspension and bulk polymers.

However, the general fit to the LI and FI models as quantified by R^2 values was lower than those obtained by the L-FI model. Thus, the results discussed in this study focus on the application of L-FI and AD spectra for polymers produced at 8000 – 24000 rpm and bulk polymers.

Table 3.2 summarises the fitting coefficients obtained using L-FIs for bulk and suspension MIP and NIP polymers, i.e. the apparent number of binding sites, binding affinities and heterogeneity. The L-FI has the advantage of being suited to fit isotherms measured over a wide concentration range, i.e. the L-FI was better able to model the linear sub-saturation including the curved saturation portions of the isotherms.

Table 3.2 **Binding parameters obtained using L-FIs for bulk and suspension imprinted MIP and NIP polymers. Results based on average values from triplicate analysis.**

Polymer	N_t (µmol g^{-1})*	a (mM^{-1})	m	K_o (mM^{-1})**	Limits of Affinity (mM^{-1})***	R^2
8000 MIP	707	0.112	0.737	0.051	0.16 - 62.5	0.981
8000 NIP	116	0.358	1.000	0.358	0.18 - 24.9	0.930
9500 MIP	215	0.858	0.897	0.843	0.17 - 66.2	0.970
9500 NIP	75	2.908	0.995	2.106	0.12 - 62.5	0.749
13500 MIP	333	0.439	0.811	0.362	0.17 - 71.9	0.981
13500 NIP	186	0.275	1.000	0.275	0.13 - 28.9	0.996
20500 MIP	322	0.483	0.808	0.407	0.16 - 78.7	0.983
20500 NIP	182	0.266	1.000	0.266	0.13 - 29.9	0.987
24000 MIP	222	0.914	1.000	0.914	0.16 - 43.3	0.957
24000 NIP	77	0.708	1.000	0.708	0.12 - 26.2	0.808
Bulk MIP	2200	0.098	0.986	0.095	0.27 - 12.4	0.980
Bulk NIP	4513	0.013	1.000	0.013	0.14 - 4.82	0.979

* N_t is the total number of binding sites.

** The average association constant $K_o = a^{1/m}$.

*** Limits of affinity distribution were calculated from the maximum and minimum free analyte concentrations (F_{min} and F_{max}) by the relationships $K_{min} = 1/F_{max}$ and $K_{max} = 1/F_{min}$ [6].

The suitability of the L-FI in assessing the binding characteristics of the imprinted polymers was determined by plotting the experimental isotherm in log B versus log F format. Linearised form of the L-FI equation is shown in Table 3.1. The

experimental binding isotherms for the suspension MIP and NIP polymers prepared at 8000 and 24000 rpm in log-log format are shown in Figure 3.1.

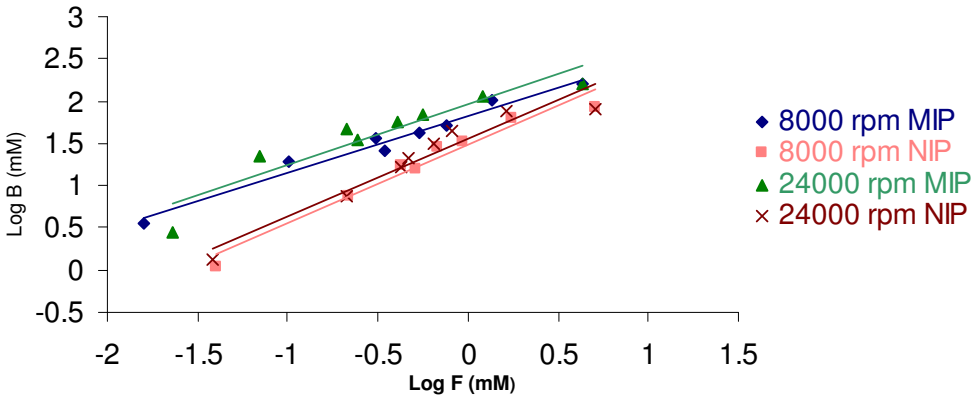

Figure 3.1 **Equilibrium binding isotherms for suspension MIP and NIP polymers prepared at 8000 and 24000 rpm in log-log format (symbols represent the experimental data; lines are L-FI fitting functions).**

As a result of plotting the experimental isotherm for log *B* versus log *F* improved linear regression values were obtained. Additionally, better fit to the experimental data was found for all suspension and bulk polymers.

- **Number of binding sites (N_t values)**

In this study the total number of binding sites (N_t values) for suspension polymers was found to be greater in the MIP than in the NIP. The N_t values for the 8000 rpm polymers yielded values of 707 μmol g^{-1} for MIP and 116 μmol g^{-1} for NIP (Table 3.2). The difference in capacity between the MIP and NIP is large (ΔN_t = 589 μmol g^{-1}). The differences in affinity distributions of the evaluated polymers show that the binding capacity of the MIPs is always higher than the corresponding NIPs over the measured concentration range. A possible explanation is that the high affinity sites, which distinguish the MIP and NIP, make up a large fraction of the total number of sites and that the high affinity sites are filled first followed by the low affinity binding sites. Similar capacity differences were observed in rebinding studies between MIP and NIP for suspension polymers in Chapter 2.

A trend between 13500 and 20500 rpm polymers was observed, i.e. values of N_t for the MIPs were similar, 13500 rpm = 333 μmol g^{-1} and 20500 rpm = 322 μmol g^{-1}, respectively. Likewise N_t values for NIPs were comparable, 13500 rpm = 186 μmol g^{-1} and 24000 rpm = 182 μmol g^{-1}, respectively. The difference in capacity between the MIP and NIP was quite big (ΔN_t = 147 μmol g^{-1} for 13500 rpm and 140 μmol g^{-1} for 20500 rpm). A trend between the 13500 and 20500 rpm polymers was expected as the overall capacity is greater for these polymers in comparison to the other suspension polymers. These results point towards a high degree of specific and non-specific binding.

The total number of binding sites was found to increase significantly for bulk polymers in comparison to suspension polymers (Table 3.2). Higher agglomeration in the bulk polymers is linked to higher N_t values. However, the calculated N_t values for the bulk MIP were less than the NIP, i.e. MIP = 2200 μmol g^{-1} and NIP = 4513 μmol g^{-1}, respectively.

- **Heterogeneous parameter (*m* values)**

A trend was observed in the *m* values for suspension polymers prepared at the higher speeds, where *m* values were closer to 1. For the lower speeds, i.e. 8000 and 9500 rpm a reverse trend was seen. Comparison of the heterogeneous parameter (*m*) for the suspension and bulk polymers (MIP and NIP) in Table 3.2 reveals that all the MIPs have a lower heterogeneity index (*m*: 0.737 – 1.000) than the corresponding NIPs (*m*: 0.995 – 1.000). The lower heterogeneity index means a more heterogeneous polymer was obtained for the 2-apy based MIPs in comparison to NIPs.

- **Binding energies (K_o values)**

The binding energies (K_o values) for all the polymers fell within the limits of affinity distribution for all suspension polymers, with the exception of 8000 rpm MIP (K_o = 0.051 mM^{-1}). The K_o values for bulk polymers fell outside the limits of affinity distribution also, i.e. bulk MIP (K_o = 0.095 mM^{-1}) and bulk NIP (K_o = 0.013 mM^{-1}), respectively.

In Table 3.2, 8000 rpm and 9500 rpm MIP polymers had lower binding energies compared to the NIP; a reverse trend was seen for 13500 – 24000 rpm polymers and bulk polymers. In general, a shift to higher binding energies from 13500 – 24000 rpm was observed in MIP and NIP polymers, with the exception of the 9500 rpm MIP and NIP polymers which exhibited a significant increase in binding energy values (a possible anomaly). The highest speed, 24000 rpm had the highest K_o values, MIP = 0.914 mM^{-1} and NIP = 0.708 mM^{-1}. Therefore, the suspension polymers were characterised by higher K_o values than the particles. The large differences in K_o values between suspension and bulk polymers were caused as a result of a higher temperature employed in bulk polymerisation which caused disruption to the interactions thus affecting the binding energies.

The L-FI binding model does not disprove the abilities of the LI and FI models but presents a more general case that covers both models. The L-FI has yielded a better fit to the experimental isotherm than either the L or FI. It follows then, by applying the L-FI in this study to the experimental isotherm for suspension polymers, a more accurate estimate of the fitting coefficients N_t, a and m (refer to Section 3.3.1) can be made. The variable a is related to the median binding affinity (K_o) via $K_o = a^{1/m}$. For values to be accurately obtained K_o must fall within the limits of $1/F_{min}$ and $1/F_{max}$ (the limits of affinity distributions), determined by $K_{min} = 1/F_{max}$ and $K_{max} = 1/F_{min}$, where F is the concentration of free analyte in solution. This is a requirement in determining the suitability of the L-FI. In the present work, this condition was met, with the exception of 8000 rpm MIP and the bulk MIP and NIP polymers which fell outside the limits of affinity distribution.

The influence of polymer morphology on the performance of MIPs was evaluated by Holland *et al*. [7]. A series of 2-apy MIPs were prepared by bulk polymerisation with varying amounts of cross-linker (EGDMA) and characterised by utilising LI, FI, L-FI and AD Spectra. The L-FI isotherm was judged to be the most appropriate isotherm for analysis in the concentration range used (0.025 – 4.0 mM). This was as a result of improved linear regression values obtained when it was fit to the experimental data. All the K_o values fell within the limits of distribution. Furthermore, the L-FI was sensitive to changes in the binding site energies with changes in composition. The total number of binding sites increased with increasing flexibility, i.e. with decreasing

EGDMA content [7]. The N_t values for polymers prepared between 40 – 10 mmol EGDMA ranged from 88.6 – 281.9 μmol g^{-1}. Conversely, the binding energies decreased with decreasing EGDMA content.
The K_o values for polymers prepared with 40 and 10 mmol EGDMA were 0.94 and 0.46 mM^{-1}, respectively.

The binding energy (K_o) values for the polymers prepared with 40 and 10 mmol EGDMA by Holland *et al*. were (K_o: 0.94 and 0.46 mM^{-1}) [7]. These binding energy values demonstrated the greatest similarity to polymers prepared at the higher speeds in this study, i.e. 24000 and 20500 rpm MIP (K_o: 0.914 and 0.407 mM^{-1}). However, in comparison to the total number of binding sites for polymers prepared with 40 and 10 mmol EGDMA, the values were, N_t: 88.6 and 281.9 μmol g^{-1}, respectively [7]. In this study, the MIP polymers prepared at 24000 and 20500 rpm exhibited N_t values of 222 and 322 μmol g^{-1}. The 20500 rpm MIP polymer demonstrated the greatest similarity to the polymer prepared with 10 mmol EGDMA content in terms of K_o and N_t values.

Holland *et al*. also reported on the heterogeneity of the polymers prepared with varying amounts of EGDMA. The m values ranged from 0.97 – 0.80 for polymers with 40 – 10 mmol EGDMA content [7]. Interestingly, a similarity was again observed between the 10 mmol EGDMA polymer [7] and for the suspension polymer prepared at 20500 rpm (m = 0.808) in this study.

3.4.1 Affinity distributions

Affinity distribution diagrams were generated with the derived affinity distribution function (Equation 1.4) in Section 1.7.1, Chapter 1. The affinity distribution shows the population of binding sites, N, with a particular association constant, K. The area under the curve corresponds to the total number of binding sites, N_t. Calculation of affinity distributions for any range of association constants is limited to a specific concentration range by which the adsorption isotherm was measured and these limits are set by $K_{min} = 1/F_{\max}$ and $K_{max} = 1/F_{\min}$. Within these limits, the affinity distribution is precise. Outside these limits, considerable errors can arise, especially if

the isotherm covers only the saturation or subsaturation region [6]. The L-FI models the adsorption isotherm by imposing a particular shape on the affinity distribution. For example, Figures 3.2 (a) and (b) shows the calculated affinity distributions for suspension MIP and NIP polymers respectively.

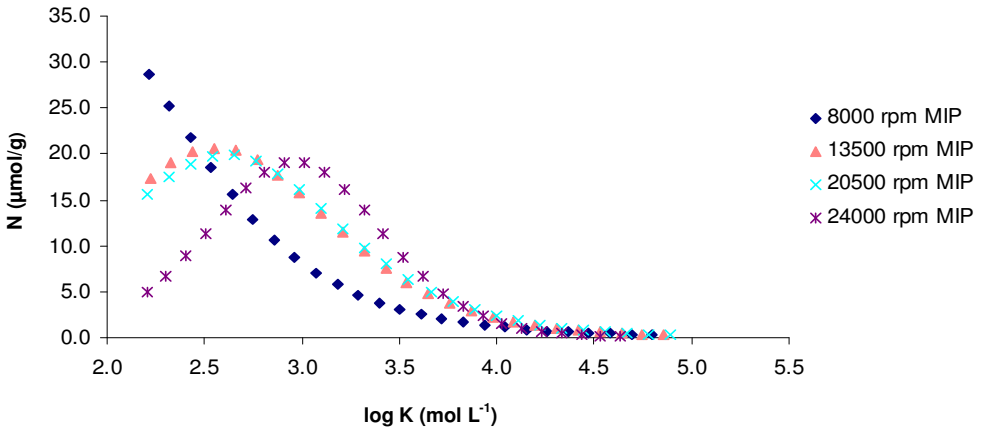

(a)

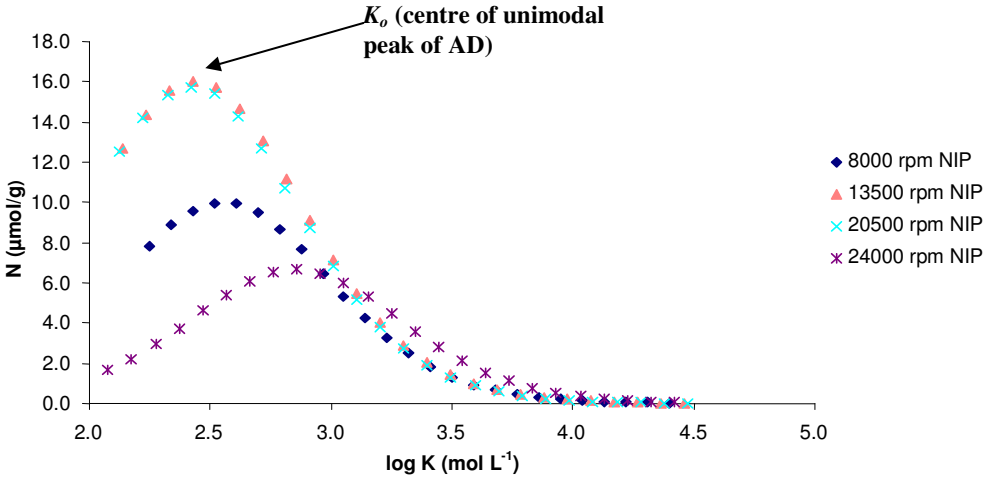

(b)

Figure 3.2 (a) & (b) Overlay of affinity distribution spectra for suspension MIP and NIP polymers. Data determined by substituting L-FI fitting parameters into (Equation 1.4, Section 1.7.1, Chapter 1) using Microsoft Excel Solver function.

From Figures 3.2 (a) and (b) it is evident that the suspension MIP polymers have a greater number of binding sites in comparison to the NIPs. There is also a greater spread in binding energies in MIP polymers across all speeds in comparison to NIPs. The spread in binding energies was determined from calculating the peak widths at half the peak height. The affinity distribution spectra for the 9500 rpm MIP and NIP

polymers were not included in Figure 3.2 (a) and (b). Polymers prepared at 9500 rpm exhibited out of trend binding energy values (possible anomaly) in comparison to the other polymers. A similar binding energy spread in affinity distribution spectra was exhibited for the 13500 – 24000 rpm MIP polymers (≈ 2.8). A shift towards higher binding energy spread was seen for the 24000 rpm MIP (≈ 3.0). Also the maximum number of binding sites in the MIP polymers at a particular energy seems to be similar for MIP polymers ranging from 13500 – 24000 rpm.

In Figure 3.2 (b), identical affinity distribution spectra were exhibited by NIP polymers prepared at 13500 and 20500 rpm (binding energy spread ≈ 2.6). Additionally, these polymers demonstrated the maximum number of binding sites. A similar spread in affinity distribution was exhibited by the 8000 rpm NIP but with a decrease in the number of binding sites. The biggest spread in AD was seen for the 24000 rpm NIP polymer (≈ 2.9) with a shift towards a higher binding energy but with the biggest reduction in the number of binding sites.

Application of the affinity distribution limits for suspension MIP and the NIP yields affinity distributions that are centred about the unimodal peak with a maximum at $K_{o,}$ as shown in Figure 3.2 (b). The heterogeneous unimodal distributions shown for the L-FI model are appropriate for modelling MIP and NIPs due to the difference in the strength of interactions of the pre-polymerisation complexes [8]. Reloading in a lower concentration range to assess the high affinity sites correlates with an exponential decaying region. The affinity distribution spectra exhibited in Figure 3.2 (a and b) are unimodal distributions, with the exception of 8000 rpm MIP, in contrast to exponential decaying regions. This implies that a wide concentration region has been used and the polymers assessed have reached saturation. From the shape of the affinity distribution spectra for MIP and NIP polymers, differences were observed in the width of the distributions between them. The MIPs exhibited broader distributions as shown in Figure 3.2 (a). The MIPs also demonstrated a greater number of binding sites and binding energies in comparison to the NIPs.

By contrast, the affinity distributions for bulk MIP and NIP polymers covered only the exponentially decaying tail of the distribution, as shown in Figure 3.3.

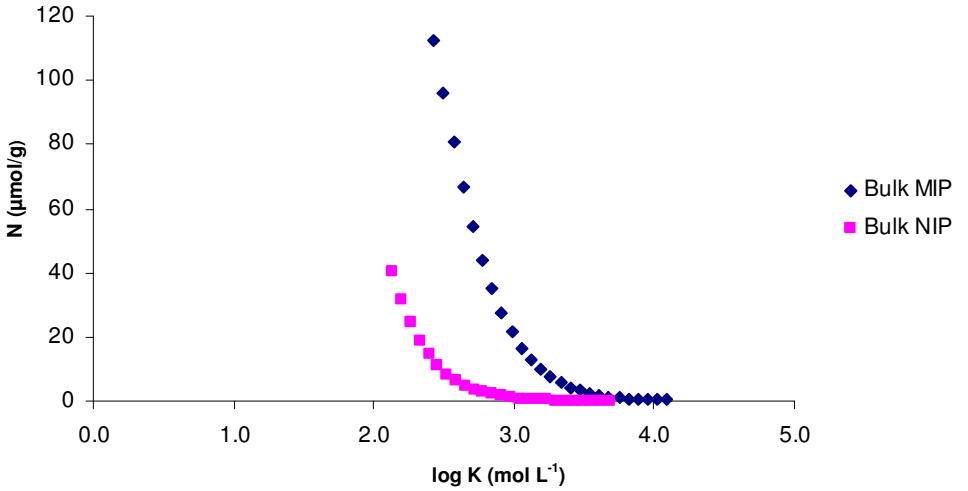

Figure 3.3 **Overlay of affinity distribution spectra for bulk MIP and NIP polymers prepared with TRIM as cross-linker. Data determined by substituting L-FI fitting parameters into (Equation 1.4, Section 1.7.1, Chapter 1) using Microsoft Excel Solver function.**

The K_o values for bulk polymers were outside the affinity distribution limits (Table 3.2) which accounts for considerable errors, this illustrated the limitations of the L-FI. The affinity distribution spectra for the bulk polymers are similar to the 8000 rpm MIP polymer as shown in Figure 3.2 (a). However, the binding energies involved in the bulk also appear to be lower than those of the rest of the suspension polymers and demonstrate a key difference between the bulk and suspension polymers. The affinity distribution spectra for bulk MIP and NIP polymers covered only the exponentially decaying tail of the distribution. A reason could be due to differing synthetic procedures employed for both sets of polymers. A higher temperature employed in the bulk synthesis disrupts the strength of interactions resulting in a decrease in binding energy. Therefore, the heterogeneous unimodal distribution of the L-FI model seemed to be more appropriate for modelling suspension polymers compared to bulk polymers.

3.5 Conclusions

The most suitable model for assessing the binding behaviour of suspension polymers was determined to be the Langmuir-Freundlich isotherm model (L-FI). Data obtained employing the affinity distribution spectra correlated with results received using the L-FI. A relationship is proposed between the number of binding sites and binding energies which was illustrated by the affinity distribution spectra. The key findings were:

- The suspension MIP polymers had a greater number of binding sites in comparison to the NIPs. There was a greater spread in binding energies in MIP polymers across all speeds (with the exception of 9500 rpm MIP). Also the maximum number of binding sites in the MIP polymers at a particular energy seems to be similar for MIP polymers ranging from 13500 – 24000 rpm, with a shift towards higher binding energy observed for the 24000 rpm MIP.

- By contrast to suspension polymers, the affinity distributions for bulk MIP and NIP polymers covered only the exponentially decaying tail of the distribution. A reason could be due to differing synthetic procedures employed for both sets of polymers. A higher temperature employed in the bulk synthesis disrupts the strength of interactions resulting in a decrease in binding energy.

The application of the L-FI method may also be restricted by the concentration region of the binding assays. The limitations in measuring the binding isotherm by L-FI within this narrow range for bulk polymers could be circumvented by additional binding experiments over a greater concentration range.

Reference List

1. Garcia-Calzon, J. A.; Diaz-Garcia, M. E. *Sensors and Actuators B: Chemical* **2007,** *123*, 1180-94.

2. Rampey, A. M.; Umpleby, R. J.; Rushton, G. Y.; Iseman, J. C.; Shah, R. N.; Shimizu, K. D. *Analytical Chemistry* **2004,** *76*, 1123-33.

3. Wei, S.; Mizaikoff, B. *Biosensors and Bioelectronics* **2007,** *23*, 201-09.

4. Sellergren, B.; Shea, K. J. *Journal of Chromatography A* **1995,** *690*, 29-39.

5. Allender, C.; Brain, K. R.; Heard, C. M. *Chirality* **1997,** *9*, 233-37.

6. Umpleby, R. J.; Baxter, S. C.; Chen, Y.; Shah, R.; Shimizu, K. D. *Analytical Chemistry* **2001,** *73*, 4584-91.

7. Holland, N.; Frisby, J.; Owens, E.; Hughes, H.; Duggan, P.; McLoughlin, P. *Polymer* **2010,** *51*, 1578-84.

8. Umpleby, R. J.; Baxter, S. C.; Rampey, A. M.; Rushton, G. T.; Chen, Y.; Shimizu, K. D. *Journal of Chromatography B* **2004,** *804*, 141-49.

Chapter 4

Characterisation of 2-aminopyridine suspension and bulk imprinted polymers using thermal desorption GC-MS

4.1 Introduction

This chapter describes an approach for the comparison of suspension and bulk methodologies through the application of GC-MS analysis for the thermal pre-treatment, characterisation and analysis of MIP polymers. One useful property of MIPs is that they are temperature resistant. An investigation was performed on the thermal stability of an (MAA-EGDMA) co-polymer by Nicholls *et al*. [1]. MIPs were found to retain affinity for the template at high temperatures of up to 150 ^{o}C for 24 h. Other studies characterising the thermal stability of cross-linked styrene-divinylbenzene polymers and methyl methacrylate-dimethacrylate cross-linked polymers, similar to those used in molecular imprinting were performed by Levchik *et al*. [2;3]. The cross-linked styrene-divinylbenzene polymers were found to be stable at temperatures of up to 250 ^{o}C. However, methyl methacrylate-dimethacrylate cross-linked polymers did not show an increase in thermal stability even though they have a high cross-link density. It was inferred that the aromatic character of the styrene-divinylbenzene cross-linked polymers was responsible for thermal enhancement.

Cummins *et al*. [4] developed a direct probe GC-MS methodology for thermal desorption analysis of MIPs in an effort to provide insight into the three-dimensional characteristics of polymers. The technique enabled analysis of specific ions which can be used to examine and assign bleed to template and monomer. The technique was also used in polymer characterisation to investigate the rebinding performance of MIPs compared to NIPs and a morphological difference between MIP and NIP was demonstrated by the result data [4]. A second study performed by Holland *et al*. [5;6] extended the use of direct probe GC-MS for characterisation of MIPs. The amount of cross-linker (EGDMA) was varied to produce polymers with different morphologies. Result data obtained by thermal desorption GC-MS demonstrated the techniques ability to identify differences in polymer performance based on composition. Additionally, the thermal GC-MS profiles correlated with the physical characteristics of the polymers, where higher levels of bleed were found to occur with larger average pore diameters [6].

In this study, polymers have been prepared by suspension and bulk polymerisation using varying conditions of reaction temperature and viscosity in the case of the

suspension procedure. These polymers were synthesised employing 2-apy as template, using the same composition as described in Chapter 2, i.e. in a (MAA-*co*-TRIM) polymer system, in contrast to previous GC-MS characterisation studies where a (MAA-*co*-EGDMA) bulk polymer system was used [4-6]. The thermal desorption of this type of co-polymer (MAA-*co*-TRIM) was investigated using direct probe GC-MS and the structure and thermal properties correlated for bulk and suspension polymers. The binding site properties and specificity of spherical beads and bulk particles were also examined in order to understand the rebinding properties of the imprinted polymer matrices at different conditions.

Objectives of the research

The main objectives of the work in this chapter were:

- To utilise direct probe thermal desorption GC-MS to study a series of 2-apy imprinted MAA-*co*-TRIM polymers prepared by suspension and bulk methodologies under varying synthetic conditions and
- To assess the 2-apy rebinding ability and specificity and correlate this to the MIP and the corresponding NIP composition for both suspension and bulk polymers.

4.2 Experimental

The methodology for the synthesis of spherical beads and monoliths was described in Chapter 2, Section 2.2.4 and 2.2.5.

4.2.1 Instrumentation

A Varian CP-3800 Gas Chromatograph coupled with a Varian Saturn 2000 Gas Chromatograph-Mass Spectrometer (GC/MS/MS) detector was used to carry out thermal desorption experiments on the polymers. A Varian Chromatoprobe was connected to one of the temperature-programmable injection ports of the gas chromatograph, which was attached via a programmable switching valve to the MS detector through a 1 m uncoated capillary column (i.d. 100 µm) housed in the GC column oven. High grade helium was used as the flow gas at 0.5 mL min^{-1}. In order to protect the MS detector from excessive exposure in the initial part of thermal treatment the programmable switching valve was employed to select fractions for MS analysis or to vent fractions to waste.

4.2.2 Polymer pre-treatment analysis

Polymers initially required thermal pre-treatment to remove any partially or unreacted monomers. Chromatographic conditions and the temperature programmes employed for polymer pre-treatment studies are described in previous work [4]. Suspension polymers prepared at 9500 rpm and 24000 rpm had been filtered and washed with chloroform and acetone to remove the mineral oil. The resultant dried beads which were not sieved, were then employed in thermal desorption studies. The bulk monolith particles were washed with acetone as part of the grinding and sieving process. Fractions ranging from 25 – 75 µm were collected using Endicott sieves. Particles less than 25 µm were utilised for thermal desorption studies.

Approximately 1 mg quantities of polymer were weighed into thermal desorption glass ampoules and placed in the desorption probe. Initially polymers were pre-treated at high temperatures to desorb any remaining template species, and other

volatiles. For thermal pre-treatment of polymers the sample was held at 80 °C for 1.5 min with the ion source and detector inactive and the effluent from the injector vented via the switching device to protect the MS detector from excessive exposure to air, moisture and volatiles. After 1.5 min the effluent was switched to the mass spectrometer (MS), which was activated for electron impact (EI) analysis in the *m/z* range 40 to 350. The injector temperature was then raised to 250 °C at 15 °C min^{-1} and held for 15 min. A split ratio of 40:1 was used. The column oven, which was used to control the temperature of the transfer column, was held at 80 °C for 1 min and then raised to 170 °C at 15 °C min^{-1}.

4.2.3 Thermal desorption experiments

Polymers which had been thermally pre-treated as described above were used for desorption studies. The pre-treated polymers were loaded by injecting 5 μL of (0.4, 2.0, 4.0 or 8.0 mg mL^{-1}) 2-apy in acetonitrile, using a Hamilton 10 μL syringe. The thermal desorption programme was modified to include a delay time of 8 min at 80 °C to vent solvent volatiles. After 8 min the MS detector was activated in EI in the *m/z* range 40 to 350, and the injector was heated using two temperature ramps: 20 °C min^{-1} to 200 °C, held for 6 min, then 50 °C min^{-1} to 250 °C and held for 6.5 min. A split ratio of 80:1 was used. The column oven was held at 50 °C for 8 min and then raised to 250 °C at 100 °C min^{-1}.

4.3 Results and discussion

The co-polymerisations of MAA and TRIM were carried out by suspension and bulk polymerisation procedures using 2-aminopyridine as template. These polymers were examined and characterised using a thermal desorption GC-MS method and performance was correlated with solution phase affinity studies.

4.3.1 Polymer thermal pre-treatment analysis

Polymers initially required thermal pre-treatment to remove any partially or unreacted monomers using the GC-MS. Two consecutive pre-treatments for the same sample of MIP and NIP species were carried out for each of the polymers. The first and second thermal pre-treatment profiles obtained for 2-apy NIP and MIP suspension polymers prepared at 9500 rpm, in reconstructed ion chromatogram (RIC) mode are superimposed and shown in Figure 4.1. The chromatogram represents the summation of all ions detected within the pre-selected mass range, i.e. *m/z* 40 to 350. In the initial pre-treatment, a maximum height of 1.25 MCounts was produced from NIP pre-treatment in contrast to 0.30 MCounts by the MIP. In the compositional analysis of the thermal pre-treatment of 9500 rpm MIP and NIP polymers, it was apparent that substantially more bleed from the NIP compared with the MIP polymers was observed in the spectra ranging from *m/z* range 40 to 350 as illustrated in Figure 4.1. This observation must be treated with caution, as some compositional material would have been removed in the washing stage of the suspension polymers with acetone. A substantial reduction in the height of the thermal pre-treatment profile was observed in the MIP following the second pre-treatment step however there is still bleed present in the NIP.

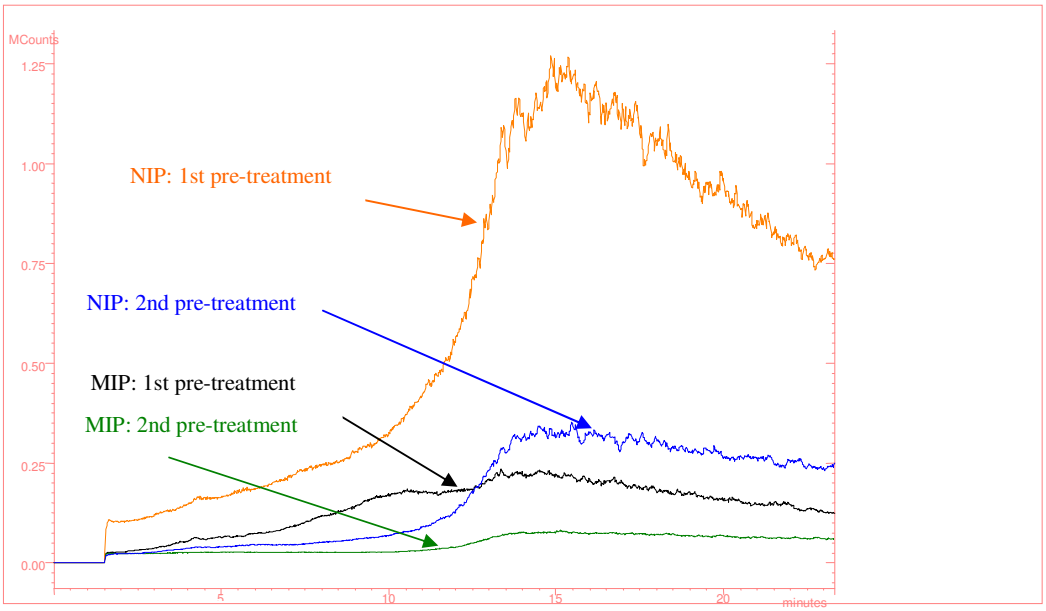

Figure 4.1 **Reconstructed Ion Chromatograms (RIC) for the first and second thermal pre-treatment profiles for 2-apy suspension MIP and NIP imprinted polymer (9500 rpm) with TRIM as cross-linker. Plot of relative abundance versus time.**

Similar thermal pre-treatments were conducted on the bulk and suspension (24000 rpm) MIP and NIP polymers. The bulk had significantly less bleed than the 24000 rpm suspension MIP and NIP polymers after the second pre-treatment. As bulk polymer monoliths were ground and sieved using acetone, some of the compositional material would have been removed in the washing stage.

As a result of the NIP bleed remaining after two successive pre-treatments on both suspension polymers, a third pre-treatment was required to follow the decline in polymer bleed in order to achieve a flat baseline. Also, the bleed did not interfere with the subsequent rebinding studies.

In order to examine the reason for significantly more bleed remaining in the NIP suspension polymers in comparison to the bulk polymer monolith after two pre-treatments, a post-analysis was used to examine specific ions. Cummins *et al.* [4] have reported that a specific benefit of MS detection is its ability to examine compounds of interest in the presence of co-eluting mixtures given that a single ion for the analyte of interest can be identified in the spectral data. The only requirement is that the analyte of interest generates a unique ion of sufficient abundance. For the

MIP polymer to exhibit a specific desorption of 2-apy, a method of analysis and a technique capable of detecting 2-apy was developed by Cummins *et al*. [4] based on *m/z* 94, the molecular ion of 2-apy.

Figure 4.2 demonstrates the 1st pre-treatment profile for the three sets of MIP and NIP polymers in this study but plotted for the *m/z* 94 ion only. For all three sets of NIP polymers, the 94 ion was not detected above the general background level, indicating that background polymer bleed did not interfere with the calculation of template pre-treatment. An increase in response for the bulk polymer monoliths was observed in contrast to both suspension polymers. A second pre-treatment was performed on all three sets of polymers and no residual template was detected as flat baselines were achieved. This signifies that one pre-treatment was adequate to remove the bound template. Triplicate analysis was performed and the amount of 2-apy which was displaced for each of the three sets of polymers was consistently reproducible.

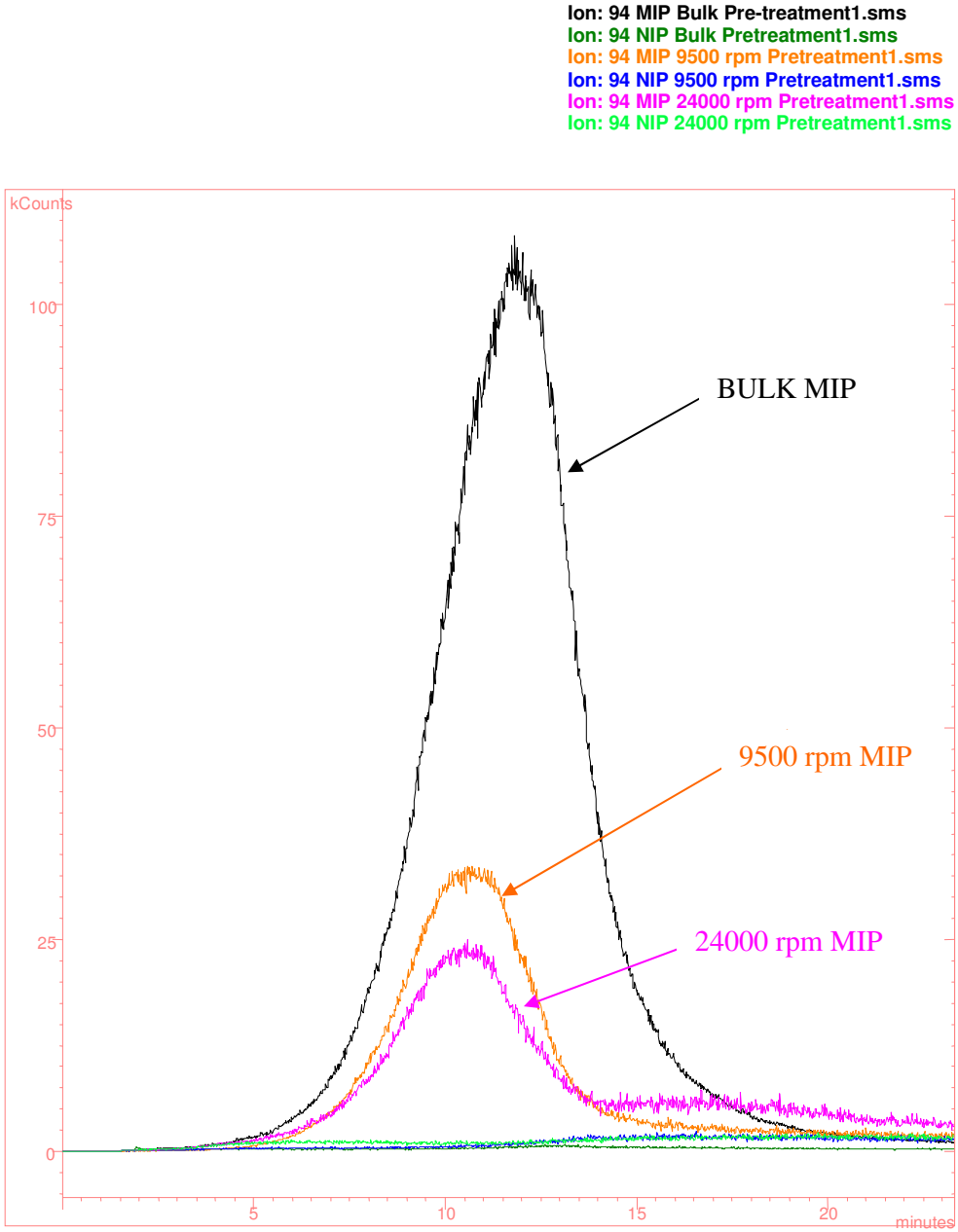

Figure 4.2 **Selected ion chromatogram for 2-apy template (*m/z* 94 ion) for first thermal pre-treatment of MIP and NIP suspension (9500 and 24000 rpm) and bulk polymer monoliths. Plot of relative abundance versus time.**

Post analysis selection of other specific ions for bulk and suspension (9500 and 24000 rpm) polymers was carried out and revealed that the bleed consisted mainly of TRIM. The 338 ion is the molecular ion for TRIM, the cross-linker and base peak is the *m/z* 69 ion (this was determined using analysis of TRIM). Figure 4.3 demonstrates the 1st

desorption profile for the three polymers but plotted for the *m/z* 69 ion only. A similar pattern was observed as in the RIC profile in Figure 4.1, with the NIP polymers showing significantly more bleed from thermal pre-treatment.

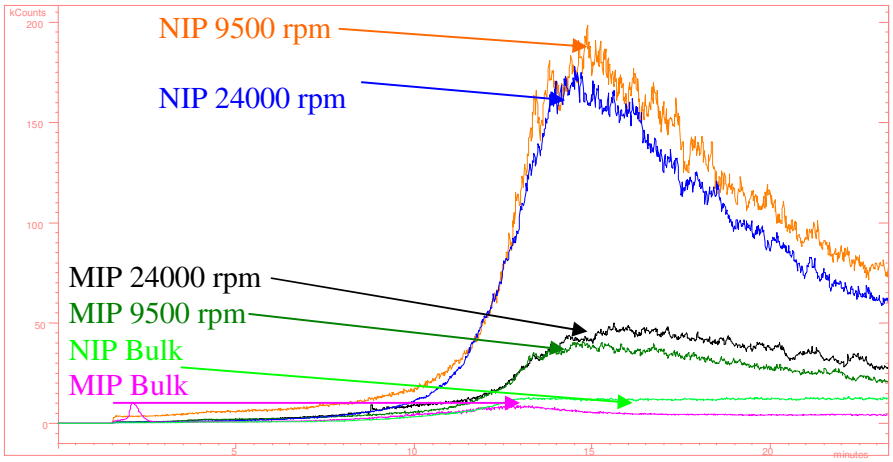

Figure 4.3 **Selected ion chromatogram for TRIM (*m/z* 69 ion) cross-linking monomer for first thermal pre-treatment of MIP and NIP suspension (9500 and 24000 rpm) and bulk polymer monoliths. Plot of relative abundance versus time.**

In this study, as TRIM was employed as the cross-linker, it could be suggested that cross-linking density of the NIP polymeric complex may be lower than that held by the MIP, which could have resulted in the high level of bleed in the NIP. There was a slight difference in bleed between the NIP polymers prepared at 9500 and 24000 rpm (Figure 4.3). This suggested that less cross-linking monomer was incorporated within the 9500 rpm polymer network as slightly more of it came off when heated. This could be due to the fact the 9500 rpm polymers are larger size beads in comparison to 24000 rpm polymers and the cross-linker is more trapped inside these beads and thus harder to wash out.

A greater difference in bleed was observed between suspension and bulk polymer bleed for the NIP and MIP. This could be due to the bulk polymer monoliths being ground and sieved with acetone, which therefore removed a lot of the soluble material. There was a definite morphology difference between NIPs and MIPs employing EGDMA [4], implying that a greater degree of cross-linking and polymerisation occurred in the imprinted polymer.

4.3.2 Thermal desorption of reloaded 2-apy

Thermal desorption/rebinding studies were performed on the MIP and NIP for all three polymer sets which were pre-treated as described in Section 4.2.2 to remove residual template and unreacted monomers. To assess the MIP and NIP polymers for a specific response to the 2-apy template, each polymer was loaded with a 2-apy solution in acetonitrile. The reloaded analyte was again placed in the probe and desorbed using a second temperature programme used for template desorption studies as described in Section 4.2.3. The displacement of the 2-apy was followed by selecting the *m/z* 94 ion. The desorption programme consisted of two temperature ramps, an initial increase from 80 to 200 °C and a more aggressive ramp from 200 to 250 °C. The temperature ramps correspond to the two peaks produced in the desorption profiles. The area of the second peak corresponds with the second ramp in the temperature programme.

4.3.2.1 Thermal desorption of reloaded 2-apy bulk and suspension (9500 and 24000 rpm) imprinted MIP and NIP polymers using a 4 mg mL^{-1} 2-apy in acetonitrile solution.

Alternate loadings of MIP and NIP were performed until each polymer had been loaded and desorbed a total of seven times. Figures 4.4 and 4.5 illustrate the first and seventh desorption profiles obtained from the loading of a 2-apy MIP and NIP plotted for *m/z* 94. The area under each peak represents the amount of material desorbed and the degradation of binding in the three sets of polymers. This suggests that the polymers maintained an affinity to bind the loaded 2-apy standard solution with the Area of Peak 2 appearing to diminish with consecutive analyses.

The area of the second peak is of different intensity to the first peak, and for the MIP is considerably larger than for the corresponding NIP in all three sets of polymers. The results present evidence of specificity by its own polymer for the template 2-apy. The MIP retained the loaded 2-apy to a bigger extent than the NIP, indicating a possible imprinting effect as seen in previous results [4].

The % Area of Peak 2 for MIPs corresponds to $\%P2_{MIP}$, calculated as shown in Equation 4.1. Similarly, $\%P2_{NIP}$ denotes the % Area of Peak 2 for NIPs.

$$\%\ P2_{MIP} = \frac{AreaPeak2}{TotalArea} \qquad \textbf{Equation 4.1}$$

Imprinting factor (IF) is a measure of the strength of interaction of the imprinted polymer towards the template molecule. Where IF represents the imprinting factor, calculated as shown in Equation 4.2:

$$IF = \frac{\%\ P2_{MIP}}{\%\ P2_{NIP}} \qquad \textbf{Equation 4.2}$$

The areas of the profiles were integrated and tabulated for the seven consecutive analyses performed on each polymer. Integrations for these analyses are presented in Tables 4.2 and 4.3, which includes the Area of Peak 2 (given as percentage) in relation to the total area for 2-apy for all three sets of polymers.

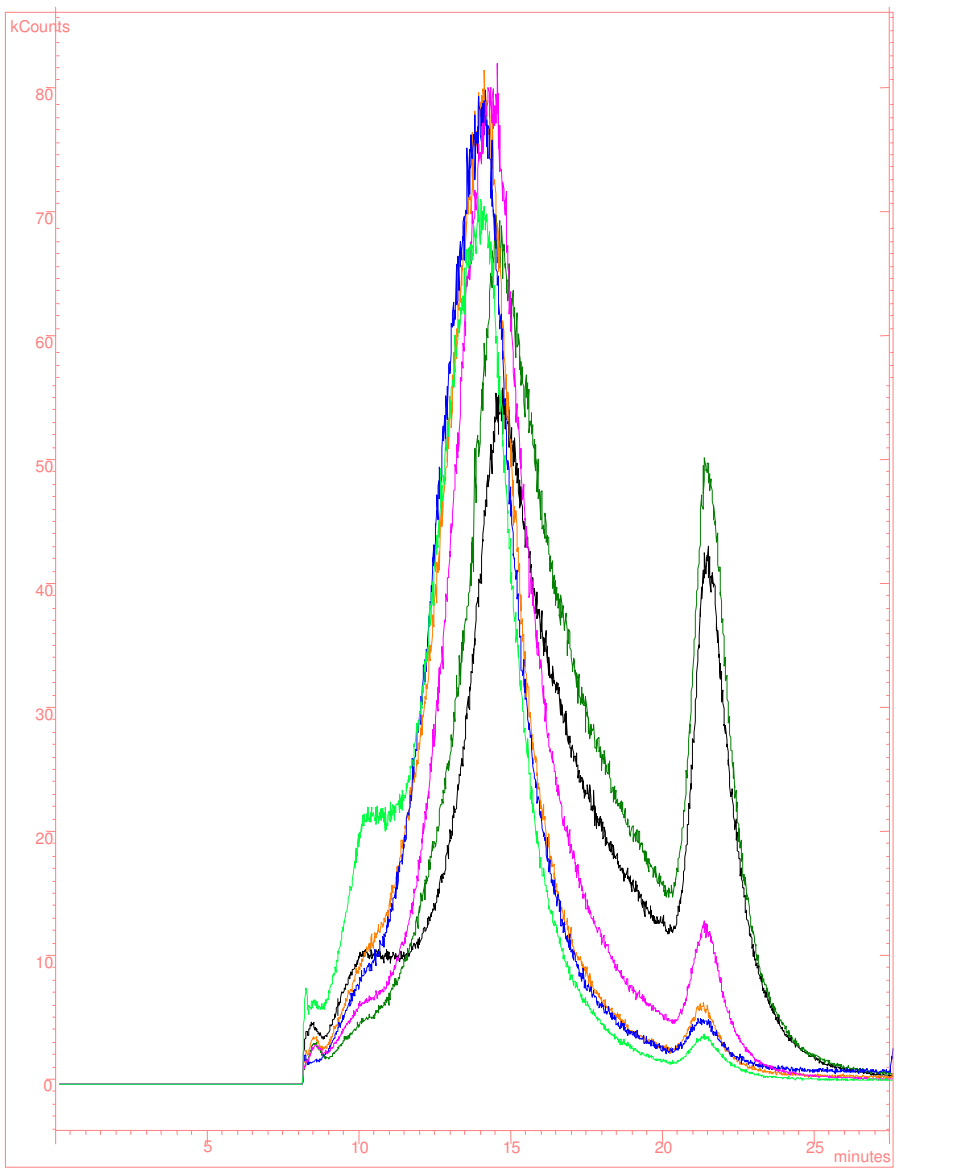

Figure 4.4 **First thermal desorption profile for a reloaded acetonitrile solution of 2-apy (*m/z* 94) (relative abundance versus time) obtained for MIP and NIP bulk and suspension imprinted polymers (9500 & 24000 rpm) with TRIM as cross-linker using a 4 mg mL^{-1} 2-apy in acetonitrile solution.**

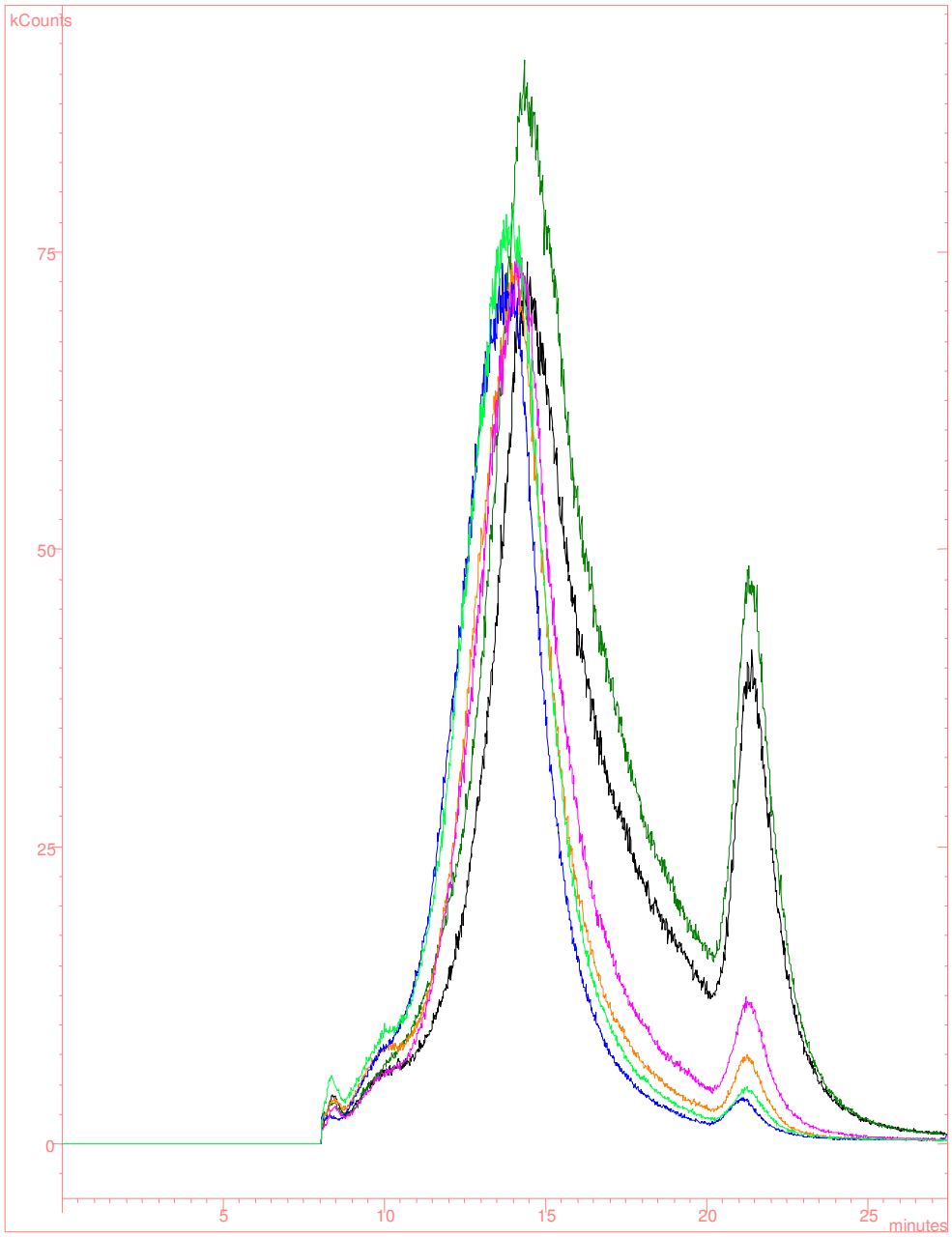

Figure 4.5 **Seventh thermal desorption profile for a reloaded acetonitrile solution of 2-apy (*m/z* 94) (relative abundance versus time) obtained for MIP and NIP bulk and suspension imprinted polymers (9500 & 24000 rpm) with TRIM as cross-linker using a 4 mg mL^{-1} 2-apy in acetonitrile solution.**

Table 4.2 **Integration of MIP and NIP thermal desorption areas for (*m/z* 94) bulk and suspension polymers (9500 & 24000 rpm) imprinted polymers with TRIM as cross-linker reloaded using a 4 mg mL^{-1} 2-apy acetonitrile solution.**

	MIP			NIP			IF
Bulk Run	**Total area kCounts**	**Area Pk2 kCounts**	**% Area Pk2**	**Total area kCounts**	**Area Pk2 kCounts**	**% Area Pk2**	$\frac{\%P2_{MIP}}{\%P2_{NIP}}$
1	13551	2865	21.14	11273	2086	18.50	1.14
2	11738	2523	21.49	13874	2164	15.60	1.38
3	12596	2503	19.87	14591	1892	12.97	1.53
4	13884	2459	17.71	14756	1964	13.31	1.33
5	12674	2243	17.70	14518	1810	12.47	1.42
6	12801	2196	17.15	15495	1886	12.17	1.41
7	15968	2303	14.42	15070	1838	12.20	1.20
9500 rpm Run							
1	12846	251	1.95	13000	191	1.47	1.33
2	13541	363	2.68	12270	170	1.39	1.92
3	12173	345	2.83	13488	164	1.22	2.32
4	11956	321	2.68	14475	184	1.27	2.11
5	12174	328	2.69	11681	154	1.32	2.04
6	12379	312	2.52	12649	164	1.30	1.94
7	11975	307	2.56	12137	145	1.19	2.15
24000 rpm Run							
1	15274	599	3.92	7647	168	2.19	1.79
2	16034	584	3.64	12386	197	1.59	2.29
3	14800	570	3.85	9637	189	1.96	1.96
4	17429	681	3.91	10839	177	1.63	2.40
5	15219	588	3.86	11495	169	1.47	2.63
6	14097	558	3.96	12415	192	1.55	2.55
7	14587	588	4.03	12848	196	1.53	2.63

Table 4.3 **Thermal desorption data for 2-apy (*m/z* 94 ion) for 2-apy bulk and suspension imprinted MIP and NIP polymers with TRIM as cross-linker reloaded using a 4 mg mL^{-1} 2-apy acetonitrile solution. Results are based on average values from seven analyses with ± 1 standard deviation.**

	MIP			NIP			IF
Polymer	**Total area kCounts (± 1 S.D)**	**Area Pk2 kCounts (± 1 S.D)**	**% Area Pk2 (± 1 S.D)**	**Total area kCounts (± 1 S.D)**	**Area Pk2 kCounts (± 1 S.D)**	**% Area Pk2 (± 1 S.D)**	$\frac{\%P2_{MIP}}{\%P2_{NIP}}$ **(± 1 S.D)**
Bulk	13316	2442	18.5	14225	1949	13.9	1.3
	(0.10)	(0.09)	(0.14)	(0.10)	(0.07)	(0.17)	(0.13)
Suspension	12435	318	2.6	12814	167	1.3	2.0
(9500 rpm)	(0.05)	(0.11)	(0.11)	(0.07)	(0.10)	(0.07)	(0.31)
Suspension	15349	595	3.9	11038	184	1.7	2.3
(24000 rpm)	(0.07)	(0.07)	(0.03)	(0.17)	(0.07)	(0.16)	(0.33)

For the bulk polymer monoliths a consistent decrease in the relative Area of Peak 2 (%P2) with repeat analysis was observed, varying from 21.5 % to 14.4 % for MIP desorptions. Similar desorptions were observed for NIP, as peak 2 degraded from 18.5 % to 12.2 % (Table 4.2). While the %P2 decreased with repeat loading, the average IF value remained essentially unchanged for the bulk polymer (1.3 ± 0.1). The %P2 was larger for the MIP desorption than that of the equivalent NIP for all desorptions conducted.

A significant decrease in %P2 for bulk MIP and NIP polymers was observed (Table 4.2); this trend was also observed for both the suspension NIP polymers (9500 rpm: 1.47 – 1.19 and 24000 rpm: 2.19 – 1.47). However, %P2 values were consistent for consecutive analyses of suspension MIP polymers, and did not diminish as in the bulk.

A second observation in Tables 4.2 and 4.3, was that the IF values were higher for both suspension polymers than bulk. The average IF value for the bulk was 1.3 ± 0.1 in comparison to the average IF values for suspension 9500 rpm and 24000 rpm polymers, which were 2.0 ± 0.3 and 2.3 ± 0.3 respectively (Tables 4.3). The difference between bulk and suspension polymers could be due to the influence of the

mineral oil on the solubilisation of pre-polymerisation components which could be affecting the suspension composition. Additionally, a higher temperature was employed in the bulk polymerisation which could also be affecting the interactions.

Also, the IF value for 24000 rpm was greater in comparison to the 9500 rpm suspension polymer (Table 4.3). The average IF values for 9500 and 24000 rpm suspension polymers were 2.0 ± 0.3 and 2.3 ± 0.3 respectively. This suggests that the 24000 rpm suspension polymer maintained its ability to retain the analyte of the loaded material with consecutive analyses better than the 9500 rpm polymer.

In Figures 4.4 and 4.5, MIP and NIP polymers reloaded with 5 μL of a 4 mg mL^{-1} solution of 2-apy in acetonitrile, displayed a difference in response for bulk and suspension polymers. In all polymers the MIPs retained the loaded material to a greater degree, i.e. a higher temperature was required to desorb 2-apy. This effect was consistent and reproducible.

An interesting observation between both bulk and suspension polymers in Figures 4.4 and 4.5 was the peak shapes. The bulk polymer monoliths had a broader peak with more tailing in contrast to the suspension polymers which were sharper peaks with less tailing, which demonstrates a possible surface phenomenon (implying the 2-apy is bound only to the surface of the polymer due to rigidity, thus preventing access.) Better particle geometry in suspension polymers could be a reason why peak tailing is reduced. SEM images of bulk and suspension polymers in Chapter 2 showed suspension polymers to be spherical in shape in comparison to the bulk polymer monoliths which were irregular shaped particles. Another possible explanation to the difference between results could be due to the diffusion of reloaded analyte into the internal binding sites (binds to good sites randomly distributed in MIP and NIP) for bulk and suspension polymers. However, the total area counts across Tables 4.2 and 4.3 for bulk and suspension polymers (9500 and 24000 rpm) exhibit similar values and the small differences in total area counts could be due to small injection differences.

4.3.2.2 Thermal desorption of reloaded 2-apy bulk and suspension (9500 and 24000 rpm) imprinted MIP and NIP polymers using a 0.4 mg mL^{-1} 2-apy in acetonitrile solution.

A second study was conducted where reloadings were performed using 5 µL of 0.4 mg mL^{-1} solution of 2-apy in acetonitrile. The aim of this study was to examine the change in IF value using a more dilute standard for the three sets of polymers, as a lower loading ratio might be expected to favour rebinding to imprinted sites. Alternate loadings of MIP and NIP were performed until each polymer had been loaded and desorbed a total of three times. Figure 4.6 illustrates the third thermal desorption representing degradation of binding which occurred in the three sets of polymers. Integrations for these analyses are presented in Tables 4.4 and 4.5.

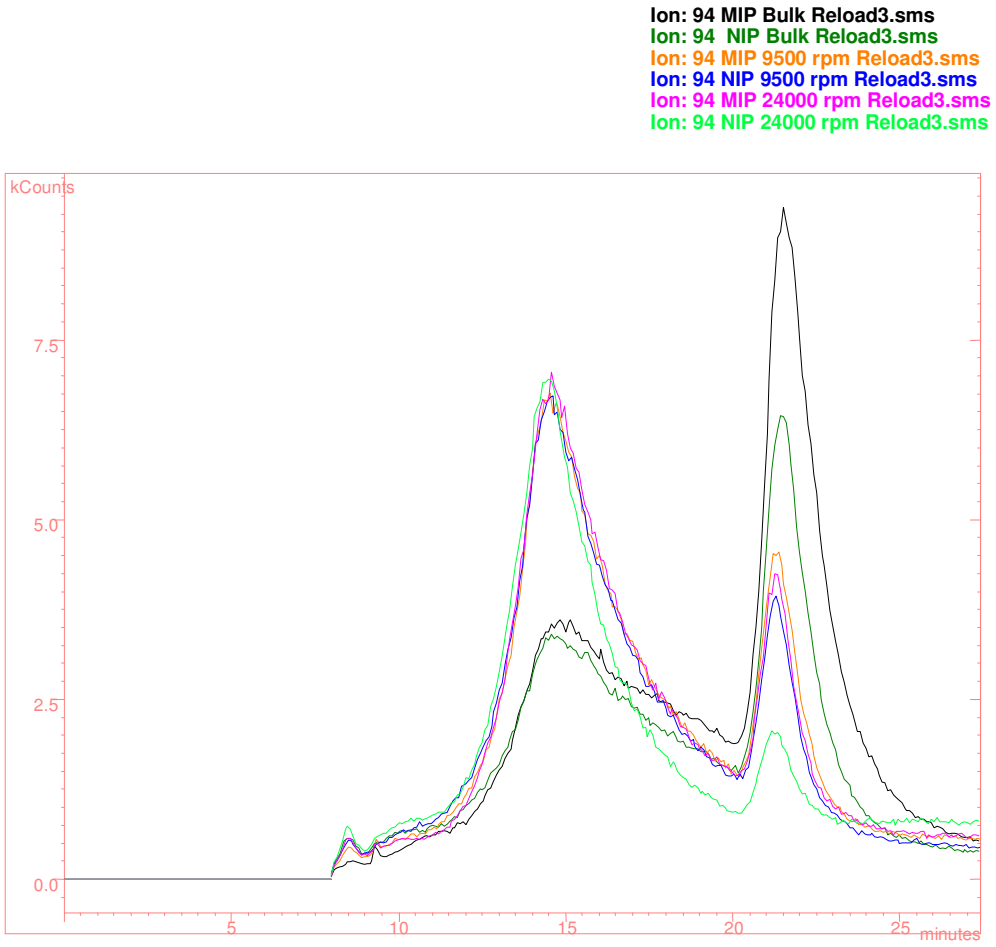

Figure 4.6 **Third thermal desorption profile for a reloaded acetonitrile solution of 2-apy (*m/z* 94) (relative abundance versus time) obtained for MIP and NIP bulk and suspension imprinted polymers (9500 & 24000 rpm) using a 0.4 mg mL^{-1} 2-apy in acetonitrile solution.**

Table 4.4 **Integration of MIP and NIP thermal desorption areas for (*m/z* 94) bulk polymers and suspension polymers (9500 & 24000 rpm) imprinted polymers with TRIM as cross-linker reloaded using a 0.4 mg mL^{-1} 2-apy acetonitrile solution.**

	MIP			NIP			IF
Bulk Run	**Total area kCounts**	**Area Pk2 kCounts**	**% Area Pk2**	**Total area kCounts**	**Area Pk2 kCounts**	**% Area Pk2**	$\frac{\%P2_{MIP}}{\%P2_{NIP}}$
1	1574	743	47.20	1439	510	35.44	1.33
2	1420	708	49.86	1409	485	34.42	1.45
3	1818	787	43.29	1393	468	33.59	1.29
9500 rpm Run							
1	1853	251	13.55	1597	175	10.96	1.24
2	1863	238	12.78	1858	207	11.14	1.15
3	1775	244	13.75	1691	170	10.05	1.37
24000 rpm Run							
1	1733	195	11.95	2342	105	4.48	2.67
2	1595	183	11.47	1114	83	7.45	1.54
3	1724	194	11.25	1241	74	5.96	1.89

Table 4.5 **Thermal desorption data for 2-apy (*m/z* 94 ion) for 2-apy bulk and suspension imprinted MIP and NIP polymers with TRIM as cross-linker reloaded using a 0.4 mg mL^{-1} 2-apy acetonitrile solution. Results are based on average values from triplicate analyses with ± 1 standard deviation.**

	MIP			NIP			IF
Polymer	**Total area kCounts (± 1 S.D)**	**Area Pk2 kCounts (± 1 S.D)**	**% Area Pk2 (± 1 S.D)**	**Total area kCounts (± 1 S.D)**	**Area Pk2 kCounts (± 1 S.D)**	**% Area Pk2 (± 1 S.D)**	$\frac{\%P2_{MIP}}{\%P2_{NIP}}$ **(± 1 S.D)**
Bulk	1604 (0.13)	746 (0.05)	46.8 (0.07)	1414 (0.02)	488 (0.04)	34.5 (0.03)	1.4 (0.08)
Suspension (9500 rpm)	1830 (0.03)	244 (0.03)	13.4 (0.04)	1715 (0.08)	184 (0.11)	10.7 (0.05)	1.3 (0.11)
Suspension (24000 rpm)	1684 (0.05)	191 (0.04)	11.6 (0.03)	1566 (0.43)	87.3 (0.18)	6.0 (0.25)	2.0 (0.58)

An interesting point of note in this study is the %P2 (a measure of the affinity binding sites) was higher at the lower loading concentration. However, analysing the IF values from the first and second study using 4.0 and 0.4 mg mL^{-1}, the IF was consistent and within experimental error for both studies, i.e. 1.3 ± 0.1 and 1.4 ± 0.1 respectively. By changing the concentration, the bulk polymer still retained affinity. However, a more dramatic effect on the IF value was seen in the suspension polymers which decreased significantly from 2.0 ± 0.3 to 1.3 ± 0.1 for the 9500 rpm suspension polymer and decreased slightly for the 24000 rpm suspension polymer from 2.3 ± 0.3 to 2.0 ± 0.6. Even though the IF for the 24000 rpm polymers decreased slightly, the IF values for the 24000 rpm polymer in the second study were very variable (Table 4.4), ranging from 1.5 – 2.7. A reason for the variable range of IF values across the three runs for 24000 rpm may be due to a very high total area count value in the first NIP value of 2342 for the 24000 rpm polymer, which could be an irregularity, yielding a high IF value for the first run (IF = 2.7).

As in the previous study, MIP and NIP polymers in Tables 4.4 and 4.5 reloaded with 5 µL of a 0.4 mg mL^{-1} solution of 2-apy in acetonitrile, displayed a difference in response for bulk and suspension polymers. In all polymers the MIPs retained the loaded material to a greater degree, i.e. a higher temperature was required to desorb 2-apy. This effect was consistent and reproducible across three successive loadings. In addition, the %P2 increased at the lower loading (Tables 4.4 and 4.5) which implied a higher degree of template rebinding (or better binding sites). However, this happened with both MIP and NIP so that no improvement in IF value was observed at the lower loading.

4.3.2.3 Thermal desorption of reloaded 2-apy suspension (24000 rpm) imprinted MIP and NIP polymers using a 2 mg mL^{-1} 2-apy in acetonitrile solution.

Extending the GC-MS studies conducted in Section 4.3.2.1 and 4.3.2.2, a third study was performed using the 24000 rpm suspension polymer with 2 mg mL^{-1} solution of 2-apy in acetonitrile. In the previous studies the IF values were highest in the 24000 rpm suspension polymer. Therefore, this polymer was employed to further study the effect of reloading in a different concentration on capacity and IF. Polymers were pre-treated and reloaded three times with 5 µL of 2 mg mL^{-1} solution of 2-apy in acetonitrile onto 24000 rpm. The integration of MIP and NIP thermal desorption areas for *m/z* 94 are tabulated in Table 4.6.

Table 4.6 **Thermal desorption data for 2-apy (*m/z* 94 ion) from a 2-apy (24000 rpm) suspension imprinted MIP and NIP polymers using a 2.0 mg mL^{-1} 2-apy acetonitrile solution. Results are based on average values from triplicate analysis with ± 1 standard deviation.**

Suspension 24000 rpm	**MIP**			**NIP**			**IF**
Run	**Total area kCounts**	**Area Pk2 kCounts**	**% Area Pk2**	**Total area kCounts**	**Area Pk2 kCounts**	**% Area Pk2**	$\frac{\%P2_{MIP}}{\%P2_{NIP}}$
1	9593	631	6.58	7279	428	5.88	1.12
2	8736	649	7.43	5838	335	5.74	1.29
3	7931	584	7.36	6116	342	5.59	1.32
Average (± 1 S.D)	8753 (0.10)	621 (0.05)	7.1 (0.06)	6411 (0.12)	368 (0.14)	5.7 (0.02)	1.2 (0.11)

Assessing the trends in Table 4.6, the % Pk2 was consistent for MIP and NIP with each consecutive loading. The total area values for MIP and NIP decreased with each consecutive reloading, which was not observed in the previous studies, i.e. the values for MIP and NIP were consistent, except for an anomaly in the first NIP values in each study (Table 4.2 and 4.4).

The data is consistent and reproducible across three successive reloadings, signifying the polymer maintained its ability to retain the analyte of the loaded material with

consecutive analyses. However, the average IF was considerably reduced, with a value of 1.2 ± 0.1 at this concentration, which contrasts with the expected trend i.e. increasing IF with increasing concentration. In the first study reloading a 4.0 mg mL^{-1} solution of 2-apy in acetonitrile onto 24000 rpm suspension polymers, resulted in an IF = 2.3 ± 0.3. In the second study which involved reloading a 0.4 mg mL^{-1} solution the IF value decreased to 2.0 ± 0.6. As a pronounced effect on the IF value was observed in this study, a higher concentration study was proposed to investigate where optimum loading was occurring.

4.3.2.4 Thermal desorption of reloaded 2-apy suspension (24000 rpm) imprinted MIP and NIP polymers using 8 mg mL^{-1} 2-apy in acetonitrile solution.

A fourth study was carried out reloading 5 µL of 8.0 mg mL^{-1} standard concentration onto 24000 rpm polymer MIP and NIP. Polymers were pre-treated before reloading. The integration of MIP and NIP thermal desorption areas for *m/z* 94 are tabulated in Table 4.7.

Table 4.7 **Thermal desorption data for 2-apy (*m/z* 94 ion) for a 2-apy (24000 rpm) suspension imprinted MIP and NIP polymers with TRIM as cross-linker reloaded using a 8.0 mg mL^{-1} 2-apy acetonitrile solution. Results are based on average values from triplicate analysis with ± 1 standard deviation.**

Suspension 24000 rpm	**MIP**			**NIP**			**IF**
Run	**Total area kCounts**	**Area Pk2 kCounts**	**% Area Pk2**	**Total area kCounts**	**Area Pk2 kCounts**	**% Area Pk2**	$\frac{\%P2_{MIP}}{\%P2_{NIP}}$
1	28540	858	3.00	23392	500	2.14	1.40
2	26755	862	3.22	24058	458	1.90	1.69
3	26977	795	2.95	23587	419	1.78	1.66
Average (± 1 S.D)	27424 (0.04)	838 (0.05)	3.1 (0.05)	23679 (0.01)	459 (0.09)	1.9 (0.09)	1.6 (0.16)

From Table 4.7, total area counts were similar in both MIP and NIP polymers, with a slight decrease for the first value in the MIP. The data is consistent and reproducible

across three successive reloadings. However, the IF was reduced employing 8.0 mg mL^{-1} solution with a value of 1.6 ± 0.2. The highest average IF value was observed in the first study employing a 4.0 mg mL^{-1} solution of 2-apy in acetonitrile was 2.3 ± 0.3, implying that optimum reloading had occurred at this concentration. The variation in IF values with different concentration implies that all the sites may not be filled reloading with a lower concentration. In addition, saturation could be reached reloading with a higher concentrated solution, and somewhere in the middle the optimum reloading occurred.

4.3.2.5 Summary of thermal desorption results for bulk and suspension imprinted polymers across four different concentrations.

The thermal behaviour of bulk and suspension polymers was studied by means of direct probe GC-MS. As previously reported [4] the MS specificity provided a way of studying template extraction and bleed composition. Similar conclusions were drawn in this study to previous findings [4], however rebinding studies to assess specificity by MIP and NIP polymers revealed differences between imprinted and non-imprinted polymers for bulk and suspension polymers.

A summary of the average IF values calculated from GC-MS data for four different concentrations (0.4, 2.0, 4.0 or 8.0 mg mL^{-1}) of 2-apy in acetonitrile for bulk and suspension (9500 and 24000 rpm) imprinted polymers is presented in Table 4.8.

Table 4.8 **IF values calculated from GC-MS data by reloading four different concentrations on bulk and suspension (9500 and 24000 rpm) imprinted polymers. Results based on average values based on ± 1 standard deviation.**

Polymer	0.4 mg mL^{-1}	2.0 mg mL^{-1}	4.0 mg mL^{-1}	8.0 mg mL^{-1}
Bulk	1.4 ± 0.1	n/a	1.3 ± 0.1	n/a
9500 rpm	1.3 ± 0.1	n/a	2.0 ± 0.3	n/a
24000 rpm	2.0 ± 0.6	1.2 ± 0.1	2.3 ± 0.3	1.6 ± 0.2

IF values are consistent and within error at 0.4 and 4.0 mg mL^{-1} standard concentrations. However, IF values increased significantly for the 9500 rpm and 24000 rpm suspension polymers for 0.4 and 4.0 mg mL^{-1} standard concentrations.

The 24000 rpm polymer was further reloaded with two different standard concentrations at 2.0 mg mL^{-1} and 8.0 mg mL^{-1}. From Table 4.8 the average IF values for both concentrations were 1.2 ± 0.1 and 1.6 ± 0.2 respectively. Both standard concentrations were lower than the 4.0 mg mL^{-1} standard solution, with an IF of 2.3 ± 0.3, possibly indicating that the optimum loading had occurred using this concentration. The change in the IF value across the four concentrations performed for the 24000 rpm suspension polymers can be analysed in the context of capacity and loading level (Tables 4.2, 4.4, 4.6 and 4.7). The %P2 decreased for the MIP by reloading in a lower to a higher concentration, i.e. %P2: 11.6, 7.1, 3.9 and 3.1 respectively. A similar decreasing trend going from lower to a higher concentration with the NIP polymers was observed, i.e. % P2: 6.0, 5.7, 1.7 and 1.9 respectively (with a slight increase in the last value). However, the total area (kCounts) for 24000 rpm MIP and NIP suspension polymer increased going from low concentration to high, i.e. 0.4 – 8.0 mg mL^{-1}, indicating a linear response for both MIPs and NIPs as shown in Figure 4.7.

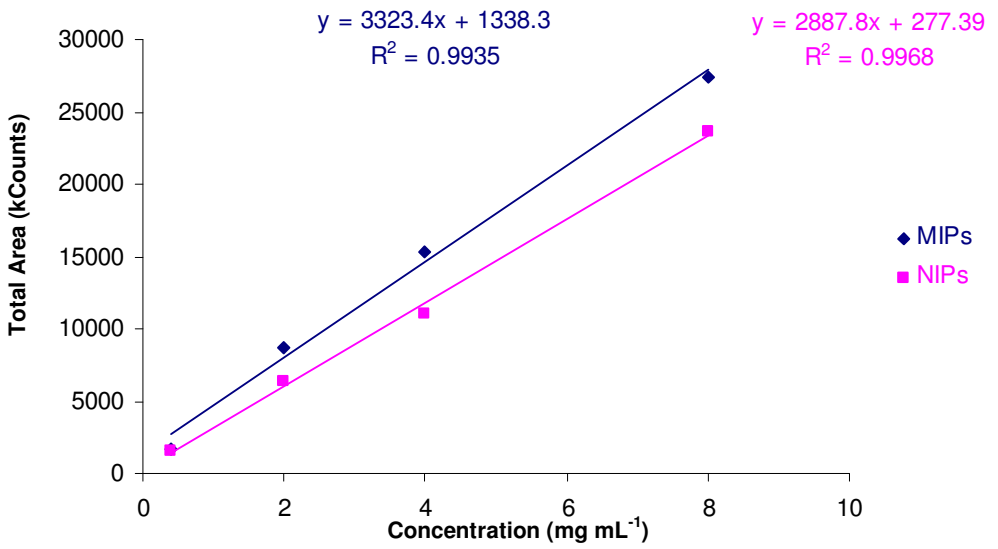

Figure 4.7 **Total area (kCounts) plotted against varying concentration (0.4 – 8.0 mg mL^{-1}) for 24000 rpm MIP and NIP suspension imprinted polymers24000 rpm imprinted polymers with TRIM as cross-linker.**

In this study, where TRIM was employed as cross-linker, it could be suggested that cross-linking density of the NIP polymeric complex may be lower than that held by the MIP, which could have resulted in the high level of bleed from the NIP suspension polymers. The behaviour of bulk and suspension polymers using TRIM was different also. Both networks are cross-linked with the same amount of cross-linker nevertheless a higher degree of thermal degradation was observed in the bulk MIP rather than the suspension. Thermal desorption profiles exhibited differing peak shapes for bulk and suspension polymers (Figures 4.4 and 4.5). The approximate spread of the peaks was quantitatively determined for bulk and suspension MIP and NIP polymers by calculating the peak widths at half the peak height from the thermal desorption profiles. The results are shown in Table 4.9.

Table 4.9 **The approximate spread in peak shapes from the thermal desorption profiles was determined by calculating the peak widths at half the peak height for bulk and suspension MIP and NIP polymers.**

Polymer	1st Peak (mins)	2nd Peak (mins)
Bulk MIP	14.8	22
Bulk NIP	14.8	21.8
9500 MIP	13.5	21.3
9500 NIP	13.5	21.3
24000 MIP	14	21.3
24000 NIP	13.5	21.3

In Table 4.9, the spread for bulk MIP and NIP polymers prepared exhibited broad distributions in comparison to the suspension polymers. The bulk polymer monoliths had broader peaks with more tailing in contrast to the suspension polymers which had sharper peaks with less tailing (Figures 4.4 and 4.5), which demonstrates a possible surface phenomenon. This could be due to differences in particle sizes between suspension polymers, i.e. the 9500 rpm suspension polymer had bigger particle size diameters than the 24000 rpm suspension polymer, and the MIPs for both polymers were smaller than the NIPs. Another difference between bulk and suspension polymers could be due to different ratios of monomers in the suspension polymers, possibly due to the influence of the mineral oil on the solubilisation of pre-polymerisation components which could be affecting the suspension composition.

Additionally, a higher temperature was employed in the bulk polymerisation which could also be affecting the interactions.

4.3.4 Comparison of UV and GC-MS rebinding analyses.

Based on UV rebinding experiments in Chapter 3, binding isotherm MIP and NIP experimental values for concentration of bound template (mM) were obtained and IF values were calculated for a concentration range spanning 0.2 mM – 8.0 mM. In this chapter, GC-MS methodology was utilised to characterise the performance of polymers synthesised under varying conditions in the absence of solvent. A correlation between the GC-MS results and the UV binding isotherm results was evaluated in terms of assessing and comparing IF values at one concentration (0.4 mg mL^{-1}). The reason only one standard concentration, i.e. 0.4 mg mL^{-1} could be used for this evaluation is due to the different concentration ranges used for the UV and GC-MS analyses, from mM to mg mL^{-1} (same units as GC-MS data). Table 4.9 presents a summary of the average IF values for UV and GC-MS results.

Table 4.9 **Comparison of IF values for UV and GC-MS results at 0.4 mg mL^{-1} standard concentration in acetonitrile.**

Polymer	Binding isotherm (IF)	GC-MS (IF)
Bulk	1.7 ± 0.1	1.4 ± 0.1
9500 rpm	1.0 ± 0.2	1.3 ± 0.1
24000 rpm	2.0 ± 0.2	2.0 ± 0.6

The IF values for both the binding isotherm analysis and GC-MS study exhibited great similarity for bulk and suspension polymers in Table 4.9. A direct comparison was found in imprinting performance for GC-MS and UV solution phase analysis. Therefore, the GC-MS technique used to characterise the bulk and suspension polymers is a very good methodology in terms of assessing IF values over the solution phase rebinding studies. These findings would make a case for the merit of GC-MS methodology as an alternative technique to solution phase binding studies for assessing IF values in the absence of solvent.

4.4 Conclusions

A thermal desorption GC-MS technique was employed to assess the performance of suspension and bulk polymers (MIPs and NIPs). The key findings were:

- Polymer pre-treatment experiments were conducted on bulk and suspension polymers. The bulk had significantly less bleed than the suspension MIP and NIP polymers after the second pre-treatment. This could be due to the bulk polymer monoliths being ground and sieved with acetone, which therefore removed a lot of the soluble material.

- Thermal desorption profiles exhibited differing peak shapes for bulk and suspension polymers. The bulk polymer monoliths had broader peaks with more tailing in contrast to the suspension polymers which had sharper peaks with less tailing.

- The specificity was less in the bulk polymers in comparison to the suspension polymers. IF values for the bulk polymer at 0.4 and 4.0 mg mL^{-1} standard concentrations were similar (IF: 1.4 ± 0.1 and 1.3 ± 0.1). However, IF values significantly increased for the 9500 rpm (IF: 1.3 ± 0.1 and 2.0 ± 0.3) and 24000 rpm suspension polymers (IF: 2.0 ± 0.6 and 2.3 ± 0.3) going from 0.4 to 4.0 mg mL^{-1} standard concentrations.

- A relationship between % Area of Peak 2 and standard concentrations reloaded was also observed for bulk and suspension polymers. The capacity varied with different concentrations reloaded. A significant decrease in %P2 for bulk MIP and NIP polymers was seen. A different trend was seen for the suspension polymers, values for %P2 were consistent for 9500 and 24000 rpm suspension polymers, and did not diminish as in the bulk. This suggests that suspension polymers maintained its ability to retain the analyte of the loaded material with consecutive analyses in contrast to the bulk.

- The 24000 rpm suspension polymers were reloaded with four different standard concentrations (0.4, 2.0, 4.0 or 8.0 mg mL^{-1}). The highest IF value of

2.3 ± 0.3 was found for 4.0 mg mL^{-1} standard concentration, possibly indicating that the optimum loading had occurred using this concentration. The variation in IF values with different concentration implies that all the sites may not be filled reloading with a lower concentration. In addition, saturation could be reached reloading with a higher concentrated solution, and somewhere in the middle the optimum reloading occurred.

- A direct comparison was found in imprinting performance for GC-MS and UV solution phase analysis, implying that thermal desorption is quite a sensitive technique and a very good method of studying MIP performance. Thus the application of thermal desorption GC-MS presents a suitable characterisation technique for polymers.

Reference List

1. Nicholls, I. A.; Adbo, K.; Andersson, H. S.; Andersson, P. O.; Ankarloo, J.; Hedin-Dahlstrom, J.; Jokela, P.; Karlsson, J. G.; Olofsson, L.; Rosengren, J.; Shoravi, S.; Svenson, J.; Wikman, S. *Analytica Chimica Acta* **2001,** *435*, 9-18.

2. Levchik, G. F.; Si, K.; Levchik, S. V.; Camino, G.; Wilkie, C. A. *Polymer Degradation and Stability* **1999,** *65*, 395-403.

3. Uhl, F. M.; Levchik, G. F.; Levchik, S. V.; Dick, C.; Liggat, J. J.; Snape, C. E.; Wilkie, C. A. *Polymer Degradation and Stability* **2001,** *71*, 317-25.

4. Cummins, W.; Duggan, P.; McLoughlin, P. *Analytical and Bioanalytical Chemistry* **2008,** *391*, 1237-44.

5. Holland, N.; Duggan, P.; Owens, E.; Cummins, W.; Frisby, J.; Hughes, H.; McLoughlin, P. *Analytical and Bioanalytical Chemistry* **2008,** *391*, 1245-53.

6. Holland, N.; Frisby, J.; Owens, E.; Hughes, H.; Duggan, P.; McLoughlin, P. *Polymer* **2010,** *51*, 1578-84.

Chapter 5

HPLC-based chiral separations of chlorpheniramine and its structural analogues using aqueous suspension imprinted polymer beads

5.1 Introduction

In the pharmaceutical industry resolution of chiral compounds is very important as enantiomers of drug compounds can exhibit large differences in pharmacological and toxicological properties [1]. When MIPs are used for chromatographic separations, the isomer used as the template is the one that is more strongly retained; as a result the elution order is predictable [2]. There have been a number of HPLC methods reported in the literature which involved the chiral separation of chlorpheniramine racemate (CP) on commercial chiral stationary phases [1;3] and stationary phases using MIPs [3]. A β-cyclodextrin chiral stationary phase was developed by Fried *et al*., 2002 [4] for the simultaneous determination of CP and its metabolites in human plasma. Chen *et al*., 2008 [5] studied the chiral separation and determination of CP enantiomers on an achiral column by HPLC using a carboxymethyl-β-cyclodextrin chiral additive. In HPLC chiral recognition on polysaccharide based chiral stationary phases is mainly due to hydrogen bonding and dipole-dipole interactions between enantiomeric solutes and chiral stationary phases [1].

Chlorpheniramine is an antihistamine (H_1-receptor antagonist) drug. It is often used as an ingredient in 'over-the counter' treatments for the common cold and allergic conditions [6]. CP has a chiral carbon and exhibits enantioselectivity in its pharmacological responses [5]. The antihistaminic drug is marketed as a racemic mixture. Antihistamine activity is mainly associated with *d*-chlorpheniramine (*d*-CP) which has the (*S*)-configuration [4], while the *l*-isomer is mainly responsible for the sedative side effects of this drug and has the (*R*)-configuration [7]; refer to Figure 5.1 for chemical structure. As a result, the enantiomeric separation and determination of CP in different dosage forms is important to ensure the quality of the pharmaceutical production of CP. Usually it is administered as a racemate in an 8 mg oral dose in the form of tablets and its half life is approximately 20 hrs in adults [8].

Brompheniramine (BP) differs from CP by the substitution of a bromine atom for the chlorine atom (Figure 5.1) but its actions and uses are similar to those of CP. The usual adult dose of an oral tablet is 4 mg every 4 – 6 hrs, not to exceed 12 mg in 12 hrs and it has a half-life of 25 hours [9]. Similar to CP, the antihistaminic activity of the BP exists predominantly with the *d*-isomer and is of comparable potency [10].

CP, *d*-CP, BP and *d*-BP were used as the free bases in this study. The chemical structures of *d*-CP, *d*-BP and pheniramine (PHEN) are shown in Figure 5.1.

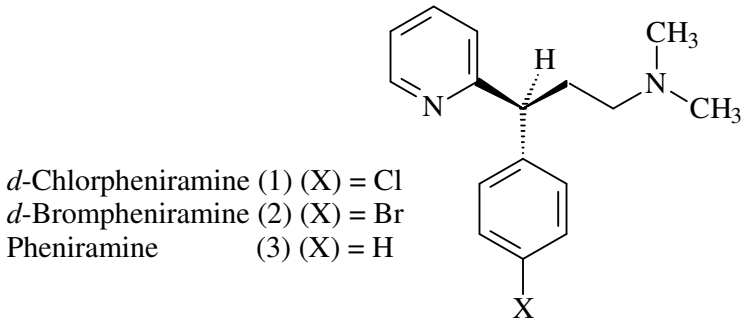

d-Chlorpheniramine (1) (X) = Cl
d-Brompheniramine (2) (X) = Br
Pheniramine (3) (X) = H

Figure 5.1 **The chemical structures of (1) *d*-Chlorpheniramine, X = Cl; (2) *d*-brompheniramine, X = Br and (3) Pheniramine, X = H.**

MIP technology presents the opportunity to tailor chiral stationary phases with pre-defined chiral recognition properties by employing enantiomers of interest as binding-site-forming templates [11]. In chromatographic applications, substantial research efforts have been concentrated on establishing efficient procedures for preparation of spherical MIP particles [12]. In particular, a multi-step swelling and polymerisation method developed by Hosoya and Haginaka [13], has been beneficial in preparing enantioselective, uniformly sized spherical polymer beads.

Chen *et al.* [14] published the first report in 2001 for the preparation of a MIP for CP using methacrylic acid (MAA) as the functional monomer, ethylene glycol dimethacrylate (EGDMA) as cross-linker and chloroform as solvent. The resultant monolith was ground and sieved producing polymer particles (< 30 μm) which were packed into stainless steel columns (150 mm x 4.6 mm i.d.). Chromatographic analysis showed that the retention and the selectivity of the imprinted polymer was greatly strengthened by molecular imprinting. The capacity factor of CP on the MIP was 4.68. Ionic interaction was proven to be the main method for the imprinted polymer to bind CP.

MIPs for *d*-CP and *d*-BP were prepared by Haginaka [15-17] which were used for chiral resolution of CP and BP. The functional monomers used were MAA or 2-(trifluoromethyl)acrylic acid (TFMAA) and EGDMA was employed as the cross-

linker. The resulting MIPs (5 – 6 µm) were packed into a stainless steel column (100 mm x 4.6 mm i.d.) and evaluated using a mixture of phosphate buffer and acetonitrile as mobile phase in HPLC. Haginaka reported that the maximum retention was seen at approximately the apparent pK_a value of the CP enantiomer due to the ionic interaction of the amino group with the negatively charged polymers [15]. In a follow up study Haginaka [16] investigated the separation of CP enantiomers on both MIPs, respectively. The highest retention factors, enantioselectivity and resolution were obtained for MIP prepared with MAA and EGDMA at mobile phase pH 6.2 (k_d = 19.4, α = 1.87, R_s = 0.53) and 8.0 (k_d = 43.1, α = 1.66, R_s = 0.56), and for MIP prepared with TFMAA and EGDMA at mobile phase pH 5.3 (k_d = 70.6, α = 2.16, R_s = 0.86) and 6.2 (k_d = 113, α = 2.12, R_s = 0.81) respectively [16]. It was suggested that, in this pH range CP enantiomers were present as a monovalent or divalent cation because of protonations on its pyridyl and amino groups.

The pharmacological activity of CP and BP depends on their acid-base properties of these basic compounds [18]. There are two nitrogen atoms in the structures which can act as proton acceptors, the aliphatic amine [–N(CH$_3$)$_2$] group and the pyridine nucleus [19]. For CP, two pK_a values have been reported, corresponding to the ionisation of the aliphatic amino group (pK_a = 9.20) and the pyridine group (pK_a = 4.00) respectively [18]. The pH dictates the form of separation and also the stationary phase interaction with CP racemate. At a lower pH CP is more protonated and at a higher pH it is unprotonated. The pK_a value is an indicator of the acid properties of the protonated form of the structure as illustrated in Equation 5.1.

$$\underset{\text{Low}}{CPH_2^{2+}} \rightleftharpoons CPH^{+} \rightleftharpoons \underset{\text{High}}{CP} \qquad \text{pH} \qquad \textbf{Equation 5.1}$$

Using the drugs pK_a, the pH can be adjusted to ensure maximum water solubility (ionic form of the drug) or maximum stability in non-polar media (non-ionic form). In CP, the aliphatic amine is significantly more basic than the pyridine entity. The difference in basicity between the pyridine nitrogen and the aliphatic amine is linked to hybridisation on the nitrogen atom [10].

A number of possibilities for hydrogen bonding interactions between CP (template) with methacrylic acid (MAA) functional monomer are possible. These include: the amine, the pyridyl nitrogen and the chlorophenyl ring of the CP. Riahi *et al*. [20] presented a computational approach for the study of MIP selectivity. CP was chosen as the template and MAA as functional monomer in order to simulate the complex formation between template and monomer at the pre-polymerisation step. The interaction energies, atomic charges, IR spectroscopy results, dipole moments and polarisability results from the computational optimisation were studied. CP was strongly bonded to the monomer and each template molecule interacted with three functional monomers as depicted in Figure 5.2. The study also confirmed that employing chloroform as a solvent increased monomer/template interactions, expected as chloroform is an aprotic solvent with low dielectric constant [20].

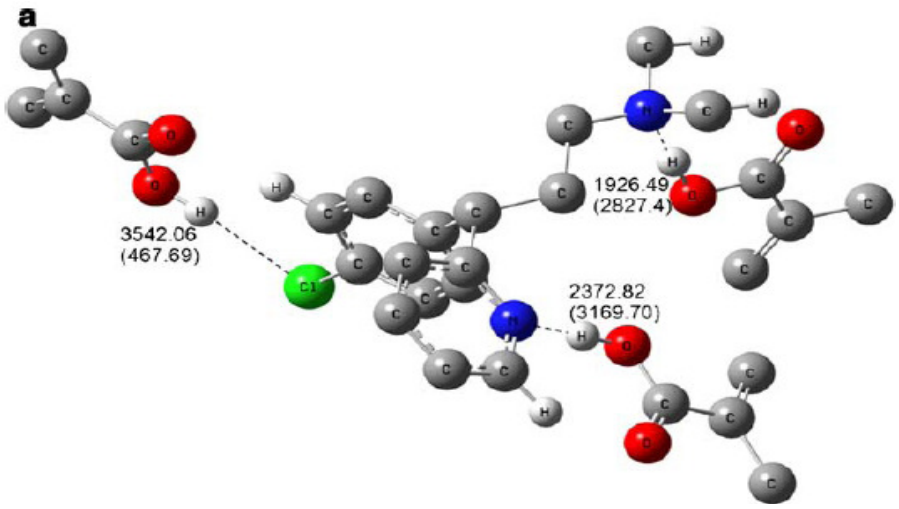

Figure 5.2 **Proposed pre-polymerisation complex between CP and MAA (1:3) [20].**

There is very little difference between the pK_a values for CP, BP and PHEN respectively [18;21;22], as shown in Table 5.1.

Table 5.1 **The pK_a values for CP, BP and PHEN.**

Compound	pK_a values
CP	4.00 & 9.20
BP	3.59 & 9.12
PHEN	4.20 & 9.30

Figure 5.3 shows a schematic representation of the proposed interaction mechanism of CP as template with MAA as functional monomer. The proposed hydrogen bonding interactions between the CP and MAA are expected to be the same for BP and MAA.

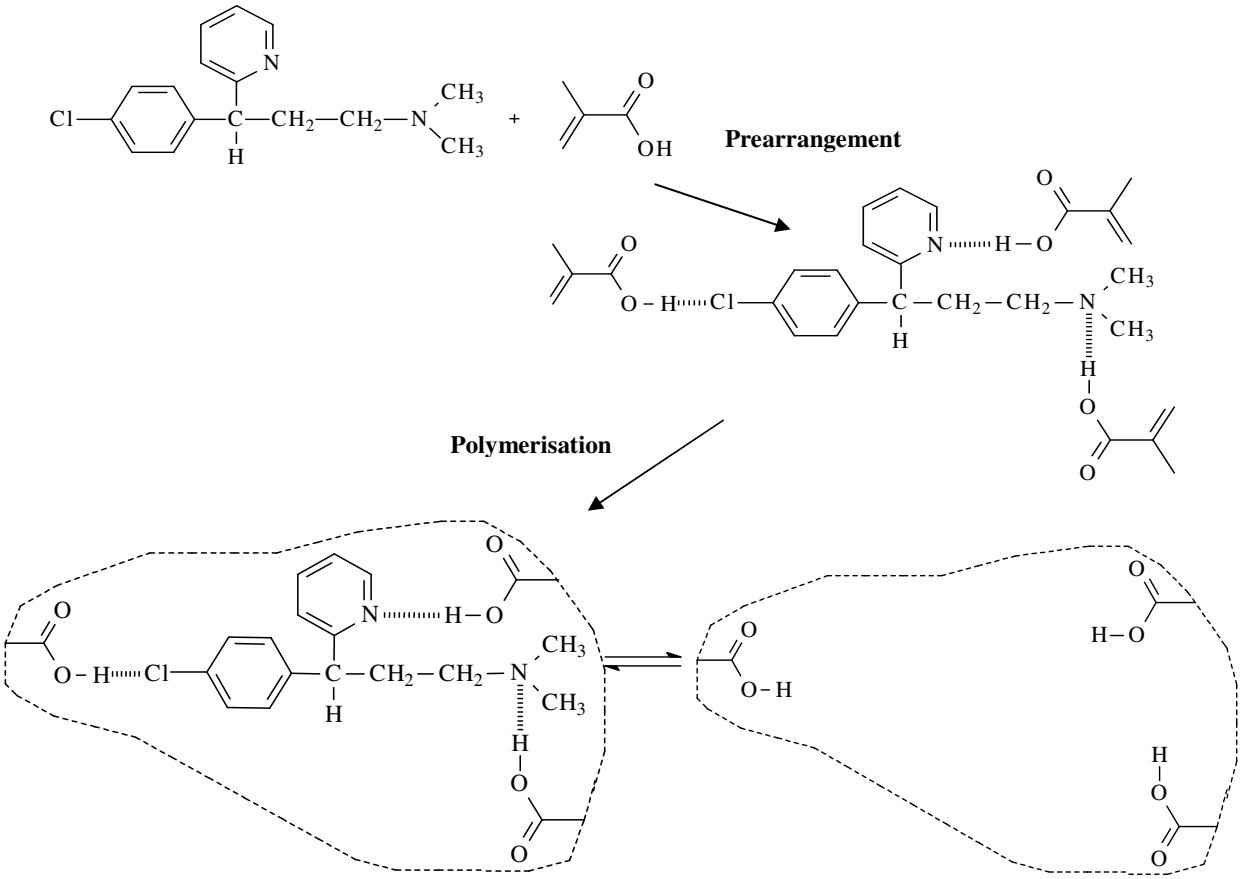

Figure 5.3 **Proposed interaction mechanism of CP as template with MAA as functional monomer.**

In this study MIPs were prepared using CP, *d*-CP, BP and *d*-BP as the template molecules. Spherical beads were obtained employing an aqueous suspension polymerisation method adapted from a procedure reported by Kempe [23;24] in Chapter 2. In this environment, pre-polymerisation mixtures prepared using chloroform as porogen were found to form stable suspensions after mechanical dispersion. Chloroform was chosen as porogen as all species were soluble in the organic solvent and because it was used in previous experimental work [14]. UV irradiation at 4 ºC produced spherical MIP particles in the size range 2 – 6 µm.

The application of MIPs as chiral stationary phases in HPLC is reported in this chapter. This is the first work dealing with the use of MIP formats as stationary

phases prepared by suspension polymerisation utilising water as a continuous phase. The novelty of this approach lies in the fact that the organic phase (containing the functional monomer, the cross-linker, the solvent, the template and the initiator) is dispersed initially, with a homogeniser, in the aqueous continuous phase without the use and influence of special solvents or stabilisers. Non-covalent interactions, like hydrogen bonding are stable in the aqueous suspension. This approach for preparing molecularly imprinted polymer beads has not been previously reported.

In addition to evaluating the retentivity and enantioselectivity of CP and BP, the use of MIP formats as stationary phases in HPLC aimed at achieving simultaneous separation of the antihistamines pheniramine (PHEN), CP and BP using an aqueous mobile phase was also investigated. PHEN is an antihistamine (structure illustrated in Figure 5.1) and differs from CP and BP by the elimination of a chlorine atom and bromine atom. The pK_a values for pheniramine are 4.2 and 9.3 respectively [22].

Objectives of the research

The main objectives of the work in this chapter were:

- To prepare MIPs for CP, *d*-CP, BP and *d*-BP by an aqueous suspension polymerisation procedure employing MAA as the functional monomer and trimethylolpropane trimethacrylate (TRIM) as the cross-linker and chloroform as the porogen,
- To optimise a HPLC method for chiral separation and determination of CP and BP enantiomers in terms of resolution and capacity values using the chiral MIPs,
- To assess the polymer performance by equilibrium binding studies using chiral HPLC analysis,
- To prepare HPLC columns using imprinted polymers and assess their ability to separate CP, BP and PHEN using an aqueous mobile phase in terms of enantioselectivity and retention properties and
- To examine the effect of column temperature on the retention factors, enantioseparation factors and resolution of CP and structurally related compounds using the *d*-$CP_{MIP(9500rpm)}$ column.

5.2 Experimental

5.2.1 Chemicals

Table 5.2 List of reagents employed

Reagent	Supplier	Assay
Chlorpheniramine Base	Schering-Plough	> 99 %
d-Chlorpheniramine	Schering-Plough	> 99 %
Brompheniramine Base	Schering-Plough	> 99 %
d-Brompheniramine Base	Schering-Plough	> 99 %
Pheniramine Maleate	Aldrich	
Methacrylic acid	Aldrich	99 %
Trimethylolpropane trimethacrylate	Aldrich	
2,2′-Azo bis(2-methylpropionitrile)	Aldrich	98 %
Methanol	Romil	> 99.9 %
Chloroform	Riedel-de Haën	> 99.8 %
Diethyl ether	BDH	> 99.5 %
Acetic Acid	Fluka	> 99.8 %
Magnesium sulphate	Aldrich	> 97 %
Sodium hydroxide	Riedel-de Haën	> 99 %
Water	Fluka	99.8 %
n-Hexane	Romil	95 %
Propan-2-ol	Romil	99 %
Diethylamine	Merck	> 99 %
Potassium dihydrogen phosphate	Merck	98 – 100.5 %
Dipotassium hydrogen phosphate	Merck	> 99 %
Orthophosphoric acid	BDH	< 85 %
Acetonitrile	Romil	> 99.9 %
Molecular sieves	Aldrich	3Å 3.2 mm

All the above reagents in Table 5.2 were purchased from Sigma-Aldrich (Dublin, Ireland). HPLC grade solvents were obtained from Lennox (Dublin, Ireland) and were used without further purification. To maintain the absence of moisture, chloroform, methanol and acetonitrile were stored over molecular sieves.

5.2.1.1 Preparation of pheniramine free base.

Pheniramine maleate salt (2.5 g) was converted to the free base form by dissolving 8 mL of 10 % aqueous sodium hydroxide (NaOH) in distilled water (15 mL). The mixture was then stirred for 30 min at room temperature and thereafter stirred for an additional 30 min while maintaining a temperature of 45 – 55 ^{o}C. The reaction mixture was allowed to settle for 15 min. The pH of the reaction should be between 10.5 and 13 (pH = 12.24), if not, additional 10 % aqueous NaOH was added to bring the pH within range, stirred for 15 min and allowed to settle. The upper organic layer consisting of the pheniramine free base was extracted into diethyl ether and dried over anhydrous magnesium sulphate. The diethyl ether layer was washed again by mixing it with water and saturated sodium chloride. After which, the solvent was evaporated from the combined ether layers in a rotary evaporator. The actual percentage yield of the free base was found to be 48.8 % (actual mass = 1.2176 g) based on the theoretical starting amount (mass of pheniramine maleate salt). GC-MS was used to confirm the molecular structure of the free base.

5.2.2 Equipment and instrumentation

- Stuart Scientific Orbital Incubator S150.
- Sterile syringes: Omnifix – Lennox Laboratory Supplies.
- Syringe nylon filters: 0.45 µm, 13 mm diameter – Antech Technologies Ltd.
- Chiralpak AD-H (250 mm x 4.6 mm I.D) column – Diacel Chemical Industries, Ltd.
- CARY-50-Varian Ultraviolet-Vis spectrometer (JVA Ireland, Ltd.).
- Hewlett-Packard (Model 1050) HPLC system employing ChemStation software.
- 'Pack in a Box' dual piston pump column packing System (Lab Alliance/Scientific Systems Inc., PA, USA)
- Thermo Electron Corporation Orion pH meter (4-Star Series) equipped with a combined Ag/AgCl glass electrode.

5.2.3 Synthesis of beads by suspension polymerisation in an aqueous media

Preparation of MIPs and NIPs for CP, *d*-CP, BP and *d*-BP as template molecules was carried out as previously reported (Section 2.2.4). Water was employed instead of mineral oil as the suspension media and chloroform was substituted for acetonitrile as the porogen.

5.2.4 Equilibrium binding studies

Equilibrium binding studies were conducted to evaluate the binding properties of the polymers. Triplicate 50.0 mg quantities of both MIP and NIP polymers were accurately weighed out and placed in 10 mL volumetric flasks. Each polymer (MIP and NIP) was loaded with 5 mL of 0.2 mM concentrated standard solution in chloroform. Samples were placed on an orbital shaker for 16 h at room temperature. After equilibration, polymer solutions were filtered to remove polymer particles using 10 mL syringes fitted with syringe nylon filter tips (0.45 µm, 13 mm diameter). The filtrates were subsequently analysed by HPLC and UV.

The IF values were calculated from the results of equilibrium binding studies. The quantity of template bound was determined from HPLC and UV analysis of the reloading solution after equilibration. The IF is expressed in Equation 2.2, Section 2.3.1, Chapter 2.

In addition, the binding capacity (*Cp*) of each of the polymers was also calculated. Approximately 50.0 mg of polymer was reloaded with 5 mL of 0.2 mM standard solution (CP, *d*-CP, BP or *d*-BP). For CP or *d*-CP, 1 mM standard solution is equivalent to 274.8 mg L^{-1}, therefore, a 0.2 mM standard solution is equivalent to 54.96 mg L^{-1}. Consequently, 5 mL of 0.2 mM CP or *d*-CP standard solution would be equivalent to reloading the polymer with 0.2748 mg 5 mL^{-1} of standard solution (in order to fill all the theoretical number of binding sites in the polymer and to achieve 100 % binding of the template to the polymer). The *Cp* of the polymers rebound in CP and *d*-CP standard solution was calculated by multiplying the percentage polymer rebound by this value, 0.2748 mg 5 mL^{-1}. Therefore, this determined the actual

binding capacity of 50.0 mg of polymer with the addition of a 5 mL quantity of 0.2 mM standard solution. For BP and *d*-BP standard solutions, the percentage polymers rebound were multiplied by 0.319 mg 5 mL^{-1} respectively.

5.2.5 HPLC analysis

A HP Agilent liquid chromatograph (Model 1050) employing ChemStation software system was utilised in this study and consisted of a HPLC quaternary Agilent pump, fitted with a Rheodyne Injector and a UV spectrophotometer detector. All chromatographic runs were performed using a flow rate of 0.75 mL min^{-1}, at 25 ^{o}C, UV detection at 254 nm and an injection volume of 5 µL, unless otherwise specified. Chiral separations were performed on a Chiralpak AD-H column [25] (5 µm particle size, 250 mm x 4.6 mm i.d.).

The mobile phase composition was a mixture of *n*-hexane:propan-2-ol:diethylamine (90:10:0.1 (v/v)). The addition of diethylamine to the mobile phase is necessary for the separation of basic enantiomers. Prior to analysis, the mobile phase was degassed and filtered using 0.45 µm nylon filters. The system was equilibrated with the mobile phase before injection.
The retention factor, *k* was calculated from Equation 5.2:

$$k = \frac{(t_R - t_o)}{t_o} \qquad \textbf{Equation 5.2}$$

where t_R and t_o are retention times of retained and unretained solutes, respectively.
In this study, t_o was estimated based on the retention time of the solvent peak.

A slightly modified method was used to calculate the resolution R_s: a straight line was drawn perpendicularly from the peak maximum to the baseline, and the baseline peak band divided into two halves.

Resolution was calculated from Equation 5.3:

$$R_S = \frac{(t_2 - t_1)}{1.7 \times 0.5 (w_{0.5,1} + w_{0.5,2})} \qquad \textbf{Equation 5.3}$$

where t_1 and t_2 are the retention times of the first and second eluted enantiomers, respectively, and $w_{0.5,1}$ and $w_{0.5,2}$ are the peak widths at half the peak height of the first and second eluted enantiomers, respectively. The enantioseparation factor was calculated from Equation 5.4:

$$\alpha = \frac{k_d}{k_l} \qquad \textbf{Equation 5.4}$$

where k_l and k_d are the retention factors of the first and second eluted enantiomers, respectively.

5.2.5.1 Validation procedure

Linearity was tested at five concentrations of the standard mixture ranging from 0.2 to 1.0 mM for CP, *d*-CP, BP and *d*-BP.

5.2.5.2 HPLC equilibrium binding analysis

The procedure for preparing rebinding solutions was described in Section 5.2.4. The filtrates were analysed on the HP1050 LC system using a Chiralpak AD-H column and a mobile phase mixture consisting of n-hexane:propan-2-ol:diethylamine (90:10:0.1 (v/v)). The average values of triplicate independent results were obtained. The % rebound values for all polymers were calculated from the HPLC equilibrium binding results. Additionally, the use of the chiral column allowed assessment of enantioselective rebinding.

5.2.6 UV/Visible equilibrium binding analysis

UV analysis was used to follow the removal of both template and acetic acid from the filtrate stream (Section 5.2.3). To demonstrate the robustness of the polymerisation procedure, UV equilibrium binding analysis was used to study the binding of CP, *d*-CP, BP and *d*-BP imprinted polymers to its own template. For UV/Vis spectroscopy analysis the amount of template bound to the polymers, was calculated by subtracting the absorbance of free substrate remaining in the post equilibrium solution, from the initial absorbance (0.2 mM standard solution). The quantity of reloaded template (CP, *d*-CP, BP and *d*-BP) bound to the polymer, was analysed by UV analysis at the pre-determined wavelength (CP and BP: λ_{max} = 260 nm). The average values of triplicate independent results were obtained.

5.2.7 Column packing

HPLC columns were packed using a dual piston pump system ('Pack in a Box' Column Packing System - Lab Alliance/Scientific Systems Inc., PA, USA) which includes: electric packing pump and software, slurry packing reservoirs and stand and column hardware. The column packer was mounted to the stand and the lower fitting of the column was assembled to it.

The MIPs used were prepared at 9500 rpm employing *d*-CP as template molecule and was abbreviated to *d*-$CP_{MIP(9500rpm)}$. The MIP particles for packing were spherical in shape with a narrow distribution (5.15 ± 0.008 µm). An adequate amount of polymer (approximately 0.8 g) was suspended in 20 mL of methanol and the mixture was sonicated for 20 min and slurry packed in a 50 mm stainless steel HPLC column (i.d. 4.6 mm). The packing of the stationary phase was performed by adding the slurry of the polymer into the reservoir. The reservoir was attached to the high-pressure pump, and then the slurry was forced into an empty column blank and eluted with methanol at constant pressure of 7000 psi. This was accomplished while holding the packing column outlet with a porous frit (2.0 µm) that allows the solvent to pass through while retaining the packing. When the column was full, it was disassembled from the apparatus and a second porous frit placed on the open inlet of the column.

5.2.7.1 Chromatography – Separation of CP and BP on *d*-$CP_{MIP(9500rpm)}$ stationary phase

A HPLC (Model 1050) was used as described in (Section 5.2.5). The flow rate was maintained at 0.075 mL min^{-1} and detection was performed at 254 nm at ambient temperature. The mobile phase consisted of acetonitrile and 50 mM potassium dihydrogen phosphate (KH_2PO_4) + 50 mM dipotassium hydrogen phosphate ($K_2HPO_4.3H_2O$) (70:30, v/v). A phosphate buffer was selected to study responses over a wide pH range. The pH was adjusted with orthophosphoric acid or sodium hydroxide (5 %). All analytes were prepared at a concentration of 0.2 mM standard solution in mobile phase. The flow rate was maintained at 0.075 mL min^{-1} as back pressures were very high. The pH values were 'apparent' because a mixture of phosphate buffer and acetonitrile was used as the mobile phase. Prior to analysis, the mobile phase was degassed and filtered using 0.45 µm filter papers. The column, packed with stationary phase as described above, was then connected to the HPLC system (HP 1050 Series) and equilibrated with mobile phase until a stable baseline was obtained.

5.3 Results and discussion

5.3.1 Percentage yield recoveries for polymers

Polymers used in this study were prepared using CP, *d*-CP, BP or *d*-BP as templates, MAA as functional monomer and TRIM as cross-linker which were polymerised by an aqueous suspension methodology. Percentage yield recoveries for molecularly imprinted polymer beads (CP, *d*-CP, BP and *d*-BP) and the corresponding NIP were estimated based on the theoretical amount of starting monomers, and results are presented in Table 5.3.

Table 5.3 **Average percentage yield recoveries for CP, *d*-CP, BP, *d*-BP imprinted polymers (MIP and NIP). Results are based on triplicate analysis with errors based on ± 1 standard deviation.**

Polymers	% Yield
CP	62.35 ± 1.11
d-CP	62.28 ± 5.73
BP	58.86 ± 3.07
d-BP	57.81 ± 7.49
NIP	57.20 ± 8.39

High yields of good reproducibility beads were found, as shown in Table 5.3.

5.3.2 Chromatography

5.3.2.1 HPLC measurements

Separation of both *d*- and *l*-isomers was achieved on a Chiralpak AD-H column. To establish the elution order of the enantiomers, a 5 μL solution of 0.2 mM CP standard in mobile phase was injected onto the HPLC. This solution was then spiked with *d*-CP which was shown to be the first peak as observed in Figure 5.4. A similar procedure showed that the *d*-BP also eluted first.

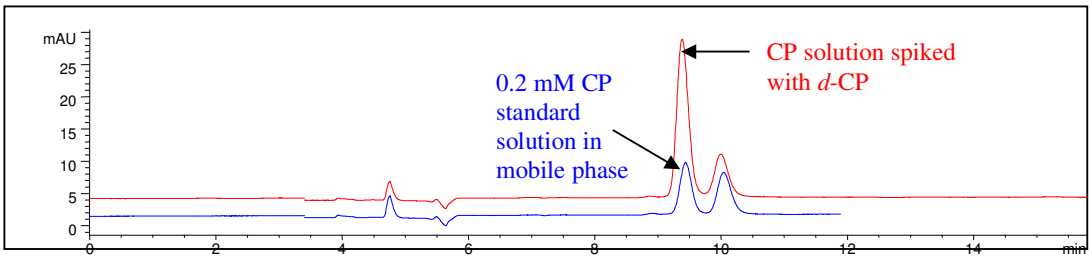

Figure 5.4 **Chromatogram of 0.2 mM CP standard solution spiked with *d*-CP ran on a Chiralpak AD-H column, mobile phase consisted of 90:10:0.1 (*n*-hexane:propan-2-ol:diethylamine) using a flow rate of 0.75 mL min^{-1} and injection volume of 5 µL.**

5.3.2.2 Method development and optimisation

Optimising separation is an important part of method development in chromatography. Once the initial separation was obtained, experimental parameters (mobile phase, injection volume and flow rate) were modified to study their influence on the resolution of compounds.

A series of investigations was performed employing a mobile phase that consisted of 90:10:0.1 (*n*-hexane:propan-2-ol:diethylamine) at varying flow rates (i.e. 0.75 – 1.0 mL min^{-1}) and injection volumes (5 – 10 µL). The optimum parameters for the separation of 0.2 mM standard solution for CP and BP were found employing a flow rate of 0.75 mL min^{-1} and an injection volume of 5 µL respectively. The chromatogram is presented in Figure 5.5 illustrates the separation of CP.

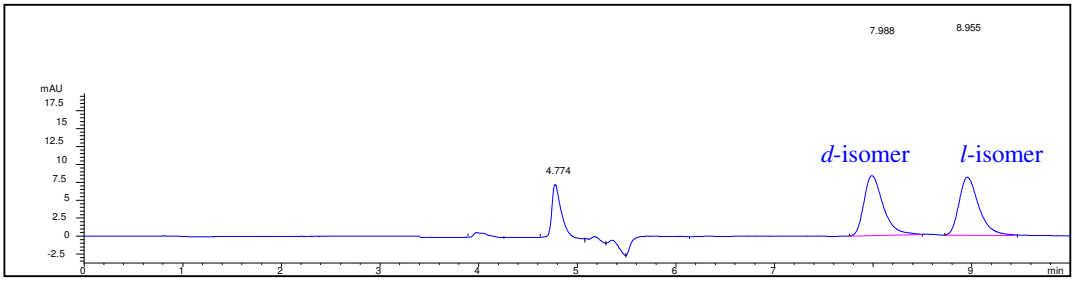

Figure 5.5 **Chromatogram of 0.2 mM CP standard solution ran on a Chiralpak AD-H column, mobile phase consisted of 90:10:0.1 (*n*-hexane:propan-ol:diethylamine) using a flow rate of 0.75 mL min^{-1} and injection volume of 5 µL.**

In Figure 5.5 sharp peaks were observed with good baseline resolution. The retention times were approximately 7.9 and 8.9 for the *d*-isomer (peak 1) and *l*-isomer (peak 2) respectively. Three injections of two standards were performed and the resolution value (R_s) for this study was 2.838 ± 0.008. Resolution values greater than 1.5 are recommended for good separation.

Therefore, the optimised HPLC conditions employed for the validation of the method and equilibrium binding studies used a flow rate of 0.75 mL min^{-1}, injection volume of 5 µL and mobile phase that consisted of a mixture of 90:10:0.1 (*n*-hexane:propan-2-ol:diethylamine).

5.3.2.3 Validation of the method

An essential parameter to ensure the acceptability of the performance of an analytical method is linearity. Under the optimum HPLC conditions, linearity was studied using five concentrations ranging from 0.2 to 1.0 mM for CP, *d*-CP, BP and *d*-BP. Calibration curves, were generated by weighted (1/*x*) least squares linear regression. The calibration curves exhibited satisfactory linearity, with correlation coefficients (R^2) higher than or approximately 0.99. The results were based on three replicates and are presented in Figure 5.6.

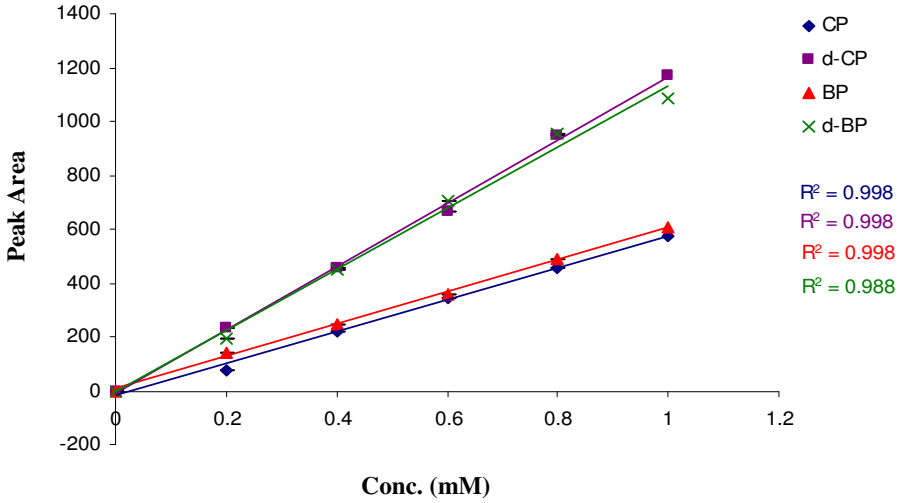

Figure 5.6 **Linearity details of CP, *d*-CP, BP and *d*-BP using peak areas under optimum HPLC conditions on a Chiralpak AD-H column employing a mobile phase that consisted of 90:10:0.1 (*n*-hexane:propan-2-ol:diethylamine). Results are based on triplicate analysis with error bars based on ± 1 standard deviation.**

5.3.3 Affinity studies

5.3.3.1 Rebinding studies using chiral HPLC analysis

Successful suspension polymerisation of MIP beads in an aqueous medium was achieved for CP, *d*-CP, BP and *d*-BP imprinted polymers rebinding experiments were carried out as previously described (Section 5.2.5.2) and the enantioselectivity of the rebinding study was determined by HPLC using a chiral column for resolution of enantiomers. Once the enantiomers were separated under the optimised HPLC conditions (Section 5.3.2.2), values of the ratio of peak areas for both *d*- and *l*-isomers (A_d/A_l) values were calculated from the HPLC chromatographic results. Table 5.4 lists the average values for the peak area of the *d*-isomer over the peak area of the *l*-isomer for each polymer reloaded in CP and BP standard solutions in chloroform respectively. The values of A_d/A_l for each polymer were listed in order of decreasing value in Table 5.4.

Table 5.4 **Values of A_d/A_l for each imprinted polymer (CP, *d*-CP, BP and *d*-BP) reloaded in 0.2 mM CP and BP standard solutions in chloroform respectively performed by chiral HPLC analysis. Results are based on triplicate analysis with errors based on ± 1 standard deviation.**

Polymers reloaded in 0.2 mM CP standard solution in chloroform	**Values of A_d/A_l**
CP standard solution	1.019 (± 0.0001)
NIP	1.033 ± 0.001
CP	0.998 ± 0.004
BP	0.977 ± 0.015
d-CP	0.976 ± 0.014
d-BP	0.914 ± 0.006
Polymers reloaded in 0.2 mM BP standard solution in chloroform	
BP standard solution	1.024 ± 0.003
CP	1.088 ± 0.008
BP	1.076 ± 0.005
NIP	1.042 ± 0.004
d-BP	1.010 ± 0.011
d-CP	1.001 ± 0.005

In Table 5.4, the A_d/A_l value for the 0.2 mM CP standard solution in chloroform was 1.019 (± 0.0001). This value is very close to 1 as expected, as CP racemate is a 50:50 mixture. For the imprinted polymers (CP, *d*-CP, BP and *d*-BP) reloaded in CP standard solution the A_d/A_l values ranged from 0.914 – 0.998.

- The highest A_d/A_l value was found for the CP MIP reloaded with CP standard solution (0.998 ± 0.004). This value is less than 1 but very close to 1.
- The second highest value was seen for the BP MIP reloaded with CP standard solution (0.977 ± 0.015). This value is slightly less than for the CP MIP, this is expected, as the BP MIP is a bigger molecule in comparison to CP and therefore has bigger binding pockets.
- The A_d/A_l values for the *d*-CP and *d*-BP MIPs reloaded with CP standard solution were (CP: 0.976 ± 0.014 and BP: 0.914 ± 0.014) respectively. A bigger drop in the A_d/A_l values was seen for these polymers. The lower figures indicate that the *d*-CP and *d*-BP polymers are selectively binding to the *d*-isomer over the *l*-isomer, indicating enantioselective imprinting in these polymers. The greatest drop in A_d/A_l value was seen for the *d*-BP polymer in comparison to the other polymers. A potential reason is the binding pocket size. Loading CP standard solution onto the *d*-BP MIP, which possesses a bigger binding pocket, allows access of more material into the binding site resulting in a lower A_d/A_l value.

The A_d/A_l value for the 0.2 mM BP standard solution in chloroform was 1.024 ± 0.003 (Table 5.4). This value is very close to 1, as BP racemate is a 50:50 mixture. However, there could be the possibility that there is a higher amount of *d*-isomer in the racemate as the A_d/A_l value is 1.02 and not 1. For the imprinted polymers (CP, *d*-CP, BP and *d*-BP) reloaded in BP standard solution the A_d/A_l values ranged from 1.001 – 1.088.

- The highest A_d/A_l value was found for the CP MIP reloaded with BP standard solution (1.088 ± 0.008). There is less access to the binding sites of the CP MIP by reloading it with BP. The A_d/A_l value is greater than 1 and also greater than the BP standard solution (1.024 ± 0.003)

- The second highest value was seen for the BP MIP reloaded with BP standard solution (1.076 ± 0.005). As similar trend in A_d/A_l value was seen for BP as was seen for the CP MIP reloaded in BP standard solution, in that the A_d/A_l values were greater than 1 and greater than the BP standard solution.
- The A_d/A_l values for the *d*-CP and *d*-BP MIPs reloaded with BP standard solution were (CP: 1.001 ± 0.005 and BP: 1.010 ± 0.011) respectively. The A_d/A_l values for these polymers were expected to be less than the standard value and this was found to be correct. As seen above with the A_d/A_l values for the *d*-CP and *d*-BP MIPs reloaded with CP standard solution, the lower figures indicate that the *d*-CP and *d*-BP polymers are selectively binding to the *d*-isomer over the *l*-isomer, again indicating enantioselective imprinting.

In addition to calculating the ratio of peak areas for the *d*- and *l*-isomers (A_d/A_l values), the optimised HPLC method (Section 5.3.2.2) was used to assess the equilibrium binding for each imprinted polymers to its own template in a 0.2 mM standard solution in chloroform. The binding characteristics were also assessed in a cross-selectivity study. Blank, non-imprinted polymers (NIPs) were also prepared in the absence of template molecules.

Table 5.5 and Figure 5.7 represents the HPLC equilibrium binding results for aqueous suspension imprinted polymers (i.e. CP, *d*-CP, BP and *d*-BP) reloaded with 0.2 mM CP, *d*-CP, BP and *d*-BP standard solution respectively. In addition, the imprinting factor (IF) values and the binding capacity (*Cp*) of CP, *d*-CP, BP and *d*-BP imprinted polymers reloaded with CP, *d*-CP, BP and *d*-BP standard solutions are also presented in Table 5.5.

Table 5.5 **Rebinding studies using chiral HPLC analysis, *Cp* and IF values for CP, *d*-CP, BP and *d*-BP imprinted polymers reloaded with 0.2 mM CP, *d*-CP, BP and *d*-BP standard solution respectively. Results are based on triplicate analysis with errors based on ± 1 standard deviation.**

Imprinted polymers	Standard solution	% MIP Rebound (*Cp* (mg 5mL^{-1}))	% NIP Rebound (*Cp* (mg 5mL^{-1}))	$IF = \frac{MIP}{NIP}$
CP	**CP**	54.69 ± 6.82 (0.150)	15.92 ± 0.13 (0.044)	3.4 ± 0.64
	***d*-CP**	46.66 ± 5.89 (0.128)	14.60 ± 0.43 (0.040)	3.4 ± 0.69
	BP	49.25 ± 4.42 (0.157)	12.18 ± 0.34 (0.039)	3.3 ± 0.90
	***d*-BP**	58.61 ± 1.46 (0.187)	13.90 ± 0.29 (0.044)	3.8 ± 0.63
***d*-CP**	**CP**	53.44 ± 7.20 (0.147)	15.92 ± 0.13 (0.044)	3.2 ± 0.71
	***d*-CP**	49.72 ± 4.06 (0.137)	14.60 ± 0.43 (0.040)	3.4 ± 0.54
	BP	53.81 ± 3.73 (0.172)	12.18 ± 0.34 (0.039)	4.0 ± 0.55
	***d*-BP**	59.90 ± 0.25 (0.191)	13.90 ± 0.29 (0.044)	4.4 ± 0.92
BP	**CP**	51.71 ± 9.67 (0.142)	15.92 ± 0.13 (0.044)	4.1 ± 0.67
	***d*-CP**	57.96 ± 4.01 (0.159)	14.60 ± 0.43 (0.040)	4.4 ± 0.60
	BP	50.85 ± 4.10 (0.162)	12.18 ± 0.34 (0.039)	4.2 ± 0.64
	***d*-BP**	55.95 ± 2.88 (0.179)	13.90 ± 0.29 (0.044)	4.6 ± 0.62
***d*-BP**	**CP**	60.09 ± 6.62 (0.165)	15.92 ± 0.13 (0.044)	4.2 ± 0.28
	***d*-CP**	63.27 ± 7.55 (0.174)	14.60 ± 0.43 (0.040)	4.3 ± 0.16
	BP	55.61 ± 3.75 (0.177)	12.18 ± 0.34 (0.039)	4.0 ± 0.41
	***d*-BP**	59.29 ± 5.46 (0.189)	13.90 ± 0.29 (0.044)	4.3 ± 0.69

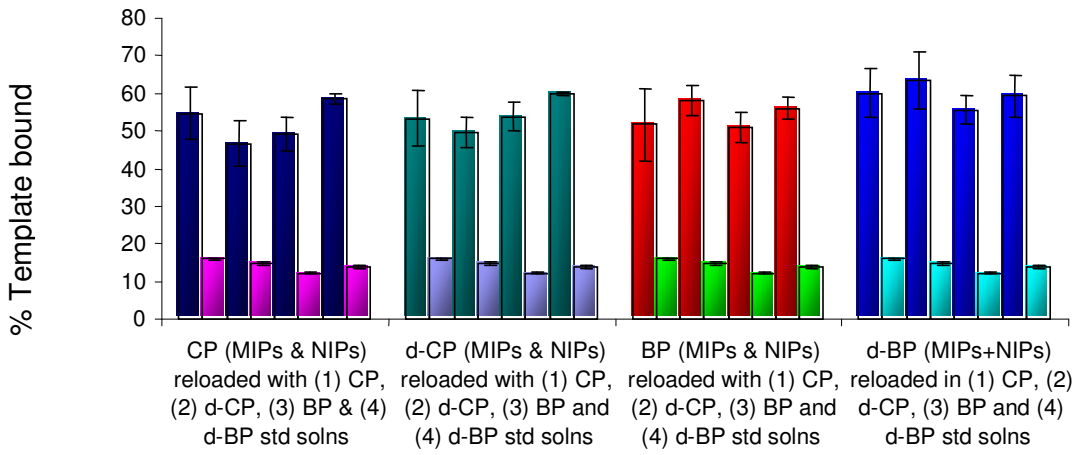

Figure 5.7 **Rebinding studies using chiral HPLC analysis, for CP, *d*-CP, BP and *d*-BP imprinted polymers (MIPs and NIPs) reloaded with 0.2 mM standard solutions (CP, *d*-CP, BP and *d*-BP) respectively. Results are based on triplicate analysis with error bars based on ± 1 standard deviation.**

As seen by the rebinding studies using chiral HPLC analysis in Tables 5.5 and Figure 5.7, binding was much higher to the MIPs in comparison to the NIPs. This resulted from the imprinting effect produced during polymerisation in the presence of template, which led to the formation of affinity binding cavities in the imprinted polymer. NIPs don't have the binding sites and recognition ability coming from the imprinting effect and, as a result binding is lower, for the NIPs. Therefore the higher binding to the MIPs confirmed the effectiveness of the imprinting technique.

It was found in the majority of cases that the *d*-BP imprinted polymers produced the highest binding capacity and IF values in all standard solutions. One possible explanation for the higher binding on the BP polymers could be the difference in binding pocket size between BP and CP polymers. The difference in molecular size of BP regarding its shape and arrangement of functionalities within the binding cavity could be facilitating a higher level of binding. Loading a CP standard solution onto a BP or *d*-BP imprinted polymer which had a bigger binding pocket allowed more access of the substrate material into the binding site within the molecule and higher binding as a result.

The *d*-CP imprinted polymers gave the second highest percentage rebound, IF value and binding capacity in BP and *d*-BP standard solutions for the MIP. However, binding was reduced for the CP and *d*-CP imprinted polymers reloaded in CP and *d*-CP standard solutions respectively. This was an unusual result as it would be expected that reloaded CP and *d*-CP standard solutions would exhibit the best binding on its own polymer.

There was slightly less binding in the CP imprinted polymer reloaded in BP standard solution and the IF was reduced (IF = 3.3 ± 0.90), which would suggest that the BP standard had less access to the CP binding site within the polymer. This was most probably a space issue within the binding pockets where CP generated a smaller cavity due to its molecular size. In contrast BP imprinted polymers reloaded with CP standard solutions produced higher binding affinities, capacities and IF values. These results suggest that the selectivity is affected not only by the functional groups but also by the size of imprinted cavities and the differences in molecular size of CP and BP. Simon *et al.* [26] performed a study investigating shape selectivity versus functional group pre-organisation in MIPs. It was reported that when the analyte is smaller than the imprinted molecule, there are reduced contacts between the analyte and the polymer matrix that makes up the binding site cavity. The reduced interactions of the analyte inside the binding cavity due to poor shape complementarity results in lower Van der Waals or hydrophobic interactions which resulted in the overall lowering of selectivity [26].

Yoshizako *et al.* reported that the rebinding capacity of the MIPs for its own template molecule will be the highest [27]. However, this effect was not seen with every template employed in this study. The high similarity of the molecular structure between CP and BP and the fact that there is very little difference between the two pK_a values for CP and BP makes it difficult to explain why a higher uptake, binding capacity and IF values were found for the BP and *d*-BP polymers over the CP polymers. It is speculated that the higher binding of BP polymers over CP depends on the differences in polarisability between Br and Cl. In addition to this, the differences in bond length distances the 3-D chemical structures of the templates CP and BP employed in this study were generated using ChemDraw Ultra software (Chem3D Pro

Cambridge software, Version 12). The 3-D chemical structures are shown in Figure 5.8 (a) and (b) respectively.

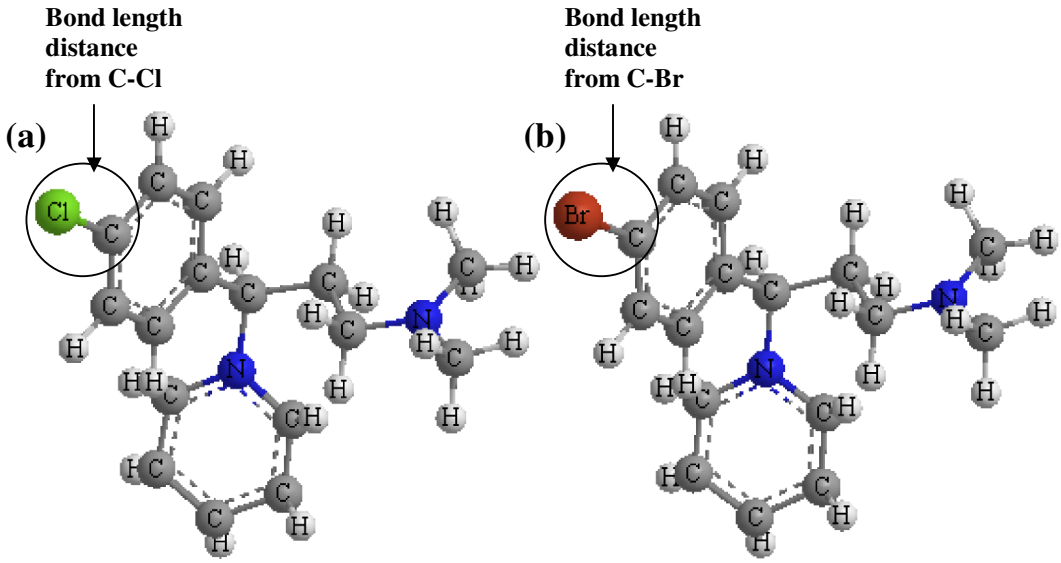

Figure 5.8 **The 3-D chemical structures of (a) CP, (b) BP.**

As highlighted in Figure 5.8, (a) the bond length distance from C-Cl for the chlorpheniramine molecule was 1.7190 Å. For (b) the brompheniramine molecule the bond length from C-Br was 1.8810 Å. These distances may be sufficiently significant to affect binding of these two molecules to the same site.

The high IF values for the *d*-BP MIPs make these MIPs very useful as group-recognition material for CP, *d*-CP and BP. Additionally, the problem of template leakage could be avoided employing structural analogues in the preparation of MIPs as stationary phases in chromatographic systems. Similarly in the literature, Ya-hui Li *et al*. [28] prepared MIPs using malachite green (MG) as template from fish water and fish feed samples and two structurally related compounds, leucomalachite green (LMG) and crystal violet (CV). The MIPs showed the highest selective binding to MG, but also exhibited high cross-reactivity with LMG and CV, showing that MIPs could be useful as potential group recognition sorbents in solid phase extraction.

The results of equilibrium binding experiments demonstrated that the imprinting strategy employing *d*-BP as the template improved the recognition ability of the MIP and increased the specific binding sites in the cavities of the polymer and thus

enhanced its molecular recognition ability. The explanation for this relies upon the creation of binding sites or cavities within the polymer.

5.3.3.2 UV rebinding studies

For comparison purposes and in order to confirm trends in IF values observed in HPLC, UV equilibrium binding analysis was used to study the binding of CP, *d*-CP, BP and *d*-BP templates to its own imprinted polymers in order to demonstrate the robustness of the polymerisation procedure.

Figure 5.9 and Table 5.6 represent the percentage amount of reloaded template (CP, *d*-CP, BP and *d*-BP), *Cp* and IF values onto their own imprinted polymers, (0.2 mM standard solution in chloroform) analysed by UV equilibrium binding analysis.

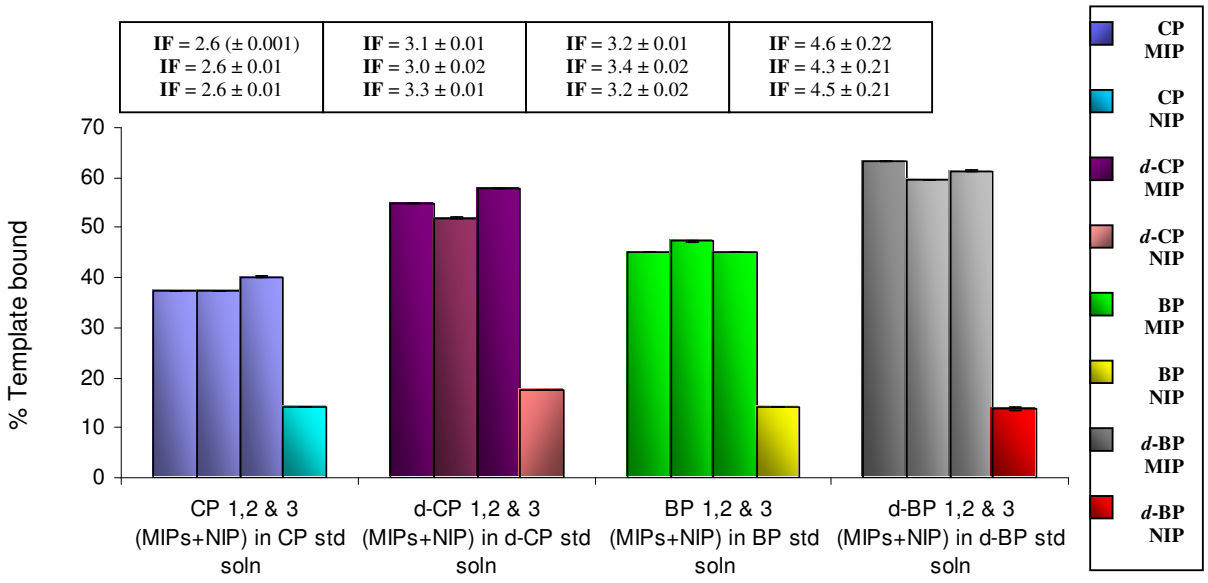

Figure 5.9 **Percentage amount of reloaded template (CP, *d*-CP, BP and *d*-BP) onto their own imprinted polymers analysed by UV equilibrium binding analysis. Results are based on triplicate analysis with error bars based on ± 1 standard deviation.**

Table 5.6 **Percentage amount of reloaded template (CP, *d*-CP, BP and *d*-BP), *Cp* and IF values bound to their own imprinted polymers. Results are based on triplicate analysis with errors based on ± 1 standard deviation.**

Imprinted polymers	% MIP Rebound (*Cp* (mg 5mL^{-1})	% NIP Rebound (*Cp* (mg 5mL^{-1})	IF
CP1	37.5 ± 0.01 (0.1031)	14.2 ± 0.02 (0.0390)	2.6 (± 0.001)
CP2	37.4 ± 0.06 (0.1028)		2.6 ± 0.01
CP3	40.2 ± 0.05 (0.1105)		2.8 ± 0.01
Average CP	38.4 ± 1.61 (0.1055)		2.7 ± 0.11
***d*-CP1**	54.8 ± 0.02 (0.1506)	17.6 ± 0.03 (0.0484)	3.1 ± 0.01
***d*-CP2**	51.9 ± 0.11 (0.1426)		3.0 ± 0.02
***d*-CP3**	57.9 ± 0.02 (0.1591)		3.3 ± 0.01
Average *d*-CP	54.9 ± 2.98 (0.1509)		3.1 ± 0.17
BP1	45.1 ± 0.01 (0.1439)	14.1 ± 0.04 (0.0450)	3.2 ± 0.01
BP2	47.3 ± 0.05 (0.1509)		3.4 ± 0.01
BP3	45.0 ± 0.03 (0.1434)		3.2 ± 0.07
Average BP	45.8 ± 1.28 (0.1461)		3.3 ± 0.09
***d*-BP1**	63.2 ± 0.03 (0.2016)	13.8 ± 0.46 (0.0440)	4.6 ± 0.22
***d*-BP2**	59.6 ± 0.03 (0.1901)		4.3 ± 0.21
***d*-BP3**	61.4 ± 0.04 (0.1959)		4.5 ± 0.21
Average *d*-BP	61.4 ± 2.52 (0.1959)		4.5 ± 0.13

These results demonstrate robustness for the polymerisation procedure. The *d*-CP, BP and *d*-BP imprinted polymers exhibited similar trends in binding capacity and IF values (with the exception of the lower IF value for BP polymers in Table 5.6) to the HPLC results in Table 5.5. Very little difference was seen across the three sets of CP imprinted polymers reloaded in CP standard solution in Table 5.5. However, the CP imprinted polymers exhibited much lower binding capacities and IF values in comparison to the HPLC results in Table 5.5. The binding to the NIP polymers was similar across all four sets of polymers in Table 5.6 with slightly higher capacity for reloading in *d*-CP standard solution. The general trends in IF values and capacities performed by UV binding analysis correlate well with HPLC results observed in Table 5.5 and Figure 5.7.

5.3.4 Applicability of MIPs as tailor-made HPLC chiral stationary phases

The imprinting effect of the MIPs was initially analysed in equilibrium binding experiments in Section 5.3.3. In order to study the imprinting effect and applicability of the polymers further as chiral MIPs, the *d*-$CP_{MIP(9500rpm)}$ was packed as HPLC stationary phase by slurry packing technique (column size of 50 mm x 4.6 i.d.). Additionally, an insight into the enantioselectivity and chromatographic behaviour of the MIP by HPLC could be gained. Packing columns for HPLC has been referred to as a 'black art' which requires a trial and error approach [29]. A reliable and reproducible column performance depends on the column fabrication. In initial studies *d*-CP MIP (24000 rpm) was selected for column packing, as it was predicted that benefits could be gained in using smaller polymer particles (≈ 2.3 µm). Unfortunately, column packing was unsuccessful employing particles of this size, due to a greater amount of fine particles in the material, which blocked the 2 µm porous frit at the column outlet. As a result *d*-CP MIP (9500 rpm) was selected for column packing, as described in Section 5.2.7.1.

5.3.4.1 Optimisation of chiral separation in aqueous media

Different mobile phase pHs (values of buffer solutions) ranging from 3 – 9 were selected for evaluation of *d*-$CP_{MIP(9500rpm)}$. The pH was screened over the 3 to 9 range, in which the charge of the analytes changes. This is indicated by the pK_a values of the antihistamines (≈ 4.00, 3.59 and 4.20 at the pyridine ring and 9.20, 9.12 and 9.30 at the aliphatic amine group) for CP, BP and PHEN respectively [18;21;22], which influence the ionic mobility of the analytes. The MIP stationary phase could not discriminate between the enantiomers at any of the pHs and mobile phase compositions studied with the exception of pH 7 and composition of 70:30 (v/v). The retention factors (*k*) of CP were observed to vary going from lower pH to higher (3 – 9). The resulting pH-retention graphs are shown in Figure 5.10 and the reproducibility was confirmed by repeating the experiments three times. Moreover, similar profiles were observed for BP (Figure 5.10).

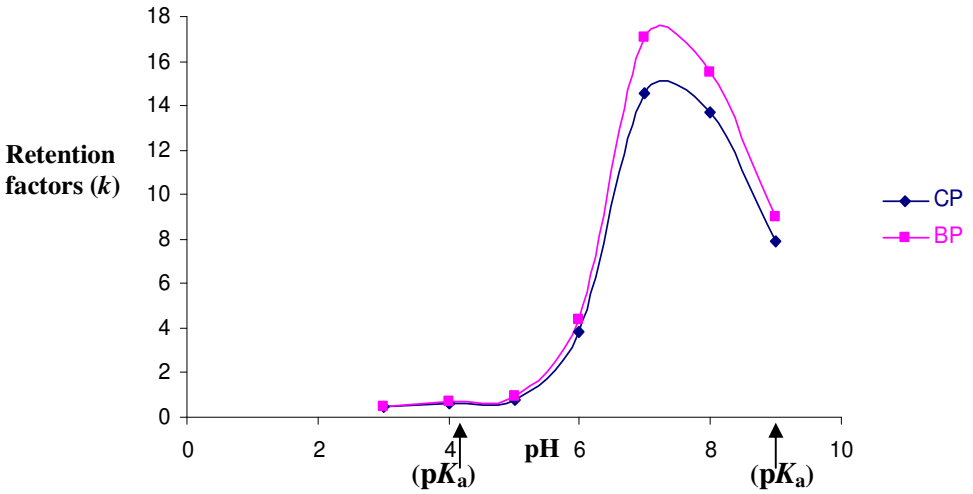

Figure 5.10 **Influence of mobile phase pH on retention factors (*k*) on *d*-CP$_{MIP(9500rpm)}$ column. HPLC conditions: column size, 50 mm x 4.6 i.d.; column temperature, ambient; mobile phase, ACN:buffer (70:30;v/v); detection, 254 nm; flow rate, 0.075 mL min^{-1}; loaded amount, 5 µL of 0.2 mM CP and BP standard solutions in mobile phase on *d*-CP$_{MIP(9500rpm)}$ column.**

The pH-influence on the retention effect was dramatic, as shown in Figure 5.10. At the high pHs the CP and BP were not protonated while the degree of ionisation of carboxylic groups on the polymer increased. Further increase in the basicity of the mobile phase pH (= 7) caused the carboxylic groups of the polymer to be deprotonated (negatively charged) and reduces the protonation of pyridyl and amino groups on CP and BP. The ionic interaction between CP (or BP) and the polymer, resulted in a swift decrease in the retention time (pH = 8 and 9) as observed in Figure 5.10. The interaction mechanism of MIPs in aqueous media depends mainly on ionic and hydrophobic interactions. Consequently, the enantiomers of CP demonstrated the strongest retention and best separation on a *d*-CP$_{MIP(9500rpm)}$ column with a mobile phase composition of (70:30) ACN:buffer at pH 7. This composition and pH were selected for future studies investigating the enantioselectivity of the *d*-CP$_{MIP(9500rpm)}$ column.

Separation of both *d*- and *l*-isomers of CP was achieved on the *d*-CP$_{MIP(9500rpm)}$ column at the mobile phase composition and pH mentioned above. To establish if the *d*-isomer was the first or second peak obtained on the chromatogram, a 5 µL solution of 0.2 mM CP standard in mobile phase was injected onto the HPLC. This solution was

then spiked with *d*-CP and injected again and it was observed that the *d*-CP isomer was the second peak as observed in Figure 5.11. A similar chromatogram was observed for the BP standard solution spiked with *d*-BP.

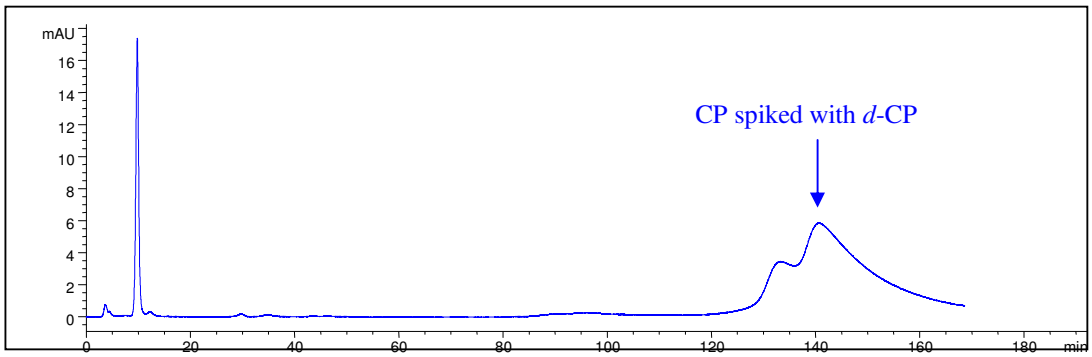

Figure 5.11 **Chromatogram of 0.2 mM CP standard solution in mobile phase spiked with *d*-CP on *d*-$CP_{MIP(9500rpm)}$ column. HPLC conditions: column size, 50 mm x 4.6 i.d.; column temperature, ambient; mobile phase, ACN:buffer (70:30;v/v) at pH 7; detection, 254 nm; flow rate, 0.075 mL min^{-1}; loaded amount, 5 µL.**

5.3.4.2 Separation of CP and BP enantiomers and *d*-CP and *d*-BP isomers on *d*-$CP_{MIP(9500rpm)}$ column

The chromatographic behaviour and separation of (a) CP, (b) *d*-CP (c) BP and (d) *d*-BP isomers were studied on the *d*-$CP_{MIP(9500rpm)}$ column at mobile phase pH 7 and are illustrated in the chromatograms in Figure 5.12 (a) – (d).

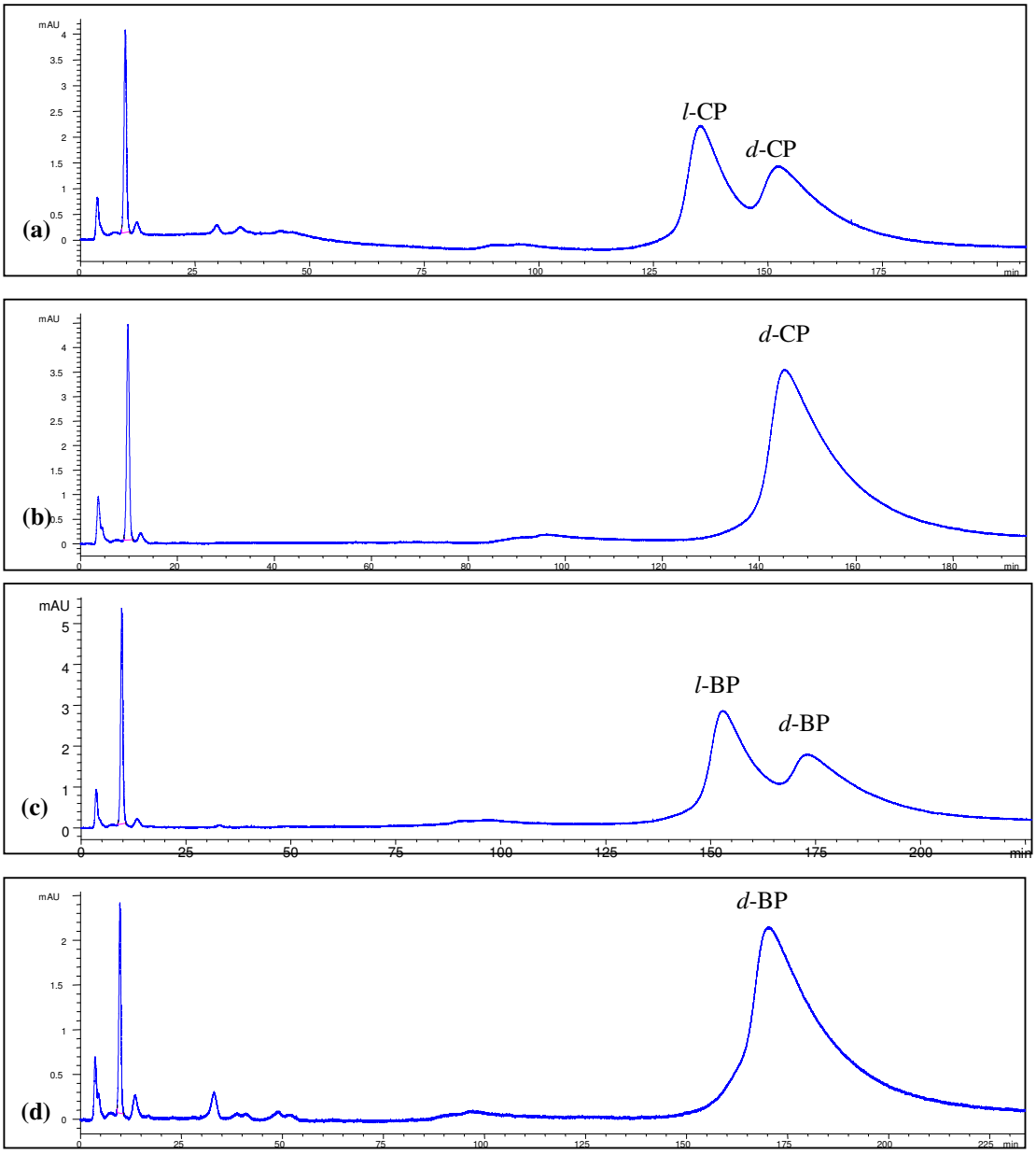

Figure 5.12 **Chromatograms for the separation of (a) CP, (b) *d*-CP, (c) BP and (d) *d*-BP isomers on *d*-$CP_{MIP(9500rpm)}$ column. HPLC conditions: column size, 50 mm x 4.6 i.d.; column temperature, ambient; mobile phase, ACN:buffer (70:30;v/v) at pH 7; detection, 254 nm; flow rate, 0.075 mL min^{-1}; loaded amount, 5 µL of 0.2 mM (CP, *d*-CP, BP or *d*-BP) standard solution in mobile phase.**

Enantioselectivity was achieved for CP and BP at pH 7 as shown in Figure 5.12 (a) and (c). The difference in retention times for the isomers separated in the chromatograms in Figure 5.12 were: (a) CP, *l*-isomer ≈ 130 and *d*-isomer ≈ 152.5 mins, (b) *d*-CP ≈ 145 mins, (c) BP, *l*-isomer ≈ 155 mins and *d*-isomer 175 mins, (d) *d*-BP ≈ 170 mins respectively. The retention of CP and *d*-CP isomers were similar to BP and *d*-BP except that BP and *d*-BP were more retained in comparison and this result is in agreement with equilibrium binding results (Table 5.5).

The retention factors, enantioselectivity factors and resolution of CP and BP enantiomers on the *d*-$CP_{MIP(9500rpm)}$ column are presented in Table 5.7. For comparison purposes the retention factors for *d*-CP and *d*-BP were also included.

Table 5.7 **Retention factors, enantioselectivity factors and resolution of CP and BP enantiomers on *d*-$CP_{MIP(9500rpm)}$. HPLC conditions: column size, 50 mm x 4.6 i.d.; column temperature, ambient; mobile phase, ACN:buffer (70:30;v/v) at pH 7; detection, 254 nm; flow rate, 0.075 mL min^{-1}; loaded amount, 5 µL of 0.2 mM standard solution in mobile phase.**

Analyte	k_l	k_d	α	R_s
CP	12.27	14.56	1.19	0.88
BP	14.98	17.04	1.14	0.60
***d*-CP**		14.8		
***d*-BP**		17.3		

Note: **k_l and k_d are the retention factors of the first and second eluted enantiomers respectively; α is the enantioseparation factor; R_s, resolution.**

As shown by the results in Table 5.7 the highest enantioselectivity (1.19) and resolution (0.88) was obtained for CP. The *d*-$CP_{MIP(9500rpm)}$ showed high cross-selectivity for CP and BP. BP was more retained than CP and this result is in agreement with equilibrium binding results (Table 5.5).

At pH 7 both the CP and BP enantiomers were charged. The results obtained above suggest that ionic and hydrophobic interactions could play a significant role in the retentivity and enantioselectivity of CP and BP enantiomers on the *d*-$CP_{MIP(9500rpm)}$ column. The retention tendencies of both *d*-CP and *d*-BP (Table 5.7) are quite similar as they possess pyridyl and amino groups. However, a higher retention factor value

was found for the *d*-BP isomer than for the *d*-CP isomer, which was in accordance with the results obtained in the equilibrium binding observations (Table 5.5).

The retention factor and resolution values reported here (Table 5.7) for the separation of BP on *d*-$CP_{MIP(9500rpm)}$ at pH 7, agreed with those of Haginaka [16] for the separation of CP enantiomers on the MIP prepared with MAA and EGDMA at pH 6.2.

5.3.4.3 Separation of PHEN, CP and BP enantiomers on *d*-$CP_{MIP(9500rpm)}$ column

It was of interest to investigate if the chiral stationary phase designed with *d*-CP MIP was able to resolve other antihistamines. The same chromatographic conditions were employed as in previous studies, the only significant difference made was to change the composition of the mobile phase (a mixture of ACN and phosphate buffer) from 70:30 to 65:35 (v/v) maintaining the same pH (= 7) in order to achieve separation of the PHEN enantiomers.

Figure 5.13 illustrates the retention properties of PHEN, CP and BP enantiomers on *d*-$CP_{MIP(9500rpm)}$.

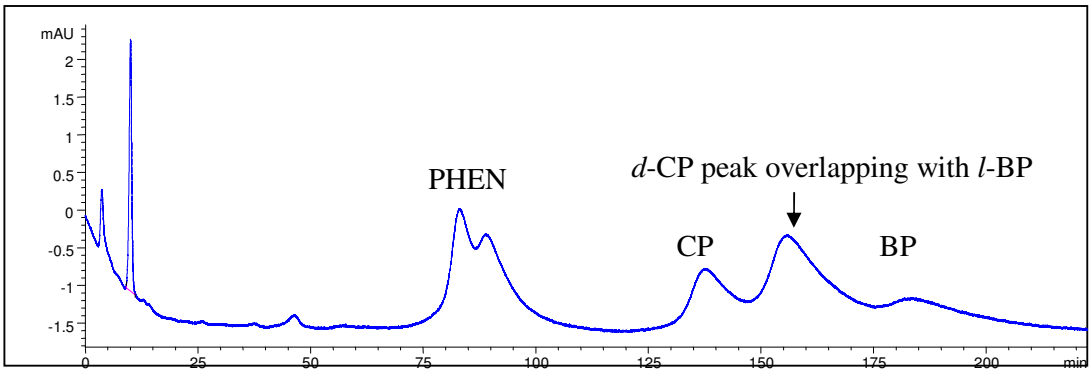

Figure 5.13 **Chromatogram for mixture of PHEN, CP and BP on *d*-$CP_{MIP(9500rpm)}$ column. HPLC conditions: column size, 50 mm x 4.6 i.d.; column temperature, ambient; mobile phase, ACN:buffer (65:35;v/v) at pH 7; detection, 254 nm; flow rate, 0.075 mL min^{-1}; loaded amount, 5 µL of a mixture containing 1 mL each of 0.2 mM PHEN, CP and BP standard solutions in mobile phase.**

The *d*-$CP_{MIP(9500rpm)}$ column successfully separated the PHEN, CP and BP enantiomers as shown in Figure 5.10. The PHEN was eluted as single peaks and the peaks are overlapping for CP and BP. Table 5.8 presents the retention factors, enantioselectivity, and resolution of PHEN, CP and BP enantiomers on the *d*-$CP_{MIP(9500rpm)}$ column.

Table 5.8 **Retention factors, enantioselectivity, and resolution of PHEN, CP and BP enantiomers on *d*-$CP_{MIP(9500rpm)}$. HPLC conditions: column size, 50 mm x 4.6 i.d.; column temperature, ambient; mobile phase, ACN:buffer (65:35;v/v) at pH 7; detection, 254 nm; flow rate, 0.075 mL min^{-1}; loaded amount, 5 µL of a mixture containing 1 mL each of 0.2 mM PHEN, CP and BP standard solutions in mobile phase.**

Analyte	k_1	k_d	α	R_s
PHEN	7.38	7.98	1.08	0.50
CP	12.72	14.66	1.15	0.64
BP	14.66	17.20	1.17	0.72

The highest retention factor, enantioselectivity and resolution were observed for BP over the PHEN and CP enantiomers. The retention tendencies of BP and CP were also similar but the BP was more retained. This may be explained by the fact that PHEN, CP and BP have almost the same pK_a values, while the hydrophobicity is in the order of BP, CP and PHEN i.e. log P_{ow} (P_{ow} = octanol-water partition coefficient) value is in the order BP (3.57), CP (3.39) and PHEN (2.79) [16]. It was concluded that hydrophobic interactions work for the retentions and enantioseparations of PHEN, CP and BP. Interestingly, this point is connected to the higher binding of BP over CP in HPLC binding analysis observed in Section 5.3.3.1, as it links to differences in polarisability of Br and Cl, as well as the size in bond lengths.

The CP enantiomers in Table 5.8 exhibited lower resolution value in comparison to Table 5.7. In contrast the BP enantiomers showed a higher resolution value (Table 5.8). The separation of PHEN, CP and BP enantiomers was performed under a different set of conditions i.e. the mobile phase composition was changed, therefore, this factor had an effect on the change in resolution values for both CP and BP enantiomers.

Table 5.9 examines the cross-selectivities of PHEN, CP and BP enantiomers on *d*-$CP_{MIP(9500rpm)}$ column by comparing the k_d values for all three compounds.

Table 5.9 **Cross-selectivity of PHEN, CP and BP enantiomers on *d*-$CP_{MIP(9500rpm)}$. HPLC conditions: column size, 50 mm x 4.6 i.d.; column temperature, ambient; mobile phase, ACN:buffer (65:35;v/v) at pH 7; detection, 254 nm; flow rate, 0.075 mL min^{-1}; loaded amount, 5 µL of a mixture containing 1 mL each of 0.2 mM PHEN, CP and BP standard solutions in mobile phase.**

PHEN	**CP**	**Selectivity Factor**
k_d	k_d	$\alpha = k_{d\,(CP)} / k_{d\,(PHEN)}$
7.98	14.66	1.84
CP	**BP**	**Selectivity Factor**
k_d	k_d	$\alpha = k_{d\,(BP)} / k_{d\,(CP)}$
14.66	17.20	1.17

The results in Table 5.9 indicated that high cross-selectivity was achieved by ionic and hydrophobic interactions in aqueous mobile phase on *d*-$CP_{MIP(9500rpm)}$ column. Leakage of trace amounts of template molecule in the MIP causes inaccuracies in analysis of the target analytes [16]. This problem could be overcome by imprinting with a structurally related analogue. The results obtained above imply that PHEN, CP and BP could be employed for such purposes.

5.3.4.4 Effect of column temperature on *d*-CP and *d*-BP isomers on the *d*-$CP_{MIP(9500rpm)}$ column

Figure 5.14 presents the separation of a mixture of *d*-CP and *d*-BP isomers on *d*-$CP_{MIP(9500rpm)}$ using a column temperature of (a) ambient and (b) 50 ^{o}C. The objective of this study was to keep the selectivity factor constant while looking for the shortest run time.

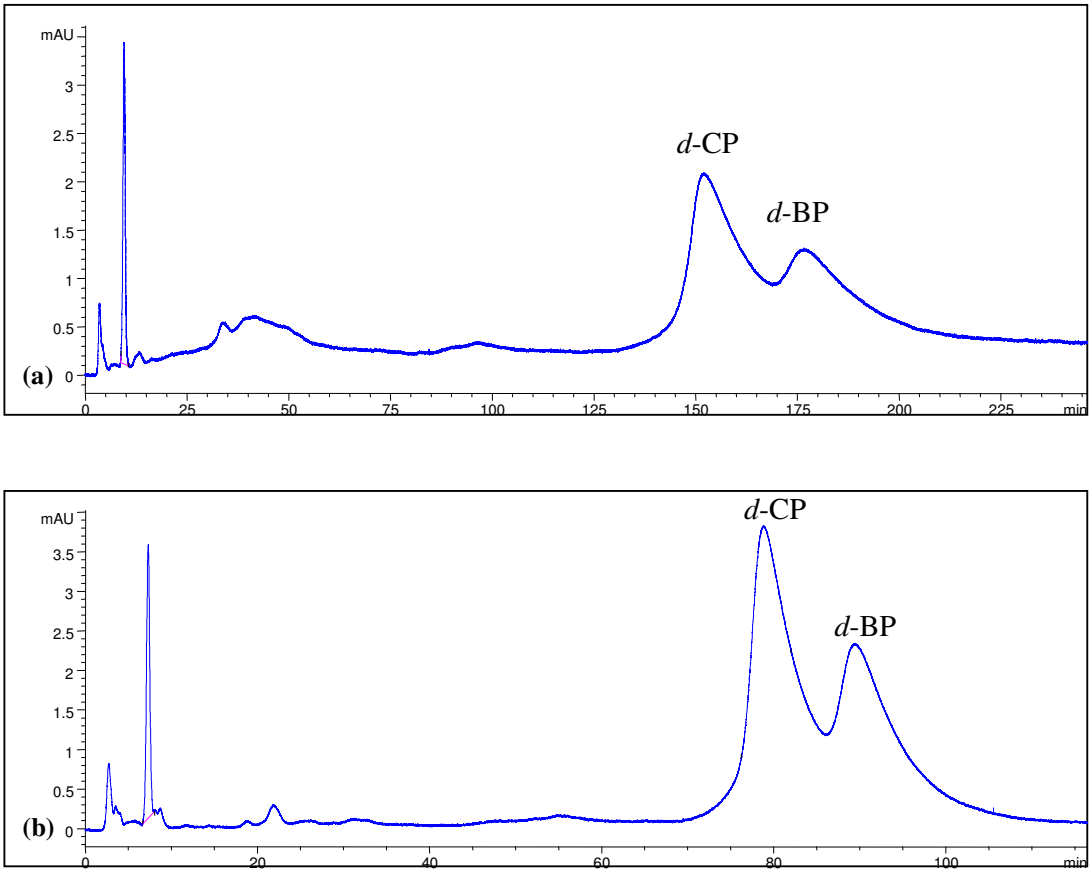

Figure 5.14 **Chromatograms for mixture of *d*-CP and *d*-BP isomers on *d*-$CP_{MIP(9500rpm)}$ using a column temperature of (a) ambient and (b) 50 ^{o}C. HPLC conditions: column size, 50 mm x 4.6 i.d.; mobile phase, ACN:buffer (70:30;v/v) at pH 7; (a) flow rate, 0.075 mL min^{-1}; (b) flow rate, 0.1 mL min^{-1}; detection, 254 nm; loaded amount, 5 µL of a mixture containing 1 mL each of 0.2 mM *d*-CP and *d*-BP standard solutions in mobile phase.**

The retention time was reduced in Figure 5.14 (b) using a column temperature of 50 ^{o}C. Additionally, the peaks were observed to be sharper at the higher temperature in

comparison to Figure 5.14 (a). The approximate spread in peaks for *d*-CP and *d*-BP at different column temperatures was determined by calculating the peak widths at half the peak height. In Figure 5.14 the spread was broader (a) *d*-CP ≈ 23 and *d*-BP ≈ 30 in comparison to the narrower peaks in (b) *d*-CP ≈ 7 and *d*-BP ≈ 9.

Table 5.10 shows the effect of temperature on the retention factors, selectivity factors and resolution of *d*-CP and *d*-BP on *d*-$CP_{MIP(9500rpm)}$ using a column temperature of (a) ambient and (b) 50 ^{o}C.

Table 5.10 **Effect of temperature on the retentivity, selectivity and resolution of a mixture of *d*-CP and *d*-BP isomers on *d*-$CP_{MIP(9500rpm)}$ using a column temperature of (a) ambient and (b) 50 ^{o}C. HPLC conditions: column size, 50 mm x 4.6 i.d.; mobile phase, ACN:buffer (70:30;v/v) at pH 7; (a) flow rate, 0.075 mL min^{-1}; (b) flow rate, 0.1 mL min^{-1}; detection, 254 nm; loaded amount, 5 µL of a mixture containing 1 mL each of 0.2 mM *d*-CP and *d*-BP standard solutions in mobile phase.**

	d-CP	*d*-BP		
Column temp. (^{o}C)	k_d	$k_{d'}$	**α**	R_s
(a) Ambient	14.94	17.56	1.18	0.61
(b) 50	9.56	11.18	1.17	0.86

From the results obtained in Table 5.10 and Figure 5.14 for the separation of *d*-CP and *d*-BP isomers on *d*-$CP_{MIP(9500rpm)}$, an increase in column temperature from ambient to 50 ^{o}C resulted in decreased retention and selectivity factors. The resolution value increased with increase in column temperature, which would be expected due to sharper peaks produced. This is a key parameter in terms of illustrating improved column performance by increasing column temperature. The selectivity factor decreased slightly from 1.18 to 1.17 at the higher temperature.

Sellergren and Shea [30] have reported on the origin of peak asymmetry and the effect of temperature on solute retention in enantiomer separations on imprinted chiral stationary phases. The temperature effects were clearly reflected in the dependence of resolution on temperature. A series of experiments was performed employing an acetic acid containing mobile phase at pH 7, which resulted in an increase in temperature leading to a decrease in the resolution.

Haginaka [15;16] investigated the effect of column temperature and flow-rate on the separation of CP enantiomers on a *d*-CP imprinted column and it was found that with an increase in the column temperature the retention factor and separation factor decreased, while the resolution increased. This was reportedly due to the suppression of the band-broadening of the second eluted enantiomers, *d*-CP. The obtained results agreed well with those reported in this study.

In another study to improve column performance it was postulated by Dauwe and Sellergren [31] that elevated column temperature can reduce the inhomogeneity of binding affinity of the imprinted sites. In addition the plate height contribution of slow kinetics in analyte-stationary phase interactions could also be reduced.

The chromatograms shown in Figure 5.14 (a) and (b) illustrate improved column performance by increasing the column temperature. The retention times are decreased and in addition, the back pressures were reduced. As a result, it was possible to increase the flow rate from 0.075 to 0.1 mL min^{-1} at the higher temperature in this study, which was also a significant parameter in terms of improving the column performance. The selectivity did not change with change in flow rate. A further objective of the study was to increase the column temperature and keep the selectivity factors, α, constant, which occurred, supported by information provided in Table 5.10. The new conditions indicate improved separation with the added advantage of time saving in the separation analysis.

5.3.4.5 Separation of CP and BP enantiomers and *d*-CP and *d*-BP isomers on *d*-$BP_{MIP(9500rpm)}$ column

The chromatographic behaviour and separation of (a) CP, (b) *d*-CP (c) BP and (d) *d*-BP isomers were also studied on the *d*-$BP_{MIP(9500rpm)}$ column at mobile phase pH 7. Similar chromatograms were observed as in Figure 5.12 (a) – (d). The retention of BP and *d*-BP on the *d*-$BP_{MIP(9500rpm)}$ column was greater in comparison to CP and *d*-CP.

The retention factors, enantioselectivity factors and resolution of CP and BP enantiomers and *d*-CP and *d*-BP isomers on the *d*-$BP_{MIP(9500rpm)}$ column are presented

in Table 5.11. The results in Table 5.6 for CP and BP enantiomers and *d*-CP and *d*-BP isomers on the *d*-$CP_{MIP(9500rpm)}$ column were also included again in Table 5.11 for comparison purposes.

Table 5.11 **Retention factors, enantioselectivity factors and resolution of CP and BP enantiomers on *d*-$BP_{MIP(9500rpm)}$. HPLC conditions: column size, 50 mm x 4.6 i.d.; column temperature, ambient; mobile phase, ACN:buffer (70:30;v/v) at pH 7; detection, 254 nm; flow rate, 0.1 mL min^{-1}; loaded amount, 5 µL of 0.2 mM (CP, *d*-CP, BP or *d*-BP) standard solution in mobile phase.**

	d-$BP_{MIP(9500rpm)}$				*d*-$CP_{MIP(9500rpm)}$			
Analyte	k_1	k_d	**α**	R_s	k_1	k_d	**α**	R_s
CP	10.30	12.30	1.19	0.68	12.27	14.56	1.19	0.88
BP	11.50	14.40	1.25	0.73	14.98	17.04	1.14	0.60
***d*-CP**		11.5				14.8		
***d*-BP**		13.4				17.3		

Note: **k_1 and k_d are the retention factors of the first and second eluted enantiomers respectively; α is the enantioseparation factor; R_s, resolution.**

In Table 5.11, the retention factors, enantioselectivity factors and resolution were greater for BP enantiomers than CP on the *d*-$BP_{MIP(9500rpm)}$ column. A similar trend was observed in the retention factors for BP over CP on the *d*-$CP_{MIP(9500rpm)}$ column. However, an opposite trend was observed for the enantioselectivity factors and resolution, as they were greater for CP enantiomers than BP on the *d*-$CP_{MIP(9500rpm)}$ column, showing that both MIPs gave the best resolution for its own template.

It was important to note that, employing the *d*-$BP_{MIP(9500rpm)}$ column to perform separations, the back pressures were observed to be a lot lower in comparison to those used for the *d*-$CP_{MIP(9500rpm)}$ column (circa 111 bar). This could result from the particles being less densely packed during the packing process for the *d*-BP MIP column. As a result the flow-rate was increased from 0.075 to 0.1 mL min^{-1} in this study.

For all studies performed, separations of the CP, *d*-CP, BP and *d*-BP compounds on *d*-$CP_{MIP(9500rpm)}$ and *d*-$BP_{MIP(9500rpm)}$ columns were achieved in an aqueous mobile phase. The retention factors and enantioselective data of these related compounds support the view that ionic and hydrophobic interactions play an important role in the retention

and enantioselectivity. Based on this information, the chiral recognition process at pH 7 can be explained. Interactions were mainly attributable to the contribution of MAA functionality on the stationary phase and the tertiary amino group in the CP and its structural analogues, which plays a predominant role in the binding of MIPs in aqueous environment. The interaction of the pyridine group of the CP and its structural analogues with a carboxylic acid group of the polymer is responsible for enantioselectivity. It was also of interest to see that the MIP stationary phase was able to separate a mixture made up of PHEN, CP and BP. The MIP may therefore be used as a stationary phase for various antihistamines.

In the literature MIP based chiral stationary phases have been produced for a vast range of chiral compounds and enantioselectivity values, α, in the 1.5 – 5 range are typical [32]. The enantioselectivity values reported in this study are within this range.

By optimising chromatographic conditions such as column temperature and flow rate, shorter analysis time and sharper peaks were attained which therefore improved the column performance for *d*-$CP_{MIP(9500rpm)}$ (Section 5.3.4.4). This was quantified by calculating the peak widths at half the peak height in Figures 5.14 (a) and (b).

A highly promising development for analytical chiral separations was represented in this study. MIPs were prepared by suspension polymerisation in an aqueous phase using the non-covalent self-assembly approach. These MIPs were subsequently packed into HPLC columns, which were prepared in 2 h from start to finish employing methanol as solvent. The MIPs were characterised by HPLC and UV binding studies and enantioselectivities were achieved on the *d*-$CP_{MIP(9500rpm)}$ and *d*-$BP_{MIP(9500rpm)}$ columns respectively. The next stage to increase efficiencies in chiral separations would be to employ polymers prepared at higher speeds as stationary phases. Additionally, combine their use with Ultra-HPLC analysis, which generate less back pressures and significantly increase column efficiency in terms of rapid chiral resolution kinetics.

5.4 Conclusions

MIPs were prepared for CP, *d*-CP, BP and *d*-BP by an aqueous suspension polymerisation method using chloroform as the porogen at an agitation speed of 24000 rpm. The enantioselectivity was determined by equilibrium binding using chiral HPLC analysis performed on imprinted polymers and structural analogues using a chiral column for resolution of enantiomers. The common trends observed for the HPLC equilibrium binding results in Figure 5.7 and Table 5.5 are outlined below.

- There was similarity in non-specific binding across all NIPs.
- *d*-BP imprinted polymer produced the highest percentage rebound and binding capacity values in CP, *d*-CP and BP standard solutions respectively.
- *d*-CP MIP gave the highest percentage bound and binding capacity in the *d*-BP standard solution (59.90 ± 0.25 and 0.191 mg $5mL^{-1}$).
- BP MIP gave the highest IF value reloaded in *d*-BP standard solution (4.6 ± 0.62).

As there is very little difference between the two pK_a values for CP and BP, it makes it difficult to explain why a higher uptake, binding capacity and IF values were found for the BP polymers over the CP polymers. It is speculated that the higher binding of BP polymers over CP depends on the differences in polarisability between Br and Cl. In order to confirm trends observed in HPLC analysis, a full comparison was performed by UV equilibrium binding analysis, which agreed well with HPLC results.

To gain a better insight into the enantioselectivity and chromatographic behaviour by HPLC, the *d*-$CP_{MIP(9500rpm)}$ was selected and packed as a HPLC stationary phase employing an aqueous mobile phase of composition 70:30 (v/v) ACN:buffer (pH 7).
The enantioselectivity results obtained in Section 5.3.4 are summarised:

- The chromatographic behaviour and separation of (a) CP, (b) *d*-CP (c) BP and (d) *d*-BP isomers were studied on the *d*-$CP_{MIP(9500rpm)}$ column: The highest enantioselectivity (1.19) and resolution (0.88) was obtained for CP over BP. The *d*-$CP_{MIP(9500rpm)}$ showed high cross-selectivity for CP and BP. The BP was more retained than CP and this result is in agreement with equilibrium binding observations (Table 5.5).

- Separation of PHEN, CP and BP enantiomers on *d*-$CP_{MIP(9500rpm)}$ column: The highest retention factor, enantioselectivity and resolution were observed for BP ($\alpha = 1.17$ and $R_s = 0.72$) over the CP ($\alpha = 1.15$ and $R_s = 0.64$) and PHEN ($\alpha = 1.08$ and $R_s = 0.50$) enantiomers. The retention tendencies of BP and CP were also similar but the BP was more retained. This was explained due to the fact that PHEN, CP and BP having almost the same pK_a values and in addition the hydrophobicity is in the order of BP, CP and PHEN.
- Effect of column temperature (a) ambient and (b) 50 ^{o}C on a mixture of *d*-CP and *d*-BP isomers on the *d*-$CP_{MIP(9500rpm)}$ column was studied. The resolution value increased with increase in column temperature from 0.61 to 0.86, which would be expected due to sharper peaks produced. The selectivity factor decreased slightly from 1.18 to 1.17 at the higher temperature.
- To further extend the enantioselectivity study, the chromatographic behaviour and separation of (a) CP, (b) *d*-CP (c) BP and (d) *d*-BP isomers were also studied on a *d*-$BP_{MIP(9500rpm)}$ column: The retention, enantioselectivity and resolution factors were greater for BP enantiomers ($k_l = 11.50$, $k_d = 14.40$, $\alpha = 1.25$ and $R_s = 0.73$) over CP ($k_l = 10.30$, $k_d = 12.30$, $\alpha = 1.19$ and $R_s = 0.68$).
- The results demonstrate that the *d*-CP and *d*-BP imprinted columns each gave the best enantioseparation for their own template (Table 5.11).

The impact of optimising chromatographic conditions such as column temperature meant that problems in terms of peak asymmetry could be overcome. This also lead to shorter analysis time as retention was reduced which therefore improved the column performance for *d*-$CP_{MIP(9500rpm)}$ by increasing resolution and improved flow rates.

Reference List

1. Zhou, L.; Welch, C.; Lee, C.; Gong, X.; Antonucci, V.; Ge, Z. *Journal Of Pharmaceutical And Biomedical Analysis* **2009,** *49*, 964-69.

2. Ansell, R. J. *Advanced Drug Delivery Reviews* **2005,** *57*, 1809-35.

3. Haginaka, J. *Journal of Chromatography B* **2008,** *875*, 12-19.

4. Fried, K. M.; Young, A. E.; Usdin Yasuda, S.; Wainer, I. W. *Journal Of Pharmaceutical And Biomedical Analysis* **2002,** *27*, 479-88.

5. Chen, Q. C.; Jeong, S. J.; Hwang, G. S.; Kim, K. H.; Kang, J. S. *Archives of Pharmacal Research* **2008,** *31*, 523-29.

6. Ismaiel, O. A.; Halquist, M. S.; Elmamly, M. Y.; Shalaby, A.; Thomas Karnes, H. *Journal of Chromatography B* **2008,** *875*, 333-43.

7. Stephani, R.; Cesare, V. *Journal of Chromatography A* **1998,** *813*, 79-84.

8. Murao, S.; Manabe, H.; Yamashita, T.; Sekikawa, T. *Internal Medicine* **2008,** *47*, 1013-15.

9. Cashman, J. R.; Celestial, J. R.; Leach, A.; Newdoll, J.; Park, S. B. *Pharmaceutical Research* **1993,** *10*, 1097-105.

10. Wilson and Gisvold's Textbook of "*Organic Medicinal and Pharmaceutical Chemistry",* Block, J. H.; Beale Jnr, J. M. Eds.; 11th Edition.; (Lippincott Williams and Wilkins, **2004**).

11. Maier, N. M.; Lindner, W. *Analytical and Bioanalytical Chemistry* **2007,** *389*, 377-97.

12. Mayes, A. G.; Whitcombe, M. J. *Advanced Drug Delivery Reviews* **2005,** *57*, 1742-78.

13. Haginaka, J.; Takehira, H.; Hosoya, K.; Tanaka, N. *Journal of Chromatography* **1998,** *816*, 113-21.

14. Chen, W.; Liu, F.; Zhang, X.; Li, K. A.; Tong, S. *Talanta* **2001,** *55*, 29-34.

15. Haginaka, J.; Kagawa, C. *Journal of Chromatography A* **2002,** *948*, 77-84.

16. Haginaka, J.; Kagawa.C *Journal Of Chromatography B-Analytical Technologies In The Biomedical And Life Sciences* **2004,** *804*, 19-24.

17. Haginaka, J.; Tabo, H.; Kagawa, C. *Journal Of Pharmaceutical And Biomedical Analysis* **2008,** *46*, 877-81.

18. Gil-Agustí, M.; García-Alvarez-Coque, M. C.; Esteve-Romero, J. *Analytica Chimica Acta* **2000,** *421*, 45-55.

19. Ismaiel, O. A.; Halquist, M. S.; Elmamly, M. Y.; Shalaby, A.; Thomas Karnes, H. *Journal of Chromatography B* **2008,** *875*, 333-43.

20. Riahi, S.; Edris-Tabrizi, F.; Javanbakht, M.; Ganjali, M. R.; Norouzi, P. *Journal of Molecular Modeling* **2009,** *15*, 829-36.

21. Foye, W. O. "*Foye's Principles of Medicinal Chemistry",* Foye, W. O.; Lemke, T. L.; Williams, D. A. Eds.; 6th Edition.; (Lippincott Williams and Wilkins, **2007**).

22. Britain, H. G.; Prankerd, R. J. Profile of Drug Substances, Excipients and Related Methodology*,* 2007.

23. Kempe, H.; Kempe, M. *Macromolecular Rapid Communications* **2004,** *25*, 315-20.

24. Kempe, H.; Kempe, M. *Analytical Chemistry* **2006,** *78*, 3659-66.

25. Diacel Chiral Columns, Esslab, UK, http://www.daicelchiral.com/appguide/data/p23/p23-08.htm. (**2009**).

26. Simon, R.; Collins, M. E.; Spivak, D. A. *Analytica Chimica Acta* **2007,** *591*, 7-16.

27. Yoshizako, K.; Hosoya, K.; Iwakoshi, Y.; Kimata, K.; Tanaka, N. *Analytical Chemistry* **1998,** *70*, 386-89.

28. Li, Y. H.; Yang, T.; Qi, X. L.; Qiao, Y. W.; Deng, A. P. *Analytica Chimica Acta* **2008,** *624*, 317-25.

29. Kirkland, J. J.; DeStefano, J. J. *Journal of Chromatography A* **2006,** *1126*, 50-57.

30. Sellergren, B.; Shea, K. J. *Journal of Chromatography A* **1995,** *690*, 29-39.

31. Dauwe, C.; Sellergren, B. J. *Journal of Chromatography A* **1996,** *753*, 191-200.

32. Mayes, A. G.; Mosbach, K. *Trac-Trends in Analytical Chemistry* **1997,** *16*, 321-32.

Chapter 6

Physical characterisation of chlorpheniramine imprinted polymer beads and its structural analogues

6.1 Introduction

In Chapter 5, the binding behaviour of the MIPs and NIPs prepared at 24000 rpm was evaluated and it was suggested that the morphology of the beads may affect the binding behaviour. Site accessibility could be a possible issue reflected in equilibrium binding studies in Chapter 5. The imprinted cavities located on the surface of the polymer were fully accessible, while cavities located in the interior of the polymer were only partially accessible or inaccessible, depending on the porosities of the polymers. It was postulated by Wei and Mizaikoff [1] that if binding sites are mainly located at the surface of the imprinted molecules, it is assumed that there are less specific binding sites available for polymers with smaller surface areas and pore volume. This assumption was reflected in the binding behaviour observed in Chapter 5. The applicability of the MIPs as stationary HPLC phases was also examined in Chapter 5. It was reported by Suárez *et al*. [2] that the porous structure of the separation media is one of the most important features needed to achieve good retention.

To further elucidate the nature of the imprinting effect and applicability of MIPs as stationary HPLC phases in Chapter 5, physical characterisation methods such as BET analysis, particle size distribution analysis, solvent swelling experiments and SEM were performed and reported in this chapter in order to characterise the macroscopic features of the polymers.

Nitrogen sorption porosimetry was used to study the adsorption mechanism of the polymers through examination of surface properties and morphological characteristics. The BET (Brunauer, Emmett and Teller) method was used to characterise the surface properties of the polymers. Various properties such as surface area, volume of pores and pore diameter were measured and this information was used to compare the adsorption properties of a series of polymers prepared at varying agitation speeds of 9500, 13500 and 24000 rpm respectively.

Additionally, particle size distribution, solvent swell studies and morphology by scanning electron microscopy (SEM) were also employed to provide an insight into macroscopic features of the polymers prepared in Chapter 5. These characteristics

were compared to polymers prepared at agitation speeds of 9500 rpm and 13500 rpm in order to assess the significance of surface area, pore volume, particle size distribution, solvent swell and morphology. Investigation of MIP materials employing these characterisation techniques present a better understanding of the morphology and textural properties of the polymers [3].

Objectives of the research

The main objectives of the work in this chapter were:

- To carry out a detailed investigation of the physical properties of MIPs prepared for CP, *d*-CP, BP and *d*-BP by suspension polymerisation method in an aqueous medium, using techniques such as nitrogen sorption porosimetry, particle size analysis, solvent swelling and SEM and
- To compare and evaluate the physical characteristics of spherical beads formed by aqueous suspension polymerisation prepared using different agitation speeds, 9500 rpm and 13500 rpm respectively.

6.2 Experimental

6.2.1 Materials and methods

The reagents and methodology for the synthesis of spherical beads by suspension polymerisation in an aqueous media was described in Chapter 5, Section 5.2.4. The equipment as described in Section 2.2.2, Chapter 2.

6.2.2 Instrumentation

- Nitrogen sorption porosimeter: Gemini VI, Micromeritics, Particular Sciences.
- Particle size analyser: Mastersizer 2000 coupled with Hydro 2000S, Malvern Instruments Particular Sciences.
- Scanning electron microscope (SEM): Hitachi S-2460N SEM system and Sputter Coater Unit PS3 Agar Aids for Electron Microscopy.

6.2.2.1 Nitrogen sorption porosimetry studies

Pore size distribution and surface areas of the washed polymers were analysed by the Brunauer-Emmett-Teller (BET) method. The analysis was performed on a nitrogen sorption porosimeter, Gemini VI Surface Area and Pore Size Analyser (Micromeritics). Sample preparation involved weighing approximately 180 mg quantity of the dry polymer into an analysis sample tube which was degassed using a constant flow of nitrogen for 2 h at 120 ºC prior to analysis. Following degassing/cleaning of the sample, the polymer was reweighed and the value was entered into the sample log information. The largest source of error in analysis of low surface area samples is free space. For all analyses, filler rods were used in the sample and references tubes. As the reference tube needs to mirror the sample tube, the height of the filler rods needs to be the same in both tubes. Therefore glass beads were added to the sample tube to guarantee equal height. This effectively eliminates free space error and thermal effects so differential pressure can be achieved.

The analyses were conducted at a cryogenic temperature (liquid nitrogen at its boiling point, 77.35 K at one atmospheric pressure). The reference tube and sample tube

were attached to the relevant sample ports on the instrument and were evacuated at 50 mmHg min^{-1} for 6 min and cooled to 77 K using liquid nitrogen. The free space (volume of sample tube unoccupied by the sample) was measured by dosing helium into both the sample and reference. Once the system was evacuated, analysis was started by exposing the sample to volumes of nitrogen gas (the adsorptive). The pressure was equilibrated and the volumes of gas sorbed were determined.

Desorption analysis followed adsorption on all polymer samples in order to generate a 109 point sorption isotherm in the relative pressure (P/P_o) range 0.01 – 0.99. Convention has established that the quantity of gas adsorbed is expressed as its volume at standard conditions of temperature and pressure (0 ºC and 760 torr and signified by STP). The pressure is expressed as a relative pressure which is the actual gas pressure P divided by the vapour pressure P_o of the adsorbing gas (nitrogen) at 77 K. For all analyses, information was gathered in the form of quantity adsorbed (or desorbed) versus pressure. This data constitutes the adsorption (desorption) isotherm for the polymer samples. Following application of the BET theory [4], information such as specific surface area (m^2 g^{-1}) was obtained from adsorption isotherms, in the P/P_o range from about 0.05 to 0.3 for a six point plot.

The instrument was calibrated with a carbon black reference standard (approximately 0.5 g) prior to use and was frequently monitored for potential errors by performing a blank test tube analysis. The BET surface area result was within specification (30.66 ± 0.071 m^2g^{-1}) and analysis was performed in triplicate.

6.2.2.2 Particle size studies

The procedure for making particle size measurements was described in an earlier chapter in Section 2.2.9, Chapter 2.

6.2.2.3 Swelling studies

Swelling ratios (S_r) of the suspension polymers were measured using three different solvents, methanol, water (solvents employed for template extraction) and chloroform

(porogen media used for polymeric synthesis). Analysis of the polymer swelling was carried out based on a method in Chapter 2, Section 2.2.10, which was previously described by Piletsky *et al*. [5].

6.2.2.4 Scanning electron microscope (SEM) analysis

The morphology of the MIPs prepared for CP, *d*-CP, BP and *d*-BP at different agitation speeds (i.e. 9500, 13500 and 24000 rpm) was characterised by SEM (Hitachi S-2460N system) with a voltage of 25 keV as described in Section 2.2.3.4, Chapter 2.

6.3 Results and discussion

6.3.1 Nitrogen sorption analysis

6.3.1.1 Isotherm analysis

Plots of quantity of gas adsorbed (desorbed) on the Y-axis against relative pressure (P/P_o) on the X-axis gives the adsorption isotherm. This information reveals much about the structure of the adsorbing material (adsorbent) simply by their shape. There are 6 types of adsorption isotherms classified by IUPAC which can be used to gain information on porosity [4], (refer to Chapter 1, Figure 1.22 for an illustration of the 6 types of adsorption isotherms).

Figure 6.1 (a) presents the overlay of CP, *d*-CP, BP and *d*-BP imprinted polymer adsorption isotherms prepared at (a) 24000 rpm (MIP and NIP) and (b) 9500 rpm (MIPs) respectively.

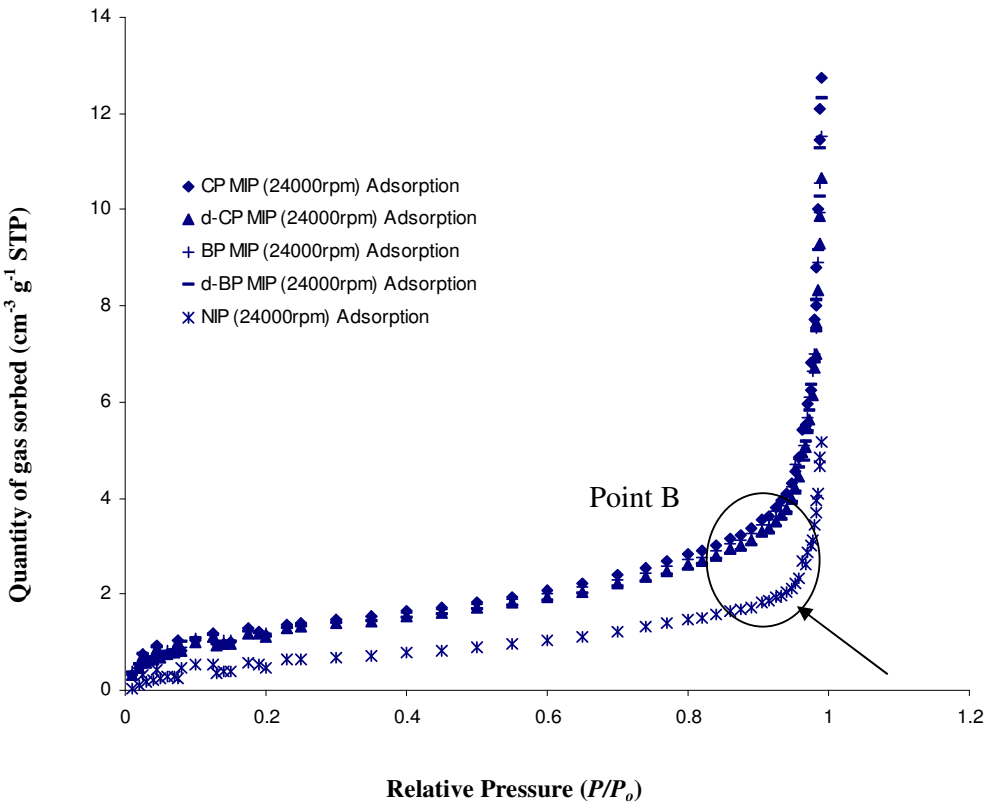

Figure 6.1 (a) **Adsorption isotherms for CP, *d*-CP, BP and *d*-BP imprinted polymers (MIPs and NIPs) prepared at 24000 rpm.**

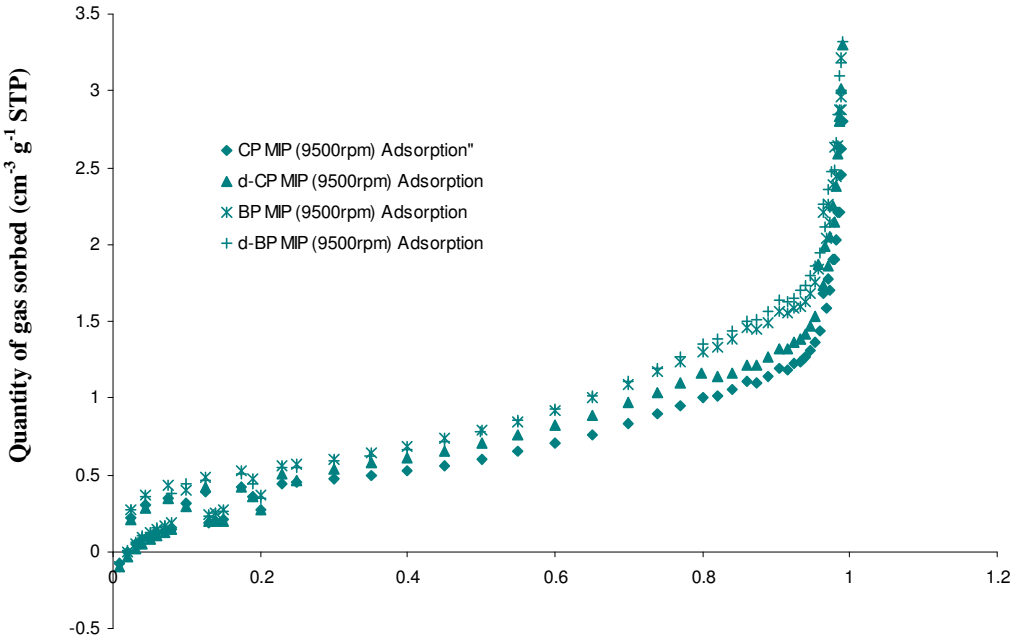

Figure 6.1 (b) **Adsorption isotherms for CP, *d*-CP, BP and *d*-BP imprinted polymers (MIPs) prepared at 9500 rpm.**

The adsorption curves shown in Figure 6.1 (a – b) have the same general shape as Type II isotherms (i.e. unrestricted monolayer-multilayer adsorption) as classified by the IUPAC [4], which is indicative of non-microporous materials (i.e. those having pores > 2 nm wide) or macroporous materials (> 50 nm). However, MIPs typically reveal Type IV isotherms which indicate mesoporosity (2 – 50 nm) [6]. In Figure 6.1 (a – b), the Type II isotherms also exhibit a Point B (which occurred at the middle, nearly linear section of the isotherm) illustrated in Figure 6.1 (a); this indicated the stage at which monolayer coverage was complete and multilayer adsorption began [4]. The adsorption and desorption curves for the *d*-CP imprinted polymer (MIP) isotherm prepared at 13500 rpm also exhibited Type II isotherms similar to those shown in Figure 6.1 (a – b).

The resulting isotherm plot (adsorbed volume versus relative pressure) was used to calculate surface area using the BET equation. The adsorption isotherms in BET coordinates are completely transformed to straight lines. The BET instrument automatically converts the monolayer/multilayer capacity to a surface area measurement in $m^2\ g^{-1}$ in the P/P_o range from about 0.05 to 0.3 for a six point plot. In Figure 6.1 (a – b) a big difference was observed between the quantities of gas sorbed for polymers made at different speeds.

Table 6.1 shows the quantity of gas sorbed at P/P_o 0.99 for the CP, *d*-CP, BP and *d*-BP imprinted polymers (MIPs and NIPs) prepared at 24000, 13500 and 9500 rpm respectively.

Table 6.1 **Quantity of gas sorbed (n^a) at P/P_o 0.99 for CP, *d*-CP, BP and *d*-BP imprinted polymers (MIPs and NIPs) prepared at 24000, 13500 and 9500 rpm respectively. Results based on average values for duplicate analysis with errors based on ± 1 standard deviation.**

Polymer	n^a ($cm^3 g^{-1}$ STP)
24000 rpm	
CP MIP	12.92 ± 0.02
d-CP MIP	10.65 ± 0.14
BP MIP	12.40 ± 0.10
d-BP MIP	12.33 ± 0.03
NIP	5.05 ± 0.04
13500 rpm	
d-CP MIP	4.65 ± 0.06
9500 rpm	
CP MIP	2.79 ± 0.09
d-CP MIP	3.29 ± 0.03
BP MIP	3.21 ± 0.02
d-BP MIP	3.32 ± 0.04

There are a number of observations that can be made from the results obtained in Table 6.1. Firstly there is a higher amount of gas sorbed (n^a value) on the imprinted polymers prepared at the highest speed 24000 rpm (over 3 and 4 times the quantity of gas sorbed) in comparison to 13500 and 9500 rpm. The difference in the quantity of gas sorbed between the polymers prepared at different speeds was also reflected in Figure 6.1 (a – b). This could be explained in terms of the fixed mass of polymer (approximately 180 mg) which was used for each analysis. For a fixed mass the overall surface area increases as particle diameter decreases.

Secondly, there was a large difference in the quantity of gas sorbed (n^a values) between the MIP and NIP polymers prepared at 24000 rpm, this was also observed in Figure 6.1 (a). With the exception of *d*-CP MIP prepared at 24000 rpm (a possible anomaly) the values for CP, BP and *d*-BP MIPs are all quite similar and within experimental error. However, the NIP prepared at 24000 rpm is less than half the value of the corresponding MIPs (n^a value = 5.05 ± 0.04 $cm^3 g^{-1}$ STP). The reason for this was most probably due to structural differences within the polymers due to imprinting [7].

6.3.1.2 BET surface area analysis

In order to determine the surface areas of the polymers the BET method requires a linear regression analysis on transformed isotherm data. Six point BET transform plots in the relative pressure region P/P_o 0.05 – 0.3 were generated, which is illustrated in Figure 6.2 for the *d*-CP polymers prepared at 24000, 13500 and 9500 rpm respectively.

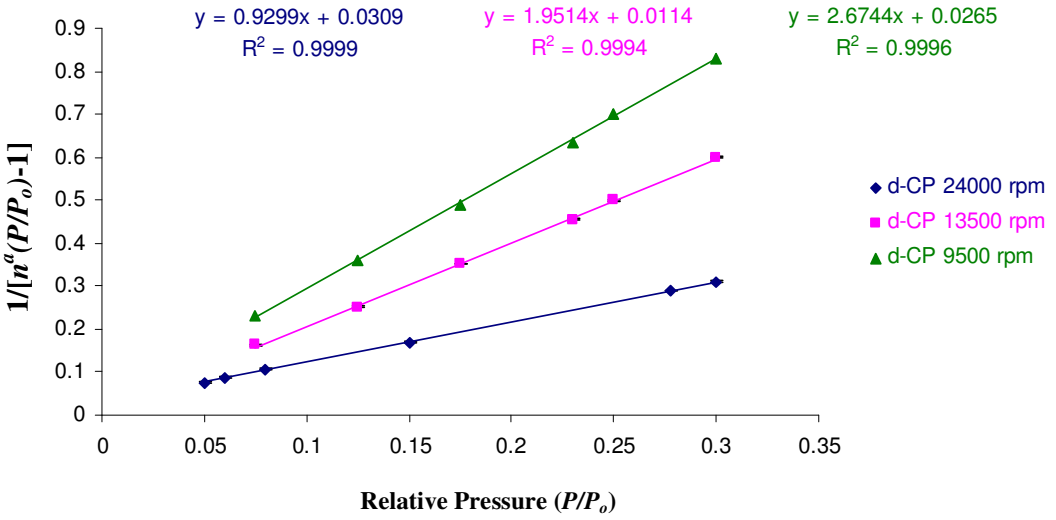

Figure 6.2 **BET plots for *d*-CP imprinted polymers (MIPs) prepared at 24000, 13500 and 9500 rpm respectively. Results based on average values for duplicate analysis with error bars based on ± 1 standard deviation.**

The BET plot in Figure 6.2 illustrates a linear relationship with a correlation coefficient of 0.999 or greater. BET plots were generated for all polymers in order to determine the surface area of the polymers using 0.162 nm^2 as the molecular cross-sectional area for adsorbed nitrogen molecules [4].

Table 6.2 presents a summary of the surface areas of the imprinted polymers prepared at 9500, 13500 and 24000 rpm.

Table 6.2 **BET surface area values for CP, *d*-CP, BP, *d*-BP imprinted polymers (MIPs) and non-imprinted polymers (NIPs) prepared at 24000 rpm, 13500 rpm and 9500 rpm respectively. Results based on average values for duplicate analysis with errors based on ± 1 standard deviation.**

Polymer	BET surface area ($m^2 g^{-1}$)	C	N ($cm^3 g^{-1}$ STP)	R^2
24000 rpm				
CP MIP	4.91 (± 0.08)	29.23 (± 0.05)	1.13 (± 0.03)	0.9997
d-CP MIP	4.55 (± 0.04)	30.51 (±0.10)	1.04 (± 0.08)	0.9999
BP MIP	4.92 (± 0.08)	35.31 (± 0.15)	1.13 (± 0.09)	0.9997
d-BP MIP	4.73 (± 0.05)	33.76 (± 0.05)	1.09 (± 0.19)	0.9998
NIP	2.61 (± 0.08)	12.10 (± 0.05)	0.60 (± 0.05)	0.9998
13500 rpm				
d-CP MIP	2.11 (± 0.04)	214.06 (± 0.69)	0.49 (± 0.04)	0.9994
9500 rpm				
CP MIP	1.52 (± 0.02)	124.67 (± 0.20)	0.35 (± 0.02)	0.9995
d-CP MIP	1.68 (± 0.01)	129.37 (± 0.49)	0.38 (± 0.01)	0.9996
BP MIP	1.84 (± 0.11)	46.06 (± 0.05)	0.42 (± 0.11)	0.9996
d-BP MIP	1.86 (± 0.02)	73.00 (± 0.03)	0.43 (± 0.02)	0.9998

C is a constant derived from the linear plot and it is exponentially related to the enthalpy (heat) of adsorption of the first adsorbed layer [4].
N is the quantity of gas sorbed.

In Table 6.2, the values of C, N and R^2 were obtained from the regression line in the BET report for surface area determination, of the polymers which employed chloroform as porogen. Results varied from 1.52 – 4.92 m^2g^{-1} for polymers prepared at 24000, 13500 and 9500 rpm respectively, indicating that the specific surface areas of the polymers seemed to be non-porous as they illustrated extremely low surface areas in the dry state. A low specific surface area corresponds to adsorption measurement mainly on the external surface of a material.

MIP polymers prepared at the lowest speed (9500 rpm) had lower surface areas compared to the MIP prepared at the highest speed (24000 rpm) in Table 6.2. The difference in BET surface areas was large across all three speeds (Table 6.2). The surface area of the MIPs was dependent on the size of the polymer beads, with the

MIP prepared at the lowest speed showing the lowest surface area. In suspension polymerisation the size of the initial emulsified monomer droplets depends on the balance between the droplet break up and coalescence in the dispersion medium, which in turn is controlled by the speed of agitation used. The effect of agitation speed had a relatively high effect on the experimental results. This therefore, indicates that the agitation rate provides some control over the pore structure of the final beads.

Sellergren and Shea [6] employed nitrogen sorption to characterise MIPs. They found that the polymers made with chloroform as porogen were non-porous and had very low surface area (3.5 m^2g^{-1}) [6]. Their findings are in agreement to the low surface area results found for polymers prepared at varying speeds with chloroform as porogen in this study (Table 6.2).

An interesting comparison can be made between Haginaka's findings and the specific surface area result in this study. The *d*-CP MIP prepared at 9500 rpm was found to exhibit an extremely low specific surface area i.e. (1.68 m^2g^{-1}). This MIP was evaluated using aqueous mobile phases in Chapter 5 and was able to separate the enantiomers of CP, BP and PHEN. Haginaka *et al*. [8] prepared MIPs for *d*-CP by a multi-step swelling and polymerisation technique using 2-(trifluoromethyl)acrylic acid (TFMAA) and chloroform as the functional monomer and porogen, respectively. Nitrogen sorption measurements were performed and the MIPs were non-porous with low specific surface area (10 m^2g^{-1}), low specific pore volume (0.04 mLg^{-1}) and low pore diameter (11.1 nm). However, the MIP prepared with *d*-CP using TFMAA could separate CP, BP and PHEN enantiomers using aqueous mobile phase. This result indicated the presence of enantioselective binding sites in its swollen state for the MIP employed as stationary phase [8].

Kempe had previously synthesised MIP beads by suspension polymerisation in mineral oil employing an agitation speed of 13500 rpm, TRIM as cross-linker and acetonitrile as porogen [9]. BET analysis performed on the MIP beads exhibited a more porous morphology in comparison to the polymers observed in this study, with significantly higher specific surface area (50 m^2g^{-1}), specific pore volume (0.24 mLg^{-1}) and pore diameter (189 nm) measured.

The value of C obtained from the BET plot (Figure 6.2), is exponentially related to the enthalpy (heat) of adsorption of the first adsorbed layer according to the BET theory [4]. However, it is generally accepted that the value of C may be used to characterise the shape of the isotherm in the BET range. It does not provide a quantitative measure of enthalpy of adsorption but gives an indication of the order of magnitude of the adsorbent-adsorbate interaction energy [4]. This value should always be positive and the normal range for C values is most frequently observed to be between 20 and 200 when using nitrogen at 77 K (temperature of liquid nitrogen) and indicates the affinity of the sample for nitrogen. In Table 6.2, low C values were observed for polymers prepared at 24000 rpm, with values in the range 29 – 35 for MIPs and a value of 12.10 for the NIP. Higher C values (circa 100) were revealed for the MIP polymers prepared at 9500 rpm and *d*-CP MIP prepared at 13500 rpm and are consistent with the formation of well-defined monolayers on many non-porous and mesoporous adsorbents. Additionally a high value of C is associated with a sharp knee in the isotherm, thus making it possible to visually inspect the uptake at Point B [4]. This correlated with sorption isotherms observed for MIPs prepared at 9500 rpm in Figure 6.1 (b) which exhibited a sharper knee in the isotherm which was more defined in comparison to Figure 6.1 (a) for MIPs prepared at 24000 rpm.

In Figure 6.1, there was a large difference in the quantity of gas sorbed between the MIP and NIP polymers. This was reflected in the surface area values for the MIP and NIP polymers prepared at 24000 rpm in Table 6.2. The NIPs exhibited lower surface areas in comparison to the MIP polymers as a larger surface area equates to a larger amount of gas sorbed. These findings agree with published work.

In the literature, Brüggemann [7] prepared molecularly imprinted catalytically active polymers at room temperature by UV radiation. The subsequent polymers were ground and sieved and examined by BET surface area analysis. It was reported that MIPs tend to have higher surface areas than NIPs. The MIP expressed over 6 times the surface area of the corresponding NIP (i.e. MIP = 6.02 m^2g^{-1} and NIP = 1.05 $m^2 g^{-1}$) [7]. The reason for this was most probably due to structural differences within the polymers due to imprinting. This would be indicative of a better arrangement of functional sites within the pores which would lead to a larger surface area within the MIPs. This would lead to MIPs with larger sized cavities allowing easier access of

the template during rebinding. This correlates with binding trends observed in Table 5.4 for MIP and NIP in Chapter 5. Beltran prepared microspheres by precipitation polymerisation using an antiepileptic drug, carbamezapine. The MIP obtained had a well-developed pore structure (specific surface area = 758 ± 8 m^2g^{-1}) and (NIP = 716 ± 8 m^2g^{-1}), however with the addition of EGDMA to the polymer composition lead to materials with low specific surface areas (MIP = 23 ± 0.8 m^2g^{-1}; NIP = 3 ± 0.2 m^2g^{-1}) [10]. It is suggested from the literature that the behaviour of the MIPs versus the NIPs may be explained by the addition of template or cross-linker to the polymer and the particular reactivity of the functional monomers with the template.

6.3.1.3 Pore analysis

The data derived from the MIPs prepared at 24000, 13500 and 9500 rpm under consideration in this study by the BJH analysis were corrected for multilayer adsorption for pores between 2 and 300 nm using the Halsey thickness equation. In all samples the overall pore volume was very low indicating non-porous materials. Nonetheless, pore size distribution analysis was conducted on the adsorption isotherms but the results are non-conclusive due to the low volumes of nitrogen adsorbed.

Figure 6.3 depicts the differential pore volume distribution curves obtained for (a) *d*-CP MIP and NIP prepared at 24000 rpm and (b) *d*-CP MIP prepared at 9500 rpm during the adsorption process for polymers in this study. The x-axis scale is a logarithmic scale for all the distribution curves.

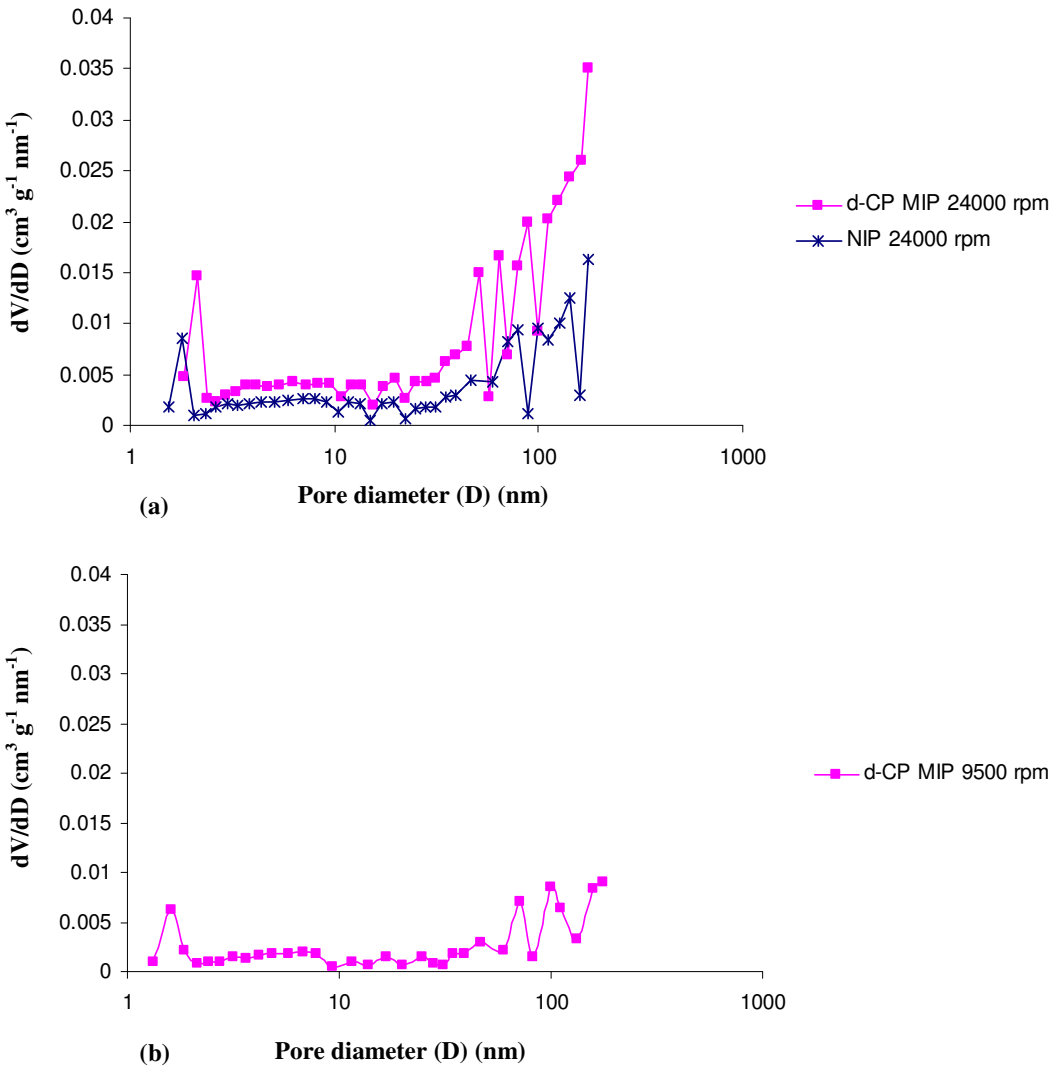

Figure 6.3 **Pore volume distribution curves for (a) *d*-CP MIP and NIP prepared at 24000 rpm and (b) *d*-CP MIP prepared at 9500 rpm.**

The differential pore volume distribution curves in Figure 6.3 (a – b) for the *d*-CP MIP and NIP polymers prepared at 24000 rpm and *d*-CP prepared at 9500 rpm exhibited disordered pore systems. The distribution curves exhibited its first sharp maximum peak at a pore diameter of approximately 3.5 nm, the small pores in the lower limit of the mesoporous region are probably generated due to the presence of solvent molecules during polymerisation procedure [3]. The distribution curves in Figure 6.3 (a – b) also exhibited several dominant groups of pores in the range of diameters 60 – 200 nm. The pore sizes of the primary and secondary pores were circa 180 and 100 nm respectively.

In Figure 6.3 (a) the pore size was smaller for the NIP than the corresponding MIP prepared at 24000 rpm. The NIP indicated a relatively homogeneous distribution in comparison to the MIP. The wide heterogeneous distributions of the MIP could be explained by formation of pre-polymerisation complexes of different composition and conformation between the template molecule and the functional monomers. The differential pore volume distributions obtained for CP, BP and *d*-BP MIPs prepared at 24000 rpm also displayed similar patterns to *d*-CP MIP.

The differential pore volume distributions obtained for CP, BP and *d*-BP MIPs prepared at 9500 rpm also displayed similar patterns to *d*-CP MIP.

Values such as the cumulative surface area of the pores, cumulative volume of pores and the average pore diameters were determined and are shown in Table 6.3. Equation 6.1 was used to determine the average pore diameter [6].

$$Average\ pore\ diameter = 4x\frac{(pore\ volume)}{(pore\ surface\ area)} \qquad \textbf{Equation 6.1}$$

The pore data must be determined from the adsorption region of the isotherm as opposed to the desorption branch of the isotherm which could lead to inaccuracies [11]. The adsorption isotherm branch was chosen for examination of the data and results shown in Table 6.3.

Table 6.3 **BJH adsorption data obtained for pores between 2 and 300 nm using the Halsey thickness equation for CP, *d*-CP, BP, *d*-BP imprinted polymers (MIPs and NIPs) prepared at 24000 rpm, 13500 and 9500 rpm respectively. Results based on average values for duplicate analysis with errors based on ± 1 standard deviation.**

Polymer	Cumulative surface area of pores ($m^2 g^{-1}$)	Cumulative volume of pores ($cm^3 g^{-1}$)	Average pore diameter (nm)
24000 rpm			
CP MIP	5.58 ± 0.06	0.020 (± 4 x 10^{-4})	14.48 ± 0.42
***d*-CP MIP**	5.07 ± 0.20	0.019 (± 3 x 10^{-3})	13.11 ± 0.11
BP MIP	5.31 ± 0.15	0.019 (± 2 x 10^{-3})	14.63 ± 1.05
***d*-BP MIP**	4.90 ± 0.16	0.019 (± 2 x 10^{-3})	14.19 ± 2.17
NIP	3.20 ± 0.12	0.008 (± 3 x 10^{-4})	9.88 ± 0.73
13500 rpm			
***d*-CP MIP**	3.04 ± 0.10	0.007 (± 1 x 10^{-4})	9.66 ± 0.45
9500 rpm			
CP MIP	2.33 ± 0.04	0.004 (± 2 x 10^{-5})	7.44 ± 0.18
***d*-CP MIP**	2.63 ± 0.11	0.005 (± 3 x 10^{-4})	7.50 ± 0.10
BP MIP	2.80 ± 0.11	0.005 (± 1 x 10^{-4})	7.04 ± 0.56
***d*-BP MIP**	2.97 ± 0.02	0.005 (± 2 x 10^{-4})	7.15 ± 0.30

Table 6.3 shows the porous properties of the obtained microspheres. In all polymer samples the cumulative volume of pores was very low indicating non-porous materials, as was also confirmed by type II sorption isotherms in Section 6.3.1.2. For the MIP polymers prepared at 9500 rpm and 13500 rpm the values were half or less than the corresponding MIPs prepared at 24000 rpm. It was observed that the average pore diameters for all polymers are in the lower mesoporous region (2 – 50 nm) suggesting that internal micro-porosity was low for all polymers. Additionally, the average pore diameter for the MIP polymers prepared at lower agitation speeds 9500 rpm and 13500 rpm was less than the polymers prepared at 24000 rpm. This suggests that the polymers prepared at the lower speeds were less porous than 24000 rpm. Considering the fact that non-porous regions were observed in the inner part of the structure (very low cumulative volume of pores in Table 6.3) and the pore diameters are in the lower mesoporous region, it is assumed that the polymer microspheres possess a dual structure, i.e. a non-porous inner part covered by a mesoporous surface.

Studying the surface area (Table 6.2) and pore volume (Table 6.3) values for CP, *d*-CP, BP and *d*-BP polymers prepared at 24000 rpm, it is evident that the CP and BP polymers exhibited greater surface areas and pore volumes then the *d*-CP and *d*-BP polymers. The lowest values were noted for the *d*-BP polymer, which was unexpected owing to the fact that *d*-BP exhibited the greatest binding affinity in Chapter 5. One possible explanation could be the exposure of the polymer to chloroform during rebinding which enhances swelling and access to specific sites within the cavities of the polymer. However, for all polymers prepared at 9500 rpm, *d*-BP had the highest surface area in comparison to CP, *d*-CP and BP polymers (Table 6.3).

6.3.1 Particle size distribution

Particle size distribution was studied for (a) CP, *d*-CP, BP and *d*-BP imprinted MIP and NIP polymers prepared at 24000 rpm, (b) *d*-CP MIP prepared at 13500 rpm and (c) CP, *d*-CP, BP and *d*-BP MIPs prepared at 9500 rpm. The Dv10, Dv50 and Dv90 values for these polymers are presented in Table 6.4.

Table 6.4 **Dv10, Dv50 and Dv90 values obtained for (a) CP, *d*-CP, BP, *d*-BP suspension MIP and NIP polymers prepared at 24000 rpm (b) *d*-CP MIP prepared at 13500 rpm and (c) CP, *d*-CP, BP and *d*-BP MIPs prepared at 9500 rpm with TRIM as cross-linker. Results are based on the average for triplicate analysis with errors based on ± 1 standard deviation.**

Polymer	Dv10(µm)	Dv50(µm)	Dv90(µm)
24000 rpm			
CP MIP	1.61 ± 0.030	2.60 ± 0.040	4.17 ± 0.050
***d*-CP MIP**	1.48 ± 0.001	2.34 ± 0.003	3.71 ± 0.003
BP MIP	1.56 ± 0.003	2.49 ± 0.004	3.94 ± 0.003
***d*-BP MIP**	1.51 ± 0.007	2.47 ± 0.007	3.68 ± 0.005
NIP	1.99 ± 0.002	3.70 ± 0.006	16.67 ± 0.786
13500 rpm			
***d*-CP MIP**	2.42 ± 0.002	4.45 ± 0.004	7.78 ± 0.008
9500 rpm			
CP MIP	2.10 ± 0.003	5.56 ± 0.011	11.49 ± 0.048
***d*-CP MIP**	2.16 ± 0.001	5.15 ± 0.008	10.45 ± 0.043
BP MIP	2.28 ± 0.003	5.24 ± 0.002	10.53 ± 0.024
***d*-BP MIP**	2.44 ± 0.002	5.21 ± 0.005	9.67 ± 0.007

Overlay diagrams displaying the particle size distribution for the polymer samples analysed in this study are shown in Figure 6.4.

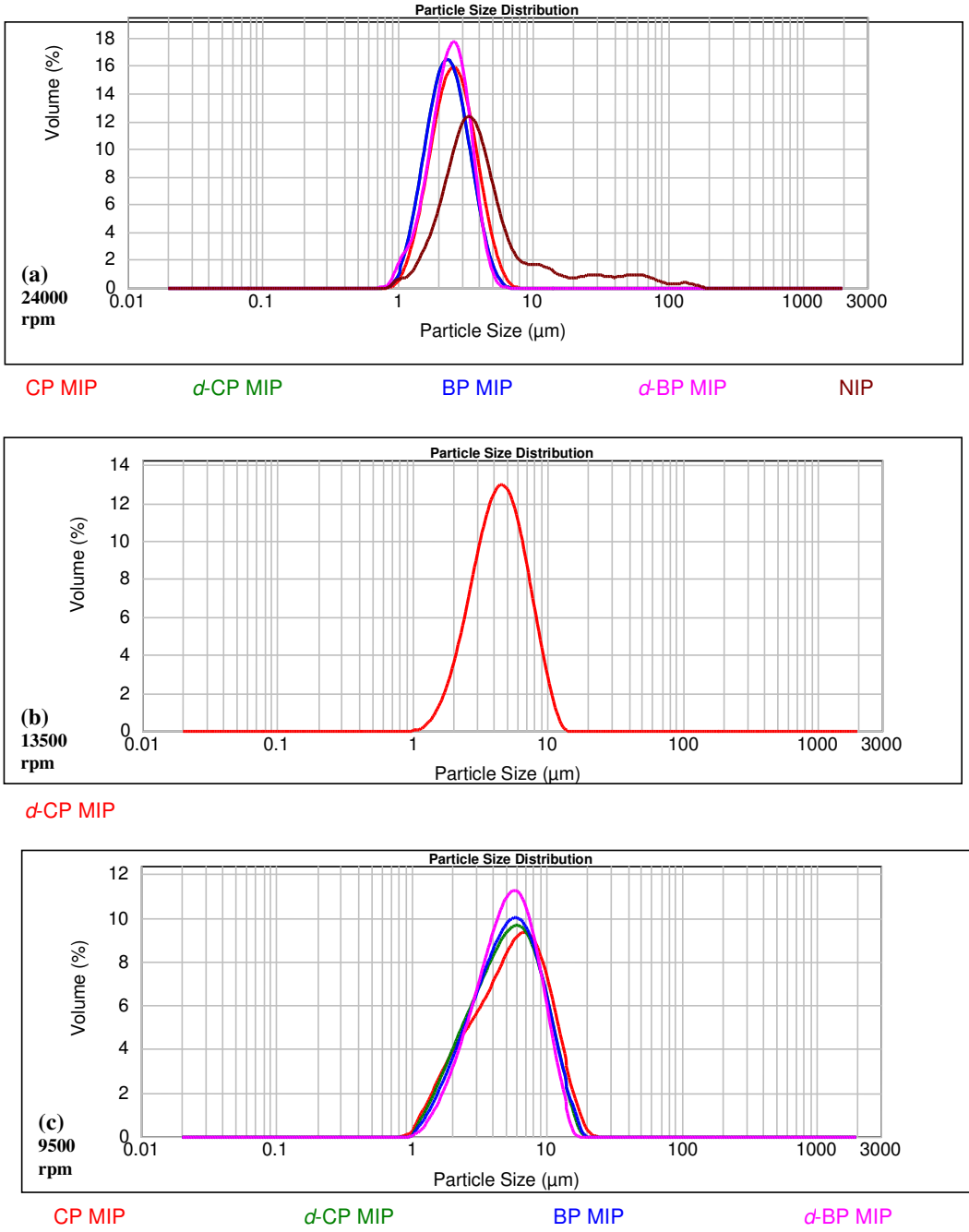

Figure 6.4 **The particle size distributions obtained for (a) CP, *d*-CP, BP and *d*-BP imprinted polymers (MIPs and NIPs) prepared at 24000 rpm, (b) *d*-CP MIP prepared at 13500 rpm and (c) CP, *d*-CP, BP and *d*-BP MIPs prepared at 9500 rpm.**

In Table 6.4, the particle size distributions for (a) CP, *d*-CP, BP and *d*-BP imprinted polymers prepared at 24000 rpm exhibited similar results. However, the NIP demonstrated greater particle size (Dv50 value = 3.70 ± 0.006 µm) in comparison to the MIPs, with Dv50 values which ranged from: 2.34 ± 0.003 – 2.60 ± 0.040 µm. In

addition, a Dv90 value of 16.67 ± 0.786 µm was observed for the NIP which was much higher in comparison to the Dv90 values for the MIPs. This high value could be due to the formation of a larger amount of agglomerates in the absence of the template. A measure of the approximate particle size spread for the polymers in Figure 6.4 (a) was performed by calculating the peak width at half the peak height. The particle size distributions for CP, *d*-CP, BP and *d*-BP imprinted polymers demonstrated similar average spread results (≈ 2.6 µm). The NIP exhibited a broader spread in comparison to the MIPs, with an approximate particle size spread of ≈ 4.1 µm.

However, the particle size for 13500 rpm *d*-CP MIP is larger in comparison to the MIP beads prepared at 24000 rpm, with an average Dv50 value of 4.45 ± 0.004 µm. Furthermore, a broader particle size distribution spread of ≈ 5.4 µm was measured. The agitation rate obviously affects the size of the beads as the size distribution was shifted toward increased bead diameters with decreasing agitation rate.

The particle size distribution for MIPs prepared at 9500 rpm were both larger (Dv50 values ranging from = 5.15 ± 0.008 – 5.56 ± 0.011 µm) with broader spreads (≈ 7.22 µm) than the MIPs prepared at 13500 and 24000 rpm in Figure 6.4 (a – b). All MIPs prepared at 9500 rpm produced polymer beads with average diameters in the low micrometer size range as required for column packing.

The application of materials as HPLC stationary phases with narrow size distribution of particles (average diameter of 3 – 6 µm) are required to possess adequate rigidity to withstand high packing pressure and appropriate column efficiency [12]. The *d*-CP MIP (9500 rpm) was successfully packed as stationary phase in HPLC (Chapter 5) with an average Dv50 value of 5.15 ± 0.008 µm, specific surface area of (1.68 ± 0.01 m^2g^{-1}) and average pore diameter (7.50 ± 0.10 nm) which were very useful for such an application. In comparison separations on a commercial reversed phase C18 HPLC column (250 mm x 4.6 mm, 5 µm particle size) from Phenomenex would typically exhibit pore properties of: (215-320 m^2g^{-1}) for surface area, pore volume (1.05 – 1.15 cm^3g^{-1}) and average pore diameter of (12.5 – 20 nm) respectively [13].

Figure 6.5 displays the particle size distribution for *d*-CP imprinted polymers (MIPs) prepared at 9500 rpm, 13500 and 24000 rpm in this study.

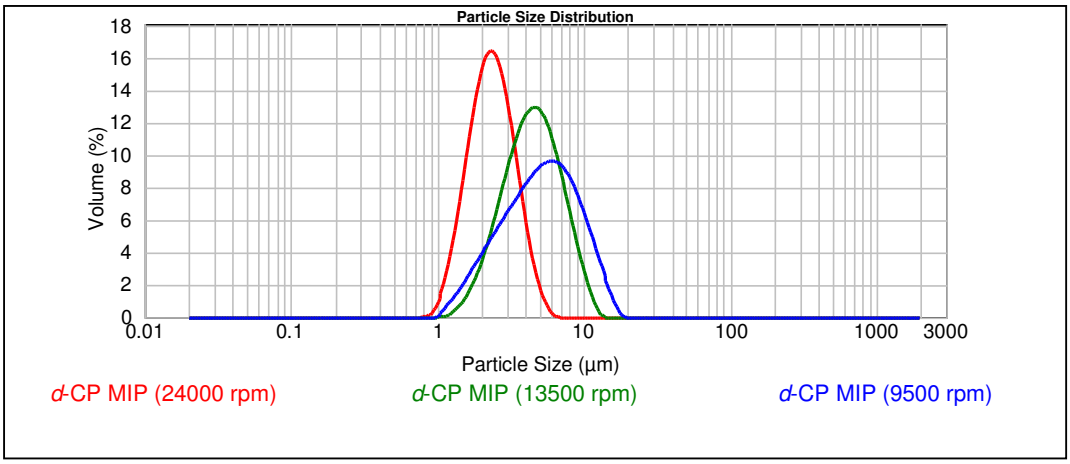

Figure 6.5 **The particle size distribution obtained for *d*-CP imprinted polymers (MIP) prepared at 9500, 13500 and 24000 rpm.**

The change in agitation speed for the preparation of *d*-CP MIPs by suspension polymerisation at 24000, 13500 and 9500 rpm respectively is reflected in the variations in average particle size values. The particle size diameter of the polymer is influenced by the rate of agitation in the initial stage of the reaction. It is expected that the higher the rate of agitation employed in dispersion of the suspension medium the smaller the globules are formed resulting in a smaller average particle size diameter [14]. The sizes of the polymers formed were affected by the mixing rate in this study and agreed with previous findings [9].

Combining the specific surface area values with particle size results a further interesting observation for the *d*-CP MIPs prepared at 24000 rpm. An average Dv50 value of 2.34 ± 0.003 µm was obtained and a pore structure with a specific area of 4.55 ± 0.04 m^2g^{-1} (Table 6.2) was found by increasing the agitation speed. However, decreasing the agitation speed had implications in terms of particle size and surface area values. An average Dv50 value was 5.15 ± 0.008 µm and a lower specific surface area (1.68 ± 0.01 m^2g^{-1}) was observed for *d*-CP prepared at 9500 rpm in Table 6.2. Analysis of the distributions showed an increase in particle size with decreasing particle agitation speed. This trend is illustrated in Figure 6.6.

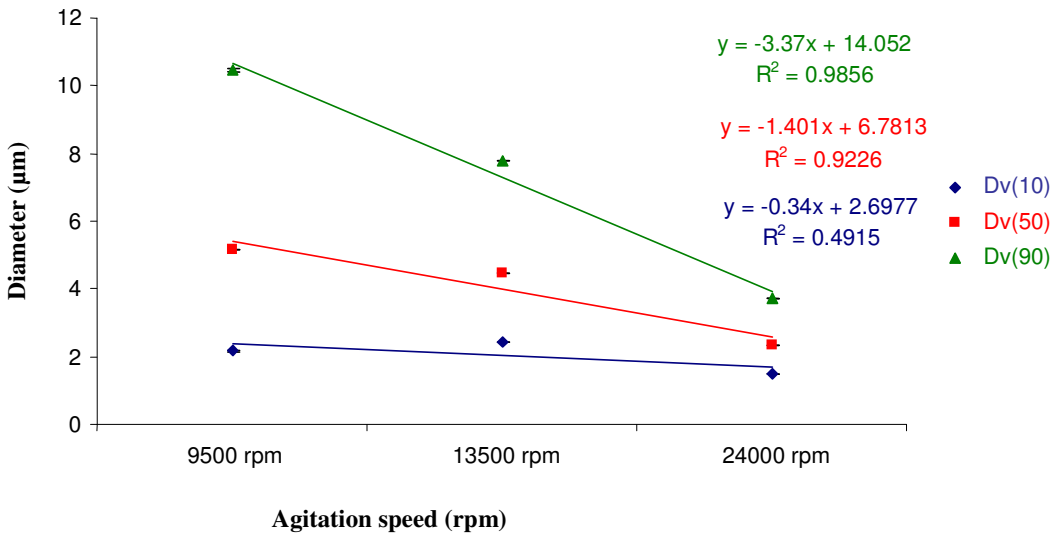

Figure 6.6 **Plot of percentile values for *d*-CP imprinted polymers (MIPs) prepared at 9500 rpm, 13500 rpm and 24000 rpm. Results are based on the average value for triplicate analysis with error bars based on ± 1 standard deviation.**

There is a general linear correlation between particle diameter and agitation speed during polymerisation. As shown in Figure 6.6 the three graphs seem to converge, if the polymers were prepared at a higher speed to 24000 rpm it could eventually converge at one point. A second observation was revealed in examining the R^2 values for Dv10, Dv50 and Dv90 values. The R^2 value for Dv10 was quite low in contrast to the Dv50 and Dv90 values, a possible reason could be due to the smaller absolute values involved. Also, the Dv10 values seem to be almost independent of agitation speed, which suggests that fines in the polymers are similar at all speeds. The size distribution was shifted toward decreased beads diameters with increasing agitation rate.

Both particle size (Dv50 values, 2.34 – 2.60 µm) and BET (specific surface areas, 4.73 – 4.92 m^2g^{-1}) for CP, *d*-CP, BP and *d*-BP MIPs prepared at 24000 rpm respectively have implications for the binding results observed in Chapter 5. This is consistent with the hypothesis proposed by Wei and Mizaikoff [1] that more specific binding sites are available at particles with higher surface areas as they confirmed by equilibrium binding isotherm studies. A greater amount of analyte will be bound to polymers prepared at 24000 rpm, exhibiting a smaller bead size with a higher surface area.

6.3.2 Solvent swell study

As imprinted polymers are generally used in solvents, the swelling ratio (S_r) for CP, *d*-CP, BP and *d*-BP imprinted polymers (MIPs and NIPs) prepared at 9500, 13500 and 24000 rpm was determined in chloroform (porogen), methanol and water and the results are presented Table 6.5.

Table 6.5 **Swell ratio (S_r) for CP, *d*-CP, BP and *d*-BP imprinted polymers (MIPs and NIPs) prepared at 24000 rpm, 13500 rpm and 9500 rpm in chloroform, methanol and water respectively. Results are based on the average value for triplicate analysis with errors based on ± 1 standard deviation.**

Polymer	**Swell Ratio (S_r)**		
24000 rpm	**Chloroform**	**Methanol**	**Water**
CP MIP	7.23 ± 0.04	1.11 ± 0.05	1.09 ± 0.24
d-CP MIP	7.30 ± 0.07	1.11 ± 0.11	1.11 ± 0.19
BP MIP	7.01 ± 0.07	1.58 ± 0.02	1.15 ± 0.10
d-BP MIP	7.22 ± 0.15	1.50 ± 0.06	1.24 ± 0.01
NIP	6.75 ± 0.08	1.45 ± 0.10	1.49 ± 0.12
13500 rpm			
d-CP MIP	7.07 ± 0.11	1.75 (± 0.004)	1.52 ± 0.01
9500 rpm			
CP MIP	7.29 ± 0.10	1.87 ± 0.09	1.40 (± 0.001)
d-CP MIP	7.10 ± 0.10	1.74 ± 0.08	1.05 ± 0.03
BP MIP	7.32 ± 0.04	2.19 ± 0.14	1.29 ± 0.03
d-BP MIP	7.41 ± 0.02	2.37 ± 0.06	1.39 ± 0.15

The swelling for all polymers in chloroform was greater in comparison to methanol and water as seen in Table 6.5. This observation was expected as the porogen would be assumed to fill the pores in accordance with polymerisation conditions [15]. No obvious trend was observed between the polymers prepared at different agitation speeds. The main trend observed in Table 6.5 was that the swell ratio was lower in methanol for the polymers prepared at 24000 rpm in comparison to polymers prepared at 13500 and 9500 rpm. The polymers prepared at 24000 rpm have higher surface

areas (Table 6.2) and higher pore volumes (Table 6.3) and lower swell ratios and this result is consistent with previous studies [15-17].

It has been reported that non-covalent (utilising hydrogen bonding interactions) MIPs demonstrate their best performance in hydrophobic organic solvents such as chloroform [18]. Solvents effect the porosity and surface area of the polymer. Chloroform is a fairly non-polar solvent which should strengthen the interactions of the monomer and template in the rebinding step by promoting hydrogen bonding formation and therefore increasing binding efficiency of the templates. Spivak and Shea [19] reported that optimum recognition was noticed when the same solvent was used in both the polymerisation and rebinding steps, because polymer swelling is increased and there is better access to specific cavities of the polymer. Furthermore, imprinted polymers will very often show different swelling properties in different solvents which will in turn change the morphology of the polymer network, the size, shape and relative positions of the functional groups of the recognition sites which are fundamental for recognition [6].

The swell ratio could have implications for rebinding in chloroform which was performed on polymers prepared at 24000 rpm. It was found in the majority of cases that the *d*-BP imprinted polymers produced the highest percentage rebound, binding capacity and IF values in CP, *d*-CP and BP standard solutions respectively. Similarly, the *d*-CP MIPs produced high percentage rebound values in BP and *d*-BP standard solutions. It was likely the higher level of binding was due to a higher degree of swelling which in turn allowed a greater degree of solvent ingress to the pores. However, in Table 6.5 the swell ratio in chloroform was the same within error for CP, *d*-CP, BP and *d*-BP MIPs prepared at 24000 rpm. Therefore, no correlation appears to exist between binding behaviour and swellability in chloroform for these polymers.

The BP compounds are larger molecular weight templates in comparison to CP and could cause a conformation change in the polymer chains. Swelling is sensitive to the molecular weight of the added template into the polymer network [20]. Hydrogen bonding is considered the driving force between template and functional monomer. For larger molecular weight templates like BP, the infusion of molecules into the

network which is hydrogen bond driven could cause a change to the equilibrium condition.

In addition to equilibrium binding experiments performed in Chapter 5 enantiomeric separation was observed in HPLC analysis when aqueous mobile phase was employed. It would be expected that for polymers prepared in chloroform a chloroform-based mobile phase would give better separation [21].

6.3.4 Characterisation of spherical beads by SEM analysis.

The surface morphologies of the *d*-CP polymers prepared at 9500, 13500 and 24000 were assessed by scanning electron microscopy (SEM). Figure 6.7 illustrates the SEM images for the *d*-CP MIP and NIP prepared at 24000 rpm and for *d*-CP polymers prepared at 13500 and 9500 rpm respectively.

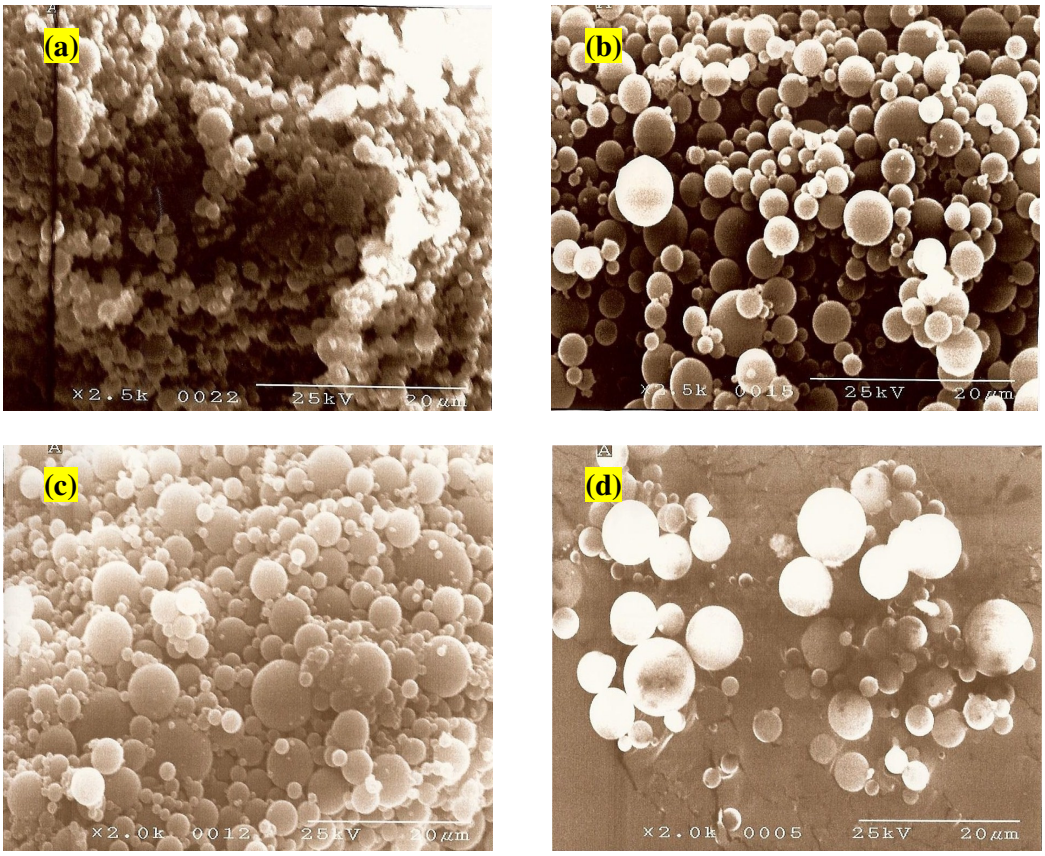

Figure 6.7 **SEM images of (a) *d*-CP MIP (24000 rpm) (b) NIP (24000 rpm) (c) *d*-CP MIP (13500 rpm) and (d) *d*-CP MIP (9500 rpm).**

SEM images are a very useful method for observing the structure of MIPs [22]. Spherical morphologies as exhibited by the SEM images in Figure 6.7 for all imprinted polymers (MIP and NIP) would make them suitable for chromatographic purposes. Three SEM micrographs were taken for each polymer. The majority of the beads were spherical with a smooth surface. These morphological images complement particle size distribution data presented above in Section 6.3.2. Particle size distribution analysis is an important technique as it gives more accurate information to SEM. Appreciable differences were observed between the images in Figure 6.7. Firstly, at 24000 rpm the MIP (2.34 ± 0.003 μm) was smaller than the NIP (3.70 ± 0.006 μm). These differences in size data can be attributed to the presence or absence of template during polymerisation.

Secondly, the rate of agitation in the initial stage of the reaction influences the particle size diameter of the polymer. A difference in the size of the beads was observed between SEM images for *d*-CP MIPs prepared at (a) 24000 rpm (2.34 ± 0.003 μm), (b) 13500 rpm (4.45 ± 0.004 μm) and (c) 9500 rpm (5.15 ± 0.008 μm) respectively. Smaller globules are formed employing a higher rate of agitation in the suspension medium resulting in a smaller average particle size diameter.

Fairhurst *et al*. [23] has previously reported that employing irregular shaped particles for chromatographic purposes caused high back pressures resulting in long retention times and poor peak shapes. The beads produced at the lowest speed 9500 rpm demonstrated good resolution of enantiomers and peak shape in Chapter 5 when employed as stationary phase packing material.

By changing the agitation speeds the properties of the MIP polymers can be examined in order to select the most favourable polymer that could be employed as a stationary phase for chiral resolution. Thus recommendations for optimising column chromatography would be to employ smaller stainless steel columns with smaller polymer bead sizes and analyse on Ultra-HPLC system. The Ultra-HPLC uses the same separation methodology as conventional HPLC, but typically uses columns packed with particles smaller than 2 μm. The advantages of employing smaller particles on such a system dramatically increase column efficiency, analytical resolution and speed.

6.4 Conclusions

A detailed examination of the characteristics of MIPs prepared at different agitation speeds, i.e. 24000 rpm, 13500 and 9500 rpm was gained from measurement of their physical properties in the dry state employing nitrogen porosimetry, particle size distribution analysis, solvent swell studies, and SEM images. The key findings were:

- Based on the BET analysis there were similarities between the three sets of polymers prepared at different agitation speeds, namely the low specific surface areas (4.55, 2.11 and 1.68 m^2g^{-1} for agitation speeds of 24000, 13500 and 9500 rpm respectively) which were non-porous in nature. The average pore volume of all samples prepared at agitation speeds of 24000, 13500 and 9500 rpm also displayed low values (0.02, 0.01 and 0.005 cm^3g^{-1}). This suggests that the main adsorption mechanism for the polymers occurs on the external surface of the material. Agitation speed had an impact on the surface area and pore volume values of the polymers.
- Particle size studies and SEM analysis was also performed on all polymers. These techniques showed an increase in particle size with decreasing particle agitation speed. In addition SEM examination shows spherical bead particles of about 2 µm for MIPs prepared at 24000 rpm.
- Swell studies were investigated on the polymers in three different solvents. The swelling ratio was greatest in chloroform and much lower for the other solvents in comparison. No obvious trends were observed across the different agitation speeds. The swell ratio was lower in methanol for the polymers prepared at 24000 rpm in comparison to polymers prepared at 13500 and 9500 rpm.
- Spherical MIPs for *d*-CP prepared at 9500 rpm were successfully packed and assessed as stationary phase in HPLC in Chapter 5. The morphology and porosity of this polymer were characterised by BET, particle size analysis and SEM. From physical characterisation results, MIPs obtained had an average diameter of 5.15 ± 0.008 µm, BET surface area of 1.68 (± 0.01) $m^2 g^{-1}$, average pore volume of 0.005 (± 0.0003) $cm^3 g^{-1}$ and an average pore diameter of 7.50 ± 0.10 nm. The SEM image of *d*-CP exhibited a spherical shape.

Reference List

1. Wei, S.; Mizaikoff, B. *Biosensors and Bioelectronics* **2007,** *23*, 201-09.

2. Suárez, E.; Paredes, B.; Rubiera, F.; Rendueles, M.; Villa-García, M. A.; Díaz, J. M. *Separation and Purification Technology* **2002,** *27*, 1-10.

3. Urraca, J. L.; Carbajo, M. C.; Torralvo, M. J.; González-Vázquez, J.; Orellana, G.; Moreno-Bondi, M. C. *Biosensors and Bioelectronics* **2008,** *24*, 155-61.

4. Sing, K. S. W. *Pure and Applied Chemistry* **1982,** *54*, 2201-18.

5. Piletsky, S. A.; Piletska, E. V.; Karim, K.; Freebairn, K. W.; Legge, C. H.; Turner, A. P. F. *Macromolecules* **2002,** 35, 7499-504.

6. Sellergren, B.; Shea, K. J. *Journal of Chromatography A* **1993,** *635*, 31-49.

7. Brüggemann, O. *Analytica Chimica Acta* **2001,** *435*, 197-207.

8. Haginaka, J.; Tabo, H.; Kagawa, C. *Journal Of Pharmaceutical And Biomedical Analysis* **2008,** *46*, 877-81.

9. Kempe, H.; Kempe, M. *Analytical Chemistry* **2006,** *78*, 3659-66.

10. Beltran, A.; Marcé, R. M.; Cormack, P. A. G.; Borrull, F. *Journal of Chromatography A* **2009,** *1216*, 2248-53.

11. Lowell, S.; Shields, J.; Thomas, M.; Thommes, M. *Characterisation of Porous Solids and Powders: Surface Area, Pore Size and Density,* (Kluwer Academic Publishers., Dordrecht, The Netherlands., **2004**).

12. Kirkland, J. J.; DeStefano, J. J. *Journal of Chromatography A* **2006,** *1126*, 50-57.

13. Phenomenex, http://www.phenomenex.com/, (**2009**).

14. Li, L.; Cheng, J.; Wen, X.; Pi, P.; Yang, Z. *Chinese Journal of Chemical Engineering* **2006,** *14*, 471-77.

15. Holland, N.; Frisby, J.; Owens, E.; Hughes, H.; Duggan, P.; McLoughlin, P. *Polymer* **2010,** *51*, 1578-84.

16. Joshi, V. P.; Kulkarni, M. G.; Mashelkar, R. A. *Journal of Chromatography A* **1999,** *849*, 319-30.

17. Lu, Y.; Li, C.; Wang, X.; Sun, P.; Xing, X. *Journal of Chromatography B* **2004,** *804*, 53-59.

18. Piletska, E. V.; Guerreiro, A. R.; Romero-Guerra, M.; Chianella, I.; Turner, A. P. F.; Piletsky, S. A. *Analytica Chimica Acta* **2008,** *607*, 54-60.

19. Shea, K. J.; Spivak, D. A. &. S. B. *Journal of the American Chemical Society* **1993,** *115*, 3388.

20. Fernandez-Barbero, A.; Suarez, I. J.; Sierra-Martin, B.; Fernandez-Nieves, A.; de las Nieves, F. J.; Marquez, M.; Rubio-Retama, J.; Lopez-Cabarcos, E. *Advances in Colloid and Interface Science* **2003,** *147-148*, 88-108.

21. Yu, C.; Mosbach, K. *Journal of Chromatography A* **2000,** *888*, 63-72.

22. Feás, X.; Fente, C. A.; Hosseini, S. V.; Seijas, J. A.; Vázquez, B. I.; Franco, C. M.; Cepeda, A. *Materials Science and Engineering:* **2009,** *29*, 398-404.

23. Fairhurst, R. E.; Chassaing, C.; Venn, R. F.; Mayes, A. G. *Biosensors and Bioelectronics* **2004,** *20*, 1098-105.

Chapter 7

Conclusions and Future Work

7.1 Conclusions

The first area of this research focussed on imprinting 2-aminopyridine (2-apy) by both suspension and bulk polymerisation procedures. The influence of experimental parameters such as temperature, agitation speed and cross-linker were examined in order to optimise the conditions for synthesis in suspension polymerisation. From evaluation of the binding conditions, surface morphology, percentage yield recoveries, particle size distribution and solvent swell ratio it was found that the best MIP bead was produced employing a high agitation speed (24000 rpm), low polymerisation temperature (4 °C), methacrylic acid (MAA) as functional monomer and trimethylolpropane trimethacrylate (TRIM) as cross-linker.

The impact of the optimised polymer composition on the binding parameters of the 2-apy suspension and bulk polymers was further evaluated utilising three binding models: Langmuir (LI), Freundlich (FI) and Langmuir-Freundlich (L-FI) isotherms and by generating affinity distribution (AD) spectra. For this system, binding isotherm modelling revealed that the Langmuir-Freundlich isotherm model (L-FI) was the most suitable for assessing the binding behaviour of suspension polymers for the concentration range studied. A relationship was observed between polymerisation conditions and the number of binding sites and binding energies which was also illustrated in affinity distribution spectra. The maximum number of binding sites in the suspension MIP at a particular energy appeared to be similar.

The behaviour of bulk and suspension polymers was studied by means of a direct probe GC-MS methodology. The initial pre-treatment stage of the methodology permited the removal of residual and unreacted monomeric/polymeric components. It was found that the bleed was higher for NIPs in comparison to MIPs. Furthermore, the bleed was significantly higher for NIP suspension polymers over the NIP bulk polymers. Post-analysis selection of specific ions was further examined and the bleed for the polymers in this study consisted mainly of the cross-linker (TRIM). The difference in bleed between bulk and suspension NIP polymers suggests differences in polymeric structure due to the cross-linking density.

A GC-MS technique was also used in polymer characterisation to investigate the rebinding performance of MIPs. Rebinding studies to assess specificity by MIP and NIP polymers revealed differences between imprinted and non-imprinted polymers for bulk and suspension polymers with TRIM as a cross-linker. A relationship between concentration reloaded and imprinting factor values for the bulk and suspension polymers was observed. Lower specificity in the bulk polymers in comparison to the suspension polymers was observed. A direct comparison was found in assessing imprinting performance utilising GC-MS and UV solution phase analysis. The sensitivity of the GC-MS technique was further illustrated by its ability to characterise polymers that had different physical structures arising from suspension and bulk polymerisation techniques. Based on the desorption studies the template was more strongly bound to the MIP than the NIP for bulk and suspension polymers.

The second area of this research focussed on the extension of suspension imprinting technology to other templates in an aqueous system. MIPs for chlorpheniramine (CP), *d*-chlorpheniramine (*d*-CP), brompheniramine (BP) and *d*-brompheniramine (*d*-BP) were successfully prepared by an aqueous suspension polymerisation method. As for the 2-apy MIP, similar conditions were utilised in the preparation of the MIPs for CP, *d*-CP, BP and *d*-BP. However, difference in this synthesis was that chloroform was employed as a porogen due to the pre-polymerisation mixture being suspended in water instead of mineral oil as previously described.

A cross-selectivity rebinding study was carried out on the polymers using chiral HPLC analysis. Trends observed for the HPLC equilibrium binding results found that there was similarity in non-specific binding across all NIPs. In the majority of cases binding capacity and IF values were found to be the highest for *d*-BP imprinted polymers in all standard solutions. One possible reason for the higher binding on the BP and *d*-BP compounds could be the difference in binding pocket size between BP and CP polymers. The difference in molecular size of the BP polymer regarding its shape and arrangement of functionalities within the binding cavity could be facilitating a higher level of binding. Loading a CP standard solution onto a BP or *d*-BP imprinted polymer which had a bigger binding pocket allowed more access of the substrate material into the binding site within the molecule and higher binding as a result.

The similarity between the molecular structures of CP and BP and the fact that there is very little difference between the two pK_a values for CP and BP makes it difficult to explain why higher uptake, binding capacity and IF values were found for the BP polymers over the CP polymers. It is speculated that the recognition of imprinted beads depended on multiple hydrogen bonding and cavity shape produced by the imprinting process. Interaction between the functional groups of the template and monomers are known to be very important for the formation of affinity sites. Additionally, it is speculated the higher binding of BP polymers over CP is related to differences in polarisability between Br and Cl and steric constraints.

In Chapter 5, the binding behaviour of the MIPs and NIPs prepared at 24000 rpm was evaluated and suggests that the morphology and textural properties of the polymer beads may affect binding behaviour. The morphology of the MIPs was examined by nitrogen sorption porosimetry, particle size distribution, solvent swell studies and by scanning electron microscopy (SEM). These characteristics were compared to polymers prepared at agitation speeds of 9500 rpm and 13500 rpm in order to assess the significance on surface area, pore volume and particle size. Differences were observed in terms of particle size and surface area values by decreasing the agitation speed. Nitrogen sorption measurements performed on all samples exhibited low specific surface areas (4.55, 2.11 and 1.68 m^2g^{-1} for agitation speeds of 24000, 13500 and 9500 rpm respectively). The cumulative volume of pores for the *d*-CP MIP polymers prepared at 9500 rpm and 13500 rpm was approximately half (or less) (0.01 and 0.005 cm^3g^{-1}) that of the corresponding MIP prepared at 24000 rpm (0.02 $cm^3 g^{-1}$). The average pore diameter of *d*-CP MIPs prepared at agitation speeds of 24000, 13500 and 9500 rpm also displayed low values (13.11, 9.66 and 7.50 nm). These results indicated that the MIPs were non-porous materials. A higher particle size distribution value for the *d*-CP MIP prepared at 9500 rpm was observed (Dv50 value = 5.15 ± 0.008 µm) compared to the *d*-CP MIP prepared at 24000 rpm (Dv50 value = 2.34 ± 0.003 µm).

The *d*-CP MIP prepared at 9500 rpm was successfully employed as a HPLC stationary phase for chiral resolution of CP and BP enantiomers using an aqueous mobile phase in Chapter 5. The pH of the mobile phase was screened over the 3 to 9 range, in which the charge of the analytes changes. The MIP stationary phase could not

discriminate between the enantiomers at any of the pHs and mobile phase compositions studied with the exception of pH 7 and composition of 70:30 (v/v). The retention factors (*k*) of CP and BP were observed to vary going from lower pH to higher (3 – 9). Consequently, the enantiomers of CP and BP demonstrated the strongest retention and best separation on a *d*-$CP_{MIP(9500rpm)}$ column with a mobile phase composition of (70:30) ACN:buffer at pH 7. This composition and pH were selected for studies investigating the enantioselectivity of the *d*-$CP_{MIP(9500rpm)}$ column.

The chromatographic behaviour and separation of CP and BP enantiomers were studied on the *d*-$CP_{MIP(9500rpm)}$ column. The highest enantioselectivity (1.19) and resolution (0.88) was obtained for CP over BP. The *d*-$CP_{MIP(9500rpm)}$ showed high cross-selectivity for CP and BP. It is interesting to note that the retention of BP was greater than that of CP (even though the resolution for CP was better). This result is in agreement with equilibrium binding observations (Table 5.5, Chapter 5). This strengthened the retention of the CP and BP enantiomers on the stationary phase as a result of deprotonation.

The effect of column temperature (a) ambient and (b) 50 ^{o}C on a mixture of *d*-CP and *d*-BP isomers on the *d*-$CP_{MIP(9500rpm)}$ column was investigated. The resolution value increased with increase in column temperature from 0.61 to 0.86, which would be expected due to sharper peaks produced. The selectivity factor decreased slightly from 1.18 to 1.17 at the higher temperature. Increasing the column temperature improved separation with the added advantage of time saving in the separation analysis.

The *d*-$CP_{MIP(9500rpm)}$ column also successfully separated PHEN, CP and BP enantiomers. A change in composition of the mobile phase (a mixture of ACN and phosphate buffer) from 70:30 to 65:35 (v/v) while maintaining the same pH (= 7) was required in order to achieve separation of the PHEN enantiomers. The enantioseparation factors on a *d*-$CP_{MIP(9500rpm)}$ column for PHEN, CP and BP were 1.08, 1.15 and 1.17 respectively. The resolution for PHEN = 0.50, CP = 0.64 and BP = 0.72. The BP was the most retained on a *d*-$CP_{MIP(9500rpm)}$ column compared to PHEN and CP. This was explained due to the fact that PHEN, CP and BP have

almost the same pK_a values and in addition the hydrophobicity is in the order of BP, CP and PHEN.

The *d*-BP MIP prepared at 9500 rpm was also successfully employed as a HPLC stationary phase for chiral resolution of CP and BP enantiomers using an aqueous mobile phase (pH 7). The chromatographic behaviour and separation of CP, *d*-CP, BP and *d*-BP isomers were studied on the *d*-$BP_{MIP(9500rpm)}$ column and compared to results obtained on the *d*-$CP_{MIP(9500rpm)}$ column. A similar trend was observed in the retention factors for BP over CP on the *d*-$CP_{MIP(9500rpm)}$ column. The retention of BP and *d*-BP on the *d*-$BP_{MIP(9500rpm)}$ column was greater in comparison to CP and *d*-CP. However, an opposite trend was observed for the enantioselectivity factors and resolution, which were greater for CP enantiomers than BP on the *d*-$CP_{MIP(9500rpm)}$ column. The results showed that for the *d*-CP and *d*-BP polymers, each gave the best enantioseparation for its own template.

In summary, the potential of a novel class of beaded polymers prepared by an aqueous suspension method for analytical separations of enantiomers was successfully explored.

7.2 Future work

An aqueous suspension polymerisation methodology utilised in this thesis was shown to be a simple and straightforward technique for the generation of a novel class of molecularly imprinted polymer beads.

The physical characterisation of the CP, *d*-CP, BP and *d*-BP suspension polymers was supported by nitrogen sorption indicating non-porous materials in Chapter 6. The porosity of these polymers could be further tailored by modifying polymerisation composition. For the preparation of imprinted polymers in this study a ratio of 2:3 mmol of template/functional monomer was employed. In future work the polymer composition could be modified so that MAA will interact with CP in a 1:3 mmol ratio. This could provide a means to prepare MIPs with more homogeneous distribution of binding sites. Additionally, the interaction of CP with three functional monomers, CP-MAA (1:3) could produce a more stable complex as a result. Employment of nitrogen sorption could provide more definitive answers to the possibility of differences in pore structure and chemical differences in suspension polymers.

In Chapter 4, thermal desorption GC-MS was used to analyse polymer-template interactions for 2-apy bulk and suspension polymers. Thermal desorption GC-MS could be used for a more accurate assessment of polymeric binding properties for the CP, *d*-CP, BP and *d*-BP suspension polymers in order to assess the binding affinity. This could be achieved by loading of templates and structural analogues onto pretreated MIPs and NIPs followed by selective thermal desorption.

Further correlation of the polymers physical characteristics could be investigated employing thermal analysis techniques such as differential scanning calorimetry (DSC) or thermogravametric analysis (TGA). Employment of these techniques would provide a greater insight into the thermal stability and the cross-link density of the polymers respectively. Additionally, differences between MIPs and NIPs could provide information about physical properties such as the degradation of decomposition temperature and cross-link density supported by such techniques.

The selectivity of the MIP stationary phase was studied in an aqueous-organic mobile phase in Chapter 5. The next stage would be the evaluation of the chiral MIPs using normal phase HPLC. The CP, *d*-CP, BP and *d*-BP polymers in this study were prepared with chloroform as porogen, by changing to a chloroform-based mobile phase, the enantiomeric recognition properties of the MIPs in normal-phase HPLC mode could be affected. A chloroform-based mobile phase may provide better separation than an aqueous-organic mobile phase.

For the majority of applications of specific molecular recognition, rapid chiral resolution kinetics is essential. Further studies, could comprise optimisation of the chromatographic conditions by employing smaller stainless steel columns with small polymer bead sizes (prepared at the higher speed of 24000 rpm) and assess their potential application on an Ultra-HPLC system. This could address issues surrounding the resolution kinetics and improve separations; leading to shorter analysis times with improved column performance.